DESIGN, SYNTHESIS AND EVALUATION OF TWIN-TUBE VALVE MODE MAGNETO-RHEOLOGICAL (MR) DAMPER FOR SEMI-ACTIVE AUTOMOTIVE SUSPENSION SYSTEM

Thesis

Submitted in partial fulfilment of the requirements for the degree of

DOCTOR OF PHILOSOPHY

by

RANGARAJ MADHAVRAO DESAI

DEPARTMENT OF MECHANICAL ENGINEERING

NATIONAL INSTITUTE OF TECHNOLOGY KARNATAKA,

SURATHKAL, MANGALORE - 575025

JULY - 2021

D E C L A R A T I O N

I hereby declare that the Research Thesis entitled **"DESIGN, SYNTHESIS AND EVALUATION OF TWIN-TUBE VALVE MODE MAGNETO-RHEOLOGICAL (MR) DAMPER FOR SEMI-ACTIVE AUTOMOTIVE SUSPENSION SYSTEM"** which is being submitted to the **National Institute of Technology Karnataka, Surathkal** in partial fulfilment of the requirements for the award of the Degree of **Doctor of Philosophy** in **Mechanical Engineering** is a *bonafide report of the research work carried out by me*. The material contained in this Research Thesis has not been submitted to any other University or Institution for the award of any degree.

Register Number   : **1 6 5 0 6 2 M E 1 6 F 1 2**

Name of the Research Scholar   : **Rangaraj Madhavrao Desai**

Signature of the Research Scholar   :

Department of Mechanical Engineering

Place   : NITK-Surathkal

Date   : 12/07/2021

CERTIFICATE

This is to certify that the Research Thesis entitled "DESIGN, SYNTHESIS AND EVALUATION OF TWIN-TUBE VALVE MODE MAGNETO-RHEOLOGICAL (MR) DAMPER FOR SEMI-ACTIVE AUTOMOTIVE SUSPENSION SYSTEM" submitted by **Mr. Rangaraj Madhavrao Desai (Register Number: 165062ME16F12)** as the record of the research work carried out by him, *is accepted as the Research Thesis submission* in partial fulfilment of the requirements for the award of Degree of **Doctor of Philosophy.**

Research Guide (s)

16/07/2021

Dr. Hemantha Kumar
Associate Professor
Department of Mechanical Engineering
NITK, Surathkal

16/07/2021

Dr. Sharnappa Joladarashi
Associate Professor
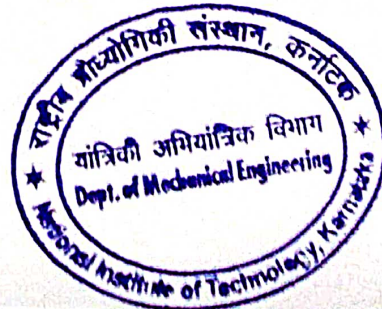Department of Mechanical Engineering
NITK, Surathkal

Chairman – DRPC
Department of Mechanical Engineering

Place   : NITK-Surathkal

Date   : 16 JUL 2021

Dedication

This thesis work is dedicated to my parents, wife and sister,

without whom this would not have been possible.

Also dedicated to my dear daughter Saanvi

ACKNOWLEDGEMENTS

Finally, I wish to express gratitude, love and affection to my beloved family members, my father **Mr. Madhavarao D Desai**, my mother **Mrs. Geeta Desai**, my wife **Mrs. Vaishnavi T** and my sister **Miss. Rashmi Desai** for their encouragement and moral support on the road to the completion of my research.

Rangaraj Madhavrao Desai

ABSTRACT

The change in rheological properties of smart materials like magneto-rheological (MR) fluid when brought under the influence of a magnetic field can be utilized to develop MR devices where the output has to be continuously and quickly varied using electronic control interface. A viscous damper which uses this MR fluid as the viscous medium is called as MR damper and the damping force generated by the MR damper can be varied by modulating the current given to the electromagnetic coil in the MR damper. Hence MR dampers have electronically controlled variable damping co-efficient and have a promising future for application in automotive semi-active suspensions. The main aim of the present work is to explore the design and application of twin-tube valve mode MR damper for use in automotive semi-active suspension.

A viscous damper of twin tube design working in the passive mode is evaluated on a damper testing machine and its performance is characterized. Its behaviour at different velocities and frequencies of excitation is studied using sinusoidal excitations of fixed amplitude and varying frequencies. The force vs displacement plots show that the size of the loops increase with increase in frequency of excitation. Using the dissipated energy method, the equivalent damping coefficient of the damper is calculated for different frequencies of excitation. Mathematical models are developed for the force vs velocity behaviour of the damper as the damper force is a function of the damper piston velocity. These mathematical models based on the experimental results will be very much useful in designing an alternative or improved suspension system for the vehicle under consideration.

A commercial MR damper, RD-8040-1 by Lord Corporation, USA, is experimentally evaluated for its application in a semi-active suspension. The experiments were carried out in damping force testing machine. Sinusoidal displacement input was given to the test damper. The set of experiments were repeated for different levels of current (0A to 1.5A in steps of 0.25A) supplied to the MR damper. Plots of force vs displacement for each frequency of excitation and plots of maximum force vs frequency of excitation show that higher values of current leads to elevated values of MR damper forces. This increase of MR damper force with current supplied is studied and analysed to develop a mathematical model of the MR damper under investigation. The non-linear softening hysteretic behaviour of the MR damper is simulated by using Genetic Algorithm (GA) provided in the optimization toolbox of MATLAB. Calculations on energy dissipation and

equivalent damping coefficient of the MR damper show that the same damper can make the suspension system behave as an underdamped system, critically damped system or overdamped system depending on the value of current supplied to it. The performance of this MR damper in a spring-mass vibrating system is studied with the help of MATLAB simulations.

A commercially available passive damper of a passenger van is tested to find the characteristic damping requirement of the vehicle. With this as reference, a twin tube MR damper working in valve mode is designed and fabricated. The magnetic flux density induced in the fluid flow gap is maximized using Taguchi analysis and Finite Element Method Magnetics (FEMM) software. The FEMM results are validated with results obtained analytically using electromagnetic circuit theory. The MR damper filled with commercially available MR fluid was experimentally tested in damper testing machine. The results demonstrate that the force developed by the MR damper is indeed increasing with the value of the current supplied. At various frequencies of input oscillation, the energy dissipated by the MR damper in a single cycle increases significantly with current supplied. The novelty of this work is that a twin tube MR damper working in valve mode was designed as a replacement for the passive damper used in a passenger van. The MR damper thus developed is capable of producing practical levels of damping force at actual operating frequencies and amplitudes of the passive damper in the passenger van. For further analysis, the behaviour of the MR damper is modelled by using the Bouc-Wen model for hysteretic systems. A Proportional-Integral-Derivative (PID) controller is used to track the desired damping force in time domain to demonstrate the application of the MR damper in a semi-active suspension system.

MR fluid was synthesized to be used as a smart fluid in a twin tube MR damper operating in valve mode. The behaviour of the MR fluid is experimentally characterized in a rheometer and mathematically modelled using Herschel-Bulkley (HB) model. The parameters of the HB model are expressed as polynomial functions of strength of magnetic field in order to find the shear stress developed by MR fluid at any given strength of magnetic field applied. This fluid is filled in the MR damper which was designed for application in a passenger van and it is tested in damper testing machine. The performance of the damper at different damper velocities and current supplied is studied. The range of values for the parameters of the experimental testing are chosen to emulate the actual conditions of operation in its intended application. Non-dimensional analysis is performed, which links MR fluid rheological properties and geometrical parameters of MR damper

design with the force developed by damper. Finite Element Method Magnetics (FEMM) is used to find the strength of the magnetic field at the fluid flow gap. Analytical methods are used to calculate the damper force developed due to the field dependent yield stress and compared with experimental force values. The resulting dynamic range of the MR damper is also assessed.

A mathematical model of the quarter car suspension is built for numerical simulation to compare the performance of semi-active suspension and passive suspension. Vibrations coming from the wheel due to road roughness and unevenness are given as input displacement to the suspension model. Sinusoidal excitation and random road excitation are used as input displacement. Based on experimental characterization, mathematical models are developed for the hysteresis behaviour of commercial and twin-tube MR damper using a polynomial model of hysteresis. These are used for implementing skyhook control in the semi-active suspension model. The current given to the MR damper is varied in order to achieve the best ride comfort which is demonstrated as a reduction in the sprung mass acceleration of the quarter car suspension. The dynamic behaviour of the MR damper based semi-active suspension is studied using MATLAB Simulink to show that its performance is better than passive suspension.

The twin-tube MR damper working in valve mode is further developed for application in a semi-active SUV suspension system. In order to prove the superiority of semi-active suspension, a single degree of freedom quarter car test rig is built and ground excitation is given in the form of displacement input from a hydraulic actuator. Constant current control, Skyhook control and Rakheja-Sankar (RS) control are employed as three different control strategies and compared with passive suspension to study the advantages. Peak acceleration response of the sprung mass is studied for better passenger ride comfort and peak ground force is studied for preventing damage to road surface as well as to vehicle suspension elements. RS control method provides better ride comfort to passengers due to lower peak vertical acceleration when compared to constant current control or Skyhook control method. RS control method also generated much lower peak ground force values when compared to Skyhook control, especially in the high frequency region.

Keywords: Magneto-rheological dampers, twin-tube valve mode, MR damper optimization, FEMM, MR fluid synthesis, nondimensional numbers, MR fluid rheology, automotive dampers, semi-active suspension, SDOF quarter car, Rakheja-Sankar control.

CONTENTS

LIST OF FIGURES

xiv

LIST OF TABLES

ABBREVIATIONS

ADC	Analog to Digital Converter
AWG	American wire gauge
CIP	Carbonyl iron powder
DAQ	Data Acquisition
DC	Direct Current
DOF	Degrees of freedom
ER	Electro-rheological
FE	Finite Element
FEM	Finite Element Magnetics
FEMM	Finite Element Method Magnetics
FESEM	Field Emission Scanning Electron Microscope
FFT	Fast Fourier Transform
FLC	Fuzzy Logic Control
GA	Genetic Algorithm
HB	Herschel-Bulkley
HP	Horse Power
IEPE	Integrated Electronics Piezo-Electric
LGQ	Linear Quadratic Gaussian
LVDT	Linear Variable Differential Transformer
MR	Magneto-rheological
NSGA	Non-dominated Sorting Genetic Algorithm
PC	Personal Computer
PID	Proportional Integral Derivative
PSO	Particle Swarm Optimization

PWM	Pulse Width Modulation
QFT	Quantitative Feedback Theory
RMS	Root Mean Square
RS	Rakheja-Sankar
SDOF	Single degree of freedom
SEM	Scanning Electron Microscopy
SN	Signal to noise
SUV	Sports Utility Vehicle

CHAPTER 1

INTRODUCTION

1.1 INTRODUCTION

Automobiles are an important part of modern civilization and their state of technology reflects the progress made by mankind in science and technology. As the requirements of the customer increased, automobile manufacturers responded with improved products using innovations in design and manufacturing. Automotive suspension system is primarily responsible for providing a comfortable ride to the passengers and also to provide a safe and balanced handling of the vehicle. Spring and damper are the most significant parts of any automotive suspension.

1.1.1 Need for vehicle suspension

On a straight road with smooth and flat surface, there is no need of a suspension system. In reality however, there are various types of unevenness and roughness present on the road surfaces. Hence, in order to provide ride comfort for the passengers of a vehicle and maintain a permanent contact between tyres and road surface, a suspension system is necessary. The suspension system of a vehicle isolates it from the exciting vibrations of the road unevenness so as to provide ride comfort and good ride stability for vehicle. The ride stability of vehicle is particularly important as vehicle is turning, accelerating, or braking. They are also necessary for protecting the road surface from excessive tyre forces and hence prevent pavement damage.

1.1.2 Working of typical vehicle suspension and its components

The typical construction of the suspension system of a vehicle consists of suspension units, which are placed at the vehicle corners. They connect the vehicle chassis to the vehicle wheels via a linkage system. Each suspension unit is comprised of two basic suspension elements namely the spring and the damper which are set in parallel. The springs absorb the shock-excitations which are caused by the road surface irregularities. As the suspension hits the undulations of road surface, the spring gets compressed and stores the energy of the shock. After that, it expands and releases the absorbed energy gradually to the vehicle body. On the other hand, the function of a damper is to dissipate the energy

of suspension vibrations. When the suspension moves over an undulation of road surface, the damper directly damps a part of the shock energy. In addition, it dissipates the stored energy in the spring. In this way, it controls the action of the springs. Likewise, springs and dampers control the motion of the vehicle body, caused by driving manoeuvres.

1.2 MAGNETO-RHEOLOGICAL FLUID (MR) FLUID

Magneto-rheological fluids have attracted considerable interest recently because they can provide a simple and rapid response interface between electronic controls and mechanical systems. MR fluids can significantly change their rheological behaviour on the application of suitable magnetic fields. The basic phenomena in magneto-rheology are related to controlling the structure and properties of a fluid-particle mixture by applying a magnetic field. MR fluids are far less sensitive to contamination and extreme temperature. MR fluids can operate at temperatures from -40^0 C to 150^0 C with only slight variations in yield stress. As shown in Figure 1.1, the applied field polarizes the ferromagnetic particles of the MR fluid, and thus induces a chainlike agglomeration of particles in the direction of the magnetization and gives rise to a significant effective viscosity increase. The magnetic moment of particles is induced by the applied field and the process of effective viscosity change is largely reversible. Under the magnetic field, an MR fluid behaves as a non-Newtonian fluid with controllable viscosity. However, if the magnetic field is removed, the suspension turns to a Newtonian fluid and the transition between these two phases is highly reversible, which provides a unique feature of magnetic field controllability of the flow of MR fluids.
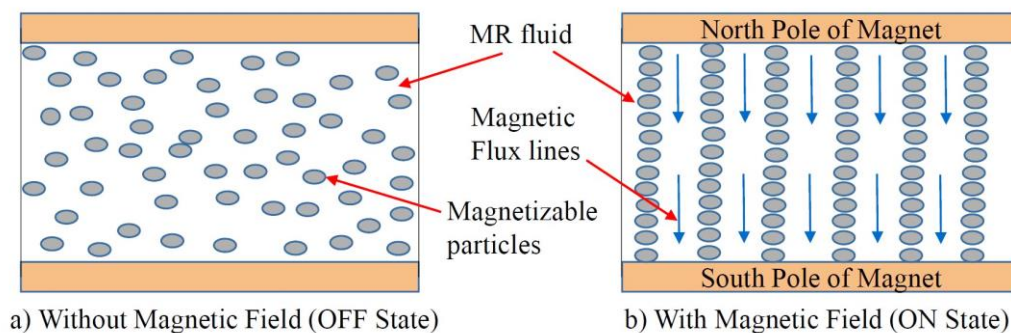
Figure 1.1 Behaviour of MR fluid under magnetic field

1.2.1 Constituents of MR fluid

An MR fluid is basically a suspension of micron sized magnetizable particles in a suitable carrier liquid. The most widely used magnetizable particle is carbonyl iron powder

(CIP), which is obtained by the thermal decomposition of iron pentacarbonyl. This method yields CIP with highest purity. Choi and Han (2013) and Goldasz and Sapinski (2015) showed that the desired properties of magnetizable particles are uniformity of size and shape, low magnetic coercivity, high magnetic saturation and chemical stability. The preferred range of particle size is 1 to 10 µm. The carrier liquid has to be non-magnetic and non-corrosive in nature. In addition, the liquid should have low thermal coefficient of expansion, good lubrication properties, wide range of operating temperature, should be non-toxic and be chemically compatible with device materials. Some examples for carrier liquid used in MR fluid are mineral oils, hydraulic oils, paraffin oils, silicone oils, synthetic hydrocarbon oil, water and silicone copolymers. Depending on the application of the MR fluid, certain additives are also added to obtain desired properties. Most commonly used additives help in dispersion of the solid phase (magnetizable particles) in the carrier fluid and to prevent rapid settling of the particles in the MR fluid. Other additives help in reducing friction, improving durability, achieving compatibility with device materials and increasing the range of working temperature.

1.2.2 Rheology of MR fluid

The off-state behaviour of MR fluid depends on the properties of carrier fluid, the type of additives used and volume fraction of the magnetizable particles in the fluid. The properties of the solid phase play a significant role in the on-state behaviour of the MR fluid. The rheology of MR fluids can be classified into pre-yield and post-yield regions as

$$\tau = \begin{cases} G^* \gamma_e, & \dot{\gamma}_e = 0\, , \tau < \tau_0 \\ \mu\dot{\gamma}_e + \tau_0, & \tau \geq \tau_0 \end{cases}$$

(1.1)

where τ is shear stress, $\dot{\gamma}_e$ is shear rate, μ is viscosity and G^* is complex modulus. The yield stress τ_0 is a function of the strength of the applied magnetic field. A wide variety of nonlinear models have been used to characterize MR fluids, including the Bingham plastic model, the bi-viscous model and the Herschel–Bulkley model. It is found that at high shear rates, non-linear effects such as shear-thinning and shear-thickening dominate the MR fluid behaviour.

1.2.3 Modes of operation of MR fluid

MR devices can be operated under three different fluid operational modes: the flow or valve mode, direct shear mode and squeeze film mode.

1.2.3.1 Valve or flow mode

The fluid flows in the gap between two static surfaces which may be planar or concentric, due to a pressure difference. The behaviour of the MR fluid is controlled by an external magnetic field whose flux lines pass through the fluid in a direction perpendicular to the direction of fluid flow.
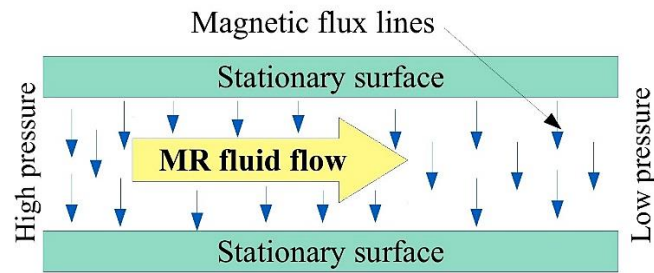
Figure 1.2 MR fluid operation in valve mode

1.2.3.2 Direct shear mode

The fluid flows between two surfaces where one of the surfaces is stationary but the other surface is in relative motion. The flow of fluid is due to a pressure difference and the magnetic flux lines pass through the MR fluid in a direction perpendicular to the direction of fluid flow.
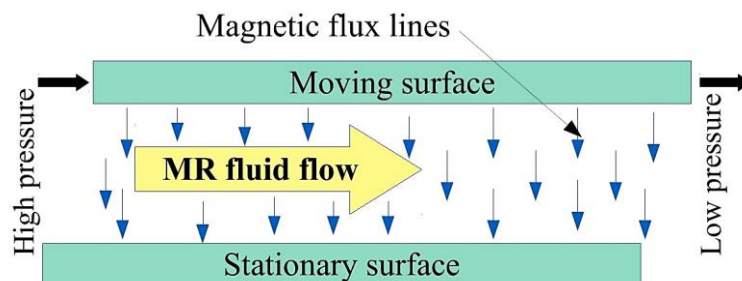
Figure 1.3 MR fluid operation in direct shear mode

1.2.3.3 Squeeze mode

The fluid is placed between two parallel surfaces. The distance between these parallel surfaces changes based on input force or displacement. The direction of the magnetic field, used for changing the MR fluid behaviour, is parallel to the direction of motion of the parallel surfaces. It is restricted to applications where the amplitudes of vibrations are very small.
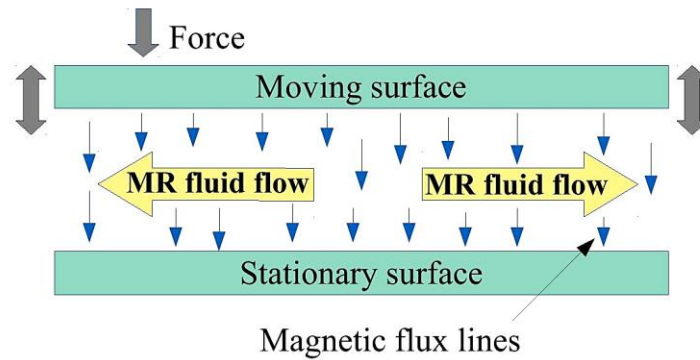
Figure 1.4 MR fluid operation in squeeze mode

1.2.4 Applications of MR fluid

MR fluids have widespread applications operating in both valve mode and shear mode in many dynamic devices. The most popular application is in vibration dampers, which are used as shock absorbers in automotive suspension. MR fluids are used in MR brakes and MR clutches which are both torque control devices. The output torque can be controlled by varying the external magnetic field. MR rotary dampers are used in prosthetic knee application. Structural applications include the use of MR fluid sandwich composites, whose vibration characteristics can be changed with the help of magnetic field. Squeeze mode dampers are used in buildings and bridges for structural applications to prevent damage due to earthquakes. MR isolation mounts find application as engine mounts in ships and automobiles and in supporting cutting tools during machining.

1.3 MAGNETO-RHEOLOGICAL (MR) DAMPER

MR dampers are semi-active control devices that use MR fluids to produce controllable damping force. The MR damper consists of a piston having electromagnetic coil embedded in it. This piston slides in a smooth cylinder, dividing the cylindrical chamber into upper and lower sections. When the MR damper's piston rod moves, the fluid flows to the other side of piston head through the annular gap. There is a coil located inside the piston head and the coil wire used for winding is heat-resistant and electrically insulated. When electrical current is applied to the coil, a magnetic field is set up around the piston head. The total force generated by an MR damper consists of three components: viscous force (uncontrollable force) due to the viscous effects F_μ, friction force F_f and field dependent force (controllable force) F_τ due to magnetic field. The controllability of the MR damper is provided by varying the excitation current. On the basis of design and

construction, MR Dampers can be broadly classified into three types namely Monotube, Twin tube and Double ended.

1.3.1 Monotube MR damper

This type is most widely used because of its compactness and better design. As the name suggests, it consists of only one tube which is completely filled with the damper fluid. There is fluid on both sides of the piston and the fluid fills the whole tube forming a single reservoir as shown in Figure 1.5. There is an accumulator at the end of the tube to accommodate the change in volume that results from piston rod movement in and out of the tube. The accumulator is usually made of a high-pressure gas chamber (usually nitrogen gas) with a diaphragm separating the gas chamber from the fluid reservoir. As the piston moves, the MR fluid flows from one side of the piston to the other. Since the chamber is completely filled with MR fluid, the fluid does not come in contact with any air, thus preventing foaming of the fluid.
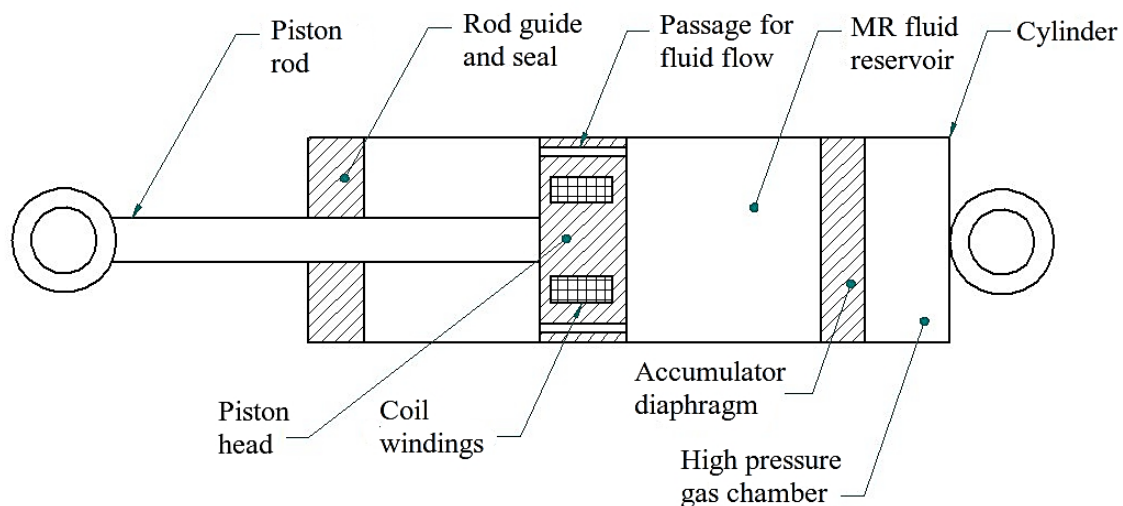
Figure 1.5 Line sketch of Monotube MR damper

1.3.2 Twin-tube MR damper

As the name suggests, it consists of two tubes, one mounted inside the other as shown in Figure 1.6. The inner tube is completely filled with MR fluid forming the inner reservoir, whereas the space between inner and outer tube is partially filled with MR fluid forming the outer reservoir. The remaining space in outer tube is either air at atmospheric pressure or some inert gas at high pressure. The MR fluid in the inner and outer tube are separated by a base valve. The piston moves in the inner tube and both sides of the piston are filled with MR fluid. The change in volume occurring due to the piston rod movement

is accommodated by the MR fluid moving from inner reservoir to outer reservoir through the base valve. This type is simpler in construction and does not require high precision manufacturing processes like in monotube MR damper.
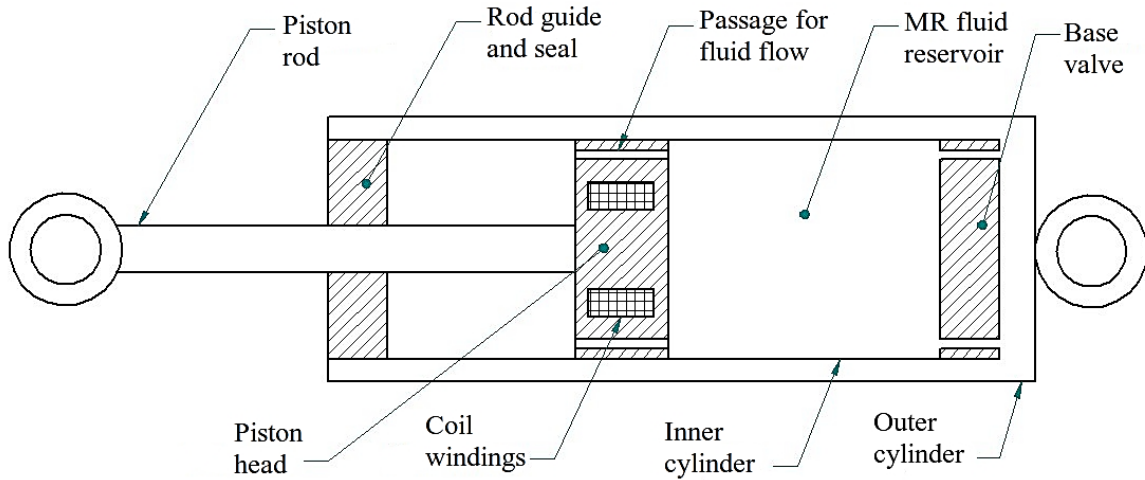
Figure 1.6 Line sketch of Twin tube MR Damper

1.3.3 Double ended MR damper

This type consists of two piston rods of equal diameter protruding from both ends of the MR damper as shown in Figure 1.7. Because of this, there is no change in the volume as the piston rod moves in and out of the damper tube. Hence this type of MR damper does not require an accumulator or another fluid chamber.
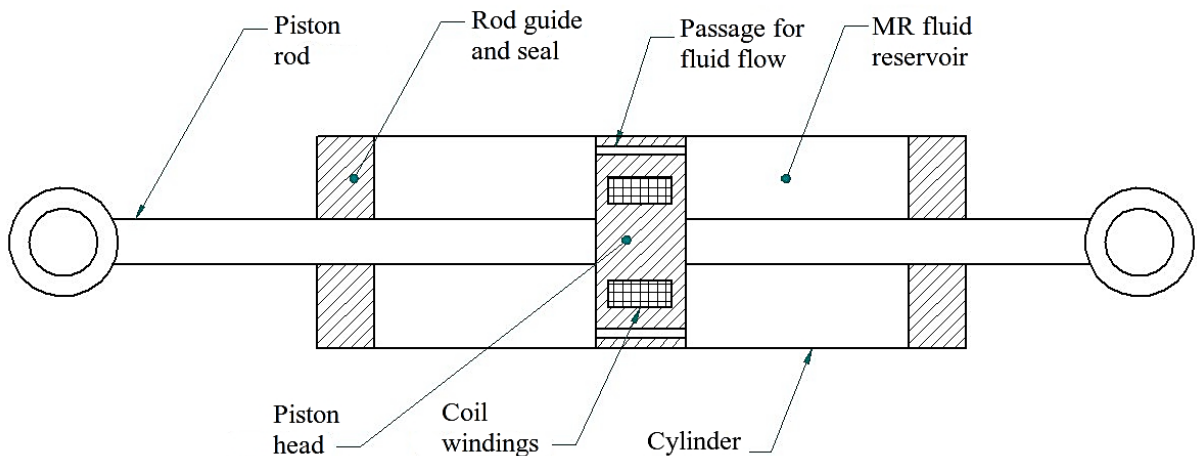
Figure 1.7 Line sketch of Double Ended MR Damper

1.4 QUARTER CAR MODEL

In order to study the dynamics of a vehicle, a two degree of freedom damped spring mass system is considered. This is called as a quarter car model, also known as heave model

of the vehicle suspension. As the name suggests, it considers one quarter of a four-wheeler automobile which is one wheel, its suspension elements and one quarter of the chassis mass. It is a simplification of the full vehicle dynamics for analysing the vertical acceleration and damper performance and it does not consider rolling or pitching of the vehicle. The model has the following elements: unsprung mass, sprung mass, spring, damper, tyre stiffness and tyre damping. Vibration input to the wheel due to the vehicle moving over uneven and irregular road is modelled as displacement input to the wheel coming from the ground.

Various elements are lumped together to form the discrete spring mass model. For example, the mass of wheel, tyre, control arms, spring, damper, brake callipers, wheel hub and wheel bearings are lumped together as unsprung mass. Similarly, the mass of the vehicle chassis, body and passengers is lumped together and one fourth of that mass is taken as sprung mass. To study the suspension performance in relative safety, the quarter car model is very practical and cost-effective. Random effects involved in a field trial can be avoided resulting in a more accurate and repeatable result set. The drawbacks of this model as compared to a full car model is the pitching, yawing and rolling of the vehicle cannot be studied. Hence the effect of full vehicle dynamics like braking, acceleration and turning cannot be studied. Also, since it is assumed that the ground is always in contact with the wheel, the effect of wheel hop cannot be studied.

1.5 TYPES OF SUSPENSION

A typical suspension consists of the unsprung mass and sprung mass. The wheel with tyre and wheel hub is the unsprung mass. The vehicle chassis is the sprung mass. Let K_s and K_t be the spring stiffness of shock absorber and tyre respectively. Let C_s and C_t be the damping coefficient of shock absorber and tyre respectively. Let u be the displacement input to the unsprung mass due to road undulations. Vehicle suspension systems are broadly classified into three types: Passive, Semi-active and Active suspension systems.

1.5.1 Passive suspension system

In these systems, the characteristics of the suspension elements are constant as shown in Figure 1.8. Most traditional vehicles come fitted with passive suspensions. In the design of these systems, there is an inherent compromise between good ride comfort and vehicle stability as the two main goals of the design. A vehicle suspension with stiff spring and firm damper is referred as 'hard' suspension. This provides good control on the vehicle

body motion and wheels vibration, and it creates optimal handling. However, this system is unable to offer effective body isolation. On the other hand, a suspension with low stiffness and soft damping, called 'soft' suspension, provides effective body isolation from road unevenness and creates good ride comfort. However, this system cannot control the motions of the vehicle body and wheels effectively. Therefore, in the design of conventional passive suspensions, a compromise has to be made between good handling and ride comfort. This limits the performance of passive suspensions.
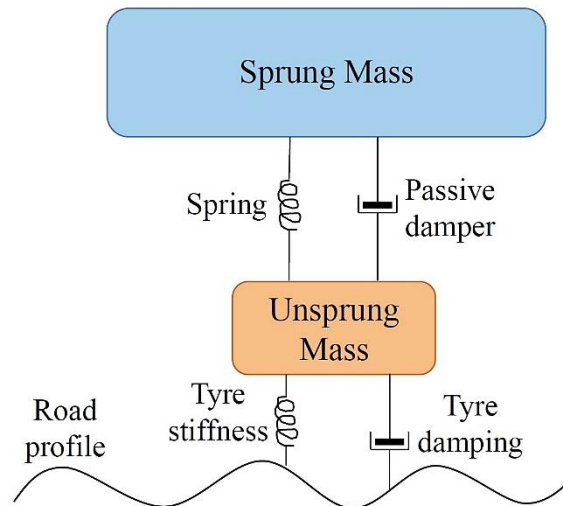
Figure 1.8 Passive suspension system

A suspension with high damping ratio damps the resonance of the sprung mass effectively. However, it increases the transmissibility of the road roughness and provides a poor ride comfort for the vehicle. Conversely, low damping ratio decreases the transmissibility of the road roughness. However, it is not able to damp the resonance of the sprung mass effectively and provides poor handling capability. Even a good design for passive suspension cannot remove this trade-off, but can only optimize it for one set of the driving conditions. Therefore, designers must decide about the priority of ride comfort or handling based on the proposed application of the vehicle. In order to overcome the drawback of passive suspensions caused by the inherent compromise, active and semi-active suspensions are considered, present the possibility of optimizing both ride comfort and handling.

1.5.2 Active suspension system

Active suspension systems involve the use of a force actuator as shown in Figure 1.9. This force actuator has the task of adding or dissipating energy from the system. The

force actuator is controlled by various types of controller determined by the designer. The correct control strategy will give better compromise between comfort and vehicle stability. Therefore, active suspension systems offer better ride comfort and vehicle handling to the passengers. In this type of suspension, the controller can modify the system dynamics by activating the actuators.
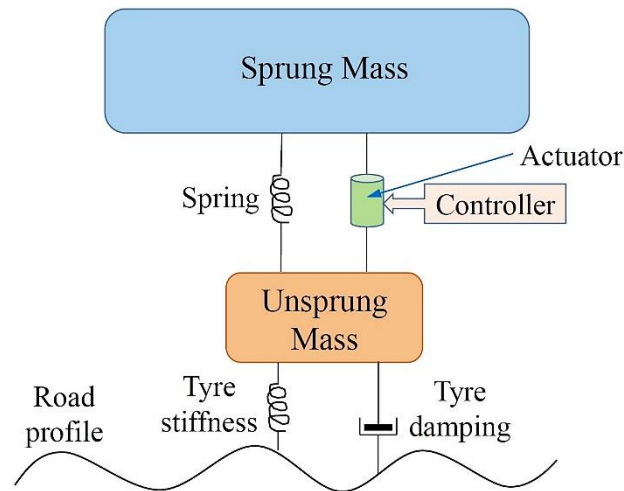
Figure 1.9 Active suspension system

The active suspension system is a close loop control system. It will correct the error and give the output to the desired level. However, increased cost, complexity, need for an external energy source and difficulty in control hardware implementation limits its wide application.

1.5.3 Semi-active suspension system

The drawbacks of passive and active suspension systems led to the development of semi-active suspension systems, which combine the advantages of both passive and active suspension systems. In the semi-active suspension system, the variable control force is achieved by means of a rapidly adjustable damper or spring or both. As shown in Figure 1.10, it replaces the actuator which provides the control force in the active suspension system. Semi-active devices have been used in a variety of applications of vibration control like in buildings and structures, rotor dynamics and vehicular applications.
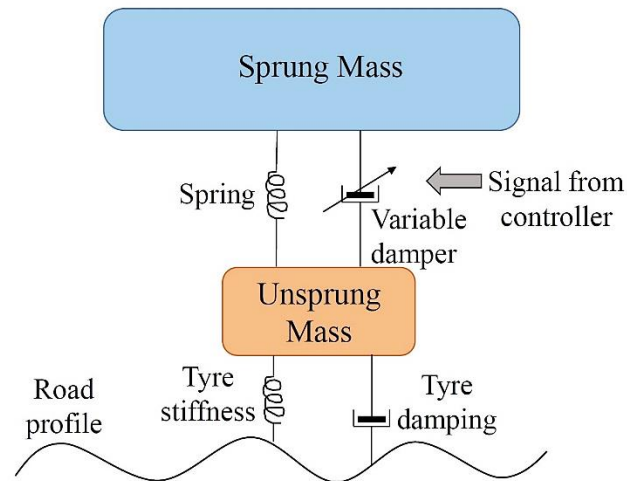
Figure 1.10 Semi-active suspension system

The semi-active devices include variable orifice dampers, variable stiffness devices, tuned liquid dampers, variable friction dampers, electro-rheological (ER) and Magneto-Rheological (MR) fluid dampers.

1.6 SEMI-ACTIVE CONTROL STRATEGIES

There are several control strategies available for semi-active suspension. The criteria for selecting one among them are cost, application, comfort, road holding and response time. One of the most important semi-active control strategies is skyhook control. It is a ride comfort-oriented strategy, where a fictional damper with damping coefficient C_{sky} is connected between the sprung mass and the sky frame. The aim is to reduce the vertical acceleration response of the sprung mass independent of the motion of the unsprung mass or the type of road surface the vehicle is travelling on. In the case of 2-states skyhook control, also known as on-off skyhook control, the damping coefficient of a semi-active damper is switched between a minimum and a maximum value in order to achieve good ride comfort. For this, the skyhook control strategy uses vertical velocity of the sprung mass and damper deflection velocity as inputs. In the case of linear skyhook control, the damping coefficient of the semi-active damper can be varied linearly between a minimum and maximum value, instead of just two states. Another control strategy, which is similar to skyhook control in terms of the sensors used, is acceleration driven damper control. Here, the vertical acceleration of the sprung mass is used as input, instead of velocity. It reduces the vertical acceleration of the sprung mass when information about the road surface is not available. This strategy too aims at improving the passenger ride comfort of the vehicle.

Groundhook damper control is a strategy used when the aim is to improve the vehicle road holding and handling characteristics. Groundhook control reduces dynamic tyre forces which helps to prevent damage to the road surface. Similar to skyhook control, a fictional damper with damping coefficient C_{ground} is used, but it is linked between the unsprung mass and the ground. This reduces the vertical acceleration of the unsprung mass consisting of tyre and wheel. Groundhook control strategy uses vertical velocity of the unsprung mass and damper deflection velocity as inputs. Both on-off and linear Groundhook control are possible.

Proportional-Integral-Derivative (PID) control can also be used to control semi-active dampers. The mathematical model of the semi-active suspension system is linearized and defined by its transfer function in the frequency domain. The accuracy of the linear model to the actual behaviour of the system determines the performance of the PID controlled system. A PID controller can be designed by selecting suitable gains for the proportional, integral and derivative terms. Several tuning methods are available to design a PID controller to obtain the desired performance from the semi-active system.

1.7 ORGANIZATION OF THE THESIS

This thesis presents a detailed study of design, synthesis and development of a twin-tube MR damper for application in a semi-active automotive suspension. A viscous damper used in a passenger van is experimentally tested to find the damping force at various velocities. Using the dissipated energy method, the equivalent damping coefficient of the damper is calculated for different frequencies of excitation. A commercial MR damper is experimentally evaluated in a damper force testing machine using sinusoidal excitation at different currents given to the damper. The increase of MR damper force with current supplied is studied and analyzed to develop a mathematical model of the MR damper under investigation. The piston assembly of a twin-tube damper is designed to accommodate electromagnetic coil. The design is optimized to increase the magnetic flux density at the fluid flow gap with the help of Taguchi analysis and FEMM results. The MR damper is fabricated and filled with commercial MR fluid. It is experimentally tested in damper testing machine at various frequencies of input oscillation and the behaviour of the MR damper is modelled by using the Bouc-Wen model for hysteretic systems. A Proportional-Integral-Derivative (PID) controller is used to track the desired damping force in time

domain to demonstrate the application of the MR damper in a semi-active suspension system.

MR fluid was synthesized for application in an automotive damper and characterized in a rheometer. The fluid behaviour is mathematically modelled using Herschel-Bulkley (HB) model. This MR fluid is filled in a twin-tube valve mode MR damper and tested in damper testing machine. Using non-dimensional analysis, the force developed by the MR damper is linked to MR fluid rheological properties and geometrical parameters of MR damper design. A model of the quarter car suspension with a commercial MR damper based semi-active suspension is built for numerical simulation. The dynamic behaviour of the suspension is studied using MATLAB Simulink models and On-Off Sky-hook control method to enhance the passenger ride comfort. A single degree of freedom quarter car test rig is built to demonstrate and study the working of the twin-tube MR damper. Constant current control, Skyhook control and Rakheja-Sankar (RS) control method are employed as three different control strategies and compared with passive suspension to study the advantages. The thesis contains nine chapters and the summary of each chapter is as follows:

Chapter 1 gives a brief introduction about automotive suspension, MR fluid, MR dampers, quarter car model used in damper evaluation, types of suspension, semi-active control strategies and organization of the thesis.

Chapter 2 provides a detailed discussion of the literature review carried out for this thesis work. It elaborates on the work carried out by other researchers in the area and highlights their major contribution. The chapter also presents the motivation, objectives and scope of the research work. The methodology followed for the research work is also presented in this chapter.

Chapter 3 discusses the experimental evaluation of an automotive passive damper and a commercial MR damper in a damper testing machine. It presents the method of finding equivalent damping coefficient. Plots of damper force vs velocity are shown and a mathematical model is developed for damper behaviour. For the commercial MR damper, equivalent damping coefficient at different currents are presented and a Bouc-Wen hysteresis model is developed. Performance of the commercial MR damper in a spring-mass vibrating system is also discussed.

Chapter 4 presents the detailed design and development of a twin-tube valve mode MR damper. Optimization of the design using Taguchi analysis and FEMM software is presented. Experimental results of MR damper testing and subsequent mathematical

modeling of the MR damper behaviour is discussed. Also, a method to track the desired damping force in time domain using s PID controller is presented.

Chapter 5 discusses the synthesis of MR fluid for application in MR dampers. The results of MR fluid characterization are presented and HB model parameters for MR fluid behaviour are identified. Analytical models for MR damper force is developed based on MR fluid rheology and MR damper geometry. These models are compared with the experimental results of MR damper testing.

Chapter 6 presents dynamic analysis of quarter car vehicle model with semi-active suspension. A commercial MR damper and twin-tube MR damper are used. Polynomial models for force vs velocity graphs of the MR dampers are presented, which are developed based on the results of experimental testing. These models are used in the quarter car semi-active suspension simulation using skyhook control, in MATLAB software. Results of the simulation for harmonic and random road excitation are discussed and compared with passive suspension.

Chapter 7 discusses the results of experimental testing of passive and MR damper in a single degree of freedom suspension test rig. Rounded ramp and sinusoidal wave are used as displacement input to the suspension test rig. Skyhook and RS control methods for semi-active suspension are compared with passive suspension using experimental results for sprung mass acceleration and ground force.

Chapter 8 draws conclusions from the present study and mentions the scope of future work.

CHAPTER 2

LITERATURE REVIEW AND RESEARCH METHODOLOGY

2.1 INTRODUCTION

The research on MR damping technology has been booming in the recent years, especially in application for automobiles ride comfort and steering stability. Thus, it's imperative to look at the current development in the field of MR damper, not only from the design point of view but also in terms of models and types of fluid used, the control strategies and many more as discussed in the following subsections.

2.2 MAGNETO-RHEOLOGICAL (MR) FLUIDS

MR fluid was discovered by Rabinow (1948) who showed its application in a magnetic fluid clutch. He described MR fluid as a suspension of magnetizable particles in a liquid of low viscosity. When a magnetic field is applied to this fluid, the particles align with the magnetic flux lines forming chain like structures, resulting in increased resistance to flow and higher shear stress in yielding. Wong et al. (2001) used Scanning Electron Microscopy (SEM) to examine the shape, size and distribution of iron particles, measured surface roughness and hence evaluated the tribological properties of MR fluid. Simon et al. (2001) used the homogenization theory to study the effective magnetic behaviour of MR composite and employ a mathematical model for the same. Phule and Pradeep (2001) briefed the properties of MR fluids and their importance in recent industrial applications. Yang et al. (2002) carried out study to evaluate essential features and advantages of MR materials. Bossis et al. (2002) carried out analysis on basic phenomenon of interparticle magnetic and hydrodynamic forces and an analytical prediction for yield stress, rheology with hysteresis and shear induced phase was also provided. Pavel et al. (2003) studied the flow of MR fluids in packed beds of magnetic and non-magnetic spheres and cylindrical porous media, theoretically and experimentally. Gong et al. (2005) studied the dynamic properties, viscoelastic properties and microstructure of MR elastomers by changing the percentage amount of each component by weight in the fluid. In the first case, the weight of iron particles was kept constant and the weight of the silicon oil was changed and in the

second case, vice versa. Jun et al. (2005) evaluated magnetic field response of MR fluid made out of 30% weight of monodisperse magnetic composite (MMC) particle. Park et al. (2009) synthesized a magnetic nano-sized additive made by decomposing pentacarbonyl iron and studied the effect of adding this material in MR fluid under the influence of magnetic material. Sunil and Jain (2009) used curve fitting method to determine coefficients of equations evaluated for fluid models of MR polishing fluids prepared by using different constituents of fluid models.

Kciuk and Turczyn (2009) studied the flow behaviour of MR fluid carrying iron Carbonyl particles under the influence of magnetic field and also tried to reduce the sedimentation of Carbonyl particles by adding fumed silica particles. Park et al. (2010) made use of single walled nanotubes in conventional MR fluid to solve the sedimentation problem and studied its effect on dynamic yield strength and magnetic field strength using the quoted universal equation. Hato et al. (2011) tried suspending submicron sized organoclay particles in the CI suspension to study its effect on rheological properties of the resulting fluid. It was found that presence of organoclay particles improved the dispersion stability of the MR fluid in solid like state. Jiang et al. (2011) developed a type of dimorphic MR fluid by adding Fe nanowires into conventional MR fluids. It was observed that in ON state, there was tremendous increase in shear yield stress and concluded that this might be the result of increased solid friction between the magnetic particles due to formation of complex networks. Kamble and Kolekar (2014) used silicon as carrier fluid with different amounts of iron carbonyl particles to synthesize a new MR fluid and studied its rheological properties. A plate and cone type rheometer was used to determine shear stress, shear strain rate, viscosity and shear modulus. Kumbhar and Patil (2014) tried to determine selection criteria for components of MR fluid and concluded that minerals oils are not fit to be used because of their sudden response to temperature change and also that the carbonyl iron particles are best suited for this use because of their nature to eliminate the shape anisotropy. Upadhyay et al. (2013) used flakes of pure iron as the dispersed phase of the MR fluid with an intention to reduce the sedimentation rate. An increase in storage modulus and elastic modulus was observed and it was predicted that this was due to field dependent solid friction between the particles. Aruna et al. (2019) performed a study to improve the sedimentation properties of carbonyl iron particles-based MR fluid. In particular, they studied the effect of adding different combinations of clay with additives to the MR fluid, during synthesis. It was demonstrated that the synthesized MR fluid was more cost effective

and had better sedimentation properties when compared to commercially available MR fluid.
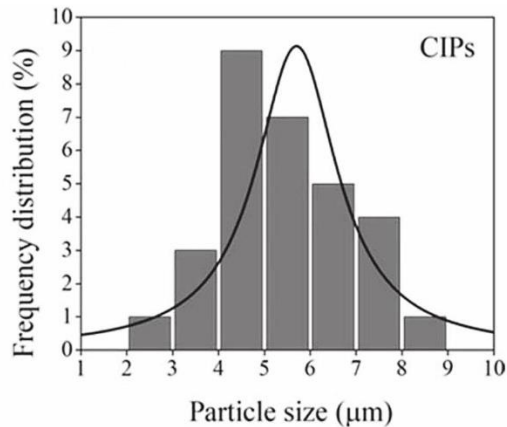
Figure 2.1 Particle size distribution of carbonyl iron particles Aruna et al. (2019)

Spaggiari et al. (2019) reviewed three different types of smart materials, which included MR fluids also. Commercial application of MR fluid in semi-active devices such as dampers, brakes or clutches are examined. The physics behind the working of these smart materials was explained with the help of equations, which would help a designer in an industrial context.

2.3 MR VALVE DESIGN AND MR DAMPER OPTIMIZATION

Jaehwan and Kyoung-Mi (2004) studied the effect of magnetic field on MR fluid in high frequency range to explore the applications of smart structures. They also investigated the effect of magnetic field applied orthogonally and parallel to the direction of wave propagation. Cortes R et al. (2005) characterized MR damper based on fluid properties such as applied current and damper design parameters. Force, velocity and displacement were determined using load cell and Shimadzu system. A numerical simulation of the suspension system was also conducted using ADAMS software. Zhang et al. (2006) studied the importance of energy dissipated and controllable force as performance parameters in MR damper. It was concluded that both are closely related to magnetic flux density that can be reached in MR fluid flow gap. Hemanth et al. (2014) carried out magneto-static analysis of MR damper using ANSYS workbench and found that in a single coil arrangement, magnetic saturation was observed for a supply of 0.7 A of current, which was also observed in the force vs velocity plot. A quarter car model was developed in MATLAB Simulink and was tested with both passive and semi-active dampers. It was concluded that the semi-active suspension system performed better than the passive one. A statistical model was

developed by Shivaram and Gangadharan (2007) using design of experiments taking into consideration various factors that affect the performance of the MR damper such as magnetic field strength, volume fraction of the magnetic particle, shearing gap between piston and cylinder, amplitude and frequency of vibration.

Nam and Park (2009) proposed a design methodology for a better performing electromagnetic circuit of the MR damper. The aim was to improve the static and dynamic characteristics of the MR damper by reducing the magnetic flux path and increasing the reluctance of the magnetic circuit. Guan et al. (2011) derived not only ordinary differential equations to represent the physical MR damper using the friction element, viscous element and spring element but also expression to determine the width of the hysteresis. Shiao et al. (2013) proposed a new piston design consisting of multi-pole magnetic core and special polarization causing almost all the magnetic flux to penetrate orthogonally in MR fluid gap, thus increasing the MRF chaining area significantly and it was found that this MR damper with this piston design performed very well compared to the conventional design. Goldsaz (2013) also proposed a new design similar to the one discussed previously. This particular design has radially projecting arms made out of a stacked silicon steel lamination. The advantage of this design was to disturb the formation of eddy currents during the transient response of the device. Another design was given by Imaduddin et al. (2013) with multiple radial and annular gap in order to increase the pressure drop of the MR valve without increasing the size and it was found that the size of outer annular gap zone contributes to viscous pressure drop and radial gap size contributes to pressure drop due to magnetic field.

Rahman et al. (2017) reviewed recent advances in MR damper technology and presented various applications of MR dampers and optimization methods for designing MR dampers. Different configurations for fabricating MR dampers are explored and an overview of different MR damper models are presented. Gołdasz and Sapiński (2017) explored the application of pinch mode of MR fluid operation in designing an MR valve. Several configurations of the pinch mode MR valve were studied with the help of magnetostatic finite element analysis. Contour maps for the flux density were generated to calculate damper performance figures. The results showed that electromagnetic force can be used to control the operation of a pinch mode MR valve. Kim et al. (2017) used permanent magnet instead of electromagnet to activate the MR damper. The magnetic flux is controlled by the shape of the housing cylinder and the piston. Ferromagnetic housing cylinder of four different types are used to carry out analytical study with FEA. A prototype MR damper was fabricated using the triangular configuration and it was demonstrated that

the force developed by the MR damper can be controlled by the position of the permanent magnet attached to the piston or by the shape of cylinder housing.
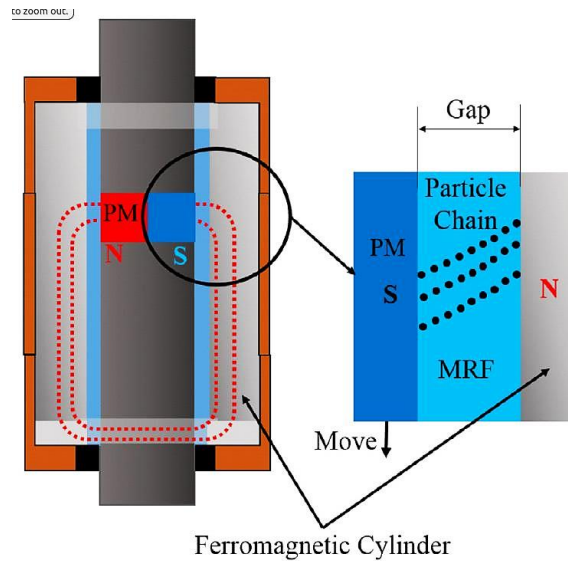
Figure 2.2 Permanent magnet in MR damper Kim et al. (2017)

Krishna et al. (2017) optimized the electromagnetic circuit of an MR damper to maximize the magnetic flux density. This was done as the force developed by the MR damper is highly influenced by the strength of the magnetic field developed at the fluid flow gap. Genetic algorithm and design of experiments approach was used for the optimization and the results showed that a fluid flow gap of 1.12 mm was optimum. Cheng et al. (2018) presented a novel MR damper, which had a meandering magnetic path in the piston so as to improve the performance of the damper. By using materials of different magnetic properties, the magnetic flux was guided to obtain a much higher controllable force when compared to traditional MR damper. Manjeet and Sujatha (2018) performed optimization of MR valve using Herschel-Bulkley (HB) model of MR fluid. Multi-objective minimization was done with an aim to improve the dynamic range and reduce the inductive time constant of the MR damper. Care was taken to see that the magnetic flux density does not reach the saturation limit of the materials used in the MR valve. Genetic algorithm was used for the optimization and Pareto fronts were found in MATLAB environment. However, experimental validation of the optimization results were not done.

Gurubasavaraju et al. (2018) used magnetostatic analysis to study the effect of choosing different materials for fabrication of MR damper on the strength of the magnetic field developed. It was found that low carbon steel and magnetic steel are ideal for piston head as they have high magnetic permeability resulting in maximum magnetic flux density. This in turn leads to higher damping force upon application of current. Gurubasavaraju et

al. (2018) developed a new computational approach to characterize a twin-tube shear mode MR damper using coupled FE and CFD analysis. This was meant as an alternative to testing experimentally in the preliminary design stage. The results were verified by experimentally testing the MR damper in a damper testing machine. The effect of fluid flow gap on damping force was determined to reveal that they are inversely related. Keshav et al. (2019) developed regression models to predict the density of magnetic flux in MR valve with current and geometric parameters of MR valve as inputs.

Figure 2.3 Geometry of MR valve Keshav et al. (2019)

For this, they used ANSYS-APDL software and design of experiment (DoE) techniques. These models were further used for geometrical design optimization in MATLAB software.

While most of the research work available in the literature made use of commercially available MR fluid which are proprietary in nature, the present work uses an in-house prepared MR fluid whose composition is definitely known. It is an added advantage that it is also more economical. Moreover, instead of relying on material specifications and technical data provided by the commercial MR fluid manufacturer, the MR fluid used in the present work was characterized experimentally in a rheometer.

The MR dampers explored in most of the available literature were either of monotube type construction or working in shear mode of MR valve. The twin tube type dampers are robust by design, simpler in construction and cheaper to manufacture when compared to their monotube counterparts. Also, shear mode type of MR valve requires high precision manufacturing processes and expensive piston rod guides to take care of the circularity and concentricity requirement of piston and cylinder for proper working of the MR damper. In the case of valve mode MR valve, a piston ring with anti-friction coating

is used which maintains physical contact between the piston and cylinder and guides its movement. Therefore, the requirements are less stringent. Hence the present work focused on the advantageous and less explored twin tube type damper construction working in valve mode.

2.4 APPLICATION OF MR DAMPER IN SEMI-ACTIVE SUSPENSION

Hrovat and Margolis (1981) used on-off semi-active pneumatic damper in air cushion vehicle to study the heave mode model experimentally. It was shown that by using a small amount of control energy, semi-active suspension provided better vibration isolation to sinusoidal input when compared to passive suspension. A hydraulic semi-active damper was recommended for better controller speed of response. Ahmadian (2017) studied the application of MR damper to increase automotive ride comfort and stability. With the help of previous studies, it was established that MR damper suspensions provide a definite advantage in performance when compared to passive suspensions. MR damper suspensions were shown to provide better compromise between the vehicle ride comfort and handling.

Yerrawar and Arakerimath (2017) presented a methodology to implement semi-active suspension using MR damper. A current controller was developed to vary the current between 0.1 A and 1 A. Ride comfort was optimized with the help of design of experiments (DOE) and Taguchi method. Relationships between the suspension parameters and their effect on ride comfort is studied with the help of a quarter car test rig. Ata and Salem (2017) performed a theoretical study to find a suitable semi-active control strategy for tracked vehicle MR damper suspension. A suspension model of the tracked vehicle with MR damper, having seven degrees of freedom, was developed to compare performance of three different controllers. Different vehicle speeds over bump and sinusoidal road profiles are simulated and the results are compared with a typical passive suspension in time and frequency domains. The results showed a marked improvement in performance of MR damper based semi-active suspension.

Jastrzębski and Sapiński (2017) evaluated an automotive MR damper under varying mechanical and electrical excitations and studied its force response and energy dissipated. The results of the experiment would help the engineers in designing an energy harvesting device for the MR damper. The effect of amplitude of piston displacement and piston

velocity are analysed. Morales et al. (2018) studied semi-active suspension which employed pneumatic spring of variable stiffness and MR dampers with variable damping to increase vehicle ride comfort and handling when compared to passive suspension. Vehicle velocity and road information gathered using GPS system were used to control the semi-active suspension resulting in 30% improvement in ride comfort and maintaining same roll angle as a comparable passive suspension. Krishnan Unni and Tamilarasan (2018) used COMSOL multi-physics software for designing an MR damper for application in an All Terrain Vehicle (ATV). The design was optimized using Taguchi method and DOE software. The aim was to improve the damping force with geometrical constraints so that the damper would fit in the ATV.

2.5 MATHEMATICAL MODELLING OF MR DAMPER BEHAVIOUR

Spencer et al. (1997) reviewed various models available at that time and proposed a new model that could predict the behaviour of a controllable fluid damper in a more effective manner. Yao et al. (2002) designed an MR damper to work in flow mode, characterized it using Bouc-Wen model to predict the damper behaviour for a quarter car model and compared the results with a passive damping system. Butz and Stryk (2002) studied various MR and ER damper in order to carry out numerical simulation of a quarter car semi active suspension system. Sapinski and Filus (2003) analysed the parametric models of MR linear dampers concerning various behavioural characteristics. The analysis shows that the basic difficulties in formulating such models was because of the presence of hysteresis and jump-type phenomenon. It could be seen that if the model is too simple then the predicted curves become less accurate, thus making the model ineligible to be used for control problems. On the other hand, when the model takes into account the appearance of hysteresis then it becomes difficult to find the numerical solution making it incompetent to be used in real-time. Song et al. (2005) used a series of continuous and differentiable mathematical functions to carry out nonparametric approach for modelling of MR damper. Kwok et al. (2007) presented a non-symmetrical Bouc-Wen model for MR fluid with an attempt to enhance the modelling accuracy by reducing the errors occurring due to taking into account the non-symmetric hysteresis characteristics. However, Bouc-Wen modelling of MR damper does not consider either the properties of materials used in the MR damper

or the geometric dimensions of the MR damper as parameters of the model. Hence this type of modelling is of little use when designing a MR damper for a new application.

Faruque and Ramaswamy (2009) proposed a technique of controlling MR damper which uses a back stepping based nonlinear monitoring method that would predict the input current directly based on system's feedback, thus ensuring smooth update of input current. Arjon et al. (2010) aimed to improve ride comfort using sensitivity control that was designed for 2 DOF quarter car model with sixth order polynomial. Kim et al. (2011) tried to estimate the performance of a continuous damping control using MR damper in a dynamic model of a large bus. The results were then compared to those of passive damper. Wang and Liao (2011) reviewed parametric dynamic modelling of MR dampers and found that although many parametric models have been proposed and validated, these models have only been able to predict only the force-displacement characteristics accurately and also that the parametric dynamic models with online updating capability need to be developed.

Prabhakar et al. (2013) studied about controlling stationary response of quarter car model subjected to random road excitation. And also, multi-objective optimization was carried out using NSGA-II to determine optimal parameter of MR damper modelled using Bingham model and modified Bouc-Wen model. Dutta et al. (2013) used skyhook control strategy to examine the dynamic performance of SDOF and 2DOF quarter car model. Arachchige et al. (2013) analysed the non-linear behaviour of an MR rotary damper and provided with a mathematical model to study the effect of Bouc-Wen model parameters on vibration response of semi-active suspension. Experimental results were compared with proposed theoretical model and it was concluded that use of MR damper reduces or eliminates undesirable vibrations in the semi-active suspension. Thakkar et al. (2013) carried out electromagnetic analysis of MR damper to determine the saturation limit of external current using FEM. Peng et al. (2014) tried to describe the distorted hysteresis behaviour of MR damper using Bouc-Wen-Baber-Noori method. Hemanth et al. (2016) proposed a novel non parametric model for MR damper and analysed it based on the magnetic flux density in the fluid gap and volume fraction of MR fluid. The results obtained from the proposed model and the results of the experiment conducted to characterize the MR damper at 1.5 Hz frequency at various input circuit current for sinusoidal excitation were in good agreement.

In order to account for the experimentally observed asymmetric hysteresis plots of MR damper behaviour, García-Baños et al. (2017) proposed a modified viscous-coulomb

friction model for a large-scale MR damper and verified it with experimental results. Tharehalli et al. (2018) modelled the behaviour of a shear mode monotube MR damper using combined CFD-FEA polynomial model. Using computational methods, influence of frequency of excitation and gap length on induced force is studied. However, the damper force is expressed as a polynomial function of current alone and fails to consider any geometric or material properties of the MR damper.
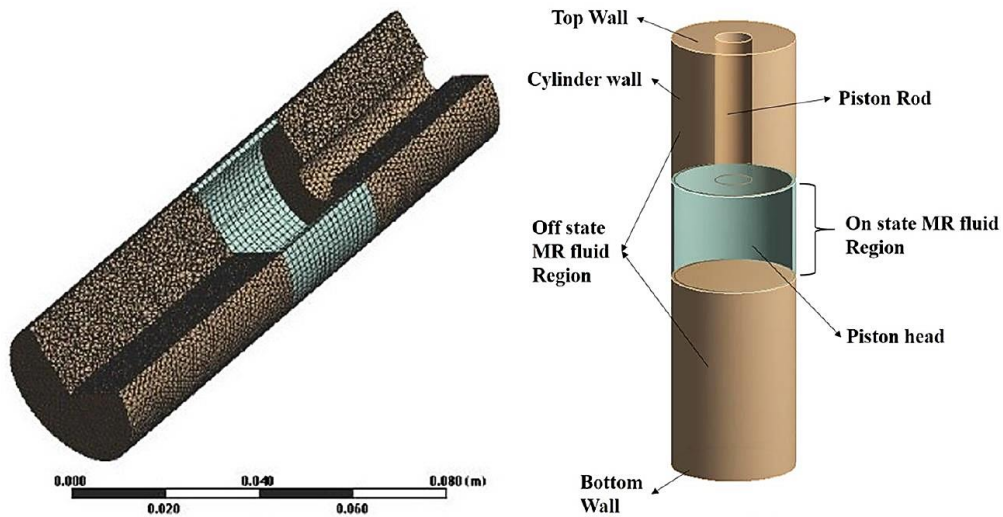
Figure 2.4 CFD meshed model with boundary conditions Tharehalli et al. (2018)

Goldasz et al. (2018) developed nonlinear hysteresis models for MR damper to improve the performance in control systems. A technique was developed to estimate the magnetic flux density without using any sensors. The response of the damper was studied for a wide range of sinusoidal excitation inputs. It was showed that both the amplitude and frequency of input excitation affects the hysteresis of MR damper. Kubik and Goldasz (2019) proposed a hysteresis model for the MR damper which was both of good quality and could be used in the design phase of MR damper.
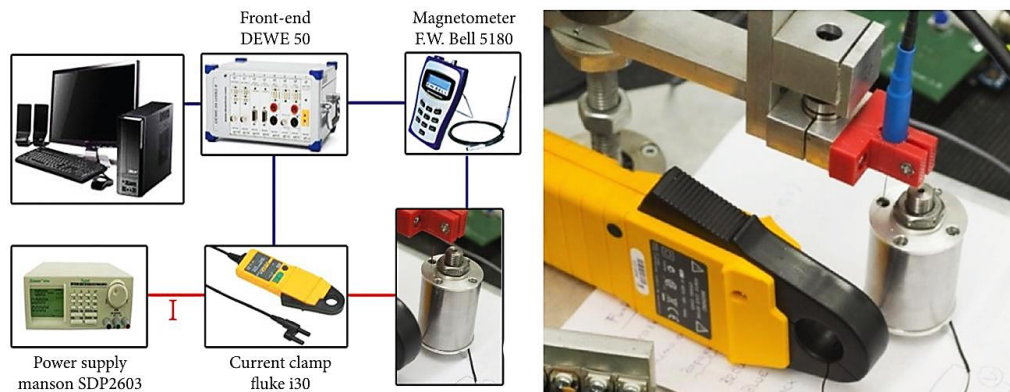
Figure 2.5 Configuration of test rig Kubik and Goldasz (2019)

A hybrid multiphysics model was developed which was based on the information available in material datasheets and engineering drawings. Parameter sensitivity study was performed to find the effect of magnetic hysteresis and other important factors on the force developed by MR damper.

Palomares et al. (2019) presented a broad review of various mathematical models of MR dampers which include the nonlinear hysteresis behaviour of MR dampers in pre-yield and post yield domains of MR fluid operation. Different models were tested by means of experimental tests and simulations done in a semi-active control case study.

2.6 MATHEMATICAL MODELING OF VEHICLE

Türkay and Akçay (2005) used a quarter car model of a vehicle having two degrees of freedom with variable vehicle velocity to study the response to white and coloured noise road input. A linear shape filter was used to demonstrate the trade-offs as a function of vehicle speed. Verros et al. (2005) presented a method for optimizing damping and stiffness value of quarter car suspension with random excitation as road input. They also studied the effect of road quality as well as other effects related to wheel hop. However, this was only a numerical study and experimental work with a physical damper was not involved.

Georgiou et al. (2007) performed multi-objective optimization of semi-active and passive suspension systems with the help of two degrees of freedom quarter car models. Optimum values of spring stiffness and damping coefficient were selected for suspension subjected to road excitation. Suitable methodologies were used to capture the dynamics of the vehicle when it moves with constant speed over roads with geometric irregularity. The aim was to improve the vehicle ride comfort, road holding and suspension travel. Rao and Narayanan (2008) implemented a look ahead preview control for the response of a four degree of freedom half car model with semi-active suspension. The vehicle moves with constant velocity on random road surface. The vehicle response is optimized for better road holding, control force and suspension stroke. Chi et al. (2008) performed comparative study of three optimization algorithms for optimizing vehicle suspension design using a quarter vehicle model. With the help of numerical simulation, it was shown that the suspension design can be improved significantly by optimizing the design variables. Investigations were also done on how vehicle velocity and road irregularity affect the design variables to get better ride quality. Salem and Aly (2009) compared fuzzy control and PID control for active suspension using a two degree of freedom quarter car suspension model in MATLAB

simulations. The application of fuzzy logic technique for a continuously variable damping suspension system was illustrated and the vehicle response for a range of input road conditions were studied.

Prabakar et al. (2009) studied the stationary response of a half car vehicle model moving over rough road with uniform velocity. The control of the suspension using MR dampers is considered. Monte-Carlo simulation was used to verify the control and response of vehicle model obtained using equivalent linearization method.
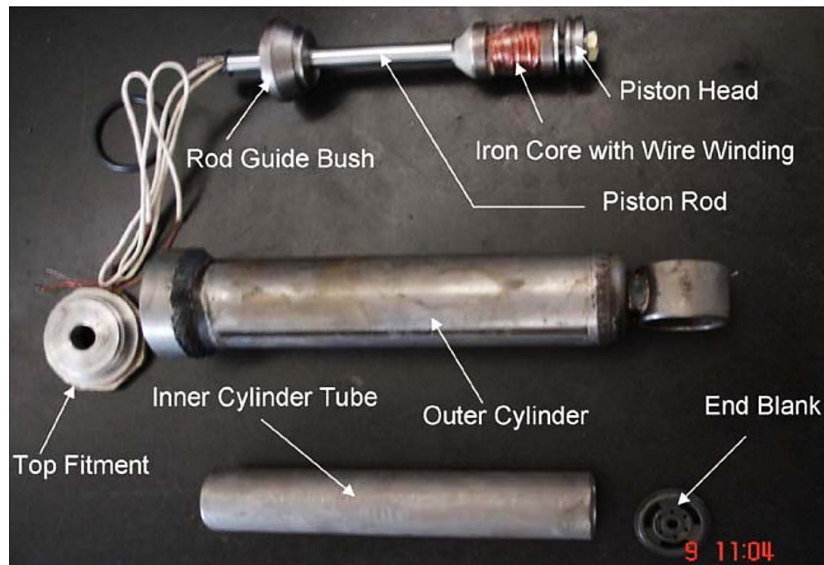
Figure 2.6 Components of fabricated MR damper Prabakar et al. (2009)

Havelka and Musil (2012) studied optimal preview control strategy with MR damper-based quarter car model using sensor data of approaching road disturbances. MR damper was represented by a non-linear hysteretic model and the effect of tyre lift-off was studied. Sultoni et al. (2014) investigated the performance of a regenerative electromagnetic shock absorber with the help of a quarter car dynamic model. The effect of vehicle acceleration and excitation due to road irregularity were studied using numerical simulations on quarter car model. The power generated by the damper and the RMS value of suspension velocity when the vehicle moves over different classes of road were analysed.

Yıldız et al. (2015) proposed a nonlinear adaptive controller for mitigation of vibration in a quarter car suspension model with a semi-active MR damper. A mathematical model of the MR damper was used to predict the damping force for different voltage and velocity input. Efficiency of the controller is compared with linear controller and passive cases under harmonic, bump and random road inputs.

Park et al. (2016) used a quarter car model to compare the performance of two different designs of MR damper. A skyhook controller was used for semi-active suspension

and simulations were carried out for two different road profiles, bump and random road excitations. One of the MR dampers had a bypass hole provided in the piston to reduce the slope of pre-yield damping force. The damping force characteristics are studied using both numerical simulations and experiments. The results showed that the MR damper with bypass holes provide better ride comfort. Hu et al. (2017) used a hyperbolic tangent model to represent the nonlinear damping of MR damper. Using this model, a quarter car model with MR damper was established and a new hybrid fuzzy PID controller was developed to improve the performance of the semi-active suspension. Results of the numerical simulation showed that sprung mass acceleration, tyre displacement and damper deflection can be reduced effectively under sinusoidal excitation from road.

Jamali et al. (2017) developed a MATLAB Simulink model to study the dynamic behaviour of a passive suspension system used in an electric vehicle. A two degree of freedom quarter car model was used for the study. Transmissibility ratio was plotted against frequency of excitation for different values of damping. A match between results of simulation and theoretical calculation showed that the Simulink model was accurate. Omar et al. (2017) designed and implemented experimental test rigs for quarter car suspensions. Performance of an electro-hydraulic active suspension was compared with passive suspension using both experiments and numerically. A single degree of freedom quarter car model was used.
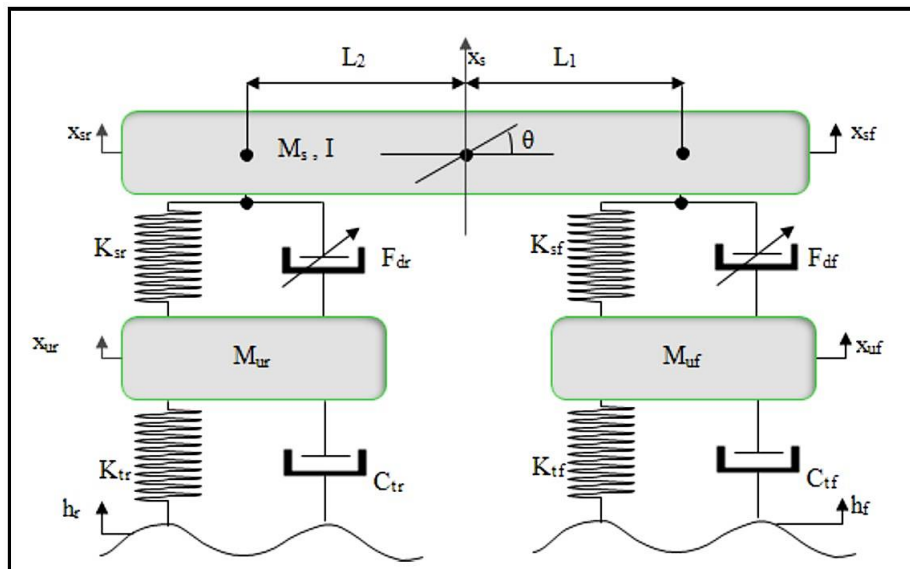
Figure 2.7 Half-car suspension with MR damper Hemanth et al. (2018)

Hemanth et al. (2018) performed dynamic analysis of MR damper-based suspension using half car model. A Bouc-Wen mathematical model was used to predict the force

developed by the prototype MR damper. Using the half-car model, the ride comfort and road holding of passive and semi-active suspension with MR damper are compared to show that the performance of the MR damper suspension is better.

2.7 CONTROL STRATEGIES OF SEMI-ACTIVE SUSPENSION

Rakheja and Sankar (1985) studied the implementation of on-off semi-active damper with the help of a SDOF spring mass damper system. Computer simulations were used to evaluate the vibration isolation. A new control scheme, known as RS control method was introduced, which used the readily measurable relative position between the sprung mass and actuator to generate the command signal for the damper. They demonstrated that the performance of the on-off damper with RS control, where the current can only be switched between zero and maximum value, was superior to that of the passive damper. It was also found that the quickness with which the damper responds, significantly affects the response behaviour of the system. However, experimental verification of RS method was not provided. Liu et al. (2005) used model of a SDOF system with harmonic base excitation with five different control algorithms to demonstrate that semi-active systems provide better vibration isolation at high frequencies when compared to passive systems, at a fraction of the cost and energy requirement of an active suspension system. Anti-jerk control algorithms were also proposed, which solved the chatter problem which arose, when semi-active dampers are simulated numerically.

Shen et al. (2006) investigated three methods of control for the semi-active suspension namely, limited relative displacement method, the modified skyhook method, and the modified Rakheja–Sankar method. The performance of the controllers was evaluated analytically using the method of averaging and experimental verification was done under sinusoidal and random excitation. The result of the investigation showed that modified skyhook method and modified Rakheja-Sankar method, both reduced the RMS response of sprung mass acceleration and relative displacement of the suspension. The limited displacement method showed reduction in relative displacement only. Song (2009) proposed a new skyhook controller that uses a single sensor instead of two sensors used in the traditional skyhook controller. The simulation results showed that this particular version of the controller can achieve comparable ride comfort as compared to the traditional one. The main aim of this study was to reduce the cost of the controller without compromising the reliability by reducing the number of sensors. Although the author suggested further

studies before implementing commercially. Chen (2009) applied skyhook surface sliding mode control method for a two degree of freedom dynamic model of a vehicle with semi active suspensions system to study its ride comfort performance in MATLAB/Simulink with some initial conditions. It was found that this controller provided better control on ride comfort performance than the Fuzzy logic control and passive suspensions system, but in the high frequency range the FLC performed better to some extent.

Zapateiro et al. (2012) proposed two different semi active suspension control systems. The first one was based on an adaptive back stepping technique with some H constraints and the other one was designed based on the Quantitative Feedback Theory (QFT). Both the controllers were simulated in MATLAB/Simulink and was found that despite behaving differently in same conditions both the controllers were able to reduce the response if the suspension system. Seong et al. (2011) proposed various control algorithms namely, sky-hook controller, LGQ controller, H∞ controller, sliding mode controller, moving sliding mode controller and fuzzy moving slide controller for MR suspension system of quarter vehicle. The effectiveness of these controllers was verified experimentally. It was found that these controllers not only reduce the unwanted vibration under bump excitation but also reduce the sprung mass acceleration under random excitation in body resonance region thus proving the effectiveness of MR suspension system in providing better comfort ability. Tu et al. (2012) carried out FE analysis on magnetic circuit of MR damper with accumulator and relation between damping force, circuit and speed was fitted by experimental results. Kasemi et al. (2012) tried to develop a Fuzzy-PID controller of MR suspension system. It was observed that a simple PID controller performed very well for step and impulse type of input but failed when the input conditions were changed hence a Fuzzy-PID controller with variable gains, as opposed to fixed gains in the former type, were used. The experimental results showed that the MR damper can be modelled after the force response over current and displacement thereby reducing the number of constant parameters to be evaluated.

Choi et al. (2016) presented different control strategies for systems using MR fluids and MR elastomers. Based on the application intended, the advantages and drawbacks of various control schemes are discussed. Qin et al. (2017) studied and compared the effect of time delay on the performance of five different semi-active control methods. A continuous damping control (CDC) damper was used for this purpose and it was tested experimentally on a load frame to obtain force-velocity plots. Models were developed to predict the dynamic behaviour of the damper. Numerical simulations were done with three different

time delays. The results showed that a larger time delay had an adverse effect on the ride comfort as well as road holding of the semi-active suspension.

Nie at al. (2017) proposed a new semi-active control algorithm to achieve a reasonable trade-off between ride comfort and road holding, and also to achieve a comprehensive vehicle suspension performance. In particular, the resonance arising at second-order is studied to address the conflict in performance. The results of the new control algorithm showed significant improvement in ride comfort without any loss of road holding when compared to passive suspension. Pang et al. (2018) combined fuzzy neural network (FNN) and particle swarm optimization (PSO) to propose a novel control design for semi-active control of vehicle suspension using MR damper. Experiments were conducted on quarter-vehicle test rig using MR damper and the data collected was used to develop a non-parametric model of MR damper. A Takagi-Sugeno (TS) fuzzy controller was designed to control the current supplied to MR damper. The proposed control scheme was validated with the help of simulation study.

2.8 MOTIVATION

Based on the open literature review, it was found that a lot of experimental and theoretical work has happened in the field of MR dampers but there is still no widespread use of MR dampers for commercial application. In the automotive field especially, the use of MR dampers is limited to high end luxury cars. After surveying a considerable amount of literature, the following gaps in the research have been identified:

a) There are surprisingly few studies done on development of MR damper as a replacement for a passive damper in a vehicle. Most of the MR damper prototypes do not develop sufficient damping force so that they can be used in an actual vehicle. The prototypes are not tested at operating frequencies and amplitudes.

b) Very few studies have been done on the long-term reliability of MR damper and the endurance capacity of MR damper. There is no significant literature on the factors affecting the reliability of the MR damper.

c) There are limited publications on numerical analysis using random road profile input and nonlinear behaviour of MR damper which also use nonlinear control strategy.

2.9 OBJECTIVES

1. To design, develop and characterize low-cost industrial MR damper for automotive suspension.
2. To perform characterization of commercial MR damper, which will be used as benchmark to compare with MR damper developed in laboratory.
3. To synthesize, characterize and mathematically model carbonyl iron particles-silicone oil-based MR fluid.
4. To develop mathematical models of MR dampers in order to predict the behaviour of MR damper of various designs and sizes at different operating parameters.
5. Experimentally validate performance of the developed MR damper using quarter car test rig.

2.10 SCOPE

1. Experimental evaluation of commercial passive dampers and commercial MR damper in damper testing machine using harmonic excitation. Measurement of damping force and damper displacement at different frequencies of excitation.
2. Design, material selection, optimization, fabrication and characterization of a twin-tube valve mode MR damper for a passenger van. Developing a mathematical model for MR damper to predict the damping force output at different velocities and frequencies of excitation and at different values of current.
3. Synthesis of silicone oil-based MR fluid in laboratory and its rheological characterization in rheometer. Developing mathematical model for MR fluid behaviour in order to predict the shear stress at different shear rates and at different magnetic field strengths. Modeling of controllable force of MR damper based on MR fluid rheology and MR damper geometry. Use of a non-dimensional approach to generate analytical equation for controllable damping force.
4. Dynamic analysis of quarter car mathematical model with MR damper based semi-active suspension subjected to harmonic and random road excitation using skyhook control and comparison with passive suspension. Performance testing of MR damper in suspension testing machine using a single degree of freedom quarter car model and a single sensor control scheme.

2.11 RESEARCH METHODOLOGY

The primary work was to design and develop a twin-tube MR damper which can be used in an automotive suspension to implement semi-active vibration control. Both commercial MR fluid and MR fluid prepared in the lab were used for this purpose. Finally, the performance of the developed MR damper is evaluated using a quarter car suspension test setup. Figure 2.8 shows the methodology flowchart of the research work followed. It shows the entire sequence of works involved in designing a twin-tube MR damper for application in a semi-active automotive suspension.

2.11.1 Characterization and mathematical modelling of automotive passive damper

An automotive passive damper was experimentally characterized in a damper testing machine in order to understand the magnitude of force that has to be developed by the damper for use in an automobile. The behaviour of the damper at different frequencies and velocities of excitation is studied. Based on the experimental results, mathematical models are developed for damper behaviour. The equivalent damping coefficient of the passive damper is also calculated based on the energy dissipated by the damper in one cycle of excitation. This step helps in the design of the twin-tube MR damper for automotive application.

2.11.2 Experimental evaluation of commercial MR damper

In order to better understand the behavioural characteristics of MR dampers, a commercial MR damper by Lord Corporation, USA, is experimentally evaluated in a damper testing machine. The change in the damping force due to change in the current supplied is studied. The variation of the dynamic range of the MR damper with frequency of excitation is observed. The damping coefficient of the MR damper at different currents suppled is calculated and a Bouc-Wen model to predict the behaviour of the damper is developed with the help of Genetic Algorithm (GA) based optimization in MATLAB.
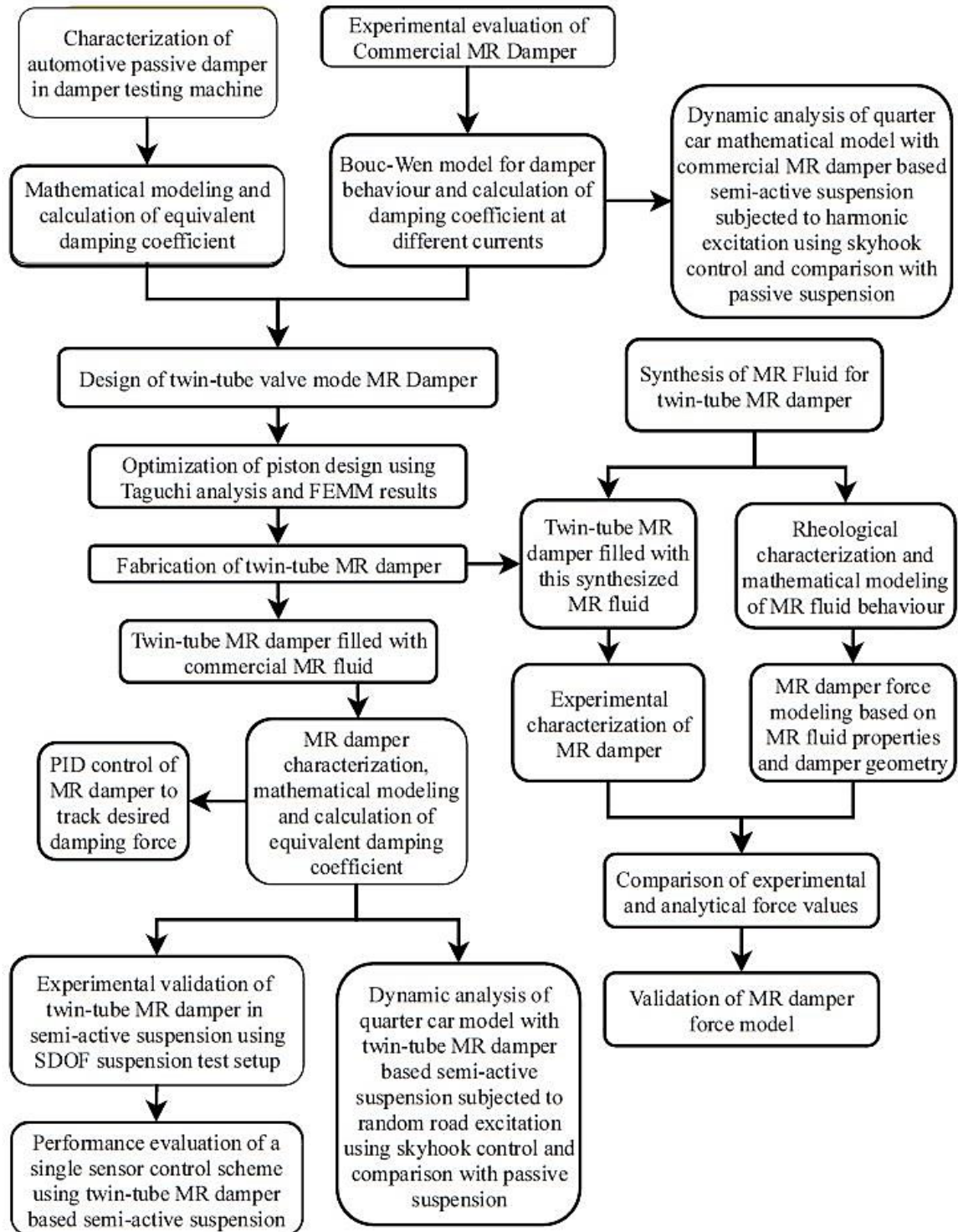
Figure 2.8 Methodology flowchart

2.11.3 Dynamic analysis of quarter car model with commercial MR damper based semi-active suspension

The mathematical model developed for behaviour of commercial MR damper is used to develop a semi-active quarter car suspension in MATLAB Simulink. Typical values

of sprung mass, unsprung mass, spring stiffness and tyre stiffness are suitably assumed. Harmonic excitation of 2.5 Hz is given as input excitation. The dynamic response of skyhook controlled semi-active suspension system is studied from the point of interest of passenger comfort. Vertical acceleration and displacement of the sprung mass for semi-active suspension is compared to that of passive suspension.

2.11.4 Design and development of twin-tube valve mode MR damper

A twin-tube MR damper working in valve mode is designed for application in an automotive semi-active suspension. The design is based on the results of experimentally testing an automotive passive damper and a commercial MR damper as explained in previous sections. The design of the piston which houses the electromagnetic coil is optimized using Taguchi analysis and Finite Element Method Magnetics (FEMM) software. The aim is to maximize the strength of the magnetic field developed in the fluid flow gap. The twin-tube MR damper is fabricated using the optimum design values and filled with commercial MR fluid for further testing.

2.11.5 MR damper characterization and PID control

The twin-tube MR damper filled with commercial MR fluid is characterized in damper testing machine using different excitation frequencies and velocities. The current supplied is varied with the help of a suitable current controller. Plots of damping force vs displacement and force vs velocity are made and mathematical model for MR damper is developed using GA based optimization in MATLAB. The equivalent damping of the MR damper at various currents are calculated based on the energy dissipated by the damper. A Proportional-Integral-Derivative (PID) control is designed and implemented for the MR damper using MATLAB Simulink to track a desired damping force as output.

2.11.6 Synthesis and characterization of MR fluid

A carbonyl iron particle-based MR fluid is synthesised in the laboratory using silicone oil as carrier fluid. This MR fluid is suitable for use in a twin-tube MR damper. The MR fluid is characterized in a rheometer with MR device cell. The shear thinning behaviour of the MR fluid is mathematically modelled using the Herschel-Bulkley (HB) model. The change in the parameters in the HB model with change in magnetic field strength is studied and modelled so that the HB model parameters can be calculated at any given strength of magnetic field.

2.11.7 MR damper force modelling based on MR fluid properties and damper geometry

A non-dimensional number approach is used to analytically express the controllable force developed by the twin-tube MR damper. These non-dimensional numbers are based on the rheological properties of the MR fluid and also the geometrical properties of the twin-tube MR damper. This type of modelling of MR damper behaviour can be used for virtual prototyping studies and provide an insight into the physics governing the behaviour of the MR damper. The damping force values calculated analytically are compared with the experimental force values to establish the validity of the MR damper force model.

2.11.8 Dynamic analysis of quarter car model with twin-tube MR damper based semi-active suspension

The mathematical model developed for twin-tube MR damper is used to develop a semi-active quarter car suspension in MATLAB Simulink. Typical values of sprung mass, unsprung mass, spring stiffness and tyre stiffness are suitably assumed. Random road excitation for two different degrees of road roughness is given as input excitation. The dynamic response of skyhook controlled semi-active suspension system is studied for a vehicle speed of 15 m/s (54 km/hr) and compared with passive suspension. RMS acceleration of the sprung mass for vehicle speed varying from 15 m/s to 20 m/s for twin-tube MR damper based semi-active suspension is compared to that of passive suspension.

2.11.9 SDOF suspension test setup

A single degree of freedom (SDOF) suspension test setup is built to study and validate the developed twin-tube MR damper for use in a semi-active suspension. The response of the sprung mass for different types of input excitation is studied. Rakheja-Sankar (RS) control method, which utilizes a single displacement sensor as input, is used to generate control signals for the MR damper. A current controller converts these control signals to input current for the MR damper. The performance of RS control is compared with the widely used skyhook control and to constant current control.

2.12 SUMMARY

From the literature review, it was found that MR devices have achieved importance because they provide a convenient, reliable and robust interface between electronic control

systems and mechanical devices. They can be used to develop semi-active systems which provide most of the benefits of an active system without the accompanying increase in cost and complexity. It is an added advantage that MR devices have low power consumption.

Many researchers have worked on developing a monotube MR damper using commercial MR fluid. In most of the cases, the MR dampers produced only nominal levels of damping force and hence, cannot be immediately used as a replacement in an automotive suspension. A clear research gap exists in the use of a twin-tube damper design, which is more robust, low cost and easy to manufacture. Though many researchers have synthesized MR fluid, very few instances exist where it was used as a replacement for commercial MR fluid in a twin-tube MR damper. In mathematical modelling of behaviour of MR damper, most of the studies done utilize phenomenological models which cannot be used for virtual prototyping studies of MR damper. They lack insight into the physics governing the behaviour of the MR device. There is a gap in research done on mathematical modelling of MR damper behaviour which utilize constitutive models of MR fluid behaviour or geometric parameters of MR damper design.

The detailed methodology of the research work was described in this chapter. The individual steps involved in design and development of a twin-tube valve mode MR damper are elaborated. Both commercial MR fluid and MR fluid synthesized in the laboratory were used. MR fluid as well as MR damper were experimentally characterized. Dynamic analysis was performed for quarter car model in MATLAB Simulink for both commercial MR damper and twin-tube MR damper based semi-active suspension. The results are compared with that of passive suspension. RS control and skyhook control were implemented as semi-active suspension control schemes using a SDOF suspension test setup for twin-tube MR damper. In the following chapters, the above said methodology has been applied to design and evaluate twin-tube MR damper for semi-active automotive suspension.

CHAPTER 3

EXPERIMENTAL INVESTIGATION AND MATHEMATICAL MODELING OF AUTOMOTIVE PASSIVE DAMPER AND COMMERCIAL MR DAMPER

3.1 INTRODUCTION

Dampers are energy dissipating devices which are used in automotive suspensions along with springs. They provide comfort to the passengers and improve the road holding of the vehicle by providing a better dynamic stability to the vehicle. The design and performance of an automotive suspension system is especially important when the vehicle travels over uneven, irregular and rough road surface. Dampers play an important role in the safety of the vehicle. The force developed by a damper is usually a strong function of the velocity of excitation and damper designers generally specify the force to be developed by the damper at various velocities in compression as well as rebound strokes. The levels of forces are also decided by the class of vehicle in which the damper is going to be used. Bigger and heavier vehicles require dampers which can generate higher levels of damping force.

MR dampers are capable of generating damping force which can be electronically controlled by means of a current controller. Such a damper can be used to implement a semi-active suspension system, which have been proved to provide better control of vibrations when compared to passive suspension system.

3.2 METHODOLOGY

A commercially available damper of a SUV (Mahindra Bolero) was used. The methodology used is represented in the form of a flow chart in Figure 3.1. The damper was harmonically excited on the damper testing machine at different frequencies and a fixed amplitude of 20 mm. The damping force produced by the damper and the displacement of the damper piston were acquired in real time. The acquired data were further analysed to find the equivalent damping coefficient of the damper and plots of damper force vs damper velocity were also generated. The damping force is a function of damper piston velocity in the case of a viscous damper. Hence, using the experimental data, mathematical model was

developed to predict the hysteretic behaviour of the passive damper. With the help of this mathematical model, the force generated by the damper at any frequency and amplitude can be calculated. This will be very useful when designing a new type of suspension for the vehicle under consideration. For example, a new semi-active suspension can be designed for the vehicle on the basis of the performance data and mathematical models of the damper presented here.
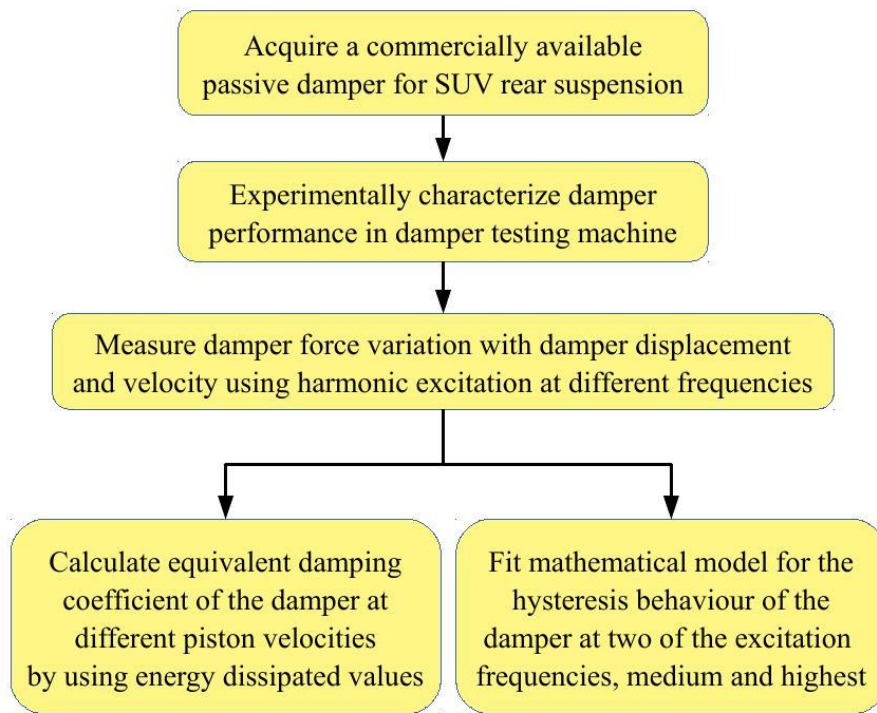
Figure 3.1 Methodology flowchart for passive damper

The damper used in this study is shown in Figure 3.2. It has a maximum stroke of 210 mm, eye diameter of 16 mm and outer tube diameter of 41.5 mm.
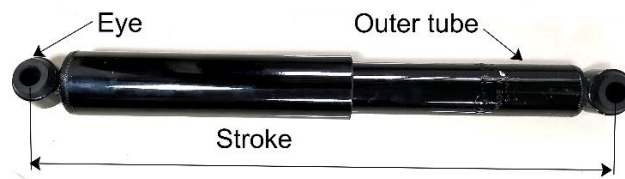
Figure 3.2 Damper used in rear suspension of SUV (Mahindra Bolero)

It is a viscous damper of twin tube type construction. It consists of two concentric metallic tubes, the inner pressure tube and an outer reserve tube as shown by Dixon (2007). The piston containing hydraulic valves along with the piston rod is placed in the inner tube filled with hydraulic oil. This piston rod is supported and guided by a rod bearing located in the top end of the inner tube. An oil and dirt seal placed in the top end of the outer tube

helps to prevent leakage and contamination of hydraulic oil. A foot valve is fitted at the bottom of the inner tube and it regulates the flow of oil between the pressure tube and the reserve tube. The reserve tube compensates for the increase in volume as the piston rod enters the inner tube during compression stroke. Circular eyes are provided at both ends of the damper for mounting it between the body and wheel assembly of the vehicle.

Lord RD-8040-1 is an MR damper which is commercially manufactured by Lord Corporation, USA. This MR damper, shown in Figure 3.3, is experimentally evaluated. It is a short stroke model and it has a stroke of 55 mm, an extended length of 208 mm and a body diameter of 42.1 mm.

Figure 3.3 Commercial MR damper Lord RD-8040-1

The flow chart of the methodology followed for commercial MR damper is shown in Figure 3.4. A commercial MR damper was experimentally characterized on a damping force testing machine.
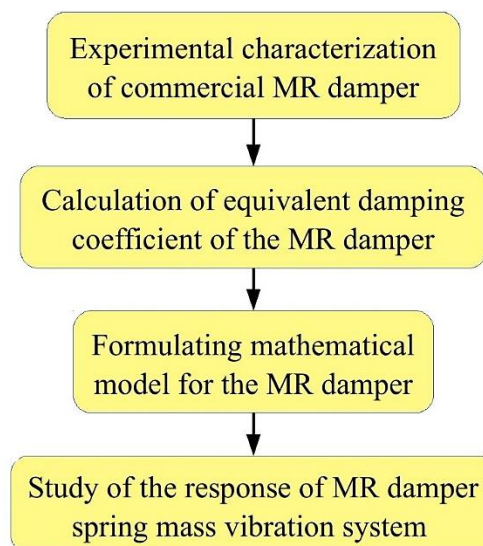
Figure 3.4 Methodology flowchart for commercial MR damper

The force developed by the damper at different frequencies of sinusoidal excitation for different values of current supplied was measured. Using the force-displacement curves thus obtained, the equivalent damping coefficient of the damper at different levels of current supplied is calculated. A mathematical model is developed for the MR damper

behaviour using the Bouc-Wen equations. A spring mass vibrating system, using this MR damper was modeled and its response to displacement pulse input at different values of current supplied is studied numerically using MATLAB Simulink toolbox.

3.3 EXPERIMENTAL EVALUATION OF PASSIVE DAMPER

3.3.1 Experimental setup

The rear damper used in Mahindra Bolero, a Sports Utility Vehicle (SUV), was tested in the damper force testing machine, as shown in Figure 3.5. The hydraulic actuator is controlled by Moog servo valve connected to a Moog portable test controller, which in turn is programmed using Moog integrated test suite software running in a PC. This DAQ and control system uses high speed 32-bit data acquisition with 6 kHz sampling rate on all primary channels. Automatic PID controller is employed to send signals to servo valve to operate in displacement mode using DSP based closed loop servo controller with closed loop update rate of 10 kHz. All this ensures high precision, accuracy and high sensitivity of the experimentation.
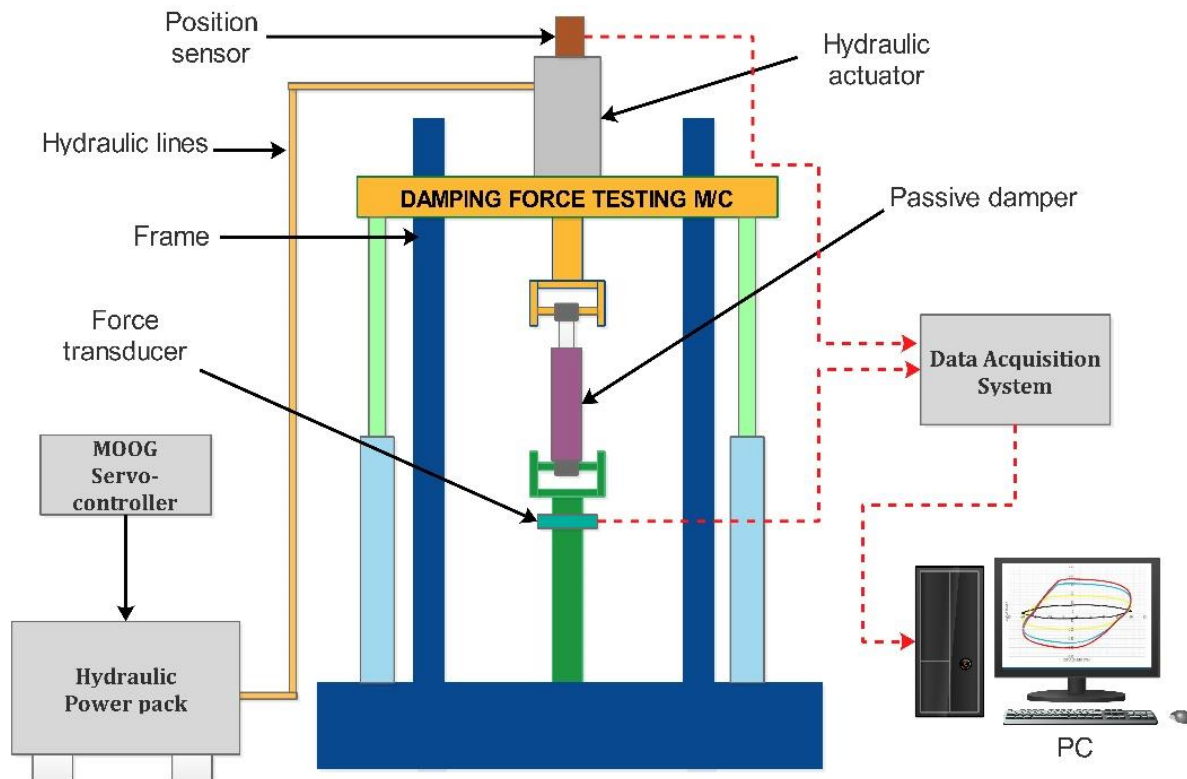
Figure 3.5 Schematic diagram of damper force testing machine

In order to capture the dynamic behaviour of the damper, it was excited at different piston velocities. This was achieved by giving harmonic displacement to the damper with the help of a servo controlled hydraulic actuator. The displacement amplitude was fixed at 20 mm and velocity amplitude of excitation was increased from 50 mm/s to 500 mm/s in steps of 50 mm/s. This is because both damper manufacturing industries and automotive designers use damper velocity for specifying damping force. As the displacement amplitude X is fixed, velocity and frequency are proportional to each other. For our ease of analysis and understanding, we have used frequency for reference and the corresponding frequencies of excitation are as shown in Table 3.1.

Table 3.1 Frequencies of harmonic excitation at 20 mm amplitude and corresponding piston velocities

Frequency level	Frequency of excitation (Hz)	Velocity level	Piston velocity (mm/s)
f1	0.4	V1	50
f2	0.8	V2	100
f3	1.19	V3	150
f4	1.59	V4	200
f5	1.99	V5	250
f6	2.39	V6	300
f7	2.79	V7	350
f8	3.18	V8	400
f9	3.58	V9	450
f10	3.98	V10	500

The instantaneous displacement of the damper is measured using the position sensor in the hydraulic actuator at a sampling rate of 1 kHz. The damping force thus developed by the damper is measured by a force transducer mounted in series with the damper at the other end. It can measure both compressive and tensile forces with a resolution of 0.001 kN and at a sampling rate of 1 kHz. Damper characterization plot with damper displacement on abscissa and damping force on the ordinate is shown in Figure 3.6.
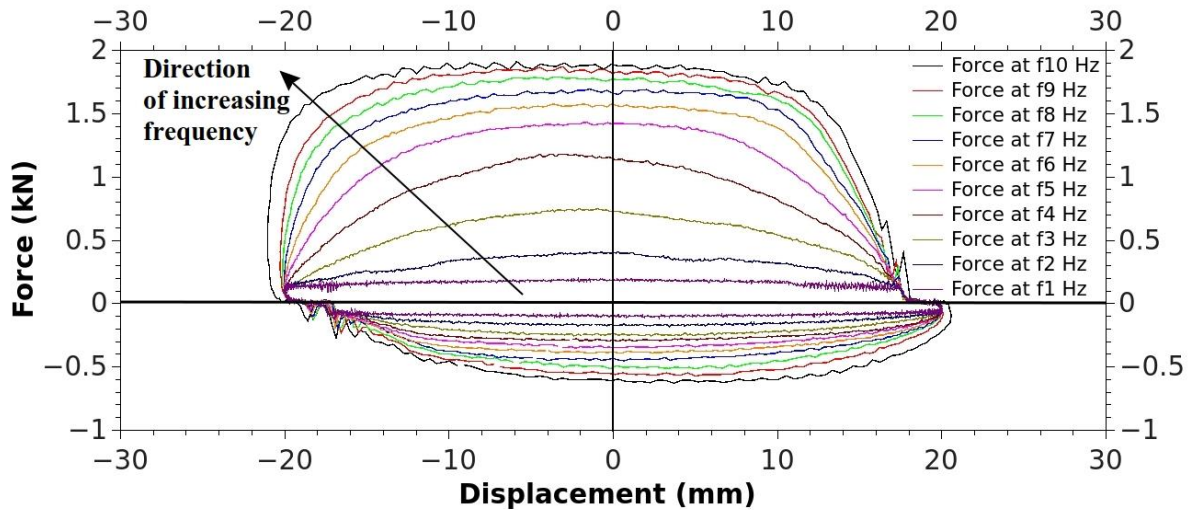
Figure 3.6 Damper force vs damper piston displacement under different frequencies of harmonic excitation at fixed amplitude of 20 mm

The convention followed is that the compressive damper force is negative and tensile damper force is taken as positive. Similarly, extension and compression are taken as positive and negative displacements respectively from the mean position. Since the amplitude of harmonic displacement is fixed, the velocity amplitude is directly proportional to the excitation frequency. Hence, as is expected, it can be seen from Figure 3.6 that damping force increases with increase in the frequency of excitation. With increase in frequency, not only does the damping force increases, but the area under the force vs displacement loop also increases.

3.3.2 Energy dissipated and equivalent damping coefficient

The area under the force vs displacement plot of a damper represents the energy dissipated by the damper in one cycle. Hence the energy dissipated by the damper in one cycle increases with the increase in frequency of excitation. This behaviour of the damper is the basic requirement for application in automotive suspension.

The automotive damper is an energy dissipation device. When the automobile encounters irregularities on the road, the suspension system absorbs the impact. The wheel moves up or down relative to the vehicle body depending on the type of road irregularity. This results in the deflection of the spring of the suspension. The energy stored in the spring has to be dissipated, otherwise it results in continuous oscillation. The damper in the suspension system does this by converting the shock energy into heat energy by way of fluid friction and viscosity. From the force vs displacement plot of the damper as shown in

42

Figure 3.6, it is possible to calculate the energy dissipated by the damper in one cycle of compression and extension. Since there are different loops for different frequencies of excitation, by finding the area of each loop, one can find the energy dissipated by the damper at different frequencies of excitation and hence at different damper piston velocities. Numerical methods were used to evaluate the area of the plot of force vs displacement. As given in Rao and Yap (2011), using these values, the equivalent damping coefficient C of the damper can be evaluated using

$$E = \pi C \omega X^2 \qquad (3.1)$$

Here, E is the energy dissipated by the damper in one cycle, ω is the frequency of excitation and X is the amplitude of sinusoidal excitation. As energy dissipated alone does not provide the whole picture, equivalent damping was calculated using equation 3.1 which incorporates frequency and amplitude parameters. The values of equivalent damping of the damper thus calculated for different piston velocities is given in Table 3.2.

Table 3.2 Equivalent damping coefficient for different piston velocities at 20 mm amplitude of sinusoidal excitation

Frequency of excitation (Hz)	Piston velocity (mm/s)	Energy dissipated (J)	Equivalent damping coefficient (kNs/m)
0.4	50	9.546	3.0226
0.8	100	16.825	2.6636
1.19	150	27.928	2.9724
1.59	200	40.941	3.2611
1.99	250	51.952	3.3064
2.39	300	59.642	3.1605
2.79	350	65.840	2.9888
3.18	400	71.462	2.8461
3.58	450	76.427	2.7038
3.98	500	83.629	2.6612

On plotting the equivalent damping coefficient of the damper against damper piston velocity as shown in Figure 3.7, it can be noticed that the equivalent damping coefficient is highest at a damper velocity of 250 mm/s. After this point, it reduces almost linearly with increase in damper velocity. It is also kept low at low damper velocity of 100 mm/s.
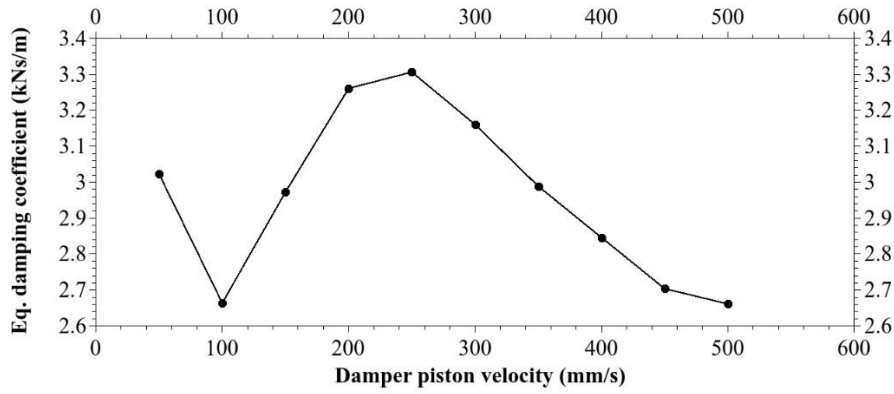
Figure 3.7 Equivalent damping coefficient vs damper piston velocity

3.3.3 Damper force vs velocity plots

The damper is further characterized by plotting damper velocity amplitude on the abscissa and maximum damping force on the ordinate as shown in Figure 3.8. Each point on the plot line corresponds to one of the frequencies of excitation V1 to V10 as given in Table 3.1. Maximum damping force during compressive stroke is taken as negative and maximum tensile force is taken as positive. Hence the plot is in first and third quadrants only.
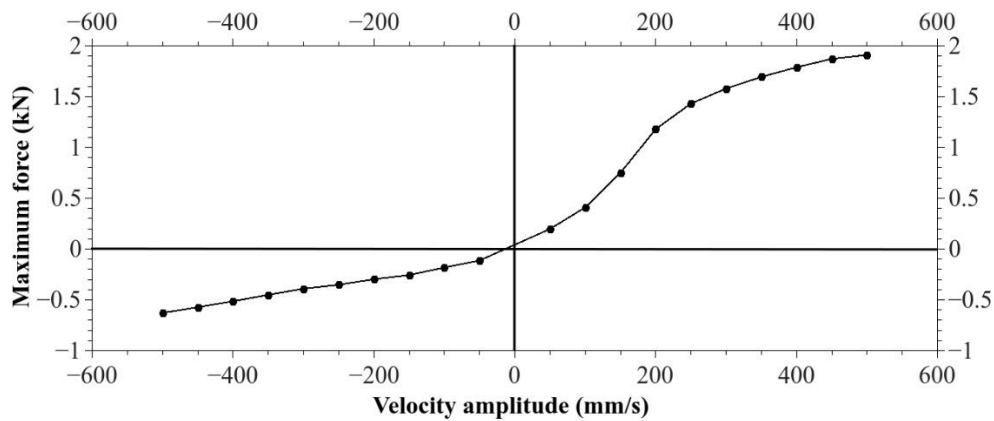
Figure 3.8 Maximum damper force vs damper piston velocity amplitude

44
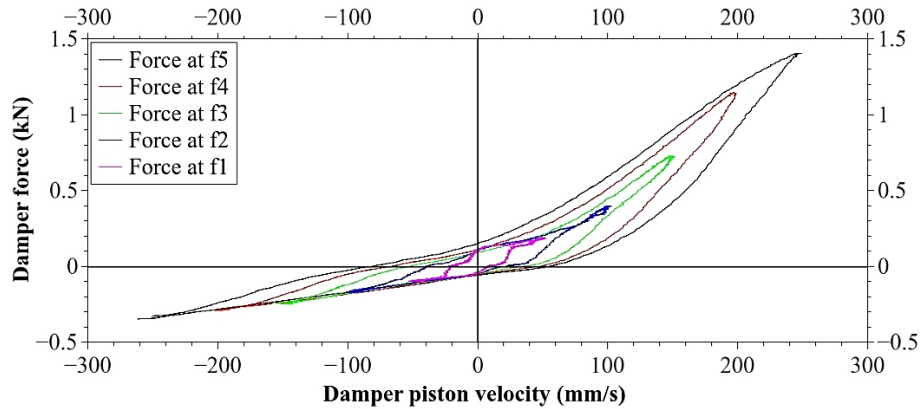
(a)
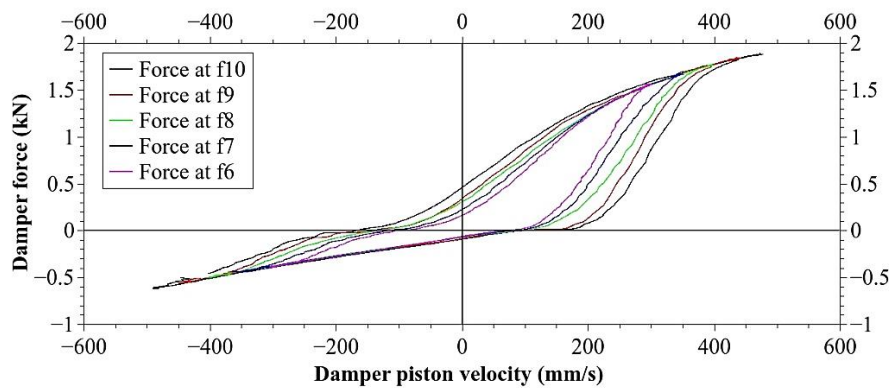
(b)

Figure 3.9 Damper force vs damper piston velocity **(a)** For frequencies f1 to f5 **(b)** For frequencies f6 to f10

The hysteresis phenomenon occurring in damper behaviour can be understood by studying the variation of damper force with damper velocity. Such a plot for different frequencies of excitation f1 to f10 as given in Table 3.1 is shown in Figure 3.9 (a) and (b). It can be observed that the damper provides higher force at higher frequencies of excitation. Also, the damping force is close to zero kN when damper velocity is close to zero mm/s. This is the expected behaviour of a typical automotive passive damper.

3.4 MATHEMATICAL MODELING OF PASSIVE DAMPER

The plot of damper force vs damper piston velocity exhibits hysteresis phenomenon as seen in Figure 3.9 (a) and (b). A mathematical model is developed for the same for two of the excitation frequencies f5 and f10. A polynomial model for force vs velocity plot of passive damper was developed so that the damper force can be predicted for any given damper velocity (up to 500 mm/s), without the need for doing any further experimentation. The curve fitting exercise helps to express the damper force as a function of damper piston

45

velocity in a closed form. This kind of representation is very useful for modeling the damper behaviour in a quarter car suspension model, which is used to study the performance of the damper. Since the plot forms a loop, it is divided into lower curve and upper curve and a polynomial model is fit for each curve separately as given by equation 3.2. F is the damper force and v is the damper piston velocity.

$$F = a_0 + a_1 v + a_2 v^2 + a_3 v^3 + a_4 v^4 + a_5 v^5 \qquad (3.2)$$

A fourth order polynomial was found to be sufficient to faithfully reproduce the experimental behaviour for f5 frequency of excitation. Similarly, for f10 frequency of excitation, a fifth order polynomial was found to be necessary. In order to reduce the computational load while running simulations which use the polynomial model of damper, the least possible order of polynomial was used which is necessary for a faithful fit to the experimental data. For lower frequencies, the dynamic content of the data is less and hence a fourth order polynomial was sufficient. For higher frequency, fifth order polynomial was found to be necessary to get a satisfactory fit with the experimental data. The coefficients of the polynomial fit are given in Table 3.3.

Table 3.3 Coefficients of the polynomial fit for force vs velocity plots

	f5 frequency (4th order polyfit)		**f10 frequency (5th order polyfit)**	
Lower curve	a_0	-0.0827801	a_0	-0.2010985564
	a_1	0.001354733	a_1	-0.0001477559
	a_2	7.73845E-06	a_2	6.3238966E-06
	a_3	3.76018E-08	a_3	3.2694698E-08
	a_4	4.55418E-11	a_4	-1.1146868E-11
			a_5	-8.9706348E-14
Upper curve	a_0	0.163555929	a_0	0.50340703073
	a_1	0.003201807	a_1	0.00371754477
	a_2	1.22393E-05	a_2	3.0238137E-06
	a_3	7.29031E-09	a_3	-9.370136E-09
	a_4	-1.03861E-10	a_4	-1.0896613E-11
			a_5	1.9829082E-14

The plots of damper force vs damper piston velocity showing both the experimental curve and the mathematical model curve are shown in Figure 3.10 (a) and (b). The simulated curve based on the polynomial model for damper behaviour closely matches the experimental data and hence it can be used to predict the damper force for any given frequency and amplitude of harmonic excitation.
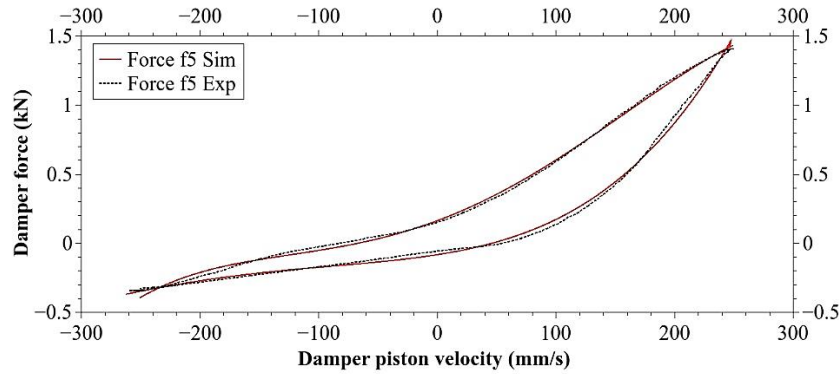
(a)
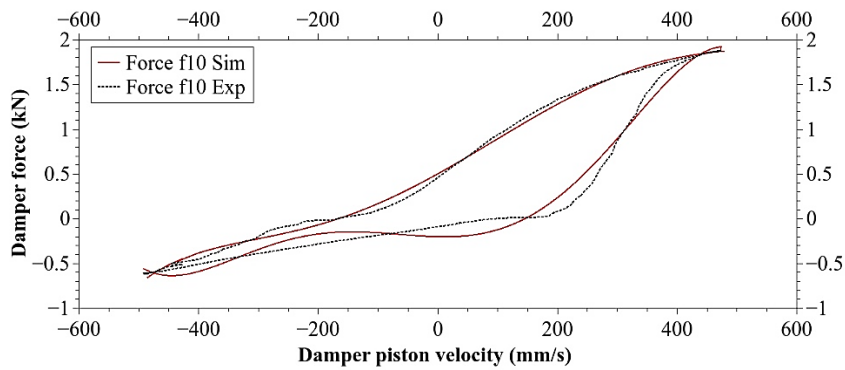
(b)

Figure 3.10 Polynomial model for damper force vs damper piston velocity **(a)** For frequency f5 **(b)** For frequency f10

3.5 EXPERIMENTAL SETUP FOR COMMERCIAL MR DAMPER

The commercial MR damper from Lord Corporation, model number RD-8040-1 was taken to Rambal India Ltd, Thiruporur, Chennai for experimental testing in the damping force testing machine as shown in Figure 3.11. The maximum force capacity of the testing machine is 1 Ton (1000 kg) and maximum velocity achievable is 1000 mm/s. A fixed displacement amplitude of 20 mm was used and velocity amplitude was increased from 50 mm/s to 520 mm/s. The corresponding frequencies are as shown in Table 3.4. At each frequency and its corresponding velocity, the current was varied from 0 A to 1.5 A in steps of 0.25 A, to give a total of seven different levels of current.
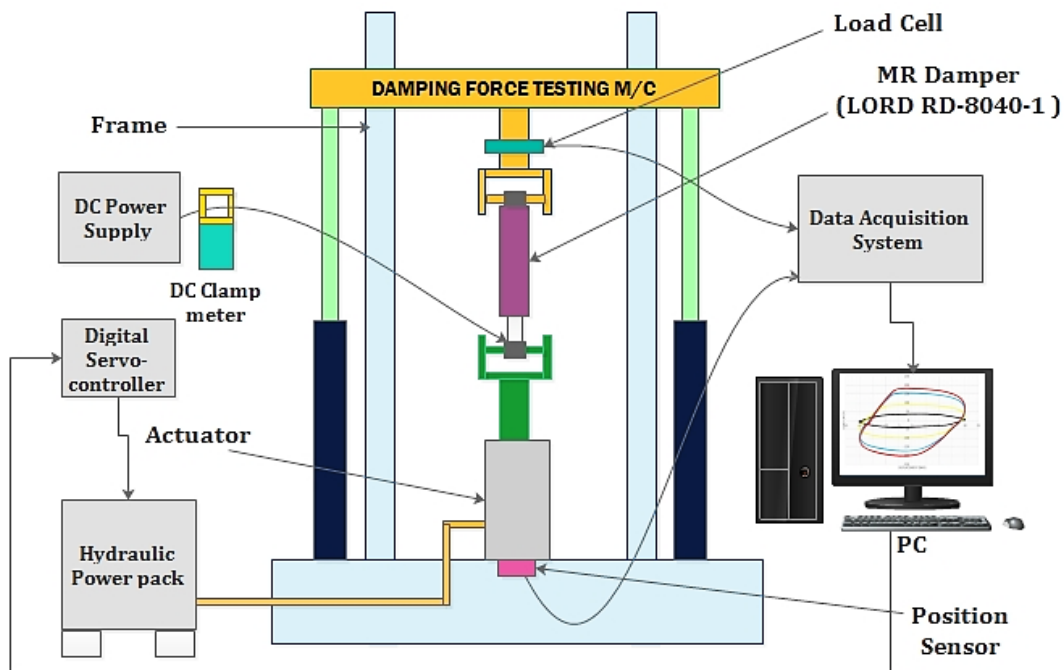
(a)

(b)

Figure 3.11 **(a)** Schematic diagram of experimental setup **(b)** Damping force testing machine

During each test run, constant current was supplied to the magnetizing coil in the MR damper through the Wonder Box of Lord Corporation, model RD-3002-03. The current being supplied was measured and verified using DC clamp current meter.

Table 3.4 Sinusoidal excitation frequencies and corresponding velocities at a fixed
displacement amplitude of 20 mm

Sinusoidal input frequency f (Hz)	Velocity amplitude 2πfX (mm/s)
0.4	50
1.03	130
2.07	260
3.1	390
4.14	520

The different levels of sinusoidal input frequency and displacement amplitude used for experimental testing were decided after consulting our industrial collaborator Rambal Ltd, who have a considerable amount of experience in manufacturing and testing hydraulic twin tube and monotube dampers for various applications. Each experimental run was measured by sensors and logged by data acquisition system to give the instantaneous displacement and damping force for different frequencies of loading. The displacement (stroke in mm) was measured by a position sensor in the hydraulic actuator and the damping force was measured by a load cell mounted in series with the fixed jaw holding the other eye of the MR damper. Test runs were carried out at different levels of current supplied to the MR Damper.

3.6 EXPERIMENTAL RESULTS AND DISCUSSIONS FOR COMMERCIAL MR DAMPER

The plots of force vs displacement for different values of current at different loading frequencies are shown in Figure 3.12 (a)-(e). Assuming negative values of displacement and force to be compression stroke and positive values to be rebound or extension stroke, the plot to the left of the ordinate is compression stroke and to the right of the ordinate is rebound or extension stroke. Similarly, the values of force above the abscissa are extension force and the values of force below the abscissa are compression force. The curve is traced clockwise as the damper is excited experimentally. The force vs displacement plots show that for any given frequency of input oscillations, the damping force increases with increase in the current supplied to the MR damper. Since the area under the force-displacement curve gives the single cycle energy dissipation, it can be observed from the force vs

displacement plots that higher values of current supplied leads to greater energy dissipation by the MR damper.
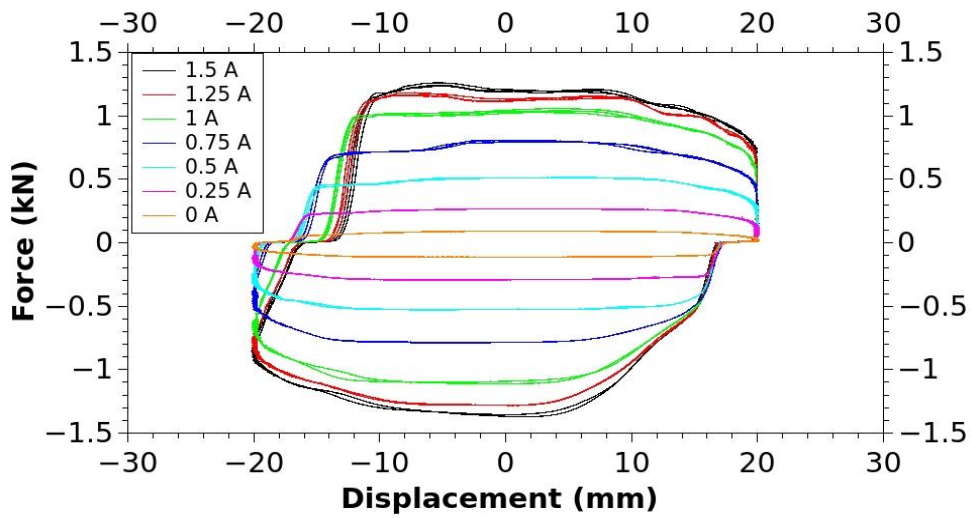
(a)
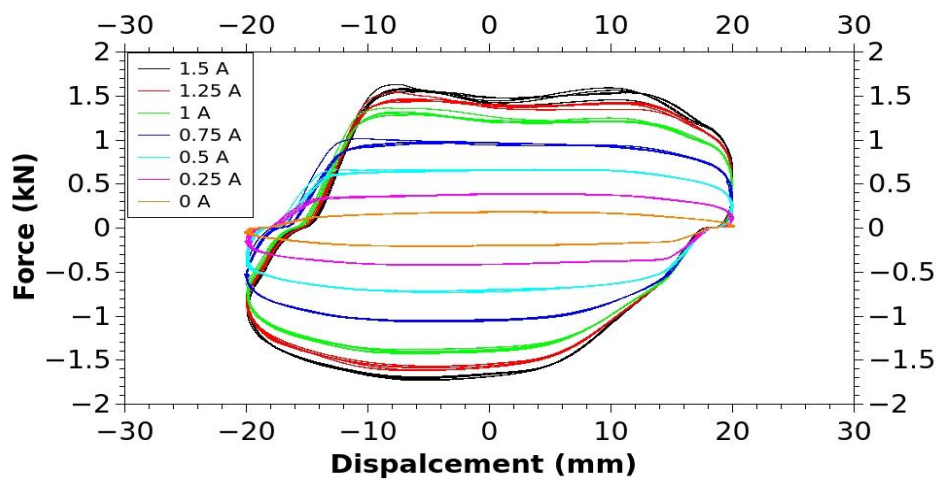
(b)
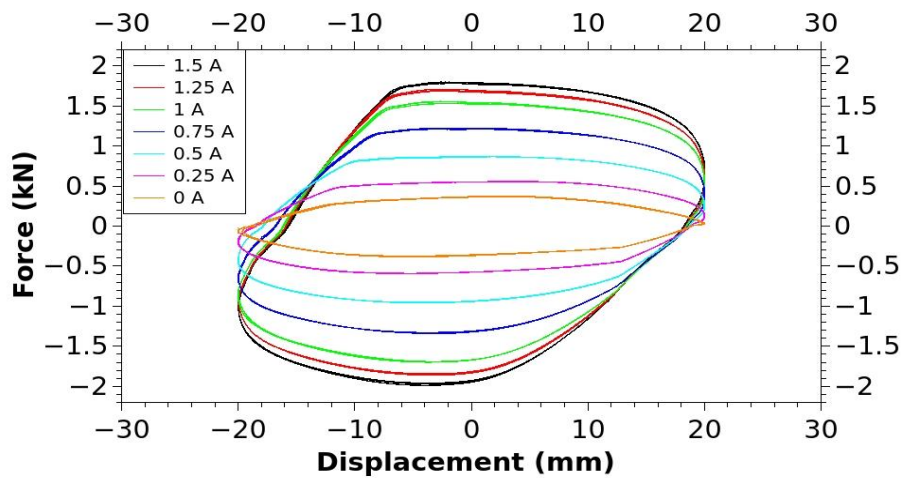
(c)
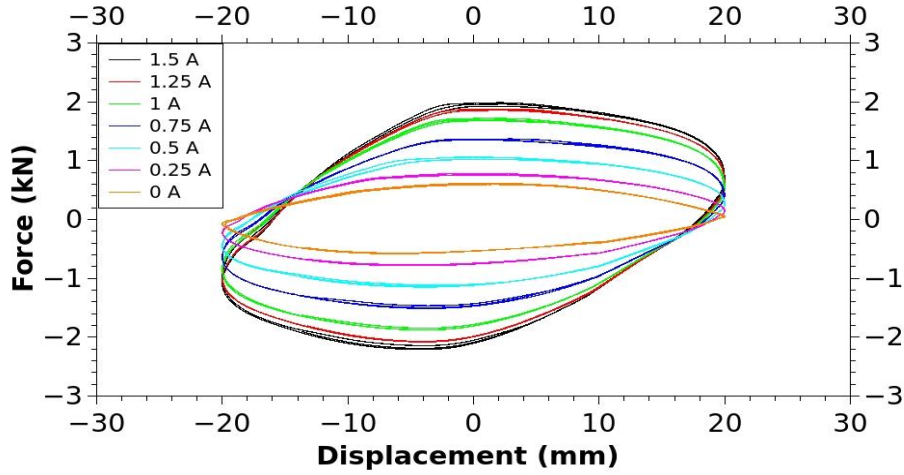
(d)
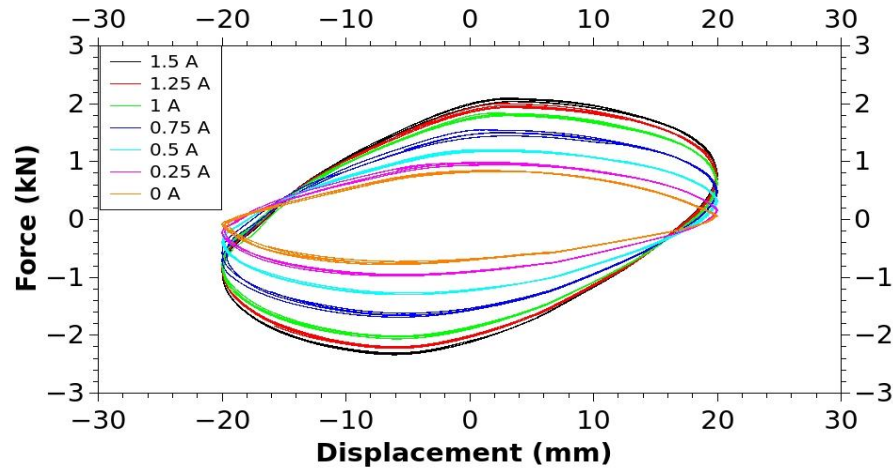
(e)

Figure 3.12 **(a)** Force vs displacement at 0.4 Hz **(b)** Force vs displacement at 1.03 Hz **(c)** Force vs displacement at 2.07 Hz **(d)** Force vs displacement at 3.1 Hz **(e)** Force vs displacement at 4.14 Hz

The force vs displacement plots for different frequencies of oscillations at three fixed levels of current, 0 A, 0.5 A and 1 A are shown in Figure 3.13 (a) - (c). At 0 A current, the MR damper works as a passive damper. Damper velocity is directly proportional to the product of frequency and stroke length. Since stroke length is kept constant for all experimental runs, increase in frequency causes proportional increase in damper velocity. The nature of a passive viscous damper is to give damping force proportional to the damper velocity as given by

$$F_d = C_{eq} . \frac{dx}{dt} \qquad (3.3)$$

Here, C_{eq} is the equivalent damping coefficient of the damper and x is the damper displacement. For any given current, it can be observed from the plots in Figure 3.13 (a)-

51

(c) that the damping force and energy dissipated by damper both increase with increase in frequency. This demonstrates that the Lord MR damper model RD-8040-1 can be used as a damper in passive and semi-active suspension systems.

(a)

(b)

(c)
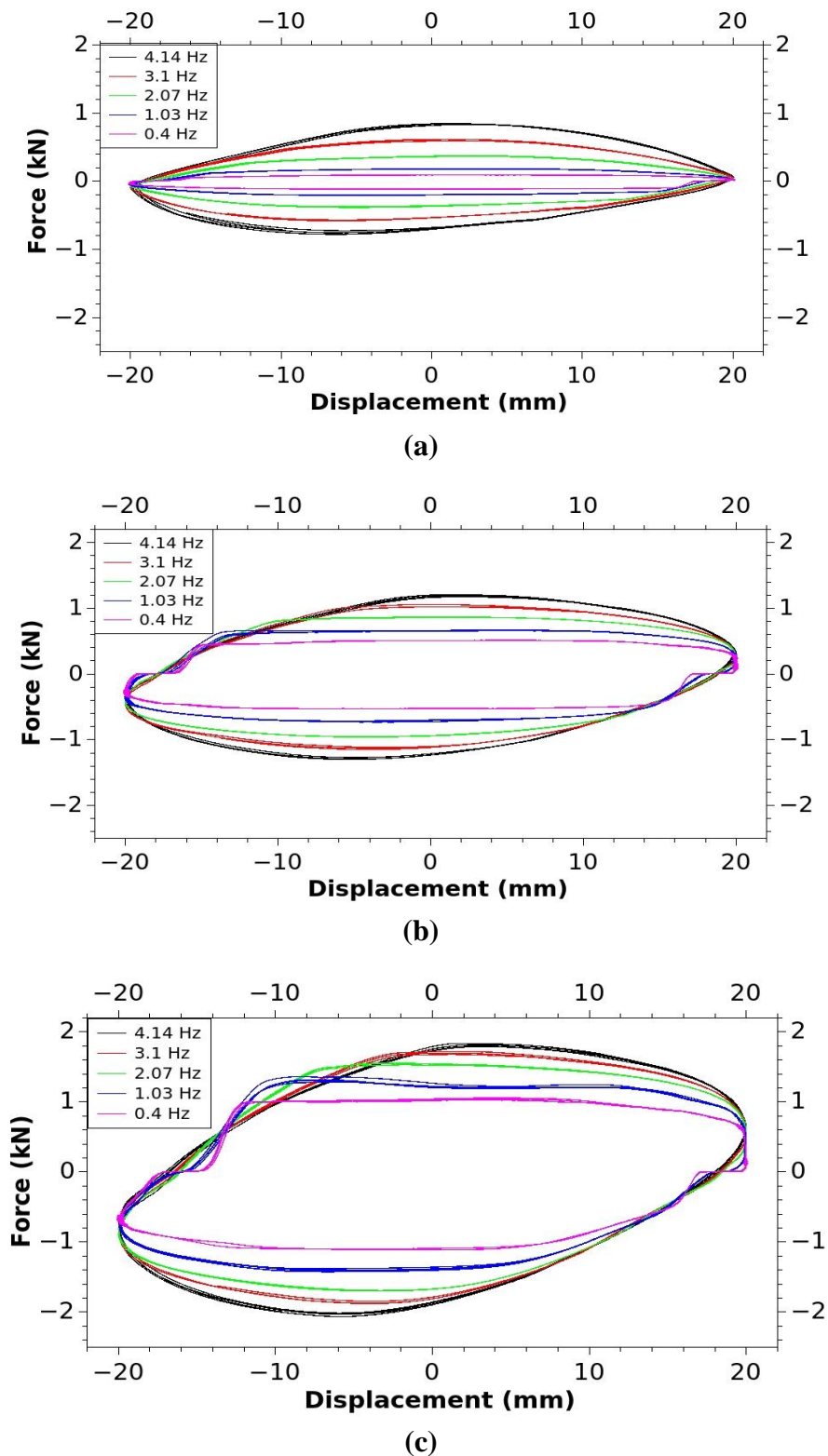
Figure 3.13 **(a)** Force vs displacement at 0 A current **(b)** Force vs displacement at 0.5 A current **(c)** Force vs displacement at 1 A current

Figure 3.14 is a plot of maximum damping force vs velocity amplitude of the damper. At 0 A current, the plot is a straight line passing through the origin as is the case in any typical passive viscous damper. At higher current values, the slope of the plot increases and it gives progressively higher values of maximum damping force for the same velocity amplitude.
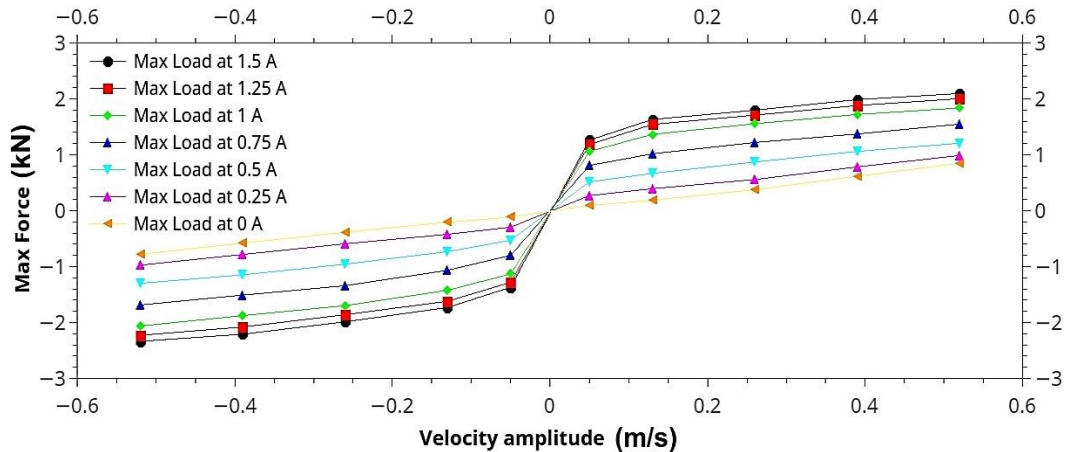
Figure 3.14 Maximum force vs velocity amplitude

Assuming negative values of velocity and force to be compression stroke and positive values to be rebound or extension stroke, the maximum force vs velocity amplitude plot will be in the third quadrant for compression stroke and in the first quadrant for extension stroke. This behaviour of the MR damper is utilized in designing a semi-active suspension system for commercial vehicle seat.
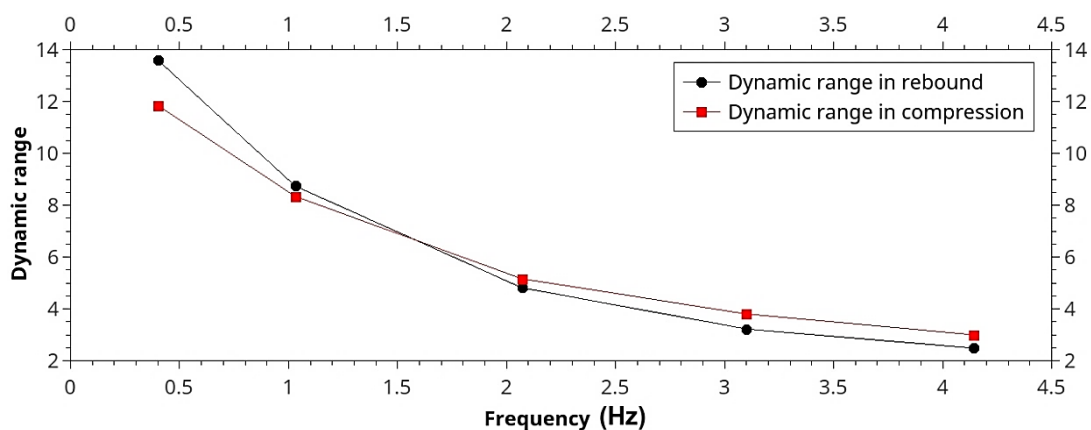
Figure 3.15 Dynamic range vs frequency for Lord RD-8040-1 damper

Dynamic range of an MR damper is defined as the ratio of the maximum damping force at full current to the maximum damping force at no current. It is a non-dimensional

53

number and the value of full current for Lord RD-8040- 1 as given in its product datasheet is between 1A and 2A. The plot of dynamic range vs frequency in Figure 3.15 shows that dynamic range reduces drastically with increase in frequency. Since dynamic range is an important parameter in effective working of a semi-active suspension system, the MR damper Lord RD-8040-1 is more suitable for low frequency applications in the range of 0.5 Hz to 3 Hz.

3.7 EQUIVALENT DAMPING COEFFICIENT OF COMMERCIAL MR DAMPER

The area of the force-displacement plot of the damper gives the energy dissipated in one cycle of compression and extension. From the experimental plots of force vs displacement for the Lord MR damper at 2.07 Hz excitation, area of the graph for one full cycle is calculated by numerical integration using the trapezoidal rule. Then using equation 3.4, the equivalent damping coefficient of the damper can be evaluated. Here W is the single cycle energy dissipation, C_{eq} is the equivalent damping coefficient, f is the frequency of excitation and X is the amplitude of excitation.

$$W = 2\pi^2 C_{eq} f X^2 \qquad (3.4)$$

For a spring-mass system having a single degree of freedom, the critical damping coefficient is given by $C_c = 2\sqrt{km}$, where k is the stiffness of the spring and m is the mass. The spring mass damper system is critically damped if C_{eq} is equal to C_c. A critically damped system returns to the mean position in the shortest time without overshooting to the other side of the abscissa. An underdamped system exhibits oscillatory motion with decreasing amplitude with time. An overdamped system also returns to the mean position without overshooting but takes longer time compared to the critically damped system.

Table 3.5 Energy dissipated and equivalent damping coefficient of MR damper at different values of current supplied

Current Supplied I (A)	Energy Dissipated W (J)	Equivalent Damping Coefficient C_{eq} (kNs/m)
0	21.8029	1.334
0.5	56.9029	3.4816
1	94.4915	5.7814

Using equation 3.4 and numerical integration of experimental plots of force vs displacement, equivalent damping coefficient of MR damper at 2.07 Hz excitation

frequency and 20 mm amplitude of excitation for different levels of current supplied is given in Table 3.5. It can be seen that the equivalent damping coefficient is increasing with increase in current supplied. The value of equivalent damping coefficient at highest current is more than four times its value at zero current.

3.8 MATHEMATICAL MODEL OF COMMERCIAL MR DAMPER

Representation of behaviour of MR damper as a mathematical model is required for simulation studies. The existing MR damper models are either non-parametric or parametric models. The parametric modeling technique uses a group of linear and non-linear springs and other elements to characterize the behaviour of the device. Based on mechanical idealizations, various parametric dynamic models for MR dampers have been explored and validated. Among these models, Guglielmino et al. (2008) showed that the Bouc-Wen model has gained wide acceptance within the engineering community as it can represent a wide range of hysteretic shapes by using simple differential equations. Spencer et al. (1997) first represented the hysteretic behaviour of MR dampers by adopting the Bouc-Wen hysteretic operator. Simple Bouc-Wen can be shown schematically as in Figure 3.16.
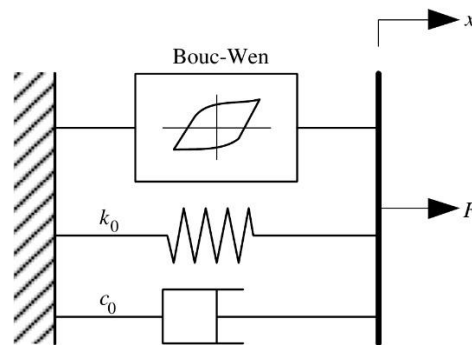
Figure 3.16 Simple Bouc-Wen Model Wang and Liao (2011)

In the equation 3.5 and 3.6, $F(t)$ denotes the total damping force predicted by the model, c_0 is the viscous damping coefficient, k_0 is the stiffness coefficient, x_0 is the initial displacement of the spring to compensate for the effect of accumulator and z is the evolutionary variable which is generally expressed in the differential form. The remaining parameters are the ones that influence the shape of the hysteresis curve.

$$F(t) = c_0\dot{x} + k_0(x - x_0) + \alpha z \tag{3.5}$$

$$z = -\gamma|\dot{x}|z|z|^{n-1} - \beta\dot{x}|z|^n + A\dot{x} \tag{3.6}$$

Determination of these parameters using different techniques is known as model fitting. Since there are 8 parameters to be defined, simple trial and error method would be impractical. Hence, a Genetic Algorithm (GA) provided in the Optimization toolbox of MATLAB was used for the purpose. GA is basically a search algorithm that looks for the best of the combination of given parameters within the given range to generate data that is very close to given experimental data. The error between the generated and experimental data is evaluated using an error function (or fitness function). The fitness function used in this study, taken from Peng et al. (2018) is given by

$$Fitness = \frac{\sqrt{\frac{1}{n}\sum_{i=1}^{n}(F_{d,i}^{exp}-F_{d,i}^{Fit})^2}}{\sqrt{\frac{1}{n}\sum_{i=1}^{n}(F_{d,i}^{exp}-(\sum_{i=1}^{n}F_{d,i}^{Fit}))^2}} \tag{3.7}$$

Here, n is the number of samples, F_d^{exp} is the force obtained from experiments, F_d^{Fit} is the force obtained from the model. For each combination of parameter values, the damping force was calculated using the equations 3.5 and 3.6 that were represented in MATLAB Simulink as shown in Figure 3.17.
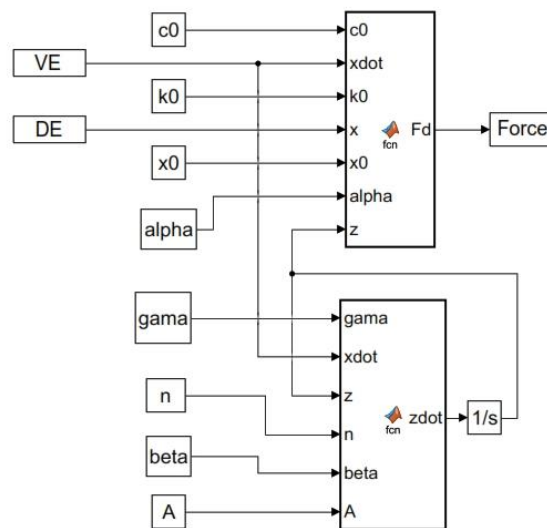
Figure 3.17 Simulink blocks for Bouc-Wen Model

To simulate the behaviour of the MR damper under forced vibration, a mathematical model of the MR damper is developed based on the Bouc-Wen model. The GA used in this study consisted of a population size of 200 with 20 generations and 50 stall generations. Since the differential equation involved is fairly complex, a fourth-order Runge Kutta method was used for computation of the model parameters. These parameters are shown in Table 3.6.

Table 3.6 Bouc-Wen model parameters

Sl. No	Parameter	Value
1	c_0 (Ns/m)	2069.6I-833.4
2	k_0 (N/m)	$6782I^2+18045I+12907$
3	x_0 (m)	0.012982
4	α (N/m)	$-128.59I^2+639.98I-276.47$
5	γ (/sq.m)	44.616
6	n	9.927883
7	β (/sq.m)	24.768
8	A	19.903

The plots of force vs displacement for the MR damper showing experimental and simulated results at current values of 0A, 0.5A and 1A for 2.07 Hz excitation frequency is shown in Figure 3.18 (a)-(c). Similarly, the plots of force vs time for the MR damper showing experimental and simulated results at current values of 0A, 0.5A and 1A for 2.07 Hz excitation frequency is shown in Figure 3.19 (a)-(c).
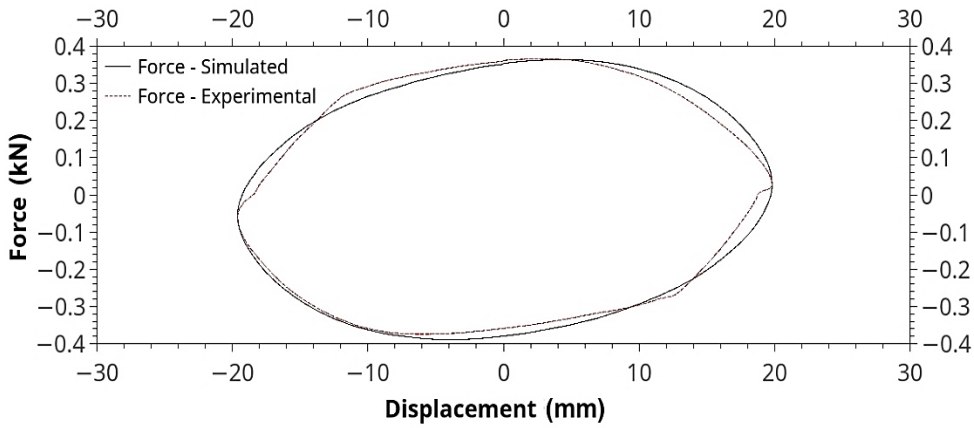
(a)
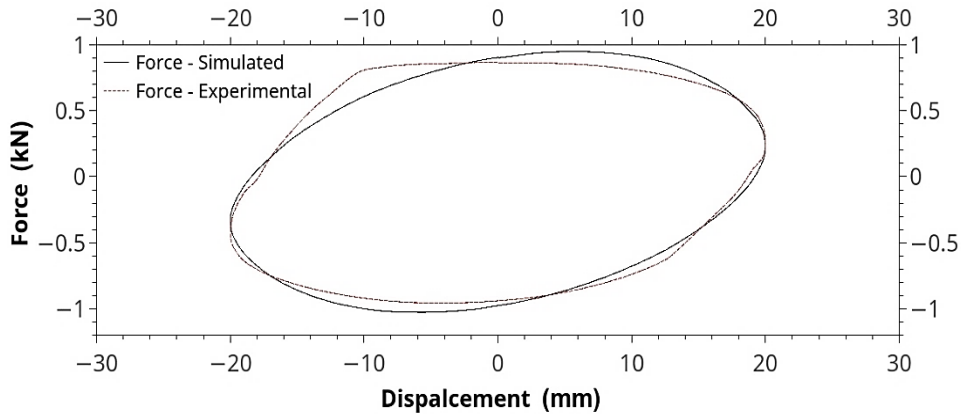
(b)
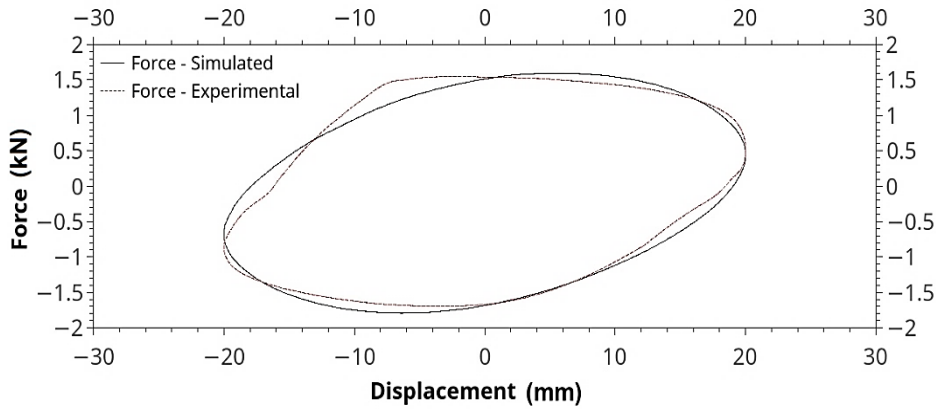
(c)

Figure 3.18 **(a)** Force vs displacement for 2.07 Hz excitation frequency at 0 A current **(b)** Force vs displacement for 2.07 Hz excitation frequency at 0.5 A current **(c)** Force vs displacement for 2.07 Hz excitation frequency at 1 A current

The plots show that there is a reasonable agreement between the experimental and simulated results. The mathematical modeling was done for one particular frequency of excitation to demonstrate the method to be used to get the mathematical model of MR damper behaviour. Hence following the same procedure, mathematical models can be developed to predict behaviour of the MR damper at various other current levels and other excitation frequencies and a more generalized model can be obtained for damper behaviour prediction. These can be further used to design semi-active control strategy for the seat suspension using MR damper.
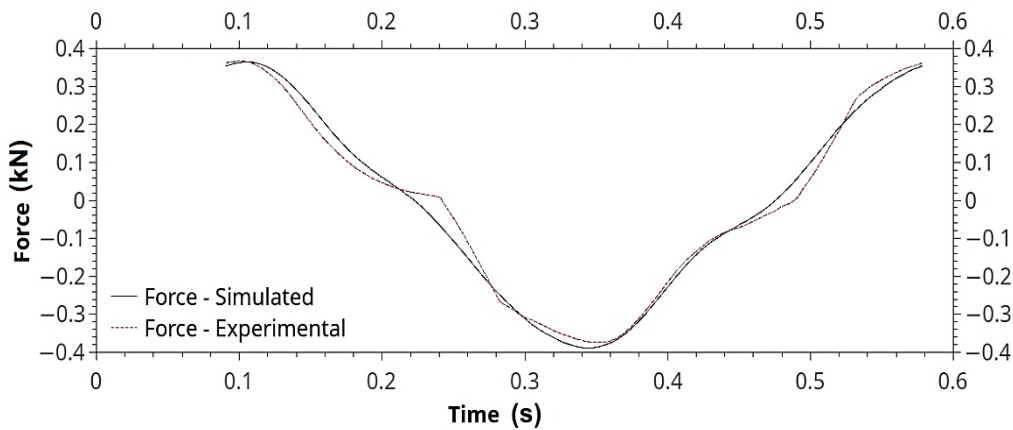
(a)
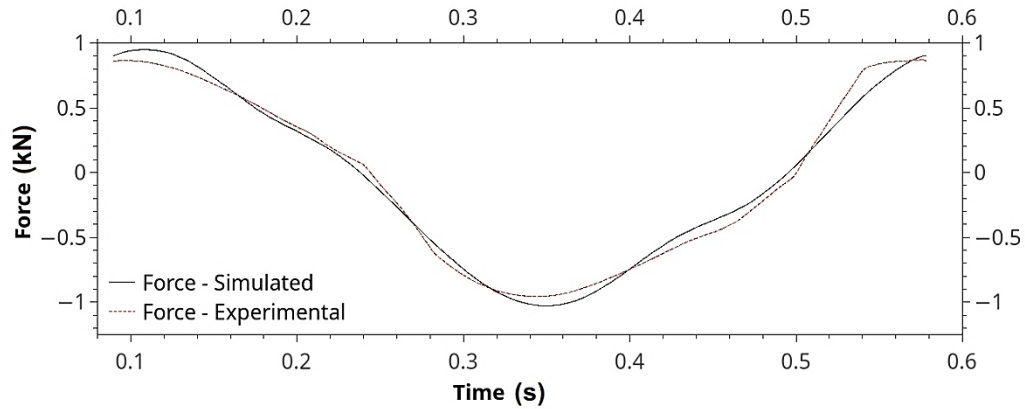
(b)
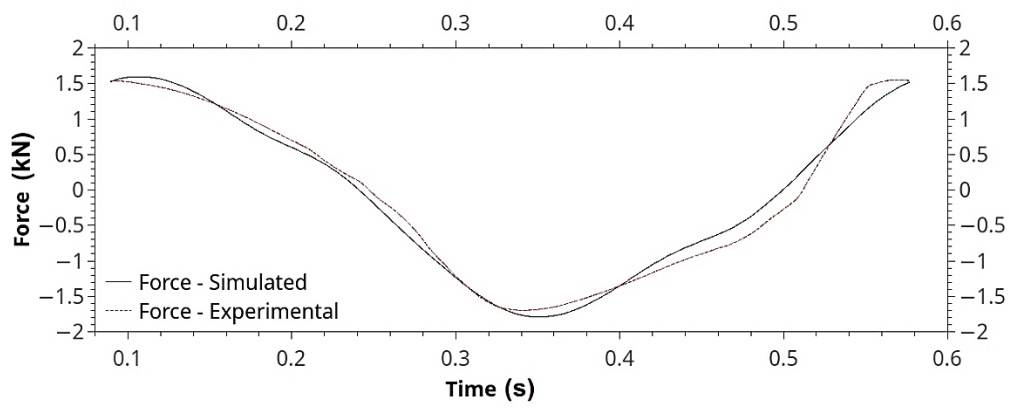
(c)

Figure 3.19 **(a)** Force vs time for 2.07 Hz excitation frequency at 0 A current **(b)** Force vs time for 2.07 Hz excitation frequency at 0.5 A current **(c)** Force vs time for 2.07 Hz excitation frequency at 1 A current

3.9 PERFORMANCE OF COMMERCIAL MR DAMPER IN A SPRING-MASS VIBRATING SYSTEM

The performance of the commercial MR damper in a spring-mass vibrating system is studied with the help of MATLAB simulations. The vibrations coming from the base are prevented from getting transmitted to the mass by introducing a spring and damper between the base and the mass as shown in Figure 3.20. The setup is modeled as a single degree of freedom spring-mass system. In the case of passive suspension, the damping coefficient of the damper is a fixed parameter based on the damper design. In the case of semi-active suspension, the damper used is a MR damper whose equivalent damping coefficient can be varied in real time with in milliseconds by changing the value of current supplied to the MR damper.
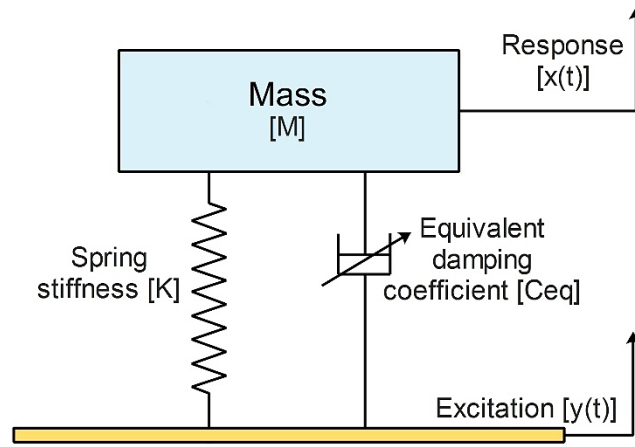
Figure 3.20 Schematic of spring-mass vibrating system

The total mass of the single degree of freedom system m is assumed to be 80 kg and the spring stiffness of the system k is assumed to be 16 kN/m. Based on these values, the natural frequency of the undamped system is 2.25 Hz. If the vibration coming from the base is having a frequency nearer to this value, use of a suitable damper becomes necessary to avoid resonance of the vibrating system. The critical damping coefficient thus calculated for this system is 2.263 kNs/m. The response of the system to a pulse displacement input of amplitude 20 mm for different values of current supplied is shown in Figure 3.21.
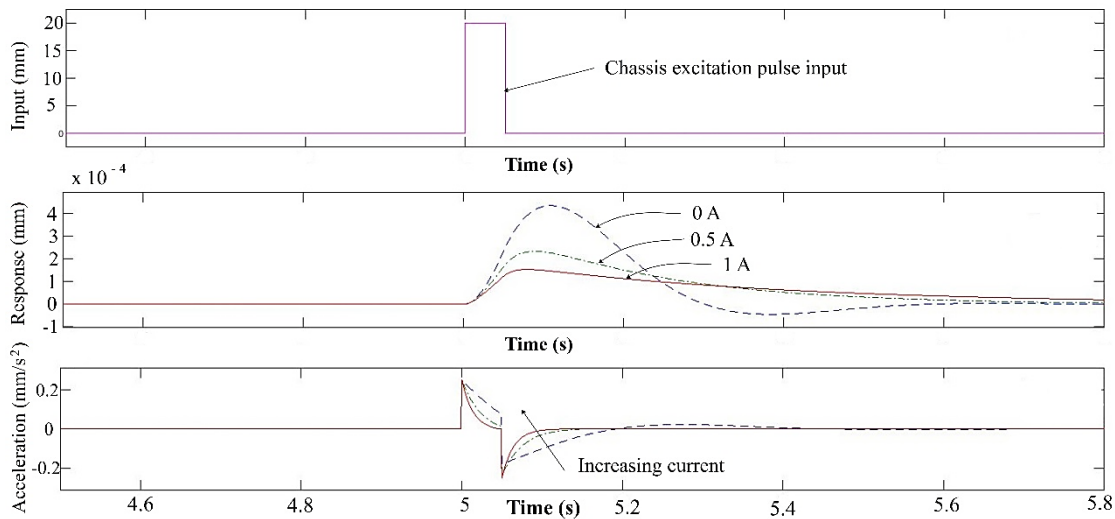
Figure 3.21 Response of spring-mass system at 0A, 0.5A and 1A, obtained from MATLAB Simulink

It can be seen that the response of the system at 0 A current is similar to the response of an underdamped system. At higher values of current, like 0.5 A and 1 A, the response of the system is similar to that of an overdamped system. This behaviour is corroborated by

60

the analytical results provided in Table 3.5 which shows that the equivalent damping of the MR damper at 0 A is less than the critical damping coefficient of the system and the equivalent damping of the MR damper at 0.5 A and 1 A are greater than the critical damping coefficient of the system. Hence it has been demonstrated that by tuning the current supplied to the MR damper, the same damper can make the system behave as an underdamped, critically damped or overdamped system of vibration.

3.10 SUMMARY

The passive damper used in a SUV automobile was tested in the damping force testing machine. Sinusoidal excitations of fixed amplitude and varying frequencies were used for evaluation. Damper force and corresponding displacement were measured along with time data. The force vs displacement plots show that the size of the loops increase with increase in frequency of excitation. As the area of the loops represent the amount of dissipated energy in one cycle, one can conclude that the passive damper dissipates higher amount of energy at higher frequencies of excitation keeping amplitude of vibration as constant. From the maximum force vs velocity amplitude plot, it was found that for the same velocity values, the damping force in bounce is more than twice that in compression. Plots of damper force vs damper velocity demonstrated the hysteresis behaviour of the damper. Results for several frequencies are plotted and to demonstrate the method, mathematical models were built for two of the frequencies, the medium and the highest one (1.99 Hz and 3.98 Hz). The simulated curves follow the experimental plots closely and for all practical purposes, the mathematical models can be used to estimate the damper force at any given damper velocity or any combination of sinusoidal excitation frequency and amplitude. These results can be utilized in designing a new suspension system for the vehicle under study as these data are not provided by the damper manufacturers.

A commercially available MR damper was evaluated in a damping force testing machine at various excitation frequencies and current supplied. Plots of force vs displacement show that damping force was increasing with velocity as well as current supplied. Calculation of area of the force vs displacement loops lead to evaluation of energy dissipated values and which in turn gave values of equivalent damping of the MR damper. The increase in equivalent damping with current supplied and plots showing high dynamic range of MR damper at frequencies between 0.5 Hz and 3 Hz made the MR damper suitable for application in commercial vehicle driver's seat suspension. Mathematical model of the

MR damper behaviour was developed using Bouc-Wen hysteresis operator and genetic algorithm (GA) provided in Optimization toolbox of MATLAB. A good match between the simulated and experimental plots confirms the veracity of the method used. It was successfully shown that by controlling the current supplied to the MR damper, a spring-mass vibrating system can be made to work as an underdamped, critically damped or overdamped system. The current supplied also controls the amount of energy dissipated by the MR damper in one cycle of input oscillation. Thus, semi-active control strategy using MR damper can be used to provide vibration isolation to the system. The learnings of this chapter have been used in the next chapter to design and test a twin-tube MR damper working in valve mode and also to develop mathematical model for MR damper behaviour.

CHAPTER 4

DESIGN AND EXPERIMENTAL CHARACTERIZATION OF A TWIN-TUBE MR DAMPER FOR A PASSENGER VAN

4.1 INTRODUCTION

A twin-tube damper design has several advantages when compared to a monotube damper design. Unlike a monotube damper, twin-tube dampers do no need any floating piston and accumulator chamber arrangement for its working. It is robust, easy to manufacture and the damper performance is not easily affected by external contaminants. In this chapter, the design and characterization of a twin-tube MR damper is presented. The piston design is optimized and mathematical models are developed for MR damper behaviour.

4.2 METHODOLOGY

The methodology used is represented in the form of a flow chart in Figure 4.1. In order to arrive at the capacity and size of the twin tube MR damper to be designed, a twin tube passive damper used in a passenger van is characterized in the lab using a damper testing machine. Based on this, the size and thickness of the inner tube, outer tube and piston rod of the MR damper is selected. General topology of the MR damper piston assembly is synthesized. Taguchi analysis using design of experiments is performed with the help of FEMM software to arrive at the optimum values of parameters used in the MR damper piston assembly to maximize the magnetic flux density at fluid flow gap. The FEMM results are validated by analytical method using electromagnetic circuit theory. Hydraulic analysis of the twin tube MR damper is performed to check for sufficient mechanical strength. Subsequently, the MR damper is fabricated and filled with commercial MR fluid MRF-132DG manufactured by Lord Corporation. The MR damper is tested experimentally on a damping force testing machine and its behaviour is characterized. Mathematical models are developed for the behaviour of the MR damper. Finally, a Proportional-Integral-Derivative (PID) control in MATLAB Simulink is used to demonstrate that the MR damper can track a desired force output.
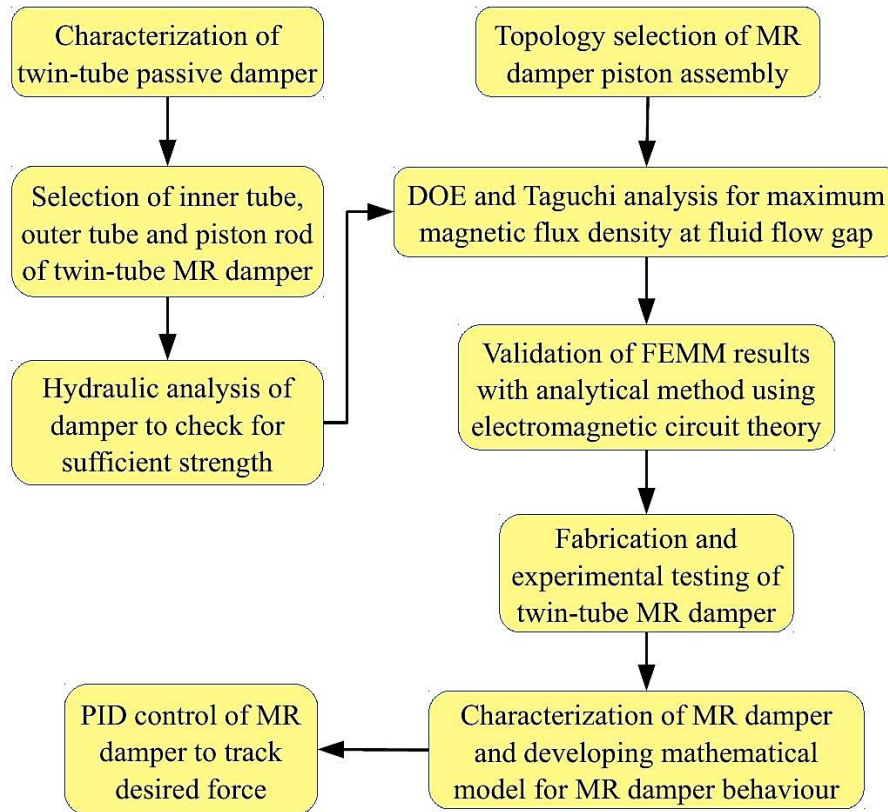
Figure 4.1 Flow chart of methodology

4.3 CHARACTERIZATION OF A TWIN TUBE PASSIVE DAMPER

Force Motors Traveller, which is a passenger van, was chosen as the application vehicle as it was readily available at the industrial partner. The van finds application as a people carrier, school bus, city bus and ambulance among other uses. The front damper of the van was chosen in particular. The damper is commercially available as spares with item code T00-686-320-0530, manufactured by Gabriel India Ltd as shown in Figure 4.2 (a). This damper was tested in the lab in order to determine the damping characteristics required for the vehicle. This testing was done on HEICO make Damper testing machine shown in Figure 4.2 (b). It consists of a hydraulic actuator powered by a hydraulic power pack of 40 HP capacity. The maximum flow rate of the pump is 64 liters per minute and maximum operating pressure is 210 bars. The hydraulic actuator is double acting, double ended and has a force capacity of +/- 20 kN. It has a stroke of 150 mm (+/- 75 mm), maximum working pressure of 210 bars and a peak actuator velocity of 1200 mm/s. The hydraulic actuator is controlled by a MOOG servo valve connected to a MOOG portable test controller. The loading frame is fixed at the base with two long vertical columns. A cross head with two

hydraulic locking cylinders slides over these columns and can be clamped anywhere over the entire length to accommodate dampers of different sizes. Arrangement is also provided to lock the crosshead at any desired position.

(a)

(b)
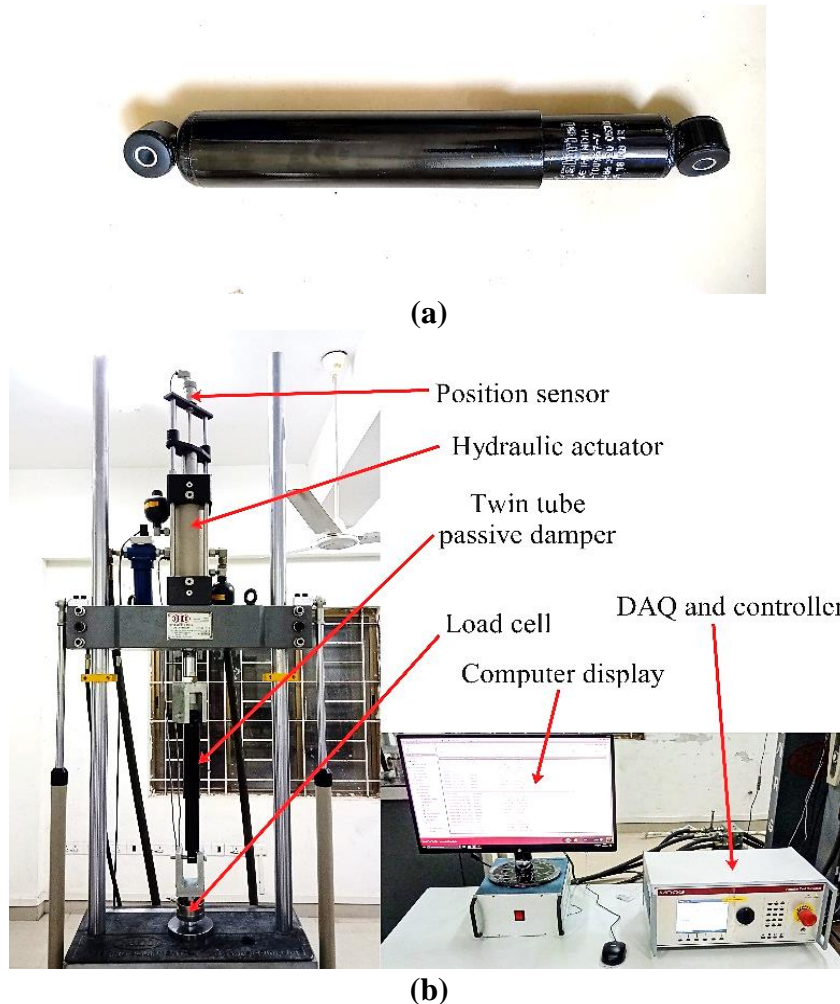
Figure 4.2 **(a)** Passive damper **(b)** Damper testing machine

There are two sensors on the damper testing machine, a displacement transducer to measure the damper displacement and a force transducer to measure the damper force. The displacement transducer is built into the actuator which is mounted on the crosshead and the force transducer is fixed on the base of the frame along with holding fixture for the shock absorber. The displacement transducer is a contactless linear position transducer with magneto strictive technology. It is Gefran make with a range of 200 mm, excitation voltage of 24 Volts D.C., sampling rate of 2 kHz and a full-scale output of 10 Volts. It has a linearity of +/- 0.02% of full scale with both repeatability and hysteresis less than 0.01 mm. The force transducer is a Micro Measurement make strain gauge based on full Wheatstone bridge configuration. The structure of the force transducer is such that it can work in both

compression and tension over a few million cycles with protection against side loading. It has a capacity of +/- 30 kN, resolution of 0.001 kN, accuracy of 0.5% of indicated value and a full-scale output of 2.0 mV/V. Data from both the displacement transducer and the force transducer are recorded with the help of Moog Integrated Test Suite at a rate of 1000 samples per second. With the help of this arrangement, a wide range of displacement waveforms like sine, square, sawtooth, trapezoid, rounded ramp and exponential. In order to evaluate the damping force generated at different piston velocities, experiment was designed with sinusoidal displacement input to the damper at a fixed amplitude of 20 mm. Different velocities were achieved by increasing the frequency of sinusoidal oscillations as shown in Table 4.1. These velocities are based on the actual operating frequencies and amplitudes of the passive damper in the passenger van. They were chosen after consultation with Rambal Ltd., who is an industrial collaborator for this research work. Rambal Ltd. has many years of expertise in mass production and testing of hydraulic mono tube and twin tube dampers for different applications.

Table 4.1 Velocity and frequency levels of input sinusoidal oscillations at a fixed amplitude of 20 mm

Velocity Level	Piston velocity(mm/s)	Frequency of excitation (Hz)	Frequency Level
V1	50	0.4	f1
V2	100	0.8	f2
V3	150	1.19	f3
V4	200	1.59	f4
V5	250	1.99	f5
V6	300	2.39	f6
V7	350	2.79	f7
V8	400	3.18	f8
V9	450	3.58	f9
V10	500	3.98	f10
V11	600	4.77	f11
V12	700	5.57	f12

The plots of damper force vs displacement for different frequencies of excitation is as shown in Figure 4.3. Damper force during compression is taken as negative and that during rebound is taken as positive force. Similarly, compressive displacement from mean position of the damper is taken as negative displacement and rebound/extension from mean position is taken as positive displacement. It can be seen that the damping force, especially during rebound, increases with increase in excitation frequency. The size of the force vs

displacement loop and hence its area is seen to be increasing with increase in frequency of excitation. A shift in the force curve is seen at extreme position of displacement, where the damper force is nearly zero. This is due to play in the damper clamping mechanism when the direction of motion of damper changes.
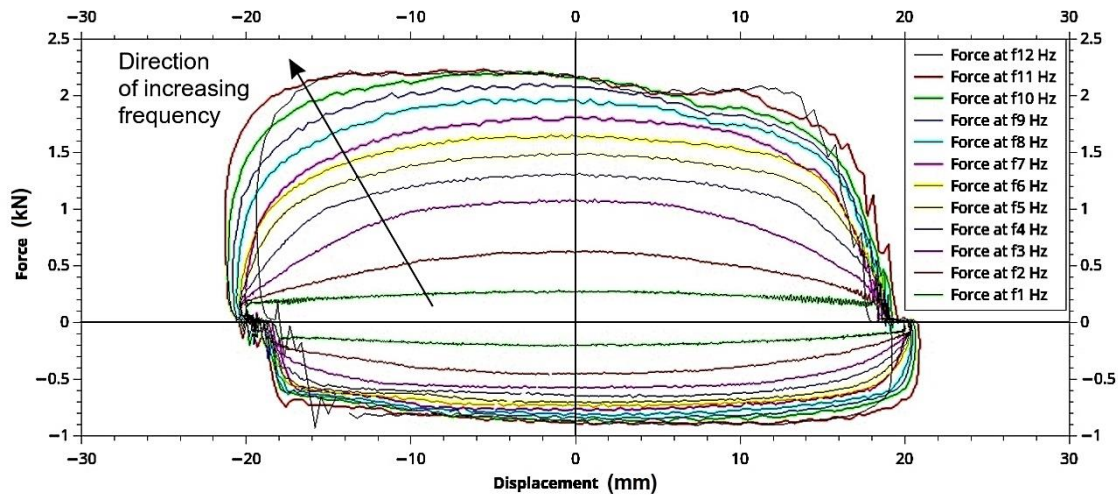
Figure 4.3 Damper force vs displacement plots for various frequencies of excitation

Velocity data for the above experiment was obtained by numerical differentiation of the displacement data and smoothening the results using moving window average method. Velocity during compression will be negative and that during rebound will be positive. The plot of damper force vs piston velocity amplitude is shown in Figure 4.4.
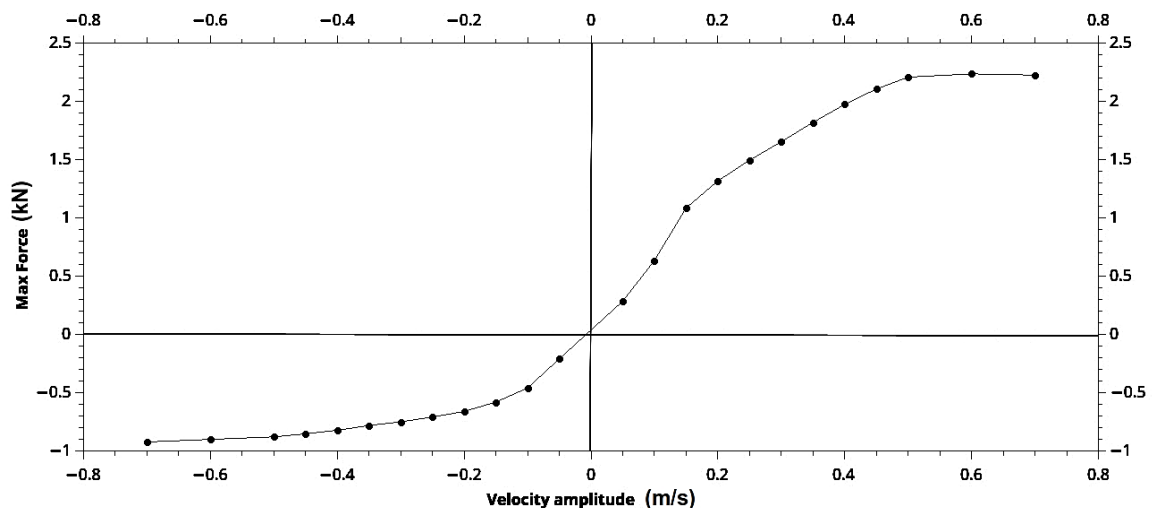
Figure 4.4 Maximum force vs piston velocity amplitude

It can be observed that the damping force during rebound is more than twice the value during compression for any given velocity. This is desirable in a vehicle suspension

because compression of the damper happens when the wheel hits a bump on the road. The energy generated due to this shock is absorbed by the spring by undergoing compression. The damper helps this process by generating a lower damping force. This energy is released by the spring during rebound and is dissipated by the damper. The damper achieves this by generating a higher damping force during rebound. As the area of the force vs displacement loop provides the energy dissipated by damper, the force vs displacement plot for one cycle of the damper at different frequencies of excitation was numerically integrated. Using this data, the equivalent damping coefficient of the damper was found, as shown in Table 4.2. The results shown are for a passive damper used in the front suspension of a passenger van. The damping requirements of the van are such that it requires high damping force near its frequencies of resonance. Hence, it can be seen in Table 4.2 that the equivalent damping force is highest at around 1.2 Hz and reduces on either side of this value of frequency.

Table 4.2 Energy dissipated and equivalent damping coefficient of the twin tube passive damper at 20 mm displacement amplitude for different frequencies of excitation

	Frequency of excitation (Hz)	Piston velocity (mm/s)	Energy dissipated per cycle (J)	Equivalent damping coefficient (kNs/m)
f1	0.4	50	15.425	4.884
f2	0.8	100	32.62	5.1641
f3	1.19	150	51.704	5.5028
f4	1.59	200	63.938	5.093
f5	1.99	250	73.222	4.6601
f6	2.39	300	80.8	4.2817
f7	2.79	350	85.231	3.8690
f8	3.18	400	94.15	3.7497
f9	3.58	450	100.142	3.5428
f10	3.98	500	106.139	3.3775
f11	4.77	600	112.852	2.9964
f12	5.57	700	105.661	2.4025

4.4 DESIGN OF TWIN TUBE MR DAMPER

A twin-tube type damper was selected because of its simplicity in construction and robust nature. It is also less susceptible to suffer the effects of imperfect machining. The basic structure of a twin tube MR damper can be seen in Figure 4.5.
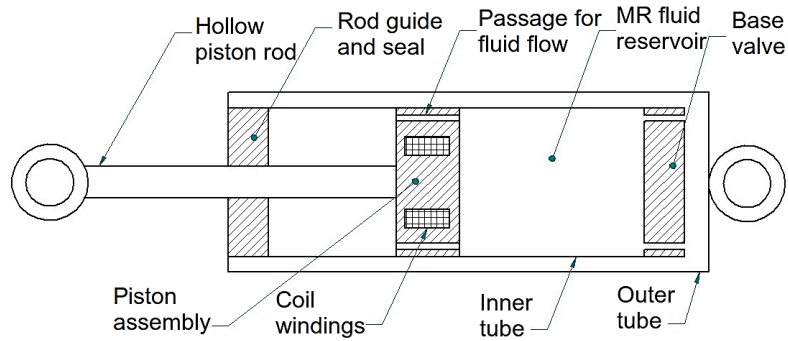
Figure 4.5 Line sketch of twin tube MR damper

The inner tube is completely filled with MR fluid and the outer tube is partially filled with MR fluid. There is a base valve fitted at the bottom of the inner tube through which the fluid has to pass to flow from inner tube to outer tube and vice versa. During compression stroke, as the piston moves from left to right in Figure 4.5, MR fluid flows from right side of the piston to the left side by passing through the annular area provided in the piston assembly. As the piston rod enters the inner tube, an equivalent volume of MR fluid flows from inner tube to outer tube through the base valve to take care of the increase in the volume of piston rod in inner tube. During rebound stroke, the same amount of fluid flows back into the inner tube from the outer tube through the base valve and MR fluid also flows from left side piston to right side of piston in Figure 4.5. In order to make the fabrication process easier and quicker, the parts of an already existing passive damper were used along with a newly designed piston assembly which acts as a MR valve. The dimensions of the twin-tube MR damper are shown in Table 4.3.

Table 4.3 Twin-tube MR damper dimensions

Parameter	Numerical value
Maximum stroke	130 mm
Closed length	397 mm
Length of the outer tube	293 mm
Outer diameter of outer tube	70 mm
Length of inner tube	254.7 mm
Outer diameter of inner tube	45 mm
Wall thickness of outer and inner tube	2 mm

A nylon wear band was incorporated on the outside surface of the piston assembly to preserve the concentricity between the inner tube and the piston assembly of the MR damper. It also helps to reduce the frictional force between the piston and the cylinder by

acting as a dynamic seal. The MR damper will be filled with MR fluid MRF-132DG from Lord Corporation which has a specific gravity of 3 and a viscosity of 0.112 Pa-s at 40^0 C.

The base valve of the MR damper was suitably modified so that the off-state (no current) damping force was around 50% of the passive damper damping force. For automotive applications, the damping force produced by MR damper at maximum current must be more than 1.5 times the passive damper damping force, according to Poynor (2001). As the new piston assembly had to fit in the inner tube of the twin tube damper, the outer diameter of the piston assembly was kept the same as the inner diameter of the inner tube. This piston assembly is made up of piston core, inner sleeve, outer sleeve, top plate, bottom plate, piston rod, countersunk screw and the electromagnetic coil as shown in Figure 4.6 (a) and (b). The electromagnetic coil is wound on the piston core in the space between the flanges and the winding is covered by the inner sleeve. The wire leads of the coils are taken out of the piston assembly by passing them through the hollow piston rod.

(a)
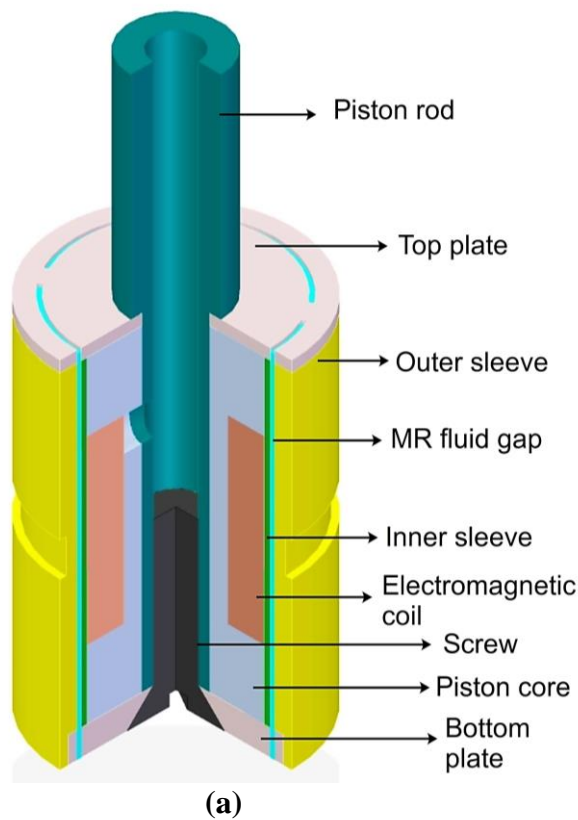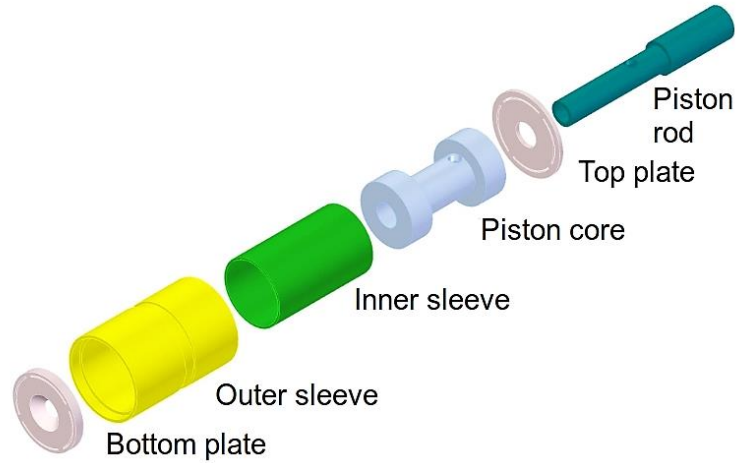
(b)

Figure 4.6 **(a)** Sectional view of the MR damper piston assembly **(b)** Exploded view of the MR damper piston assembly

The piston core, outer sleeve and piston rod are part of the magnetic circuit and hence they are made of low carbon steel (EN-1A) which is a soft magnetic material. The top plate, bottom plate and inner sleeve are made of aluminum which is non-magnetic in nature. This helps to prevent the leakage of magnetic flux induced by the electromagnetic coil.

4.4.1 Hydraulic analysis of damper

From Figure 4.4, the maximum damper force is developed during the rebound stroke at highest velocity and its value is 2.24 kN. In order to develop this force, the fluid pressure developed on the rod side of the cylinder is given by

$$p_r - p_p = 4F / \pi\left(d_p^2 - d_r^2\right) \tag{4.1}$$

Here, p_r is the rod side fluid pressure of the cylinder and p_p is the piston side fluid pressure of the cylinder, F is the maximum damper force, d_p is the piston diameter and d_r is the piston rod outer diameter. As there is no accumulator used and outer tube is vented to atmosphere, p_p will be nearly equal to atmospheric pressure and hence it can be neglected. Therefore, pressure inside the cylinder is given by

$$p = 4F / \pi\left(d_p^2 - d_r^2\right) \tag{4.2}$$

Since the wall thickness of both the inner tube and outer tube is less than 1/10th of the diameter of the respective tubes, they can be treated as thin cylindrical shells for strength estimation. The value of hoop stress is considered for design and it is given by

$$\sigma = \text{pd} / 2\text{t} \qquad\qquad (4.3)$$

Here, p is the pressure inside the cylinder as obtained by equation 4.2, d is the internal diameter of the inner tube and t is the tube wall thickness. On substituting the actual values of d and t as mentioned in previous section, the value of hoop stress obtained is 19.12 MPa. Since the material used for inner and outer tube is low carbon steel EN1A which has a yield stress of 240 MPa, the hoop stress developed is much less than the yield stress and the factor of safety achieved is 12.55.

4.5 DESIGN OF EXPERIMENTS AND TAGUCHI ANALYSIS

In order to find the values of parameters used in the design of the MR damper piston assembly which give maximum magnetic flux density at the gap where MR fluid flows, a three factor and three level experiment is designed for Taguchi analysis. The parameters and their levels are given in Table 4.4. Fluid flow gap is an important parameter and Krishna et al. (2017) have shown that, a fluid flow gap of around 1 mm is found satisfactory in most cases. Hence, this value and two values in the neighborhood of this value were chosen as the three levels for the fluid flow gap parameter. As the inner diameter of the inner tube is already selected, the outer diameter of the piston assembly is also fixed. The thickness of the aluminum inner sleeve is fixed at 1 mm and the thickness of outer sleeve is fixed as 3 mm. Hence the fluid flow gap is varied by varying the radius if the piston core r_c as shown in Figure 4.10.

Table 4.4 Parameters and their levels for Taguchi analysis

Parameter	Level 1	Level 2	Level 3
Fluid flow gap (g)	0.8 mm	1 mm	1.2 mm
Flange thickness (t_p)	12 mm	13 mm	14 mm
Copper winding wire gauge (w_g)	22	24	26

Flange thickness influences the area available for the propagation of the electromagnetic flux lines as well as the volume of MR fluid actuated in the fluid flow gap. The total length of the piston assembly is fixed. Hence flange thickness is varied by changing the height of the coil area h as shown in Figure 4.10. The levels for the wire gauge of the copper winding are chosen as 22, 24 and 26 AWG, as wires of gauge lower than 22 or higher than 26 are not suitable for the intended application. Wires of gauge lower than 22 are thicker and fewer turns of winding are possible in a given space but they can carry more current. Hence to obtain the same number of ampere-turns, a larger current need to

be supplied, which in turn consumes more power. Wires of gauge higher than 26 are very thin and as a result, higher number of turns are possible in a given space but it can only support a very low value of current. Based on practical experience, 500 turns are possible with 26-gauge wire, 400 turns with 24-gauge wire and 300 turns with 22-gauge wire in the available space for electromagnetic coil. Since there are three factors and there are three levels for each factor, the L9 orthogonal array is used to carry out the experiments for Taguchi analysis as shown in Table 4.5.

Table 4.5 L9 orthogonal array for Taguchi analysis

Exp. No.	Factor 1	Factor 2	Factor 3
1	1	1	1
2	1	2	2
3	1	3	3
4	2	1	2
5	2	2	3
6	2	3	1
7	3	1	3
8	3	2	1
9	3	3	2

The experiments are run using Finite Element Method Magnetics (FEMM) software. FEMM is a software package which uses Finite Element Method (FEM) to solve electromagnetic problems (Baltzis (2008). FEMM is an open-source software which is accurate, simple and has low computational cost. The MR damper piston assembly is analyzed as a 2D axisymmetric magnetostatic problem in FEMM. For the piston core, piston rod and outer sleeve, 1010 steel is selected from the soft magnetic materials group as its magnetic properties are very similar to the EN1A low carbon steel which is actually used for fabrication. The B-H curve for 1010 steel as available in FEMM is shown in Figure 4.7 (a). For MR fluid, a non-linear B-H relationship was defined using the B-H curve of MRF-132DG as given in Figure 4.7 (b). For the inner sleeve, top plate and bottom plate, aluminum 1100 was selected. For the electromagnetic coil, the current was specified as 1 A. For the runs with 22-gauge copper wire, 300 turns were specified, for the runs with 24-gauge copper wire, 400 turns were specified and for the runs with 26-gauge copper wire, 500 turns were specified. Since both aluminum and copper are paramagnetic materials, they have a relative permeability value of unity.
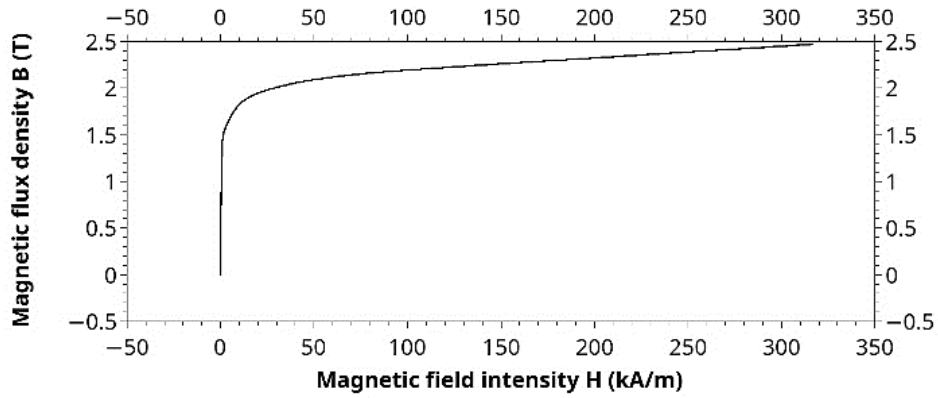
(a)
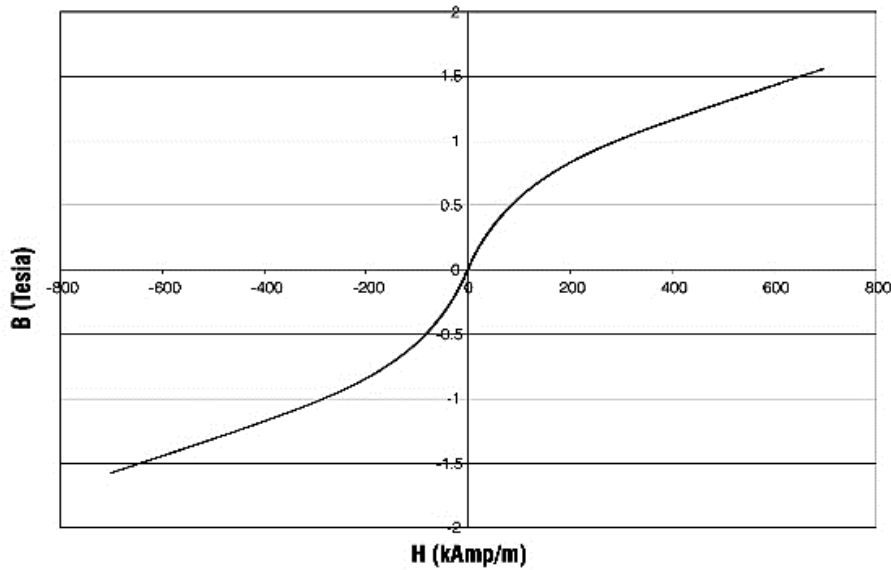
(b)

Figure 4.7 **(a)** B-H curve of 1010 steel **(b)** B-H curve of Lord MR fluid MRF-132DG

The magnetic flux density at the gap where MR fluid flows is the output or response for each experimental run. There are two such gaps in the MR damper piston assembly where activation of the MR fluid happens, one at the upper region and the other at the lower region of the piston assembly. Hence the average of the magnetic flux densities at these two regions is taken as the response for each experimental run. The results of these experimental runs along with the factors assigned to the L9 orthogonal array is given in Table 4.6. Using the Taguchi method, the variation in the response is analyzed using a suitably chosen signal-to-noise (SN) ratio, as given by Montgomery (1997). This SN ratio is formulated using the quadratic loss function and its equation which is widely applicable for 'larger the better' scenario is given in

$$SN_L = -10 \log \left(\frac{1}{n} \sum_{i=1}^{n} \frac{1}{y_i^2} \right) \tag{4.4}$$

74

Table 4.6 FEMM results with factors assigned to L9 orthogonal array

Exp. No.	Fluid flow gap (g) (mm)	Flange thickness (t_p) (mm)	Copper winding wire gauge (w_g) (AWG No.)	Magnetic flux density- Upper (T)	Magnetic flux density- Lower (T)	Avg. magnetic flux density at fluid flow gap (T)
1	0.8	12	22	0.1442	0.1465	0.14535
2	0.8	13	24	0.1831	0.1862	0.18465
3	0.8	14	26	0.2021	0.2049	0.2035
4	1	12	24	0.183	0.187	0.185
5	1	13	26	0.2046	0.2082	0.2064
6	1	14	22	0.1366	0.139	0.1378
7	1.2	12	26	0.2078	0.2122	0.21
8	1.2	13	22	0.1325	0.1354	0.13395
9	1.2	14	24	0.1718	0.1753	0.17355

The 'larger the better' condition is used since we want to maximize the magnetic flux density at the gap where MR fluid flows. The main effects plot of SN ratio plotted against different levels of each factor is shown in Figure 4.8. From the plot it can be observed that the copper winding wire gauge has a large effect on the response and 26 AWG copper wire winding gives the maximum flux density at fluid flow gap. Flange thickness is the next significant factor and a value of 12 mm provides the maximum response. Fluid flow gap does not seem to affect the response much, but a value of 0.8mm is found to be optimum from the plot in Figure 4.8.
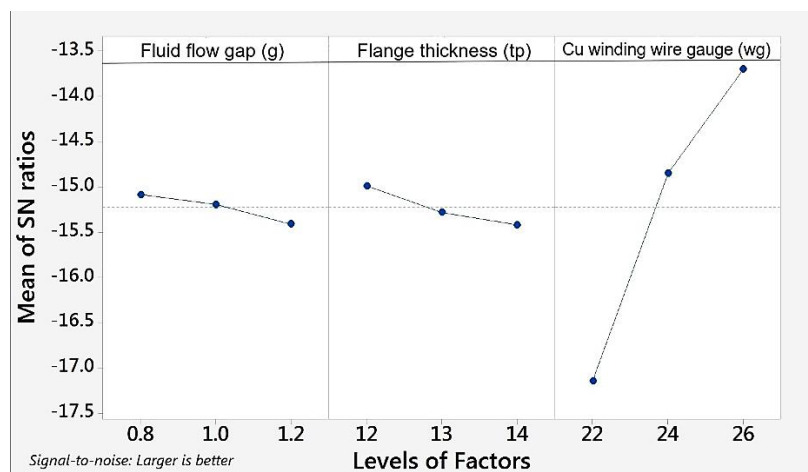
Figure 4.8 SN ratios for different levels of factors

Hence the piston assembly parameters chosen to achieve maximum flux density at the gap where fluid flows are: electromagnetic coil winding of 26 AWG copper wire with

500 turns, piston core flange thickness of 12 mm and fluid flow gap of 0.8 mm. An experimental run using these values of the parameters is done using the FEMM software.

<center>(a)   (b)</center>
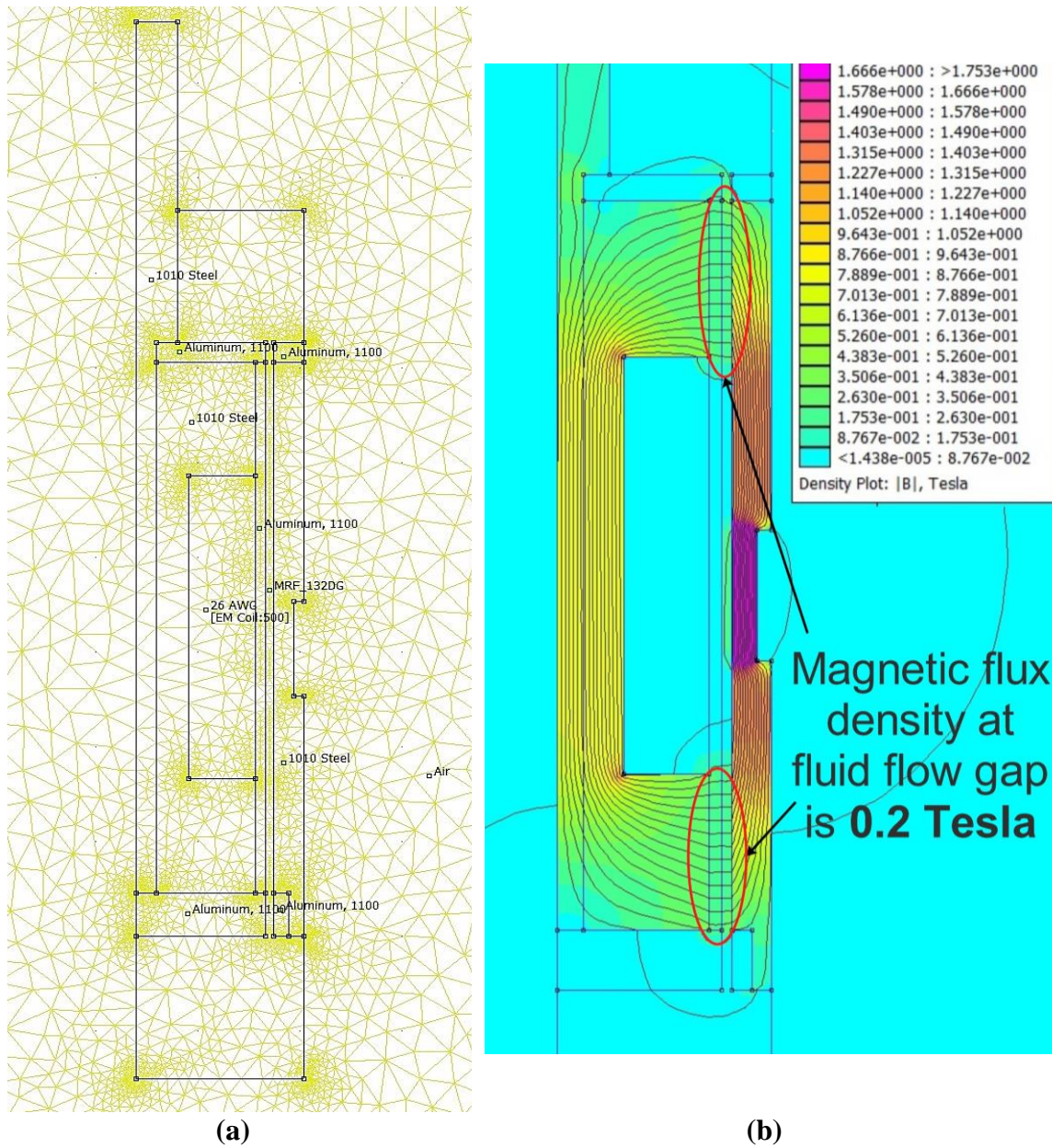
Figure 4.9 **(a)** FEMM mesh of piston assembly half cross section **(b)** FEMM contour plot of piston assembly half cross section showing magnetic flux density

The MR damper piston assembly is analyzed as a 2D axisymmetric magnetostatic problem in FEMM. A Dirichlet boundary condition is used along the boundary to keep magnetic flux from crossing the boundary. Though the problem is an open boundary problem, an Open Boundary Builder wizard is used to create a boundary structure that accurately emulates the impedance of an unbounded domain. A triangular mesh was used to discretize the piston geometry in 2D. Automatic meshing was used to generate the initial mesh. Trials were run in FEMM software using a finer mesh as well as a coarser mesh,

<center>76</center>

which showed little change in the contour plot showing magnetic flux density. Hence all further runs were made using automatic meshing.

The triangular meshing of MR damper piston assembly half cross section is shown in Figure 4.9 (a). It also shows the various block labels used for the different components of the piston assembly. Figure 4.9 (b) shows the distribution of magnetic flux lines in the half cross section of the piston assembly for the optimum values of the parameters chosen. The electromagnetic coil is made of 500 turns of 26 AWG electrically insulated copper wire with total resistance of 7.2 Ω. It also shows the magnetic flux density in different regions of the piston assembly. It can be observed that magnetic flux lines are going through the MR fluid in the fluid gap between the piston core flanges and outer sleeve. The magnetic flux density in the MR fluid at this region of the fluid flow gap is 0.2 Tesla.

4.5.1 Validation of FEMM results

In order to validate the results of the FEMM software, an analytical method is developed using electromagnetic circuit theory. The MR fluid flows through the annular space between the outer sleeve and inner sleeve of the piston assembly and hence the MR damper operates in valve/flow mode. The thickness of this annular gap 'g' is 0.8 mm and the total length of travel for the MR fluid through the piston 'L' is 56 mm as shown in Figure 4.10. When electric current is supplied to the electromagnetic coil, a magnetic field is developed at the piston core and the magnetic flux lines begin to flow from north pole to the south pole through the magnetic circuit. In doing so, the magnetic flux lines go through the MR fluid at the annular gap in a direction perpendicular to direction of flow for a total length of 24 mm. Therefore, the volume of MR fluid activated by the magnetic field is 2.056 ml.

As the exact solution to the magnetic circuit in the piston assembly of the MR damper is both complicated and hard to find, an approximate solution is generally used, as in the work by Nguyen et al. (2008). The sketch of the approximate magnetic circuit in the piston assembly of MR damper is shown in Figure 4.10. L is the height of the piston core of MR damper, t_p is the flange thickness of the piston core, r_p is the radius of the piston assembly, r_c is the radius of the piston core, r_o is the outer radius of the hollow piston rod, r_i is the inner radius of the hollow piston rod, g is the width of the fluid flow gap, t_s is the wall thickness of the inner cylindrical sleeve of the piston assembly, h is the height of the annular space available for copper winding and w is the radial width of the annular space available for copper winding.
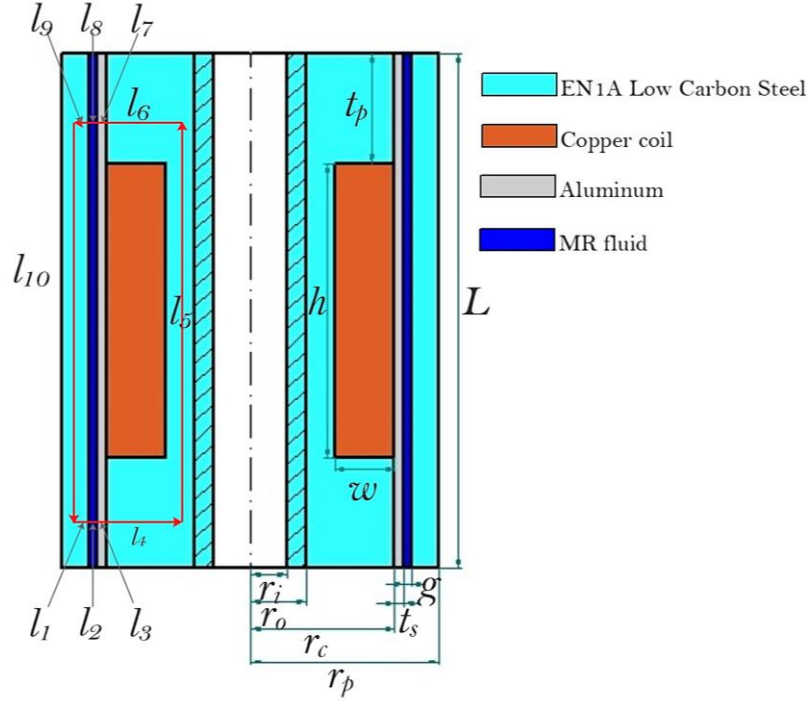
Figure 4.10 Sketch of the cross section of the piston assembly of MR damper showing the magnetic circuit and terminology

The magnetic flux in a magnetic circuit is given by equation 4.5. Here, ϕ is the magnetic flux, *mmf* is magnetomotive force, *I* is the current in electromagnetic coil, *N* is the number of turns in the coil, and *S* is the total reluctance of the magnetic circuit. The reluctance of the nth link in the magnetic circuit S_n is given by equation 4.6, where l_n is the effective length of the nth link in the magnetic circuit and μ_0 is the magnetic permeability of vacuum or free space. The value of μ_0 is a universal constant and it is taken as $4\pi \times 10^{-7}$ H/m. The relative permeability of the nth link in the magnetic circuit is μ_{rn} and a_n is the area of cross-section of the nth link in the magnetic circuit.

$$\varphi = mmf\,/\,total\ reluctance\ =\ NI\,/\,S \tag{4.5}$$

$$S_n\ =\ l_n/(\mu_0\mu_{rn}a_n) \tag{4.6}$$

The total reluctance of the magnetic circuit *S* is the sum of the reluctance of the *n* links in the magnetic circuit. Therefore, referring to the path of the magnetic flux shown in Figure 4.10, total reluctance of the magnetic circuit is given by

$$S =\ S_1 +\ S_2 +\ S_3 + \cdots +\ S_{10} \tag{4.7}$$

Since the design of the MR damper piston assembly is symmetric, $l_9 = l_1$, $l_8 = l_2$, $l_7 = l_3$ and $l_6 = l_4$ and so, $S_9 = S_1$, $S_8 = S_2$, $S_7 = S_3$ and $S_6 = S_4$. Hence,

$$S = 2(S_1 +\ S_2 +\ S_3 +\ S_4) +\ S_5 +\ S_{10} \tag{4.8}$$

The relative permeability, cross-sectional areas and effective lengths of the links as shown in Figure 4.10 are as follows:

$\mu_{r1} = \mu_{r4} = \mu_{r5} = \mu_{r10}$ = relative permeability of low carbon steel EN1A, taken as 1200 according to Parlak and Engin (2013). μ_{r2} = relative permeability of MRF-132DG, MR fluid from Lord Corporation, taken as 3.5 according to Parlak et al. (2010). μ_{r3} = relative permeability of aluminum, taken as 1, as it is a paramagnetic material.

$l_1 = (r_p - r_c - g - t_s)/2; \quad l_2 = g; \quad l_3 = t_s; \quad l_4 = r_c - [(r_c - w + r_i) / 2]; \quad l_5 = l_{10} = L - t_p$

The cross-sectional areas of the links in the magnetic circuit are:

$a_1 = 2\pi [r_p - 0.75(r_p - r_c - g - t_s)] t_p ; \quad a_2 = 2\pi (r_c + t_s + 0.5g) t_p ; \quad a_3 = 2\pi (r_c + 0.5t_s) t_p ;$

$a_4 = 2\pi (r_c - w) t_p ; \quad a_5 = \pi [(r_c - w)^2 - r_i^2] ; \quad a_{10} = \pi [r_p^2 - (r_c + t_s + g)^2].$

The numerical values of the parameters used in the piston assembly geometry are given in Table 4.7.

Table 4.7 Numerical values of the parameters used in the piston assembly geometry (All values are in mm)

Parameter	Numerical value
L	56
t_p	12
r_p	20.45
r_c	15.65
r_o	6
r_i	4
g	0.8
t_s	1
w	6.5

On evaluating equation 4.8 with the help of equation 4.6, the value of total reluctance of the magnetic circuit S is 1.82771×10^6 A/Wb. Since there are 500 turns in electromagnetic coil of the MR damper, the flux generated in the magnetic circuit for 1 A electric current is 2.7874×10^{-4} Wb using equation 4.5. Using the law of conservation of magnetic flux, the magnetic flux density at the gap where MR fluid flows is given by

$$B_2 = \varphi / a_2 \tag{4.9}$$

On substituting, its value is found to be 0.212 Tesla. This value of magnetic flux density closely agrees with that obtained using FEMM in the previous section. In order to have a good response time for the MR damper, the inductance of the electromagnetic coil was kept as low as possible. The inductance L of a coil is given by

$$L = \frac{N^2 \mu_0 \mu_r a}{l} \qquad (4.10)$$

On substituting the numerical values, the value of inductance of the electromagnetic coil in the MR damper is found to be 626.7 mH. As the resistance of the coil *R* is 7.2 Ω, the time constant of the *LR* circuit *(L/R)* is 87 ms which is a reasonably good value.

4.6 FABRICATION AND EXPERIMENTAL TESTING OF MR DAMPER

The design of the MR damper is finalized based on the results of the previous sections and fabrication of the parts is done. Optimum values of the parameters are used in the fabrication of the MR damper piston assembly and the parts thus fabricated are shown in Figure 4.11 (a). The parts of the base valve as carried over from the existing passive damper is shown in Figure 4.11 (b) as an exploded view. The final assembled MR damper is shown in Figure 4.11 (c).

The MR damper was tested at Rambal Ltd, Chennai using the damping force testing machine, the schematic of which is shown in Figure 3.11 (a) of chapter 3. This machine is equipped with a hydraulic actuator with a capacity of 1 ton and maximum stroke of 250 mm. The hydraulic actuator is operated using a servo valve that can provide a sinusoidal excitation with a maximum velocity of 1000 mm/s. The DC current required for damper operation is supplied using the Lord Wonder box that can supply a maximum of 2A current. Since the Wonder Box used is not provided with an indicator for current being supplied, a DC Clamp meter was used to measure current supplied to the MR damper. The damper testing machine is also equipped with Interface make load cell with a loading capacity of 1200 kg. The generated data was recorded using National Instruments USB 6221 Data card logger, capable of recording 10,000 samples per second. LabVIEW software was used to interface with the data logger and the servo control valve during the tests.
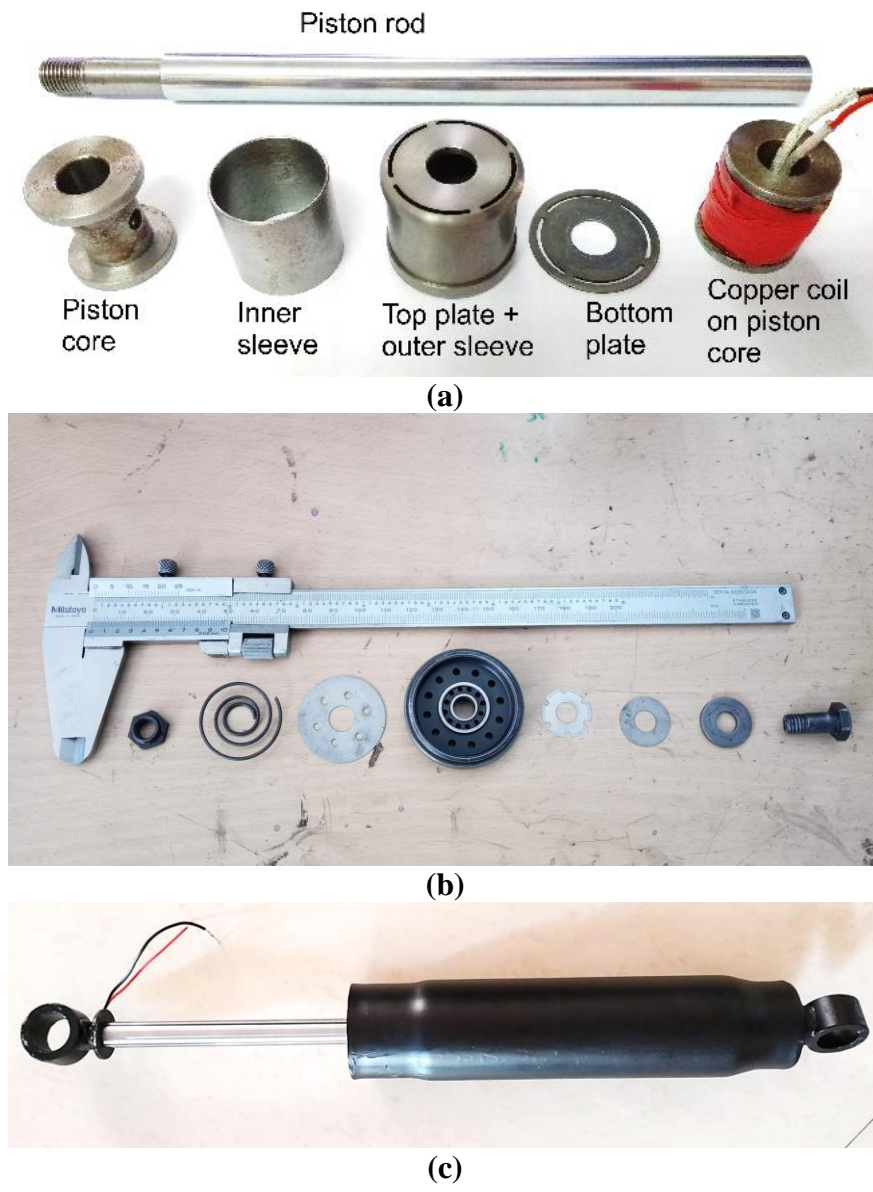
Figure 4.11 **(a)** MR damper piston assembly **(b)** Base valve of MR damper **(c)** Twin tube MR damper

The MR damper is loaded onto the damper testing machine, ensuring there is no play between the damper eye and the machine clamps. The damper is given excitation for a few seconds to ensure that there is no leakage of any kind and that the damper is operating smoothly. This part of the testing procedure is known as priming. It also takes care of any settling of the MR fluid in the damper during idle condition. After the damper is primed satisfactorily, the data recording can be commenced. The amplitude of excitation is kept constant at 20 mm while varying the excitation frequency to obtain different piston velocities. This is repeated for different values of current supplied. The frequency of excitation along with values of current supplied are provided in Table 4.8. The maximum

piston velocity was limited to 500 mm/s which corresponds to 3.98 Hz at 20 mm amplitude. This is because it was learnt from the industrial collaborator that during normal operation of the damper in the passenger van, the damper velocity rarely exceeds 500 mm/s. Also, it was observed in the passive damper test results that the maximum damping force is reached at 500 mm/s piston velocity. After this, the damping force does not increase much with increase in piston velocity. Limiting the maximum piston velocity to 500 mm/s also prevents over stressing of the MR damper which may result in undesirable consequences like overheating of the damper or leakage of MR fluid.

Table 4.8 Values of current supplied and sinusoidal excitation frequencies

Currents supplied (A): 0, 0.25, 0.5, 0.75, 1, 1.5			
Velocity amplitude of excitation (mm/s)		Frequencies of excitation (Hz)	
V1=50	V6=300	f1=0.4	f6=2.39
V2=100	V7=350	f2=0.8	f7=2.79
V3=150	V8=400	f3=1.19	f8=3.18
V4=200	V9=450	f4=1.59	f9=3.58
V5=250	V10=500	f5=1.99	f10=3.98

4.7 EXPERIMENTAL RESULTS OF MR DAMPER TESTING

The plots of damper force vs input displacement for different values of current supplied to the MR damper is repeated for different frequencies of excitation as shown in Figure 4.12 (a)-(j). The amplitude of sinusoidal displacement is fixed at 20 mm. According to generally accepted convention, damper force in compression is taken as positive and that during rebound is taken as negative. Similarly, extension of the damper from mean position is taken as positive displacement and compression of the damper from mean position is taken as negative displacement. The force vs displacement plots thus plotted have a rectangular shape for lower frequencies of input oscillations and transform into elliptical shape when the input oscillation frequency is increased. This can be explained by the fact that the coulomb damping plays a predominant role in the damping force generation at low frequencies and viscous damping effects take over a more prominent role in the damping force at higher frequencies of input at constant amplitude of vibration.
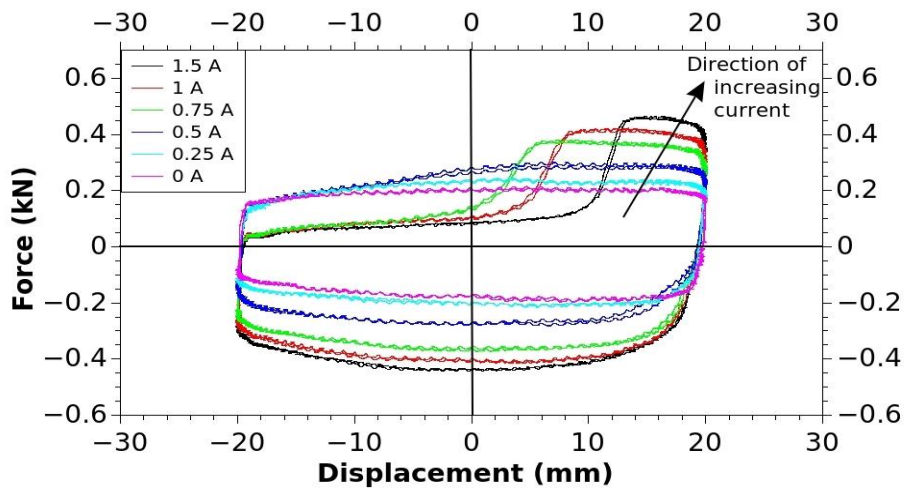
(a) At 50 mm/s peak velocity and 0.4 Hz
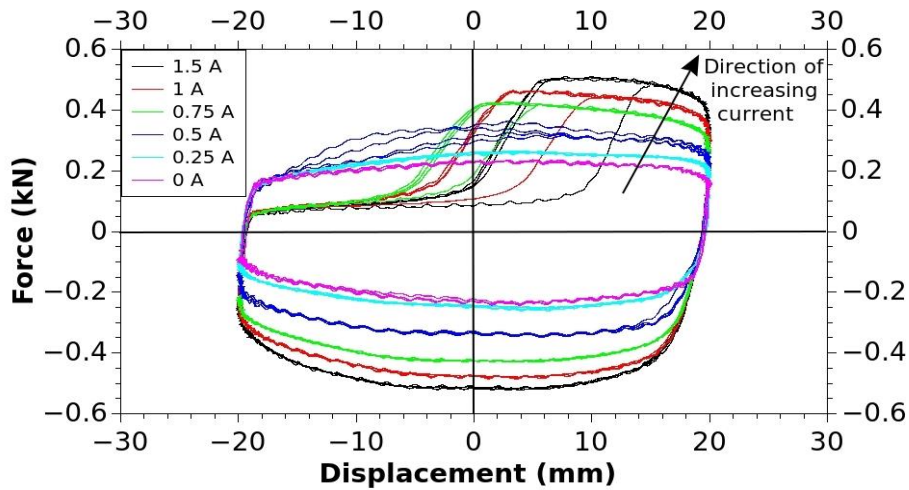
(b) At 100 mm/s peak velocity and 0.8 Hz
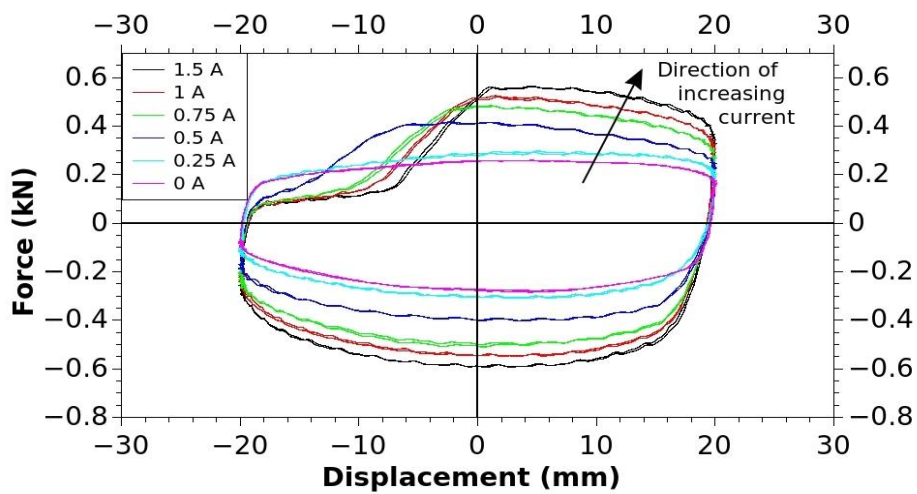
(c) At 150 mm/s peak velocity and 1.19 Hz
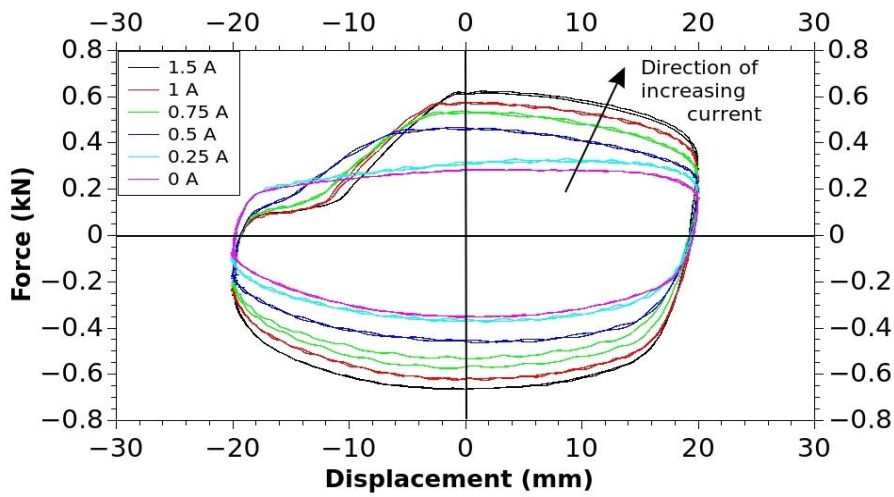
(d) At 200 mm/s peak velocity and 1.59 Hz
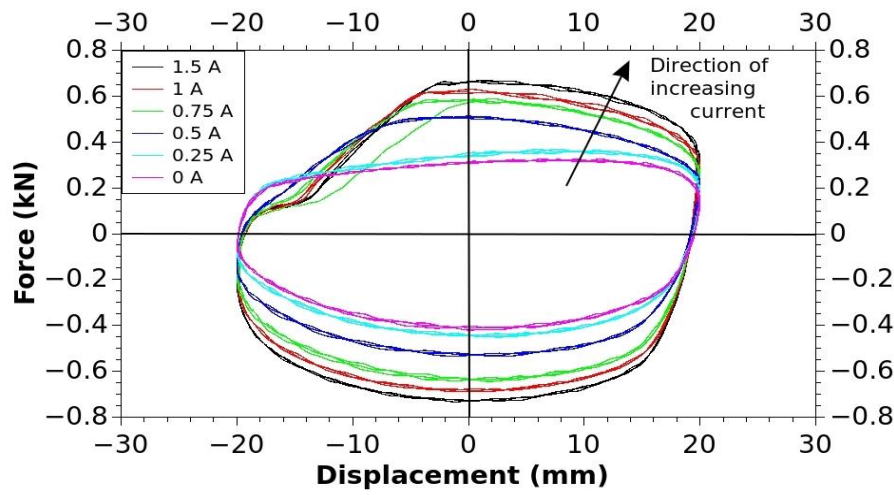
(e) At 250 mm/s peak velocity and 1.99 Hz
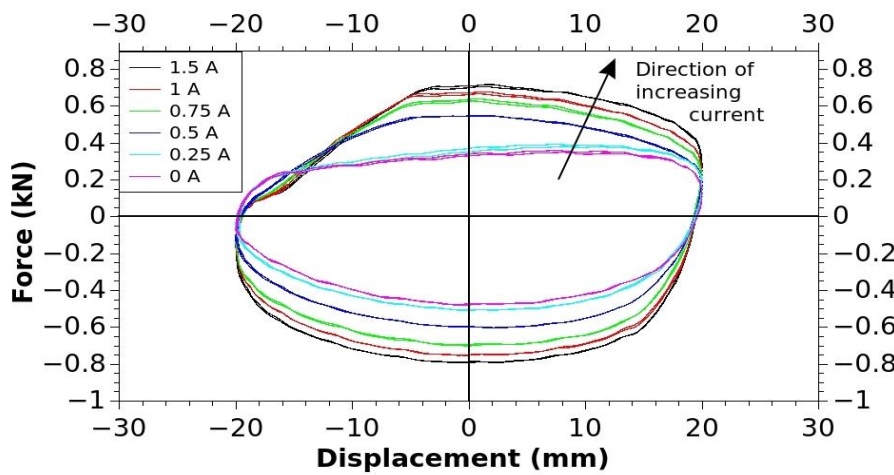
(f) At 300 mm/s peak velocity and 2.39 Hz
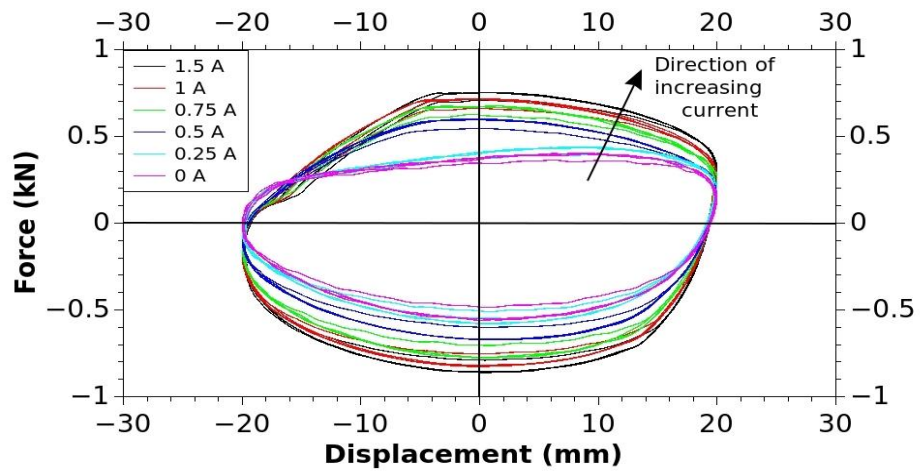
(g) At 350 mm/s peak velocity and 2.79 Hz
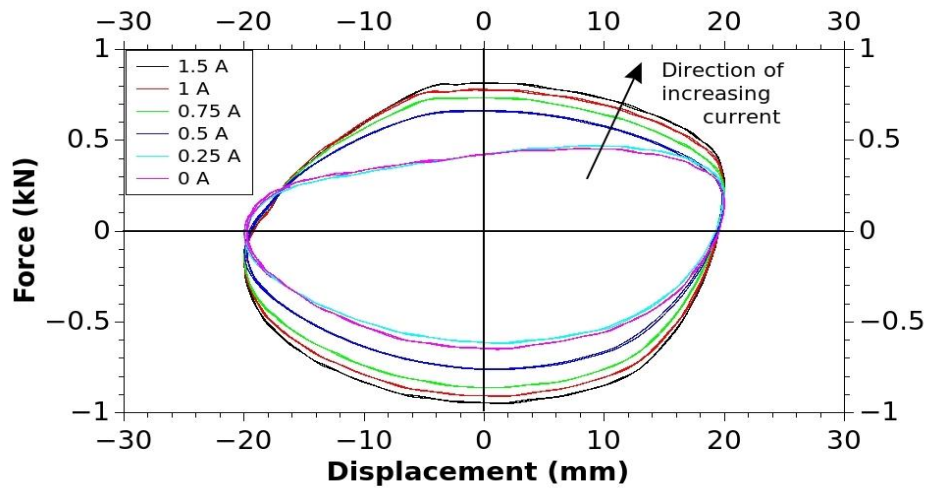
(h) At 400 mm/s peak velocity and 3.18 Hz
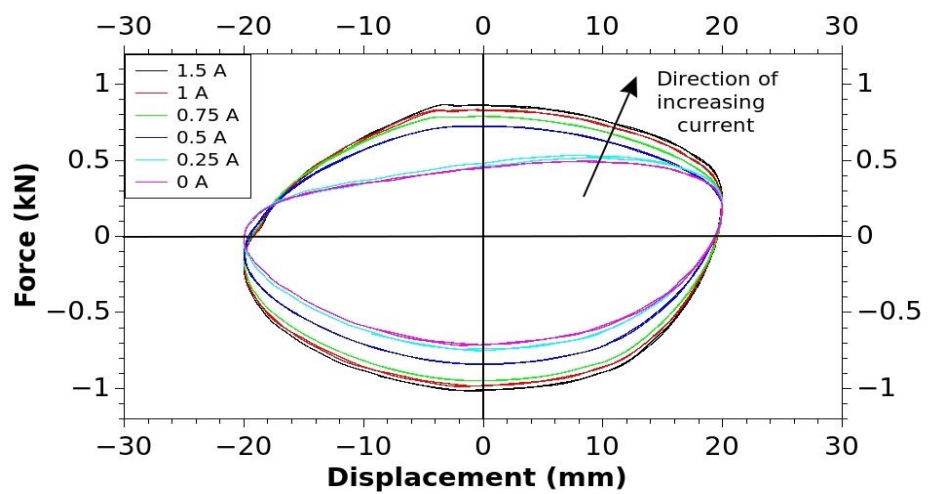
(i) At 450 mm/s peak velocity and 3.58 Hz
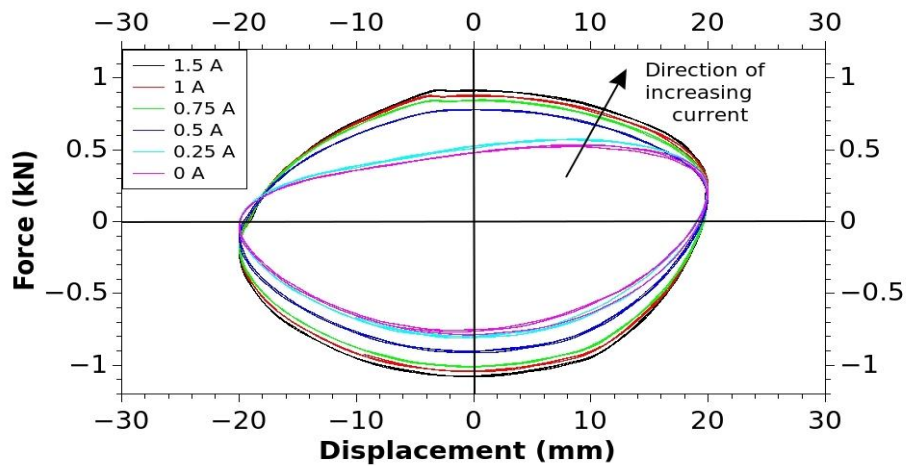
(j) At 500 mm/s peak velocity and 3.98 Hz

Figure 4.12 Damper force vs displacement at different values of current supplied

For any given frequency of input oscillation to the MR damper, it can be observed that the damper force values increase with increase in the current supplied. The size of the force vs displacement loops increases with increase in current indicating an increase in the energy dissipated by the damper in one cycle. This demonstrates the intended effect of using MR fluid in the damper along with an electromagnetic coil in the damper piston.

Another observation is that the force vs displacement plots are wavy for lower frequencies of oscillation and become progressively smoother as the frequency of input oscillation increases. The MR damper exhibits predictable behaviour at lower values of current supplied for frequencies f1 to f4. But for the same frequencies, when the value of current supplied exceeds 0.5A, there is a fall in the rebound force values as seen in the second quadrant of the force vs displacement plots. As the curve is experimentally traced clockwise, this area represents the beginning of the extension stroke after completion of a compression stroke of the damper. This may be due to the increased resistance to flow of MR fluid through the piston during the compression stroke. Consequently, some quantity of MR fluid flows to the outer tube through the base valve instead of flowing across the piston to the top side of the inner tube. This results in a drop in the fluid pressure in the top side of the inner tube during the beginning of the extension stroke, giving us a lower value of damping force.

Figure 4.13 shows the plot of damper force vs piston velocity. Here, the velocity values used are the maximum velocity at each frequency of oscillation. As per convention, compression force is taken as negative and rebound force is taken as positive. Taking the

force and velocity values to be of the same sign, damper force vs velocity plots for rebound are in the first quadrant and those for compression are in third quadrant. Hence, each data point on this plot corresponds to one frequency of input oscillation, thus giving us ten data points for compression and ten for rebound. Such a plot is shown for six different values of current supplied to the MR damper along with passive damper in Figure 4.13. The plots clearly show that the damper force values are higher for higher values of current supplied at any given frequency of input oscillation and this is true for both compression and rebound force values. It can be seen that the damping force curves generated by the MR damper during compression at different velocities fully envelop the force curve for the passive damper.
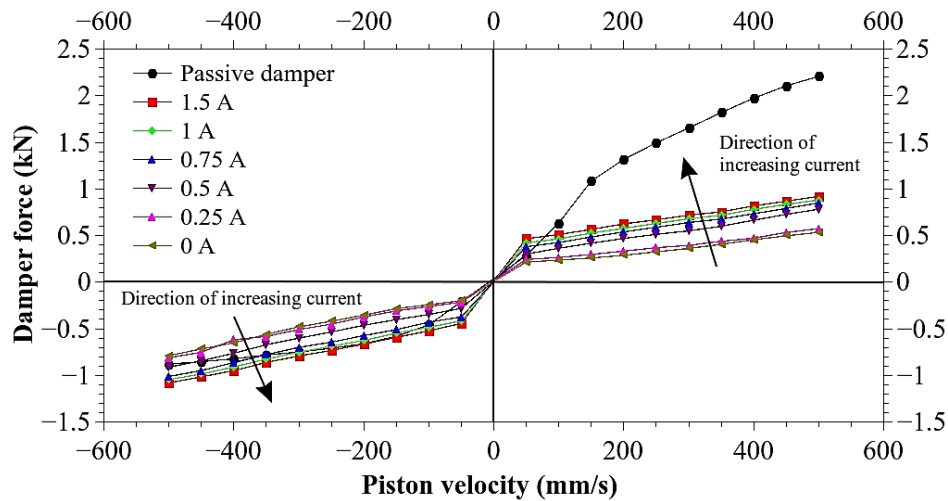
Figure 4.13 Damper force vs velocity for different values of current supplied

Passive dampers used for automotive applications have unsymmetrical damping force by design, requiring higher damping force during rebound than in compression stroke. Hence it can be seen in Figure 4.13 that the damping force for passive damper is much higher in first quadrant representing rebound stroke than in third quadrant representing compression stroke. However, the design for MR damper is a symmetric one with nearly same forces generated during compression as well as rebound stroke. It is also an added advantage to MR damper that the damper force can be controlled by changing the current supplied.

From Figure 4.12, it can also be seen that the MR damper was experimentally tested at actual values of vibration amplitude and velocities which the damper will experience in the field. As a result, the MR damper can be readily and successfully used as a replacement for the passive damper in the passenger van for which it was designed.

Similar to the method employed as mentioned in the section on characterization of twin-tube passive damper, the energy dissipated by the MR damper in one cycle for the same ten frequencies of excitation at three different values of current supplied, 0 A, 0.75 A and 1.5 A is calculated. Using these values, the equivalent damping coefficient for the MR damper at the corresponding value of frequency of excitation and current supplied is also evaluated. These values are shown in comparison to those for the passive damper in Table 4.9. From Table 4.9, it can be noted that the energy dissipated per cycle is increasing with increase in the frequency of excitation for both passive damper and MR damper at any current. The passive damper shows a decreasing trend of equivalent damping coefficient with frequency of excitation, except for the first two frequencies f1 and f2. Whereas, MR damper shows a decreasing trend with frequency for all frequencies and all currents tested. There is dissimilarity in the trend of equivalent damping coefficient with frequency for passive damper and MR damper only for the first two frequencies f1 and f2. For frequencies higher than f2, both passive and MR damper show the same decreasing trend. This is so because, in the case of passive damper, the requirement of the vehicle in which it is used is such that it requires high damping force near its frequencies of resonance. Hence, it can be seen in Table 4.9 that the equivalent damping coefficient for passive damper is highest at around 1.2 Hz (f3) and reduces on either side of this value of frequency.

Table 4.9 Comparison of energy dissipated and equivalent damping coefficient of the passive damper and MR damper for different frequencies of excitation

Frequency of excitation (Hz)		Energy dissipated per cycle (J)				Equivalent damping coefficient (kNs/m)			
		Passive damper	MR damper at 0 A	MR damper at 0.75 A	MR damper at 1.5 A	Passive damper	MR damper at 0 A	MR damper at 0.75 A	MR damper at 1.5 A
f1	0.4	15.425	14.227	20.925	21.446	4.884	4.505	6.625	6.791
f2	0.8	32.620	16.084	25.446	28.223	5.164	2.546	4.029	4.468
f3	1.19	51.704	18.354	30.083	34.174	5.503	1.953	3.202	3.637
f4	1.59	63.938	21.219	34.103	38.929	5.093	1.690	2.716	3.101
f5	1.99	73.222	23.929	38.356	43.044	4.660	1.523	2.441	2.739
f6	2.39	80.800	26.694	41.062	46.898	4.282	1.415	2.176	2.485
f7	2.79	85.231	29.757	44.804	49.966	3.869	1.351	2.034	2.268
f8	3.18	94.150	33.748	48.907	54.653	3.750	1.344	1.948	2.177
f9	3.58	100.14	36.491	53.330	57.923	3.543	1.291	1.887	2.049
f10	3.98	106.14	37.722	56.599	61.072	3.378	1.200	1.801	1.943

It can also be observed that in the case of MR damper, for any given frequency of excitation, both the energy dissipated in one cycle and equivalent damping coefficient are increasing with increase in current supplied. The plot of ratio of equivalent damping coefficient of MR damper to that of the passive damper vs frequency of excitation for three different currents supplied, 0 A, 0.75 A and 1.5 A is shown in Figure 4.14.
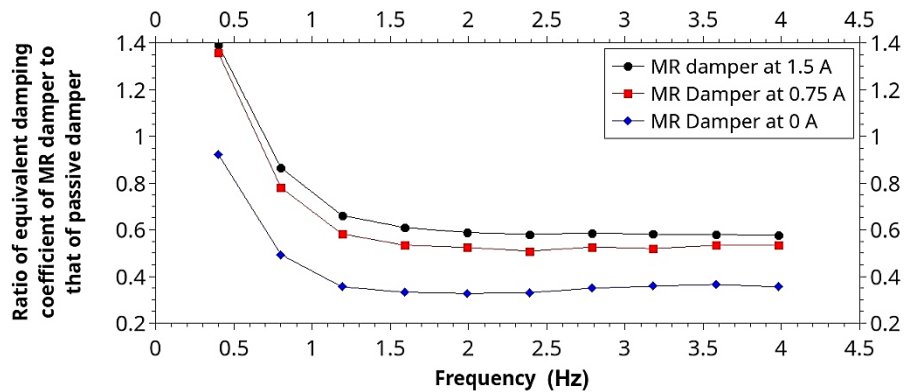
Figure 4.14 Ratio of equivalent damping coefficient of MR damper to that of the passive damper vs frequency of excitation for three different currents supplied

It can be observed that for any given value of frequency, the ratio of the damping coefficient increases with current supplied. However, for any given value of current, the damping coefficient of the MR damper reduces with increase in frequency when compared with that of the passive damper. Also, the plot area can be divided into two regions, one for which the frequency is less than 2 Hz and the other for which the frequency is more than 2 Hz. For the region having frequency less than 2 Hz, the ratio of equivalent damping coefficient is very sensitive to variation in frequency. In this region, the ratio reduces rapidly with increase in frequency. For the region above 2 Hz, the ratio is fairly insensitive to variation in frequency and changes very little with increase in frequency. This behaviour of the MR damper should be duly noted while designing the control system for the semi-active vehicle suspension using this MR damper. The equivalent damping coefficient of passive damper is higher than MR damper for most of the frequency range. This is due to the asymmetric force profile of the passive damper as can be seen in Figure 4.13. The damping force generated by passive damper during rebound is much higher to that generated during compression, for the same piston velocity. This behaviour is by design of the passive damper and a requirement of the passive suspension of the vehicle in which it

is used (passenger van). However, the design for MR damper is a symmetric one with nearly same forces generated during compression as well as rebound stroke.

Plots of the dynamic range of the MR damper vs the frequency of input oscillation for both compression and rebound loading is shown in Figure 4.15. Here, the dynamic range is the ratio of the maximum force generated by the MR damper at the highest value of current supplied (1.5 A) to the maximum force generated by the MR damper at the lowest value of current supplied (0 A). It can be observed from this plot that the dynamic range of the MR damper reduces with increase in the input oscillation frequency.
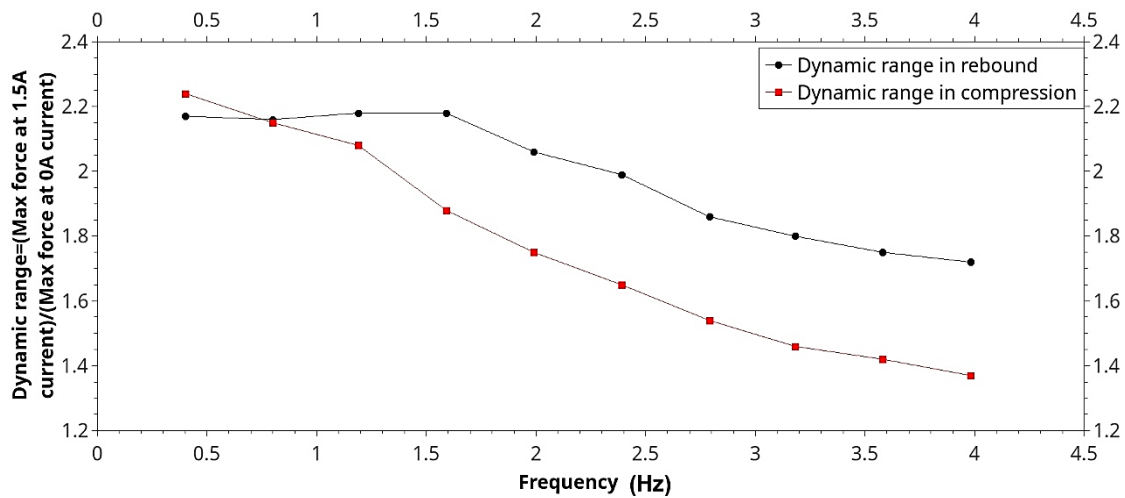
Figure 4.15 Dynamic range of MR damper vs frequency of input oscillations

4.8 MATHEMATICAL MODELING OF MR DAMPER

In order to develop a suitable control strategy for incorporating this MR damper into a semi-active suspension system, a mathematical model representing the hysteretic behaviour of the MR damper is needed. The Bouc-Wen model is one such model which is widely accepted among the engineering community because various types of hysteretic shapes can be represented by it, using simple differential equations, as shown by Wang and Liao (2011). Equations 4.11 and 4.12 are the equations for the Bouc-Wen model as given by Spencer et al. (1997). They are the equations for the total damping force as predicted by the model and the evolutionary variable respectively. Here, k_0 is the stiffness coefficient, c_0 is the viscous damping coefficient and x_0 is the initial displacement of the spring taken as -0.02 m in the present study. The force offset due to the initial displacement of the damper is corrected by introducing f_o in equation 4.11, according to Kwok et al. (2007). The five remaining parameters in the equations below determine the shape of the hysteresis curve.

$$F(t) = c_0\dot{x} + k_0(x - x_0) + \alpha z - f_0 \qquad (4.11)$$

$$\dot{z} = -\gamma|\dot{x}|z|z|^{n-1} - \beta\dot{x}|z|^n + A\dot{x} \qquad (4.12)$$

In order to find the numerical values of these parameters in the Bouc-Wen model, the optimization toolbox of MATLAB was used. Genetic algorithm (GA) was employed to find the best combination of the parameters to generate data points that is very near to the experimental values. The error between experimental and generated values was found using the fitness function as given in equation 4.13, according to Peng et al. (2018). Here, number of samples is n, experimental force obtained is F_d^{exp} and simulated force is F_d^{Sim}.

$$Fitness \; = \frac{\sqrt{\frac{1}{n}\sum_{i=1}^{n}(F_{d,i}^{exp} - F_{d,i}^{Sim})^2}}{\sqrt{\frac{1}{n}\sum_{i=1}^{n}(F_{d,i}^{exp} - \frac{1}{n}(\sum_{i=1}^{n}F_{d,i}^{Sim}))^2}} \qquad (4.13)$$

The values of the parameters thus obtained for one of the frequencies of input damper oscillation of 1.59 Hz (f4) at three different values of current is shown in Table 4.10.

Table 4.10 Parameter values for Bouc-Wen model for the MR damper at 1.59 Hz (f4) input damper oscillation

At 0 A current		At 0.5 A current		At 1 A current	
Parameter	Value	Parameter	Value	Parameter	Value
c_0	750	c_0	1050	c_0	1400
k_0	2050	k_0	2050	k_0	2050
alpha	200	alpha	350	alpha	450
beta	-900	beta	-950	beta	-950
gamma	2000	gamma	2000	gamma	2000
A	500	A	220	A	280
n	3.2	n	3.2	n	3.2
f_0	70	f_0	70	f_0	70

Figure 4.16 shows the comparison between experimental and simulated damper force for three different values of current supplied 0 A, 0.5 A and 1 A at 1.59 Hz input oscillation plotted against displacement. It can be observed that the experimental and simulated values of damping force agree very well with each other except in the second quadrant for the highest level of current supplied. In the experimental data, a fall in the damping force value is observed in this region.
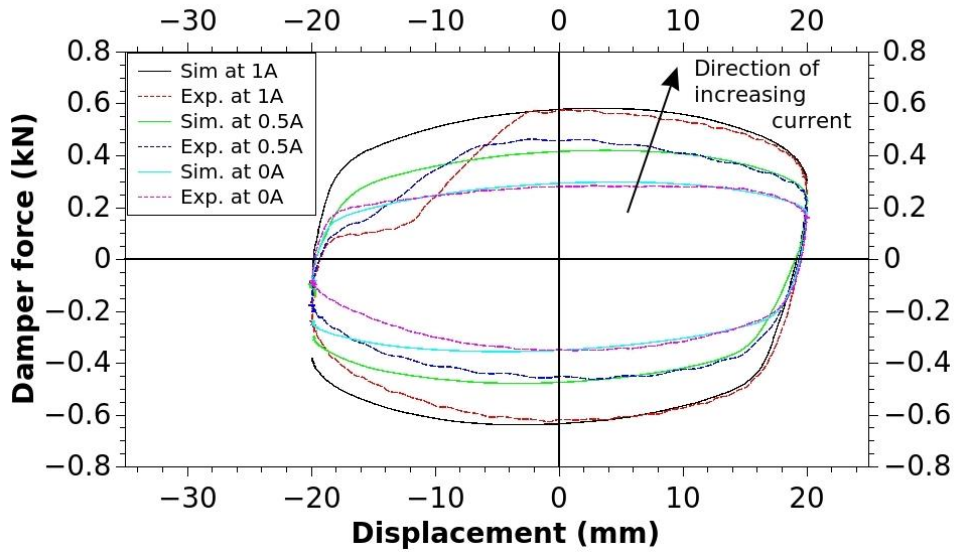
Figure 4.16 Comparison of experimental and simulated damper force vs displacement at 1.59 Hz input oscillation for different currents

Figure 4.17 shows the comparison of experimental and simulated damper force vs velocity at 1.59 Hz input oscillation for three different currents supplied. The experimental and simulated curves agree well except in the first quadrant for the highest level of current supplied. As the curve is experimentally traced anti-clockwise, this area represents the beginning of the extension stroke after completion of a compression stroke of the damper. There is a drop in the experimentally obtained value of damping force in this region and the reason for this drop has been explained in the beginning of this section.
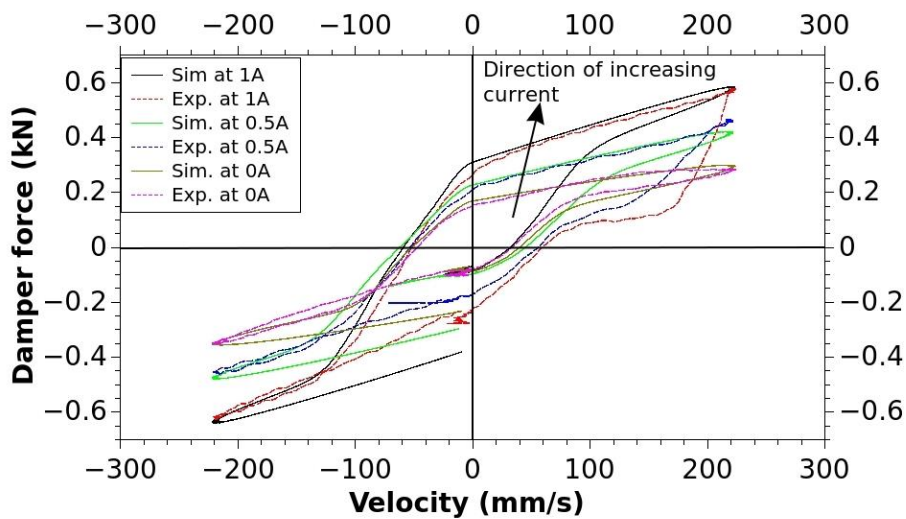
Figure 4.17 Comparison of experimental and simulated damper force vs velocity at 1.59 Hz input oscillation for different currents

Figure 4.18 shows the comparison of experimental and simulated damper force vs time at 1.59 Hz input oscillation for the three different currents supplied. The simulated force curve closely follows the experimental force curve.
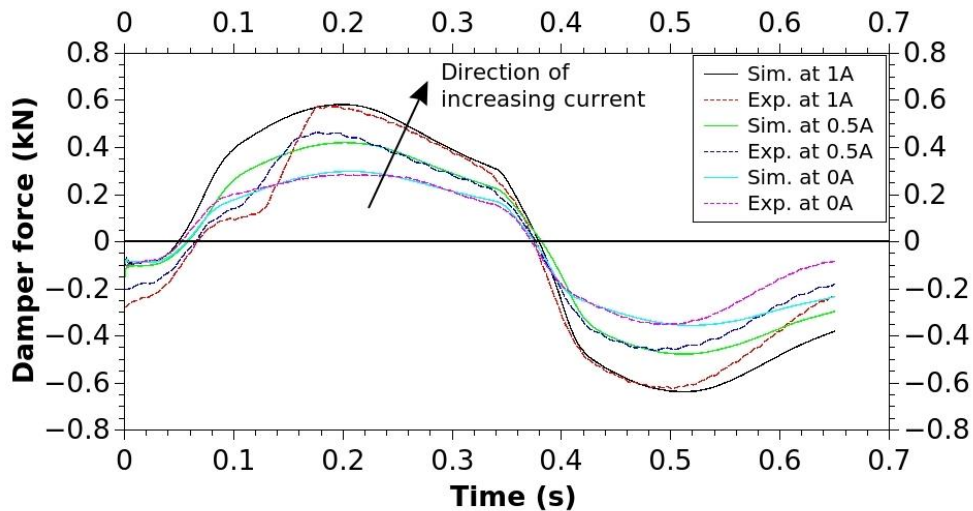
Figure 4.18 Comparison of experimental and simulated damper force vs time at 1.59 Hz input oscillation for different currents

The Bouc-Wen model curves along with the values of parameters are shown for one of the damper oscillation frequencies to demonstrate the method used. The same method can be applied for all the combinations of input damper oscillation frequency and current supplied to obtain the Bouc-Wen model curve and corresponding values of parameters. It can be observed from Table 4.10 that out of the eight parameters, four parameters c_0, α, β and A change with the value of the current and the other four (k_0, γ, n and f_0) do not change with the value of the current supplied but only depend on the frequency of the input oscillation. Hence, in Bouc-Wen model of the MR damper, the damper force is function of both current supplied I and the damper velocity $\dot{x}$.

4.9 PID CONTROL OF MR DAMPER

In order to implement a one degree of freedom Proportional-Integral-Derivative (PID) controller in time for a semi-active suspension system incorporating this MR damper, the damper velocity is assumed to be constant at 200 mm/s which corresponds to V4 in Table 4.8. The variation of the maximum damping force in compression and rebound obtained experimentally at f4 in Table 4.8 (1.59 Hz) with current supplied is modeled as a polynomial as shown in Figure 4.19.
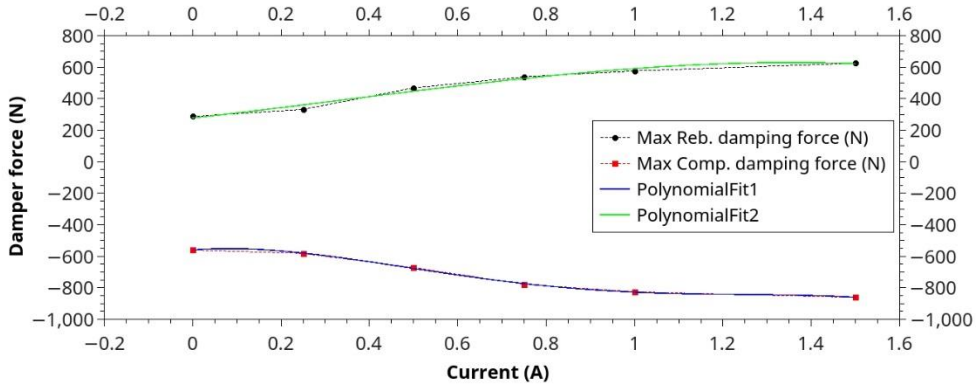
Figure 4.19 Variation of maximum damping force with current supplied at 1.59 Hz input oscillation

The polynomial equation for actual damper force F_a as a function of current supplied, I is given by

$$F_a(I) = a_0 + a_1I + a_2I^2 + a_3I^3 + a_4I^4 \qquad (4.14)$$

The coefficients of the polynomial fit to the experimental data as shown in Figure 4.19 is given in Table 4.11.

Table 4.11 Numerical values of the coefficients of polynomial in equation 4.14 fit to experimental damping force data

Parameter	a_0	a_1	a_2	a_3	a_4
Rebound	-560.441	231.48	-1581.3449	1523.53866	-440.791
Compression	277.3438	310.3244	117.463275	-114.03485	0

With damper velocity as constant, the damping force is now a function of current alone and a simple PID control can now be implemented with the help of MATLAB Simulink. The damper is assumed to be in compression. The Simulink model of PID control of MR damper is shown in Figure 4.20.
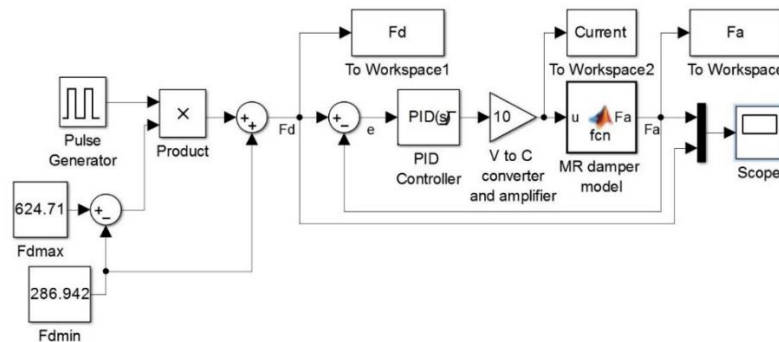
Figure 4.20 Simulink model of PID control of MR damper

The desired damping force profile F_d is taken as a pulse input with a period of 2 s and pulse width of 0.5 s. The lower value of the pulse is the damper force at minimum current 0 A and the higher value of the pulse is the damper force at maximum current 1.5 A. The actual damping force F_a is calculated based on the polynomial model given by Eq. 14. The error which is the difference between the desired force and actual force is fed to the PID controller block. The controller signal is routed through a voltage to current converter and suitably amplified and fed to the MR damper model. Care is taken to see that the current fed to the MR damper never exceeds the safe maximum limit. The force vs time plot showing the variation of desired and actual damping force using PID controller is shown in Figure 4.21.
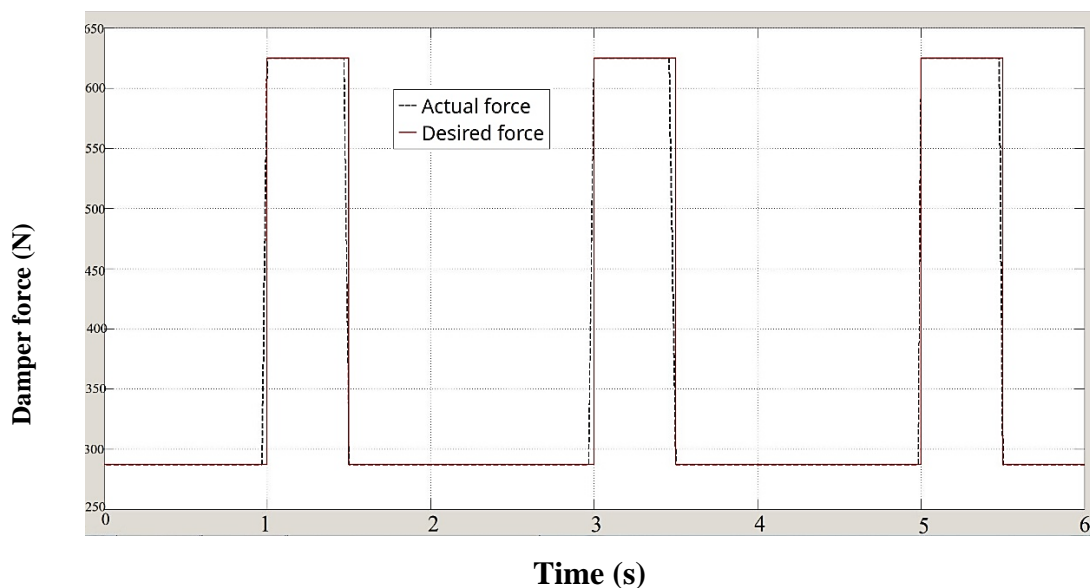
Figure 4.21 Force vs time for MR damper using PID control

It can be seen from Figure 4.21 that the actual force of the MR damper tracks very closely the desired damping force profile as a function of time. This shows that a PID controller can be effectively used to control the damping force of the MR damper in the time domain with very little lag and no overshoot.

4.10 SUMMARY

A twin tube MR damper was designed based on the damping values of a passive damper used in a passenger van. The damper piston was modified to accommodate an electromagnetic coil in order to generate a magnetic field in the fluid flow gap for the activation of MR fluid. The MR damper operates in valve mode. The magnetic flux density at the fluid flow gap is evaluated analytically by using laws of the magnetic circuit and the

value obtained closely matches with that obtained using the FEMM software. Experiments were carried out by using commercially available MR fluid by Lord Corporation. Different levels of current were supplied to the MR damper and input oscillations at operating frequencies and amplitudes were given. The force generated by the damper and displacement of the damper piston were measured. The plots of force vs displacement reveal that the damping force increases with the current supplied and hence demonstrates the field dependent yield stress nature of the MR fluid. Plots of force vs velocity further confirm the MR behaviour which shows that for a particular damper piston velocity, as the current supplied increases, the damping force increases.

Mathematical models were developed to simulate the MR damper behaviour at various values of current supplied and input oscillation frequency. The Bouc-Wen equation was used to simulate the force vs displacement, force vs velocity and force vs time plots. The eight parameter values needed for this simulation were arrived at using GA provided in the optimization toolbox of the MATLAB software. This was done for selected values of current supplied at a particular input oscillation frequency to demonstrate the method used. The plots showing comparison between experimental and simulated values for 1.59 Hz input oscillation frequency for three values of current 0 A, 0.5 A and 1 A confirm close agreement and validates the parameter values used. The maximum input current used for the MR damper operation is 1.5 A and this can be comfortably supplied by the vehicle's alternator or battery without any modifications needed. The power requirement of the MR damper is less than 18 W, which is very low. A PID controller was used to track the desired damping force in the time domain. A pulse waveform was used as input. The actual force of the MR damper tracks the desired force closely with very little lag and no overshoot. Hence the MR damper can be used to implement a semi-active suspension system in the passenger van with PID controller. Thus, this twin tube valve-mode MR damper can be used as a replacement for the passive damper in the passenger van. The twin-tube MR damper fabricated and tested in this chapter has been used in the next chapter, where the commercial MR fluid is replaced by MR fluid synthesized in the laboratory.

CHAPTER 5

SYNTHESIS OF MAGNETORHEOLOGICAL FLUID AND ITS APPLICATION IN A TWIN-TUBE VALVE MODE AUTOMOTIVE DAMPER

5.1 INTRODUCTION

In the previous chapter, a commercially available MR fluid was used in the development of a twin-tube MR damper. In this chapter, a carbonyl iron particle and silicone oil-based MR fluid is synthesized in the laboratory for use in the twin-tube MR damper. Methods and procedure to prepare the MR fluid in laboratory are presented. This chapter also explains the experimental characterization of MR fluid in a rheometer with MR device cell. A novel method of expressing the controllable damping force in terms of MR fluid characteristics and damper geometry is presented.

5.2 METHODOLOGY

The methodology followed in the present work is shown in Figure 5.1. MR fluid was prepared in the lab by mixing magnetizable particles with the carrier fluid. This fluid was experimentally characterized in the rheometer to understand the behaviour of MR fluid under an externally applied magnetic field. The variation of the shear stress of MR fluid with strength of the magnetic field as well as the shear rate is studied. This behaviour is modelled mathematically using the HB model which accounts for the non-linear behaviour of the shear stress at high shear rates, particularly the shear thinning and shear thickening of non-Newtonian fluids. The variation of the parameters of the HB model with the strength of the applied magnetic field is modelled as a polynomial so that the shear stress vs shear rate behaviour of MR fluid can be calculated at any given strength of the magnetic field.

The prepared MR fluid was used as the working fluid in the twin-tube MR damper. This MR damper was experimentally characterized using damping force testing machine. The plots of force vs displacement, force vs peak velocity and force vs real-time velocity at various currents supplied to the MR damper were determined. The MR damper was further analysed to arrive at the force generated value with the help of the relationship between flow rate through MR valve and the resulting drop in pressure across it. A non-

dimensional scheme was used to relate the MR fluid properties and geometry of the MR damper to arrive at the force developed by the MR damper.
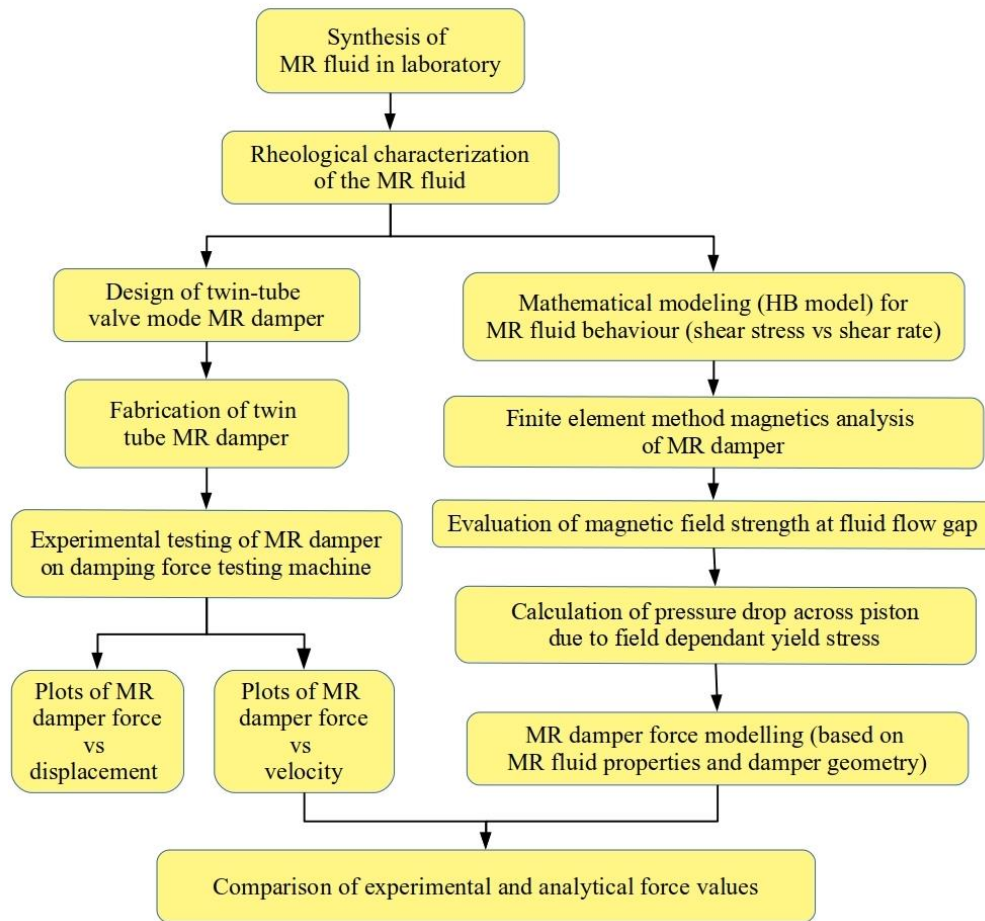
Figure 5.1 Flowchart of methodology followed

5.3 SYNTHESIS AND CHARACTERIZATION OF MR FLUID

5.3.1 Synthesis of MR fluid

Magneto-rheological fluid is a smart fluid whose behaviour can be controlled with the use of a magnetic field. It is a multi-phase non-colloidal suspension of magnetizable particles in non-magnetic fluid known as the carrier liquid. The particles are usually micron sized and a stable and inert fluid like silicone oil, hydrocarbon oil, mineral oil and paraffin oil can be used for the liquid phase according to Goldasz and Sapinski (2015). In the present case, the particles used are magnetic iron particles obtained from thermal decomposition of iron pentacarbonyl because of their higher limit of magnetic saturation, high purity and unique particle shape, as shown by Wereley (2013). The magnified image of carbonyl iron powder (CIP) taken using a field emission scanning electron microscope (FESEM) of Zeiss

Sigma make is shown in Figure 5.2. It can be seen that the particles are roughly of spherical shape which is advantageous from tribological point of view. The CIP was also analysed in a particle size analyser CILAS 1064 to find the distribution of size of the particles. The mean diameter was found to be 9.38 µm and 50% of the mass of the sample is made of particles having diameter less than 8.24 µm. The histogram of the results showing the distribution of particle size is presented in Figure 5.3. It can be observed that it has a narrow distribution about the mean size.
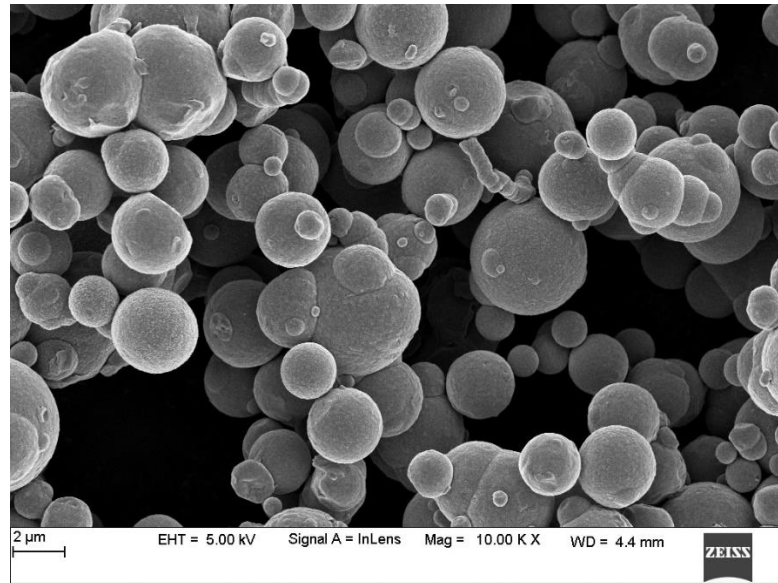
Figure 5.2 FESEM image of CIP

The carrier liquid used is silicone oil as it has a high range of operating temperature, ideal viscosity, is chemically inert and inexpensive. The mixing ratio used is 70% by volume of silicone oil and 30% by volume of CIP as this is found to be the ideal ratio for application in an automotive damper according to Acharya et al. (2019). The criteria used for choosing this mixing ratio is the magnitude of the damping force developed for a given amount of current supplied. The yield stress developed by the MR fluid in the presence of a magnetic field increases when the proportion of CIP is increased. However, it would also result in higher off state viscosity of the fluid according to Acharya et al. (2019). This would result in a lower value of dynamic range of the MR damper and it is undesirable. Moreover, using Particle Swarm Optimization (PSO), Gurubasavaraju et al. (2017) found that 31-33% of volume fraction of CIP with silicone oil as carrier fluid is the optimum ratio for application in MR damper. A small quantity of SKF grease (about 2 gms for 100 ml of silicone oil), which is a thixotropic material is used as an additive. According to Ashtiani et al. (2015), it works as an anti-settling agent and enhances the stability of the iron particles

in the suspension. Experimental sedimentation study of MR fluid with CIP as magnetizable particles and silicone oil as carrier fluid was carried out by Allien et al. (2019). The composition of the MR fluid used is also the same (70:30 by volume). Sedimentation ratio was calculated for different time interval. The sedimentation ratio was found to be 0.022 after 24 hours which showed that the MR fluid had good sedimentation stability.
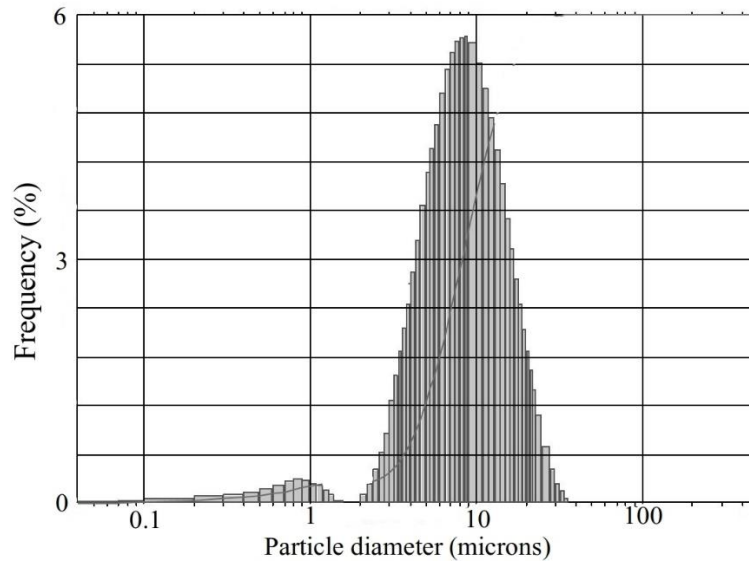
Figure 5.3 Particle size distribution of CIP used in MR fluid synthesis

Initially, the additive grease is added to silicone oil while it is kept stirring in a beaker, with the help of a mechanical stirrer. Mixing process is continued for a couple of hours until the mixture becomes a homogenous solution. The CIP particles are then added in small quantities to this liquid as it is kept constantly stirring. Finally, the suspension is stirred for 8 hours to obtain MR fluid.

5.3.2 Characterization of MR fluid

In order to evaluate the rheological properties of the prepared MR fluid, it was characterized in a rheometer. A rheometer provides experimental results of variation of shear stress and viscosity of the fluid with change in shear rate. A parallel plate type rheometer by Anton Paar, model number MCR 702, as shown in Figure 5.4 was used for this purpose. A magnetorheological device cell was employed to apply different magnetic field strength to the test fluid sample. The electromagnetic coils, parallel plates and the MR fluid sample is maintained at a constant temperature of 25 °C by circulating cooling water around it.
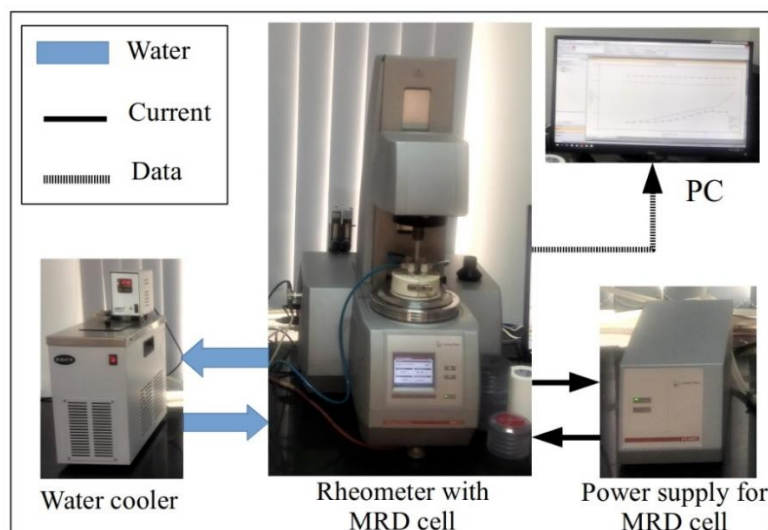
Figure 5.4 Rheometer device with magnetorheological device cell

A small quantity of a homogenous sample of the MR fluid is placed between the parallel plates of the rheometer. A fixed gap is maintained between the parallel plates and one of the plates is rotated at different speeds to vary the shear rate. The rheometer is constructed in such a way that a very precise control of the speed of rotation of the parallel plates is possible. In this way, the shear rate of the fluid sample is varied from 0.1 to 1000 /s on a logarithmic scale. The fluid shear stress is measured at different values of shear rate and it is repeated for different values of magnetic field strength applied through the magnetorheological device cell. The values of current supplied to the cell, the resulting magnetic field strength values and magnetic field levels are given in Table 5.1. It was found that for current values above 4 A, magnetic saturation of MR fluid sets in and there is no appreciable rise in the shear stress values.

Table 5.1 Different levels of magnetic field strength applied in rheometer

Magnetic field level	Current supplied to MR device cell (A)	Magnetic field strength (kA/m)
H0	0	0
H1	0.75	29.148
H2	1.5	53.797
H3	3	95.162

The plot of shear stress vs shear rate for four different values of magnetic field strength applied is shown in Figure 5.5. As can be seen from this plot, MR fluid exhibits linear behaviour when there is no externally applied magnetic field (off-state) denoted by 0 kA/m. However, when an external magnetic field is applied, the variation of shear stress

with shear rate becomes non-linear and we get a higher value of shear stress as the applied magnetic field strength is increased from H1 to H3. Hence the MR fluid exhibits Newtonian behaviour at H0 magnetic field level and Non-Newtonian behaviour when magnetic field level is H1, H2 or H3. In the case of non-linear behaviour, as the slope of the curve is decreasing with an increase in shear rate, it is said to exhibit shear thinning behaviour.
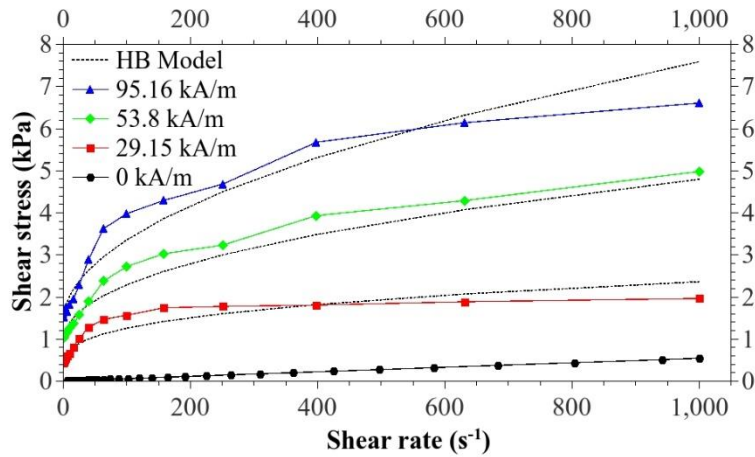
Figure 5.5 Variation of shear stress with shear rate for different magnetic field strengths and corresponding HB model fit

A very well-known and versatile mathematical representation of the non-linear behaviour of Non-Newtonian fluids is given by the Herschel-Bulkley (HB) model. HB model was used instead of Bingham plastic model because it closely predicts the actual non-linear behaviour of the MR fluid under high rate of shear in the post-yield region. Bingham plastic model assumes that the dynamic viscosity remains constant and the fluid exhibits linear Newtonian behaviour in the post-yield condition, which is an approximation for simplification. H-B model better characterizes the shear-thinning and shear-thickening behaviour of non-Newtonian fluids. According to Goldasz and Sapinski (2015), it consists of three parameters as given in equation 5.1 and relates the shear stress τ of MR fluid to the shear rate $\dot{\gamma}$

$$\tau = \tau_0 + \mu\dot{\gamma}^p \tag{5.1}$$

where τ_0 is the yield stress whose value depends on the strength of the applied magnetic field. The parameter μ is indicative of the viscosity of the fluid and p is the flow behaviour index. The RheoCompass software of the rheometer provides the values of the parameters in the HB model equation by fitting curves to the experimental data. The values of the parameters are given in Table 5.2 and the corresponding curves fit to the

experimental curves are shown by dotted lines in Figure 5.5. It can be observed that the HB model curves agree well with the measured experimental data.

Table 5.2 Parameters of the Herschel-Bulkley (HB) model for different levels of magnetic field strength

Magnetic field strength (kA/m)	Herschel-Bulkley model parameters		
	τ_0 (kPa)	μ (kPa-s)	p
29.148	0.27211	0.22073	0.32546
53.797	0.88387	0.18193	0.44424
95.162	1.4046	0.19476	0.50066

The flow behaviour index p represents the nonlinearity of variation of shear stress with shear rate for a non-Newtonian fluid like MR fluid. For values of p<1, the fluid behaviour is said to be shear thinning and for values of p>1, the fluid exhibits shear thickening. The values of p shown in Table 5.2 are all less than 1, indicating a shear thinning behaviour of MR fluid. This means that there is a fall in the rate of increase of shear stress with shear rate, at high shear rates.

By studying the variation of the HB model parameters with the strength of the magnetic field, it is possible to estimate their value at any given value of magnetic field strength with a fair amount of accuracy. Graphs are plotted with magnetic field strength on the abscissa and the HB model parameters on the ordinate. Spline curves are drawn through the data points and second order polynomial functions are fit for the curves as shown in Figure 5.6 (a)-(c). The polynomial functions for the HB model parameters are of the form

$$y = a_0 + a_1 x + a_2 x^2 \tag{5.2}$$

where y is any of the three HB model parameter and x is the magnetic field strength.
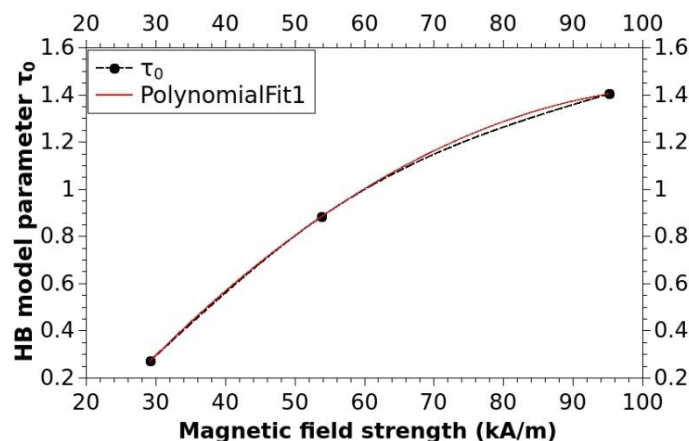
(a)
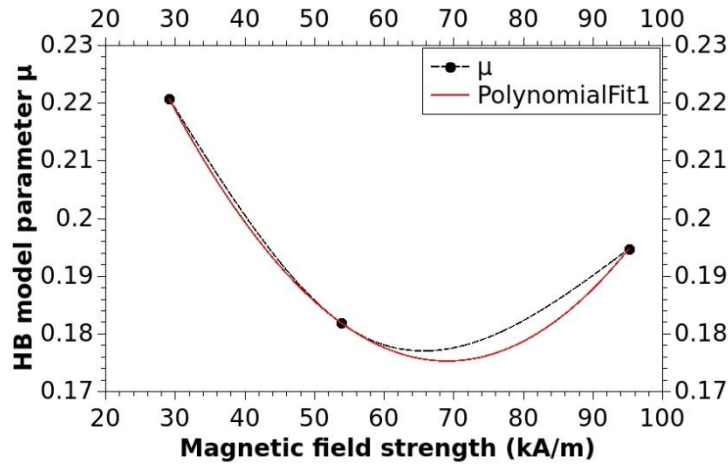
(b)
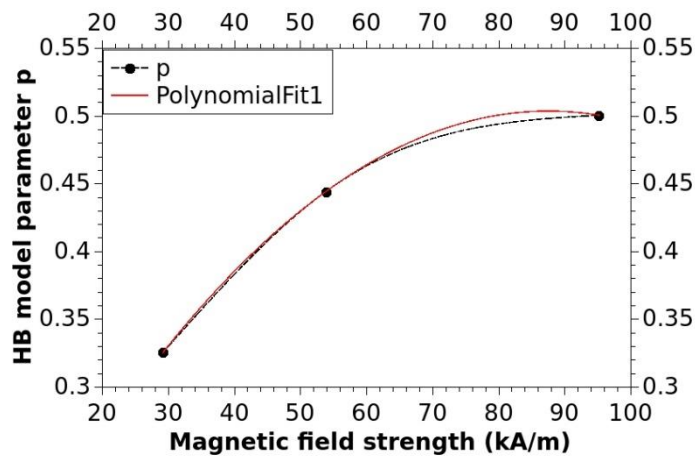
(c)

Figure 5.6 Polynomial fit for variation of the HB model parameters with the strength of the magnetic field **(a)** HB model parameter τ_0 **(b)** HB model parameter μ **(c)** HB model parameter p

In this way, the three parameters of the HB model for MR fluid are expressed as functions of strength of the magnetic field and the coefficients calculated are provided in Table 5.3. Using this, one can calculate the shear stress of MR fluid at any given value of magnetic field strength and shear rate with the help of equation 5.1.

Table 5.3 Values of coefficients for polynomial fit of HB model parameters

HB model parameter	a_0	a_1	a_2
τ_0	-7.418221E-01	4.018580E-02	-1.852667E-04
μ	3.113701E-01	-3.941635E-03	2.854343E-05
p	1.029334E-01	9.159857E-03	-5.233589E-05

Based on the experimental data, the valid range of strength of magnetic field is 20 to 100 kA/m and for shear rate it is 0 to 1000 s^{-1}. In order to validate this, shear stress values of MR fluid are evaluated for a magnetic field strength of say 40 kA/m for shear rate varying between 0 to 1000 /s. This is plotted along with the already known shear stress values for magnetic field strengths H1, H2 and H3 as shown in Figure 5.7.
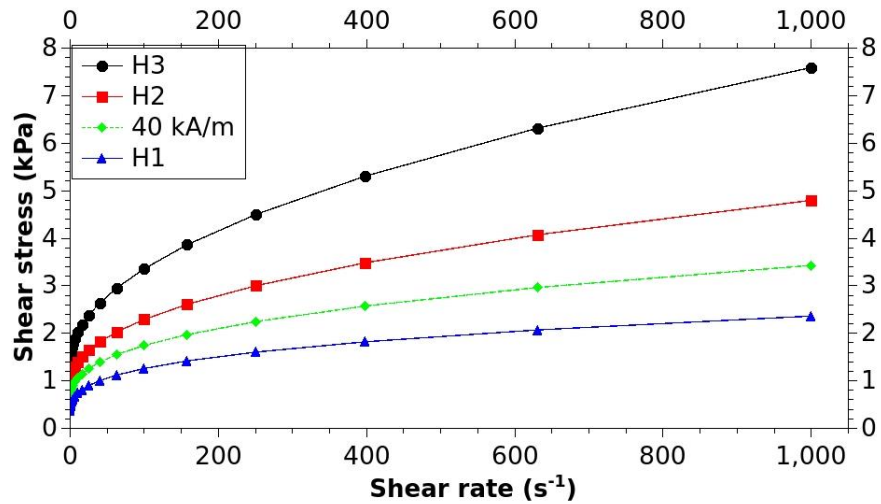
Figure 5.7 MR fluid shear stress vs shear rate for H1-H3 and 40 kA/m

It can be seen in Figure 5.7 that the shear stress vs shear rate curve for MR fluid at a magnetic field strength value of 40 kA/m is as expected and satisfactorily interpolates between the curves for magnetic field strength of H1 and H2.

The rheometer experimental data also provides information about the variation of dynamic viscosity of MR fluid with variation in shear rate. The plot of dynamic viscosity of the MR fluid in the off-state (no magnetic field applied H0) against shear rate on a logarithmic scale is shown in Figure 5.8.
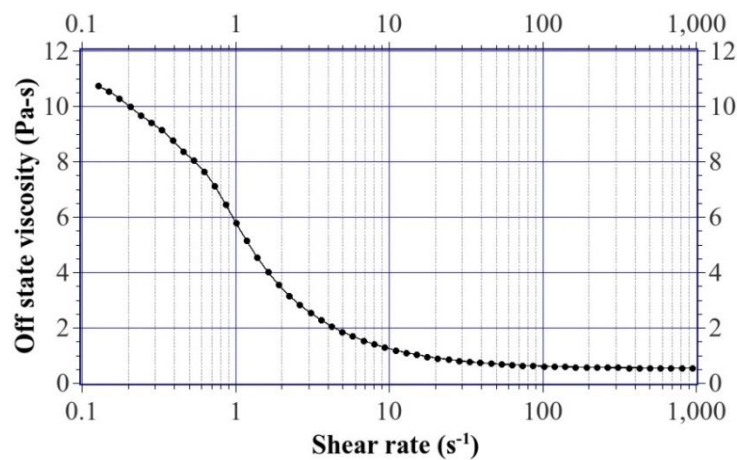
Figure 5.8 Off-state viscosity of MR fluid vs shear rate

It can be observed that the off-state viscosity falls rapidly with increase in the shear rate and reaches a very low value of less than 1 Pa-s at a shear rate of more than 15 s^{-1}, exhibiting shear thinning behaviour.

The variation of the viscosity of MR fluid with shear rate under various strengths of magnetic field is shown in Figure 5.9. As the shear rate is varied over a very wide range, it is plotted on a logarithmic scale. Three curves corresponding to different levels of applied magnetic field of H1, H2 and H3 as detailed in Table 5.1 can be seen.
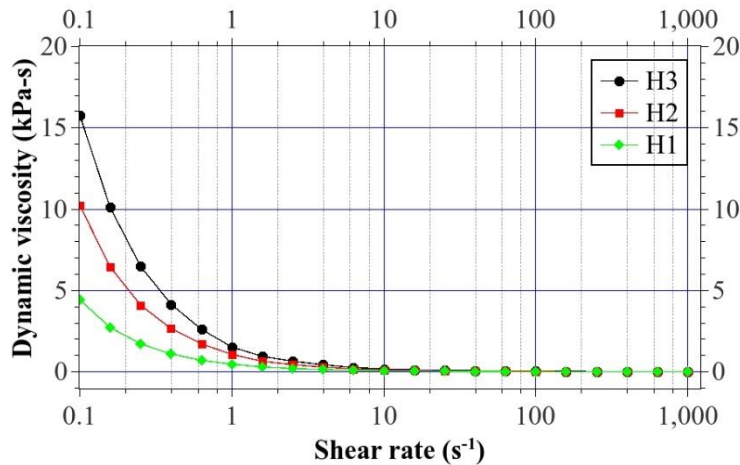
Figure 5.9 Dynamic viscosity vs shear rate for different magnetic field strengths

At very low shear rates of less than 1 s^{-1}, the dynamic viscosity of MR fluid increases significantly with the increase in applied magnetic field strength. However, at higher shear rates of more than 10 /s, the applied magnetic field has very little influence over dynamic viscosity and it attains a very low value.
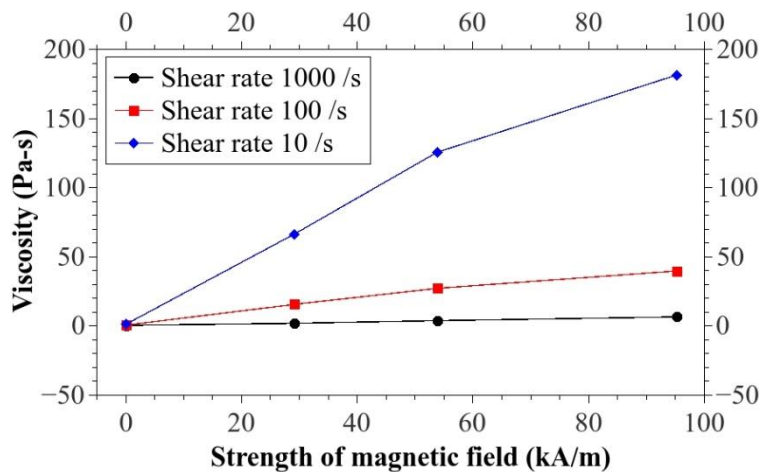
Figure 5.10 Viscosity vs magnetic field strength at constant shear rates

Figure 5.10 shows the variation of viscosity with strength of the applied magnetic field for constant shear rates of 10, 100 and 1000 s^{-1}. This confirms and further corroborates the observation from Figure 5.9 that the magnetic field influences dynamic viscosity of MR fluid only at low values of shear rates of around 10 s^{-1}. At higher shear rates, the dynamic viscosity becomes less sensitive to the strength of the magnetic field and finally approaches a very low value of viscosity when shear rate is higher than 100 s^{-1}.

5.4 DESIGN AND FABRICATION OF MR DAMPER

A twin-tube type MR damper operating in the valve mode was designed and prototype was fabricated as detailed in the previous chapter. An automotive passive damper was experimentally characterized in the damper testing machine to arrive at the forces that the MR damper is required to generate at the specified damper velocities. The design parameters of the MR damper are given in Table 5.4. The electromagnet needed for the activation of MR fluid is housed in the piston assembly and the lead wires for power supply are routed through the hollow piston rod. The MR damper piston which also acts as MR valve has a cross section as shown in Figure 5.11. All the radial measurements in the cross section are measured from piston axis, represented by vertical dashed line.
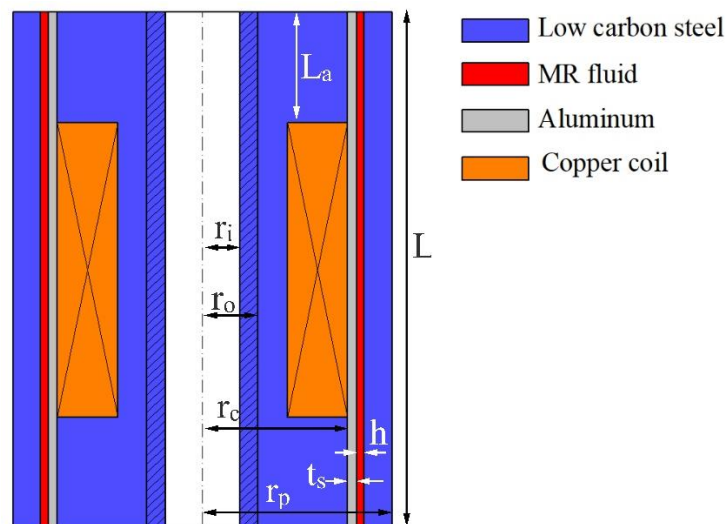
Figure 5.11 Sectional view of MR damper piston

When the piston travels in the cylinder, MR fluid is forced to flow through the annular flow gap formed between two concentric cylinders of the piston assembly. The geometrical design and material of the parts of the piston assembly are such that the magnetic flux lines generated by the electromagnet are made to pass across the MR fluid present in the annular region in a direction perpendicular to the direction of flow of the

fluid. This activates the MR fluid, changing it from a liquid into a semi-solid with a field dependant yield stress. Hence, by controlling the current supplied to MR damper, which in turn controls the strength of the magnetic field at the fluid flow gap, the resistance generated by the MR fluid to the motion of the damper piston can be controlled. This forms the basis of operation of an MR damper capable of generating a variable damper force.

Table 5.4 Design parameters of MR damper

Parameter		Numerical value
Damper related	Stroke of the damper	130 mm
	Fully compressed length of the damper	397 mm
	Length of the outer tube	293 mm
	Outer diameter of the outer tube	70 mm
	Wall thickness of the outer tube	2 mm
	Length of the inner tube	254.7 mm
	Outer diameter of the inner tube	45 mm
	Wall thickness of the inner tube	2 mm
EM coil related	Number of turns of electromagnetic coil (N)	500 turns
	Thickness of the Cu winding wire	26 AWG
	Resistance of copper winding as measured (R)	7.2 Ω
	Inductance of the electromagnetic coil (L_h)	626.7 mH
	Time constant of the circuit (t_p)	87 ms
Piston related	Total length of fluid path in piston (L)	56 mm
	Length of annular active zone ($2L_a$)	24 mm
	MR fluid gap thickness (h)	0.8 mm
	Radius of piston core (r_c)	15.65 mm
	Radius of piston assembly (r_p)	20.45 mm
	Wall thickness of inner sleeve (t_s)	1 mm
	Mean radius of MR fluid annular space (r_c + t_s+0.5h)	17.05 mm
	Mean circumference of MR fluid annular space (w)	107.128 mm
	Area of the piston rod (A_r)	113.1 mm^2
	Area of the piston (A_p)	1313.82 mm^2
	Active MR fluid volume	2.056E-06 m^3
	Gap ratio (h/r_p)	0.03912

This twin tube MR damper is filled with 410 ml of the MR fluid synthesized as detailed in section on synthesis of MR fluid. The inner tube is first completely filled with MR fluid. The base valve fitted to the bottom of the inner tube ensures that the MR fluid is

held inside without leakage. The base valve is actually a set of two non-return unidirectional flow valves with different blow off pressure settings.

Fluid flows from the inner tube to the outer tube only when sufficiently high pressure is developed in the inner tube due to an additional volume of the piston rod entering the cylindrical chamber of the inner tube during the compressive stroke. Similarly, fluid flows from the outer tube to the inner tube during the extension stroke by overcoming the non-return valve in the base valve which has a lower blow off pressure setting. The damper is assembled along with the piston rod guide and dynamic seals to ensure a leak proof operation of the MR damper.

5.5 EXPERIMENTAL RESULTS OF MR DAMPER TESTING

The MR damper was tested in the damper force testing machine at Rambal Ltd, Chennai. The experimental setup is as shown in Figure 5.12. The MR damper is mounted between the fixed jaw and the moving jaw of the machine. The fixed jaw is supported by the horizontal cross member and a force transducer is included between the two to measure the force generated by the MR damper. The moving jaw is fixed to the piston rod of a hydraulic actuator having a stroke of 250 mm and capable of producing a peak force of 9.8 kN.
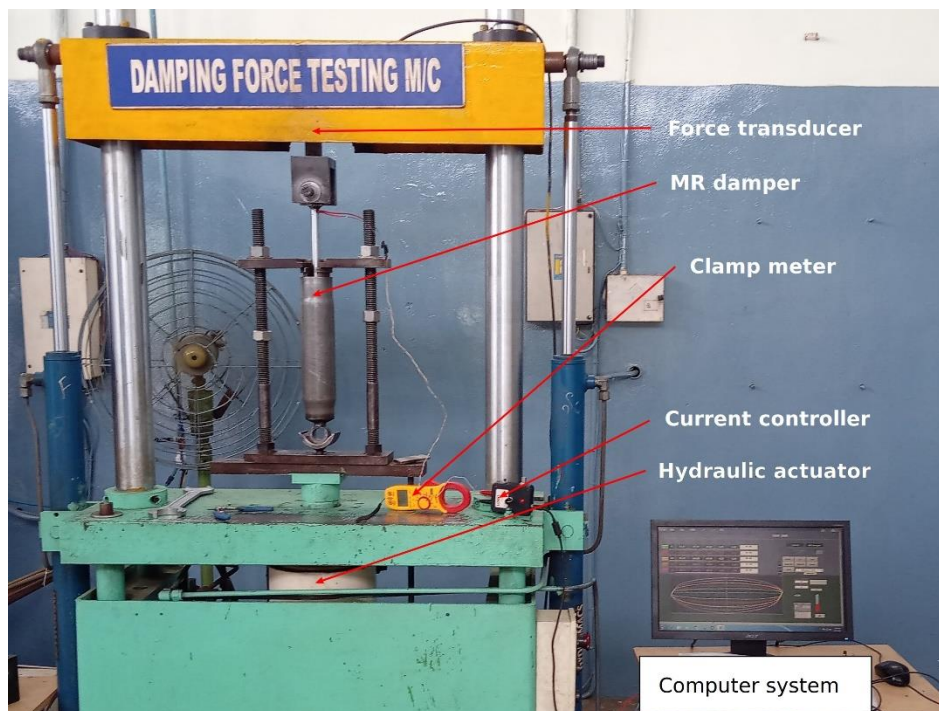
Figure 5.12 Damper testing machine experimental setup

The actuator is controlled by a servo valve, which in turn receives commands from LabVIEW software. Using this arrangement, various standard waveforms like sine, triangle, rounded square, ramp and trapezoid can be given as displacement of the hydraulic actuator. When any one of the waveforms is chosen, its parameters are to be selected so that the peak velocity of the actuator is within 1000 mm/s. This value of peak velocity is dictated by the capacity of the hydraulic power pack and the design of the hydraulic circuit. At the cap end of the hydraulic actuator, there is a position sensor which measures the displacement of the actuator and hence of the MR damper. The signals generated by the two sensors namely, the force transducer measuring the damper force and position sensor measuring the damper displacement, are acquired with the help of NI USB-6221 DAQ which is a multifunction I/O device. It has 8 differential channels for analog input with ADC resolution of 16 bits. It has a maximum sampling rate of 250 kHz. A sampling rate of 10k samples/s was used to acquire the data. LabVIEW software provides the interface between the data logger and the computer.

The electromagnetic coil in the MR damper is powered by Lord Wonder Box, a current controller from Lord Corporation, USA. A 12 Volt DC power supply provides input power to the Lord Wonder Box. This current controller works on the principle of Pulse Width Modulation (PWM) with a frequency of 30 kHz. Two modes of operation are possible for the Lord Wonder Box, manual control and external voltage control. In the present study, it is operated in manual mode, where the current output is varied by means of a control knob provided on the Wonder Box. A digital clamp meter was used to monitor the current being sent to the MR damper by the current controller. The damping force generated in MR damper is due to the flow of the MR fluid in it. When the MR damper is kept idle for some time, because of static friction, there will be "sticking" in the dynamic seals and in those surfaces, which have relative motion. Also, there will be a small amount of settling in MR fluid. Hence, priming of the MR damper for a short period of time (10-15 seconds) is needed to reach a stable and smooth operating condition. In real operation as an automotive damper, running the vehicle for a short distance in the beginning, takes care of the priming requirement. Hence, before the start of the actual experimental run, the MR damper is cycled through a few compression and extension strokes to prime the MR fluid and ensure that the fluid remains homogenous and that there is no settling of the magnetic iron particles. The setup is checked for any play between the damper and testing machine fixture. The damper is checked for any leakages. Once the damper is operating smoothly, data recording can commence. The MR damper was characterized by employing

the testing parameters as shown in Table 5.5. The operational requirements of any automotive damper are given by the vehicle designers in terms of the maximum stroke needed and damping force to be generated at different values of damper piston velocities. The maximum stroke requirement is a geometrical requirement and it is taken care of during the design of the damper components.

Table 5.5 Frequencies of harmonic excitation at 20 mm amplitude and corresponding piston velocities

Frequency level	Frequency of excitation (Hz)	Peak piston velocity (mm/s)
f1	0.4	50
f2	0.8	100
f3	1.19	150
f4	1.59	200
f5	1.99	250

In order to evaluate the damping force generated at different values of damper piston velocities, one of the most widely used and accepted methods is by exciting the damper with harmonic oscillations of varying amplitude and frequency. In the present work, a sinusoidal waveform is selected for the damper displacement for ease of analysis and to ensure that the time derivatives of the waveform remain continuous and smooth. The excitation amplitude is held constant at 20 mm and the frequency is increased so that the peak velocity varies from 50 mm/s to 250 mm/s. These piston velocities can be arrived at by using any other combination of excitation amplitude and frequency, provided that these values are within the safe operating limits of the MR damper. In actual operation on an automobile, the inputs coming to the damper due to road irregularities are random in nature. The maximum piston velocity was restricted to 250 mm/s which corresponds to the frequency of excitation f5. This was done to avoid any possibility of MR fluid leakage in the prototype damper and also to prevent overheating of the damper during continuous testing. The current supplied to the MR damper was also varied from 0 A to 2 A in steps of 0.5 A. The current was held constant and the damper was excited with frequencies from f1 to f5. This constitutes one experimental run, after which the current supplied to the MR damper is increased by 0.5 A. This is continued till all possible combinations of current supplied and excitation frequencies are obtained.

The plots of damper force vs displacement for different frequencies of excitation are shown in Figure 5.13 (a)-(e). Each plot shows the force vs displacement plots for five

different values of current supplied, 0, 0.5, 1, 1.5 and 2 A. It can be observed that the force values in both compression and rebound are increasing with increase in current supplied for all the frequencies of excitation.

(a)

(b)

(c)

112
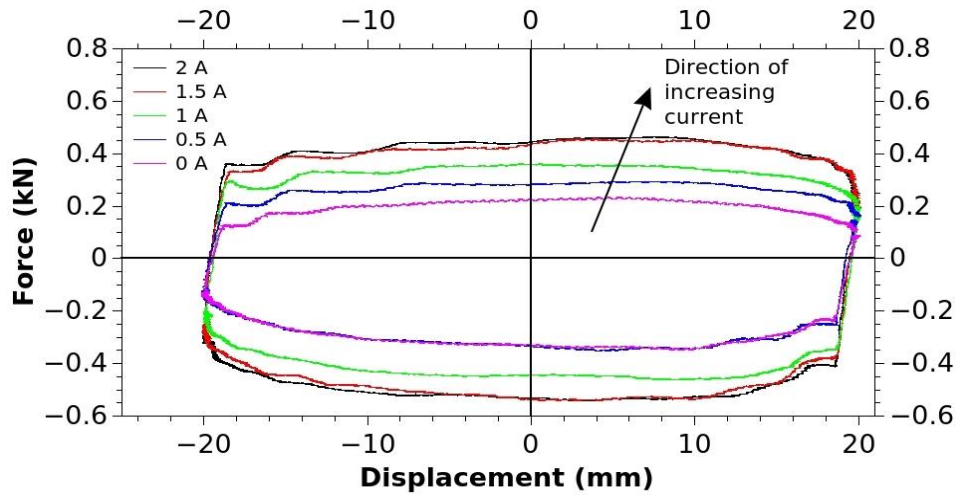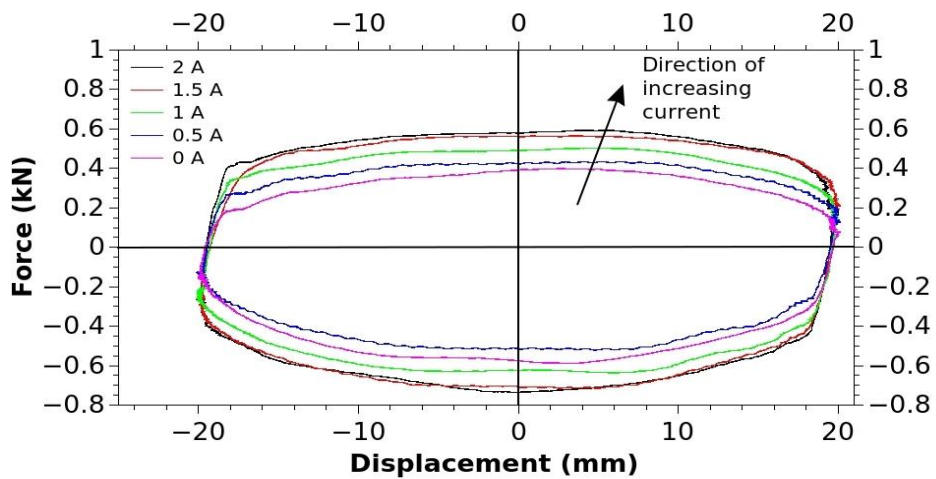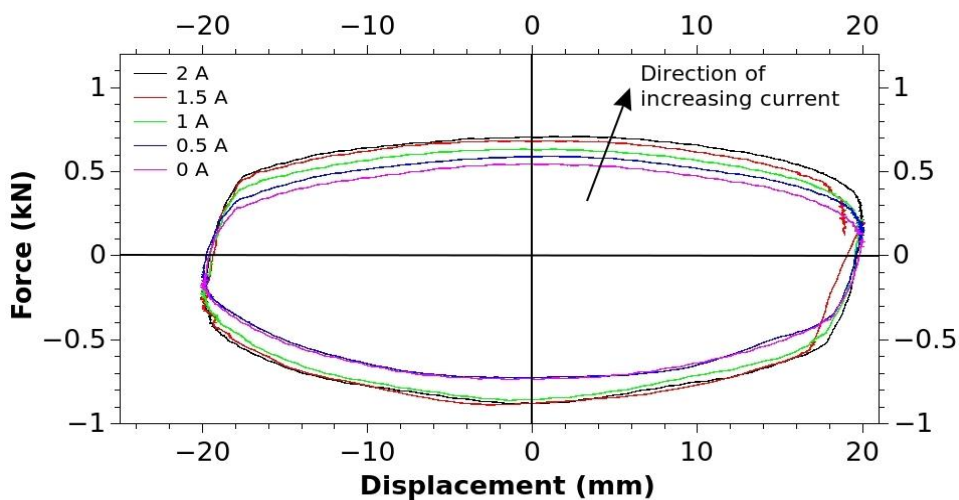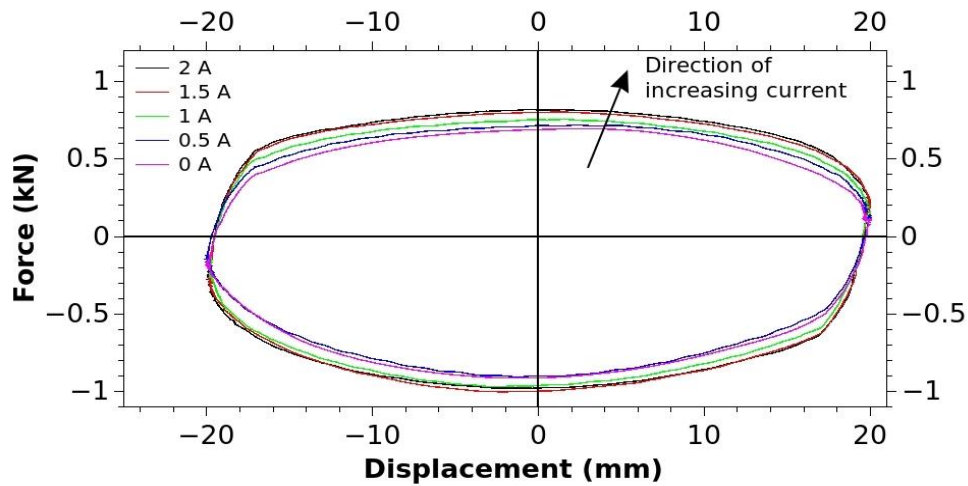
(d)
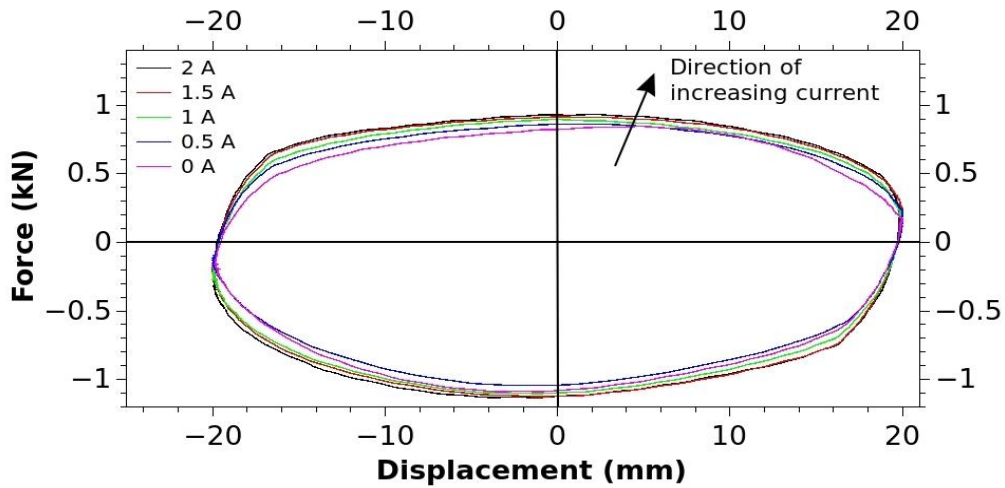
(e)

Figure 5.13 Damping force vs displacement for excitation frequencies f1 to f5 at different values of current supplied

The MR damper behaviour can also be understood by plotting the peak velocity of the damper piston for each frequency of excitation against the maximum damper force as shown in Figure 5.14. The convention followed is that the compressive forces are given negative sign and the tensile forces are given positive sign. Similarly, the velocity during the compressive stroke is given negative sign and during extension stroke it is given positive sign. Here, each data point on the plot curve represents the damper force at a particular frequency of excitation and a particular value of current supplied.
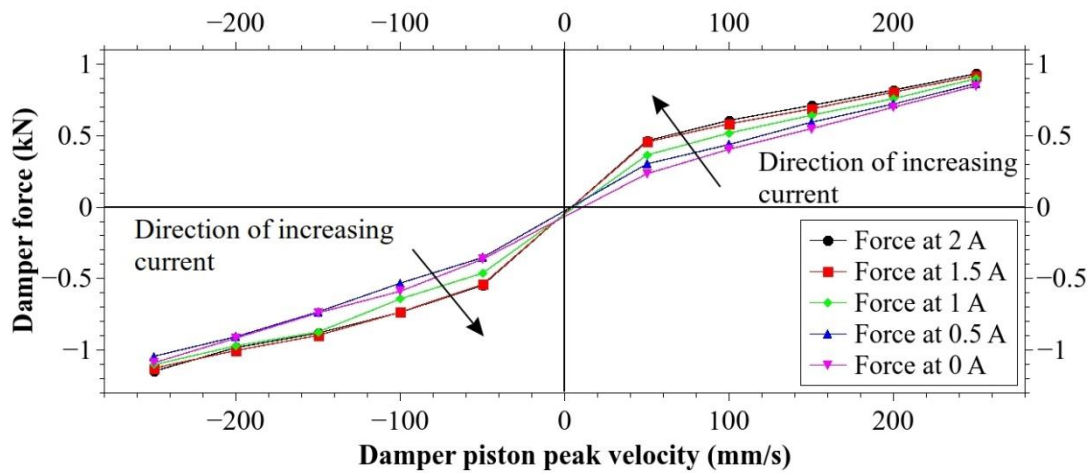
Figure 5.14 Damping force vs damper piston peak velocity at different values of current supplied

In order to study the hysteresis behaviour of the MR damper, the damper force measured in real time is plotted against instantaneous velocity of the damper piston. The velocity data is obtained by numerical differentiation of filtered displacement data. But before differentiation, the high frequency noise that may be present in the experimental data of damper displacement is removed by using a Fast Fourier Transform (FFT) low pass filter. For the experimental run with excitation frequency f1, the cut-off frequency is taken as 10 Hz and for f2 it is taken as 15 Hz. For higher excitation frequencies, the cut-off frequency for low pass filter is taken as 20 Hz. The plots of damper force vs damper piston velocity are shown in Figure 5.15 (a)-(e).

(a)

(b)

(c)

(d)
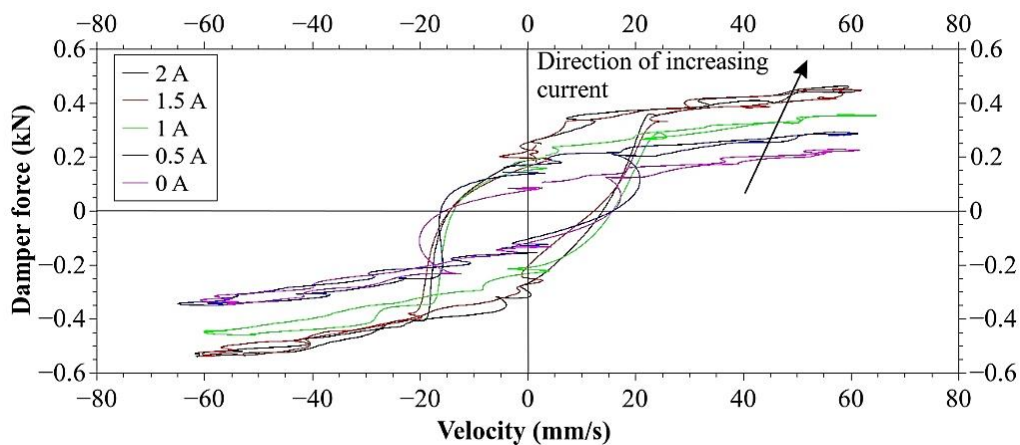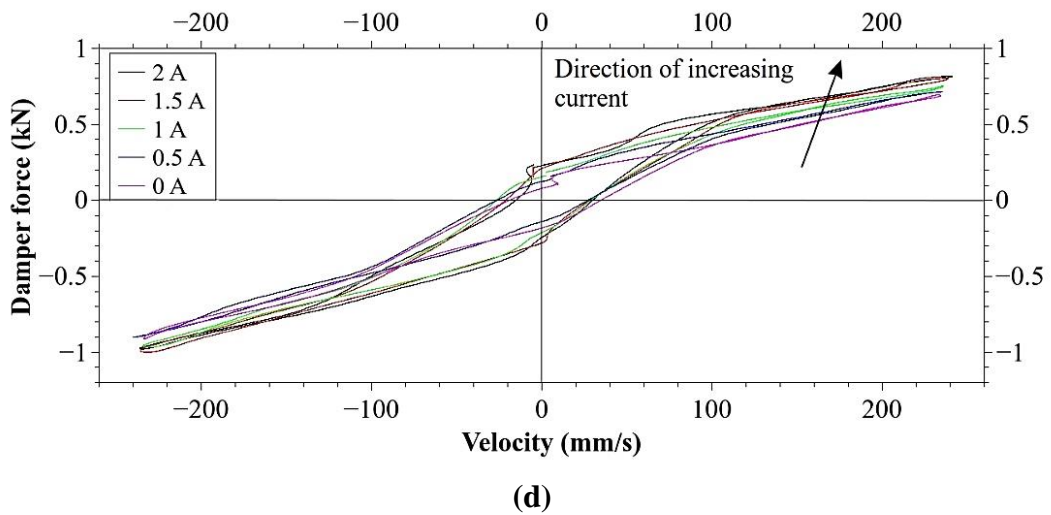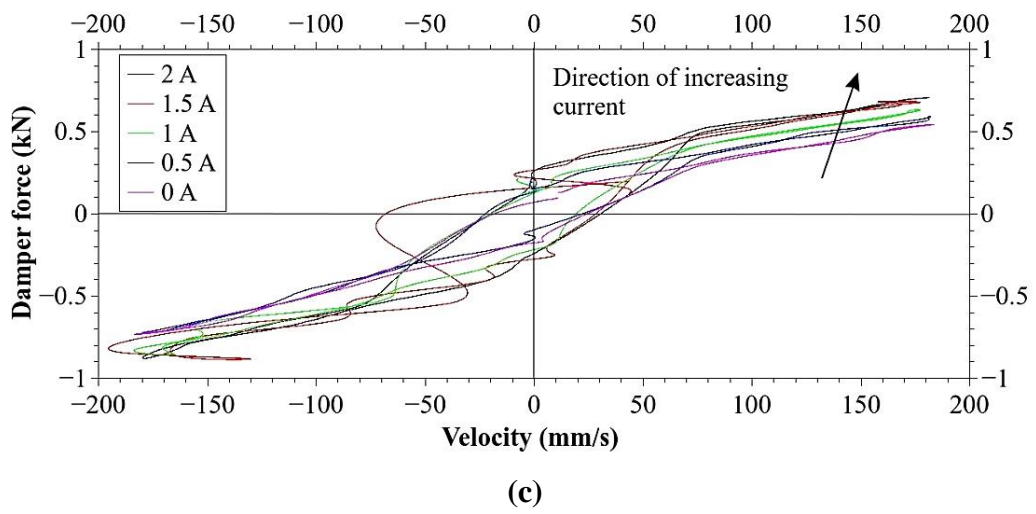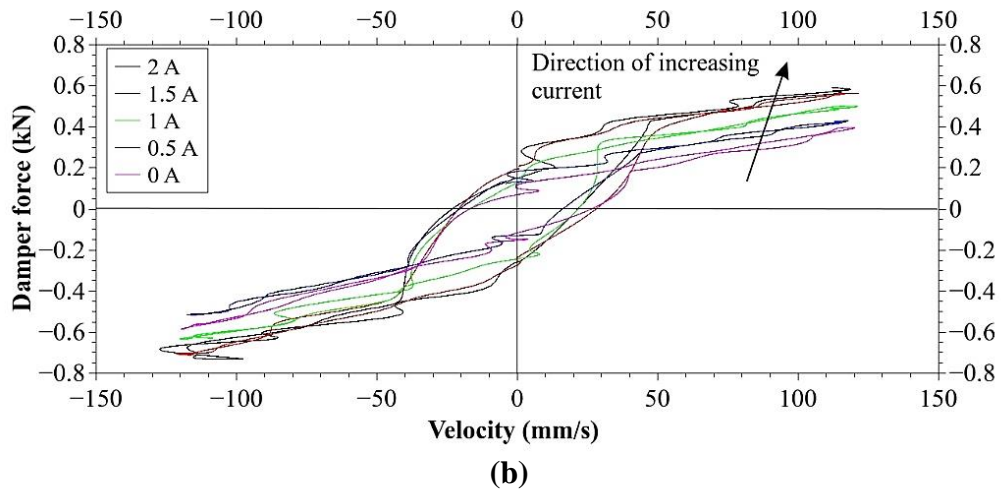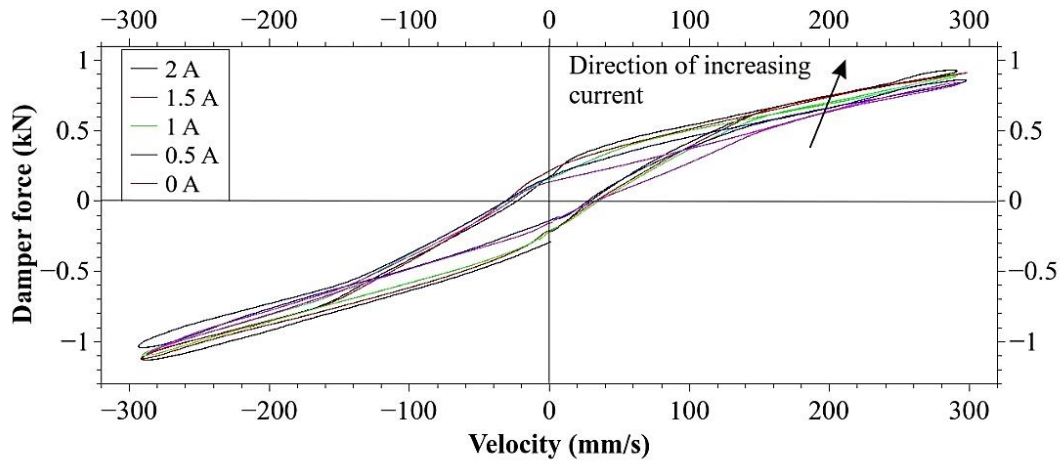
(e)

Figure 5.15 Damping force vs velocity for excitation frequencies f1 to f5 at different current supplied

It can be seen that the MR damper exhibits hysteretic behaviour and the value of force increases as the current supplied is increased for all the frequencies of excitation tested. Low velocity region (between -20 to 20 mm/s) of the plot correspond to extreme positions of the damper piston (maximum displacement), which is undergoing harmonic motion. Force curve is observed to be wavy in this region due to play in the clamping mechanism when the direction of motion of damper piston changes. Hence at this location of maximum displacement and low velocity, waviness of force is observed.
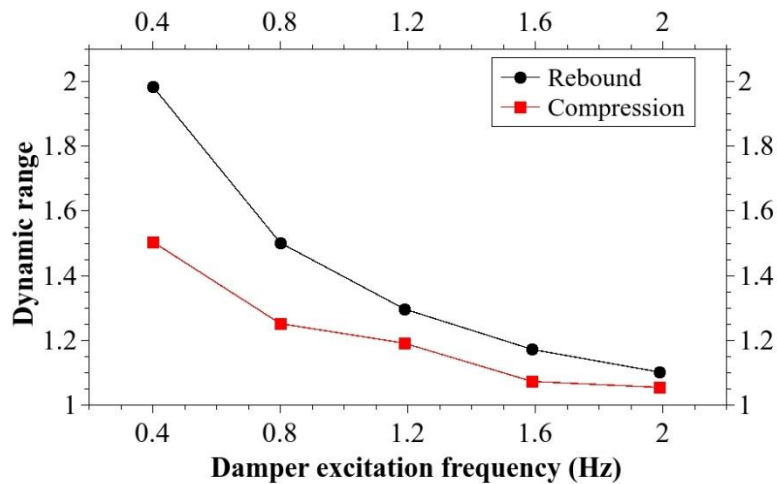
Figure 5.16 Dynamic range vs damper excitation frequency

Dynamic range is the ratio of the damper force at maximum value of current supplied (ON state) to the damper force at no current supplied (OFF state) at a given damper velocity or frequency of excitation with a fixed displacement amplitude. The variation of

this ratio with the frequency of excitation for MR damper is shown in Figure 5.16. The variation of damper compression force and damper rebound force are shown. It is seen that the dynamic range of the damper is decreasing with increase in excitation frequency.

5.6 MR DAMPER MODELING BASED ON MR FLUID RHEOLOGY AND MR DAMPER GEOMETRY

The force developed by the MR damper is the sum of controllable and uncontrollable forces. In the present case, the piston of the MR damper contains the electromagnetic coil and hence the piston assembly is analysed as an MR valve. The approach used is to establish a relationship between the applied magnetic field and rate of flow of MR fluid through the valve with the resulting drop in pressure across the piston assembly. For this, three non-dimensional parameters, the pressure number G, the yield stress number S and flow index m are defined as

$$G = -\frac{p_x h}{2\tau_0} \tag{5.3}$$

$$S = \frac{2Q(m+1)(m+2)}{wh^2}\left(\frac{\mu}{\tau_0}\right)^m \tag{5.4}$$

$$m = {1}/{p} \tag{5.5}$$

$$Q = (A_p - A_r)v_p \tag{5.6}$$

where, p_x is the pressure gradient, h, w, A_p and A_r are as defined in Table 5.4, τ_0, μ and p are parameters of HB model as explained in section on characterization of MR fluid, Q is the flow rate of MR fluid and v_p is piston velocity. The MR valve is axisymmetric by design and the fluid flow model in the annular space of this valve can be approximated to flow between parallel plates if the ratio of fluid flow gap h to piston diameter $2r_p$ is sufficiently small, according to Goldasz and Sapinski (2015). Referring to Table 5.4, this ratio calculates to 0.01956 which is very small.

For various currents given to the MR damper, the value of average strength of the magnetic field H in the active region of the fluid flow gap is found from the FEMM model of MR damper piston. The results of the FEMM program have been validated in the previous chapter, wherein an analytical method using electromagnetic circuit theory was employed. The magnetic flux density at the fluid flow gap was calculated based on the geometrical and material properties of the MR damper piston assembly. The results of the FEMM program and those of the analytical method have been shown to agree well.
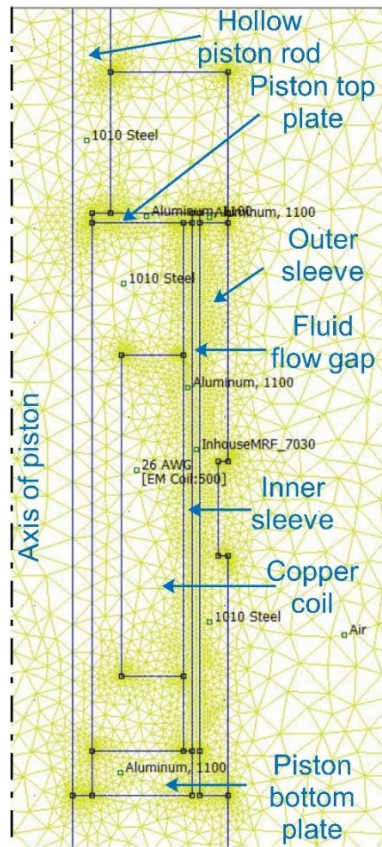
(a)
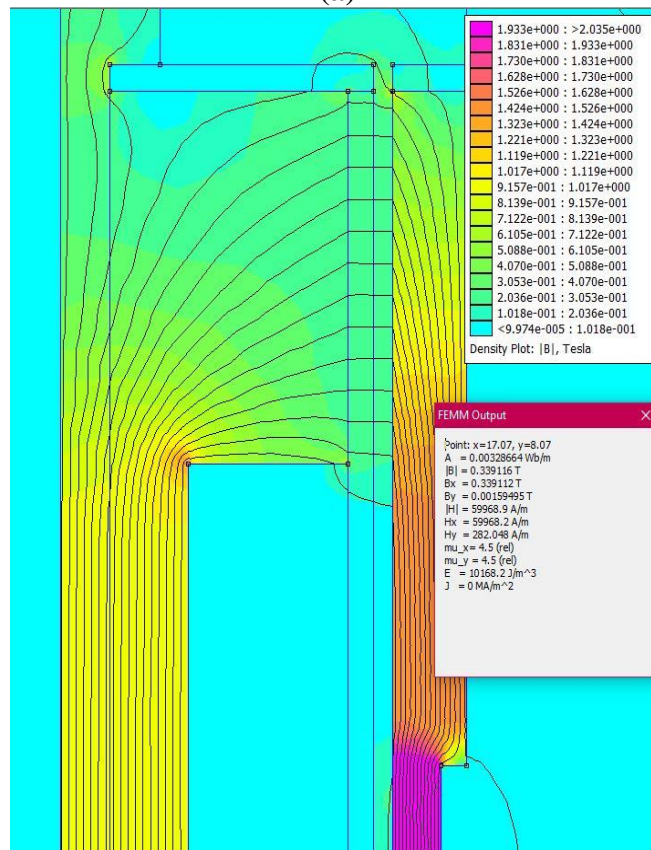
(b)

Figure 5.17 MR damper piston axisymmetric cross section **(a)** Meshing **(b)** Density plot

showing magnetic flux density and flux lines

118

Validating the results with experiment poses a practical problem as the fluid flow gap is very narrow and inaccessible to a magnetic probe. The relative permeability of MR fluid μ_r is taken as 7.5. The meshed 2D axisymmetric model of MR damper piston is shown in Figure 5.17 (a). The flux density plot of the piston cross section showing the distribution of magnetic flux density for 2 A current supplied is shown in Figure 5.17 (b). The values of magnetic field strength thus found at different currents (except 0.5 A) along with the HB model parameters at that field strength calculated using Table 5.3 and equation 5.2 are given in Table 5.6.

As the magnetic field strength in the fluid flow gap at 0.5 A is too low and less than 20 kA/m, it falls outside the valid range of strength of magnetic field to calculate HB model parameters using Table 5.3 and equation 5.2. Hence, HB model parameters at 0.5 A current supplied are not considered.

Table 5.6 Magnetic field strength at the fluid flow gap and corresponding HB model parameters for different values of current given to MR damper

Current (A)	Magnetic field strength (kA/m)	τ_0 (kPa)	μ (kPa-s)	p	$m=1/p$
1	22.5045	6.8711E-02	2.3712E-01	2.8257E-01	3.5390
1.5	27.4215	2.2082E-01	2.2475E-01	3.1476E-01	3.1771
2	31.0374	3.2697E-01	2.1653E-01	3.3682E-01	2.9690

In equation 5.4, Q is a function of damper piston velocity as given by equation 5.6, w and h are constants based on damper geometry and τ_0, μ and m are field dependent HB model parameters given in Table 5.6. The values of the yield stress number S calculated at 1 A, 1.5 A and 2 A for different piston velocities is given in Table 5.7.

Table 5.7 Yield stress number S at different values of currents supplied and damper velocities

Current (A)	Yield stress number S at different damper piston velocity (mm/s)				
	50	100	150	200	250
1	3527985.00	7055970.00	10583955.01	14111940.01	17639925.01
1.5	40055.22	80110.45	120165.67	160220.89	200276.12
2	10159.86	20319.73	30479.59	40639.45	50799.32

According to Goldasz and Sapinski (2015), the non-dimensional parameters G, S and m are related by.

$$G^2 S - (G - 1)^{m+1}[G(m + 1) + 1] = 0 \qquad (5.7)$$

The pressure number G is evaluated by solving equation 5.7 using numerical method and its values are tabulated in Table 5.8.

Table 5.8 Pressure number G at different values of currents and damper velocities

Current (A)	Pressure number G at different damper piston velocity (mm/s)				
	50	100	150	200	250
1	47.398	57.391	64.211	69.545	73.993
1.5	19.1512	23.5207	26.555	28.955	30.971
2	15.3028	19.001	21.6	23.6715	25.4224

On substituting values of pressure number G in equation 5.3, the pressure gradient p_x is evaluated. The pressure drop across the piston due to field-controlled yield stress Δp_τ is a product of the pressure gradient and the total length of the active region in the annular space of the MR damper piston as given by

$$\Delta p_\tau = p_x(2L_a) \tag{5.8}$$

The force developed due to the field-controlled yield stress (controllable force) F_τ is found using

$$F_\tau = \Delta p_\tau\left(A_p - A_r\right) \tag{5.9}$$

The values of F_τ thus calculated are tabulated in Table 5.9.

Table 5.9 Force developed due to the field-controlled yield stress F_τ in kN

Current (A)	Force developed due to the field-controlled yield stress F_τ at different damper piston velocity (mm/s)				
	50	100	150	200	250
1	0.2346	0.2841	0.3179	0.3443	0.3663
1.5	0.3047	0.3742	0.4225	0.4606	0.4927
2	0.3605	0.4476	0.5088	0.5576	0.5988

Kubik et al. (2017) showed that the MR damper force is the sum of controllable force F_τ and uncontrollable force F_u. As shown by Yang et al. (2002), controllable force is the force developed due to the field-dependent yield stress of MR fluid and uncontrollable force is due to the off-state viscosity of MR fluid and coulomb friction at the damper parts with relative motion like cylinder and piston, piston rod and rod guide, etc. According to Yang et al. (2002), the dynamic range of MR damper is an important performance parameter and it is said to be the ratio of the total damper force F_d to the uncontrollable force.

$$F_d = F_\tau + F_u \tag{5.10}$$

$$Dynamic\ range = F_d/F_u \qquad\qquad (5.11)$$

This is a novel approach as most of the researchers have carried out only theoretical and numerical analysis with no experimental data to support the work. Attempt has been made in the present work to use real experimental data as far as possible. Field controlled damping force F_τ cannot be measured experimentally as viscosity and frictional forces cannot be made to disappear in experiments. Hence, an attempt has been made here to arrive at the magnitude and behaviour of the uncontrollable force F_u using both experimental and model derived results. The force developed by the damper as measured in the experiments and the force due to field-controlled yield stress F_τ as calculated and shown in Table 5.9 are plotted for different damper peak velocity and current supplied as shown in Figure 5.18 (a)-(c).
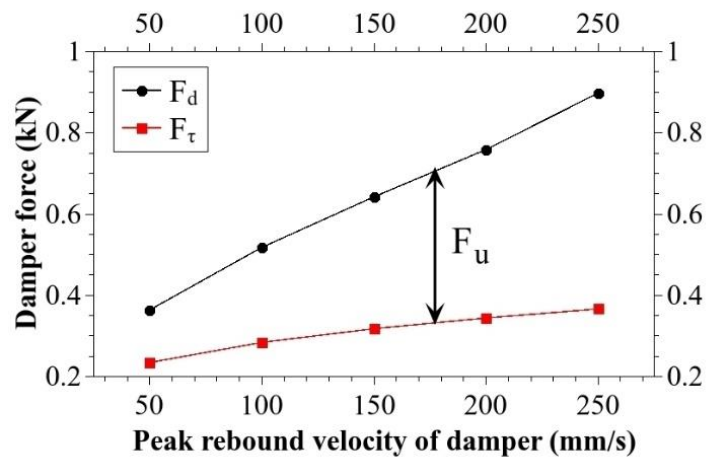
(a)
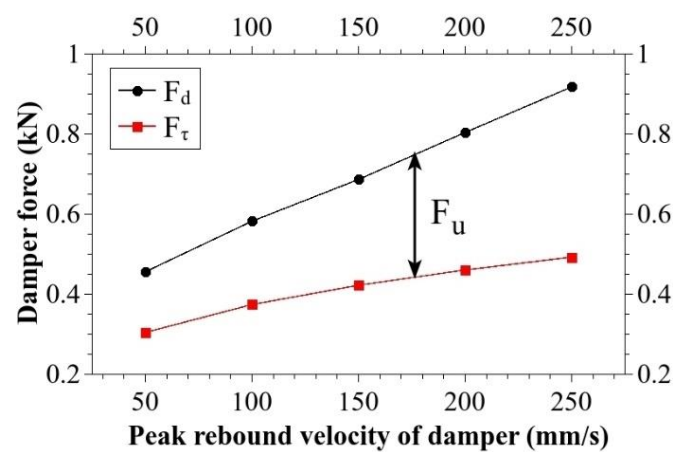
(b)
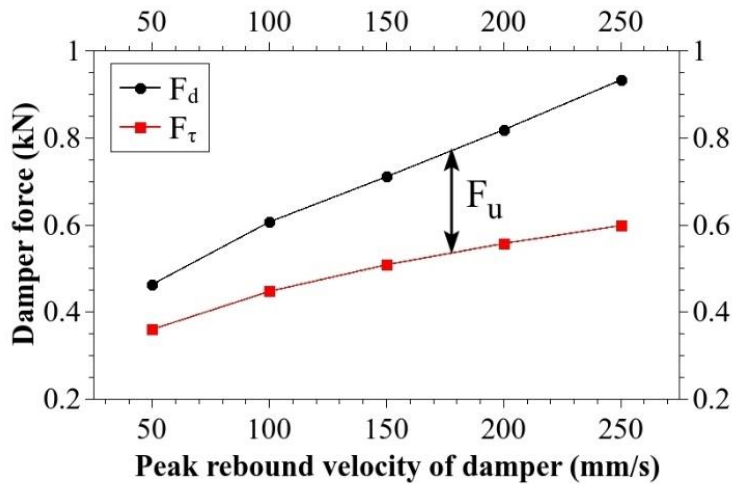
(c)

Figure 5.18 Damper force vs damper peak velocity **(a)** 1 A current **(b)** 1.5 A current **(c)** 2 A current

It can be seen that F_τ has similar trend as F_d and the difference between the two lines in each plot corresponds to the uncontrollable force F_u. The results of MR damper modelling based on MR fluid rheology and MR damper geometry can be verified based on the trend of force vs velocity plots obtained when compared to experimentally obtained plots. The magnitude of force obtained from model also corresponds to experimental data, with controllable damping force F_τ always being smaller than total damping force F_d.

The variation of the controllable force of the MR damper with current supplied for different damper piston velocities is shown in Figure 5.19. As expected, the controllable force increases when higher current is given to MR damper. This force is higher at higher damper piston velocities.
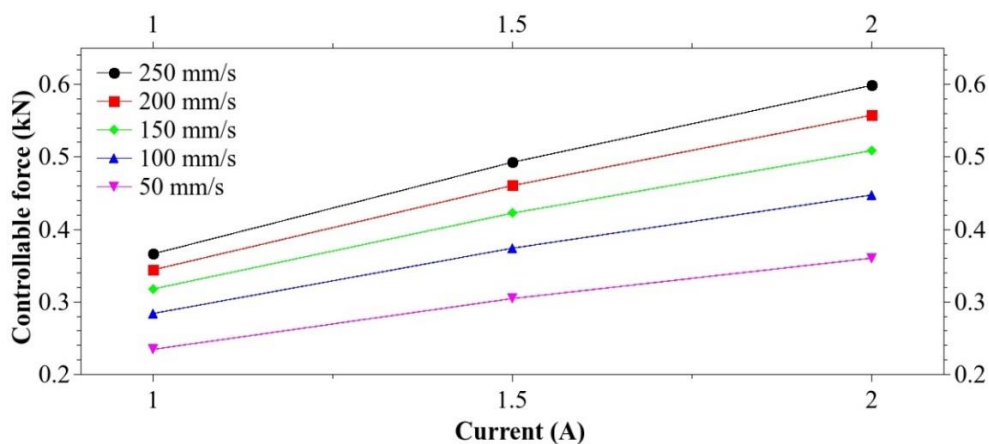
Figure 5.19 Controllable damper force vs current for different damper piston velocities

Dynamic range of MR damper for different levels of current given to MR damper is calculated using equation 5.11. Values of F_d are taken from the experimental results and F_u is calculated using equation 5.10. Variation of dynamic range with damper velocity is shown in Figure 5.20 for different values of current.
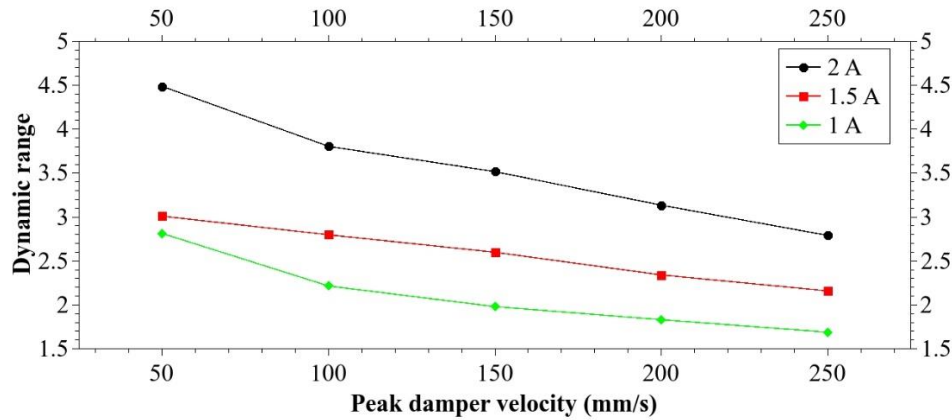
Figure 5.20 Dynamic range of MR damper vs peak damper velocity

Dynamic range of MR damper is higher for lower values of damper piston velocities and at higher velocities, which corresponds to higher frequency of vibration for a given stroke length, the dynamic range achieved has a lower value.

5.7 SUMMARY

MR fluid was prepared with CIP and silicone oil as the principal components. This fluid was characterized in a rheometer and its behaviour under varying magnetic field strengths was studied. The shear stress developed at any given shear strain was experimentally observed to increase with the applied magnetic field. The shear thinning behaviour of shear stress vs shear rate plot for MR fluid is non-linear in nature. This is successfully modelled using the HB model and the parameters of the model are expressed as polynomial functions of strength of magnetic field so that shear stress of MR fluid can be found at any given strength of the magnetic field. A twin tube valve mode MR damper containing this MR fluid is experimentally characterized in the damper testing machine under varying values of current given. Damper force vs displacement, peak velocity and instantaneous velocity plots are generated. The strength of the magnetic field at the fluid flow gap in the piston of the MR damper at different levels of current is evaluated using an axisymmetric 2D model of piston in FEMM software. It was found that the damper force

increases with current given at all frequencies of excitations tested. The value of analytically calculated force increases with current. Some important conclusions are:

- Dimensionless numbers along with H-B model for MR fluid behaviour can be used to predict the damping force of MR damper at any given piston velocity and current.

- Dynamic range of MR damper is evaluated and it is found that it decreases with an increase in excitation frequency.

- The experimental and analytical damper force are compared to conclude that the methods used are valid.

Hence, a twin tube MR damper operating in valve mode can be designed for application in an automobile using an in-house prepared MR fluid. The damping force is the sum of controllable and uncontrollable force. The controllable force can be varied by controlling the current supplied to the MR damper and thus it can be used to implement a semi-active suspension system. The MR damper piston which acts as a MR valve can be analysed using non-dimensional equations involving pressure number G, yield stress number S and flow index m. The pressure loss across the damper piston due to a field-controlled yield stress of MR fluid is calculated at different velocities using flow rate and geometrical design parameters along with dimensionless numbers.

In order to compare the performance of commercial MR damper, twin-tube MR damper with commercial MR fluid and twin-tube MR damper with in house MR fluid, experimental data for harmonic excitation of 20 mm amplitude and 2 Hz frequency is analyzed. Energy dissipated per cycle and equivalent damping coefficient of commercial damper is taken from Table 3.5, that for twin-tube MR damper with commercial MR fluid is taken from Table 4.9, and that for twin-tube MR damper with in house MR fluid is calculated from Figure 5.13 (e) using equation 3.4. The values for different current supplied is shown in Table 5.10.

It can be seen that, at zero current, twin-tube MR damper with in house MR fluid provides highest energy dissipated and equivalent damping coefficient among the three types of MR dampers. For higher currents, commercial MR damper provides the highest equivalent damping coefficient, followed by twin-tube damper with in house MR fluid and then by twin-tube MR damper with commercial MR fluid.

Table 5.10 Comparison of energy dissipated and equivalent damping coefficient of commercial MR damper, twin-tube MR damper with commercial MR fluid and twin-tube MR damper with in house MR fluid for different current supplied

Current supplied (A)	Energy dissipated per cycle (J)			Equivalent damping coefficient (kNs/m)		
	Commercial MR damper	Twin-tube MR damper with commercial MR fluid	Twin-tube MR damper with in house MR fluid	Commercial MR damper	Twin-tube MR damper with commercial MR fluid	Twin-tube MR damper with in house MR fluid
0	21.8	23.9	60.143	1.334	1.52	3.83
0.5	56.9	-	60.43	3.48	-	3.85
0.75	-	38.35	-	-	2.44	-
1	94.5	-	64.26	5.78	-	4.1
1.5	-	43.04	66.6	-	2.74	4.24

The results of experimental testing of commercial MR damper and twin-tube MR damper presented in the previous chapters are used to implement semi-active suspension with skyhook control in the next chapter. Dynamic analysis of quarter car vehicle model is performed using MATLAB Simulink software.

CHAPTER 6

DYNAMIC ANALYSIS OF QUARTER CAR VEHICLE MODEL WITH SEMI-ACTIVE SUSPENSION

6.1 INTRODUCTION

A quarter car model is the most widely used suspension model to study the vertical dynamics of a suspension system. In this chapter, experimental characterization of commercial MR damper Lord RD-8041-1 is presented and a polynomial model for force-velocity behaviour is developed. This model is used to implement skyhook semi-active control in quarter car model using MATLAB Simulink. Vertical displacement and acceleration response of the sprung mass in semi-active suspension to harmonic excitation is studied and compared to that of passive suspension of car. Polynomial model for force-velocity behaviour is also developed for twin-tube MR damper based on the experimental results presented in section 4.7. This model is implemented in semi-active suspension subjected to random road excitation using skyhook control and compared with equivalent passive SUV suspension.

6.2 EXPERIMENTAL CHARACTERIZATION OF COMMERCIAL MR DAMPER

6.2.1 Test set-up

Lord RD-8041-1 is a long stroke MR damper commercially manufactured by Lord Corporation, USA. This MR damper, shown in Figure 6.1, has a stroke of 74 mm, an extended length of 248 mm and a body diameter of 42.1 mm.

Figure 6.1 MR damper Lord RD-8041-1

The experimental setup for characterization of MR damper can be seen in Figure 6.2. A damper testing machine by HEICO Ltd is used for this purpose. It has a hydraulic

actuator of 150 mm stroke and capable of producing actuator force up to 20 kN. The MR damper is held between a fixed jaw and a movable jaw of the damper testing machine. The movable jaw is part of the piston rod of the hydraulic actuator. Sinusoidal displacements of different amplitudes and frequencies can be applied to the damper with the help of this actuator. There are two sensors on the damper testing machine, one is a position sensor built in to the hydraulic actuator and another is a force transducer fitted in the fixed jaw of the machine. These two sensors measure the damper displacement and damping force in real time. The sampling rate used was 1000 samples/second. A MOOG controller along with MOOG integrated test suite running in a computer are used to control the hydraulic actuator and for data acquisition from the sensors.
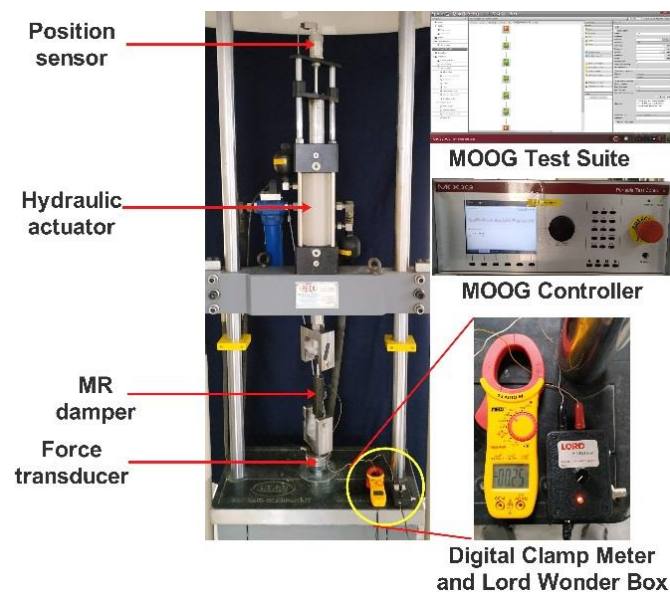
Figure 6.2 Experimental setup for damper characterization

A current controller device, Lord Wonder Box of Lord Corporation is used to supply direct current (DC) to the MR damper. It has a manual control knob which can be used to modulate the current given to the MR damper through Pulse Width Modulation (PWM). Since the Wonder Box does not have a display, a digital clamp meter was used to measure the current being supplied to the MR damper.

6.2.2 Parameters of testing

The MR damper was given sinusoidal displacement of fixed amplitude (Z) of 15 mm. Excitations of five different frequencies (f) and corresponding velocities ($2\pi fZ$) were given as shown in Table 6.1. The maximum piston velocity is limited to 300 mm/s because at higher piston velocities, the MR damper will be stressed severely and probability of

damper failure are higher. When the MR damper is used in a vehicle on road, the piston velocities may be higher than 300 mm/s but it will only be for a short time unlike in the experimental testing, where the MR damper is excited through repeated cycles of oscillations. Hence the higher limit of piston velocity during experimental evaluation are justified.

Table 6.1 Values of frequencies and corresponding velocities for sinusoidal displacement input of 15 mm amplitude

Frequency level	Frequency (Hz)	Velocities (mm/s)
f1	1	94.24
f2	1.5	141.37
f3	2	188.5
f4	2.5	235.62
f5	3	282.74

This was repeated for five different values of current supplied from 0 A to 1 A in increments of 0.25 A giving a total of 25 experimental runs. Data about damper displacement, damping force and time were logged for each of the experimental runs for further analysis.

6.2.3 Force-velocity characterization of commercial MR damper

The damper displacement and time data obtained in the characterization experiment are numerically differentiated to obtain velocity data. Moving window average method was used to smoothen the velocity data after numerical differentiation. Damping force data was also similarly smoothened to reduce the noise in the transducer signal. The plots of damping force vs damper displacement are show in Figure 6.3 for different frequencies of excitation.
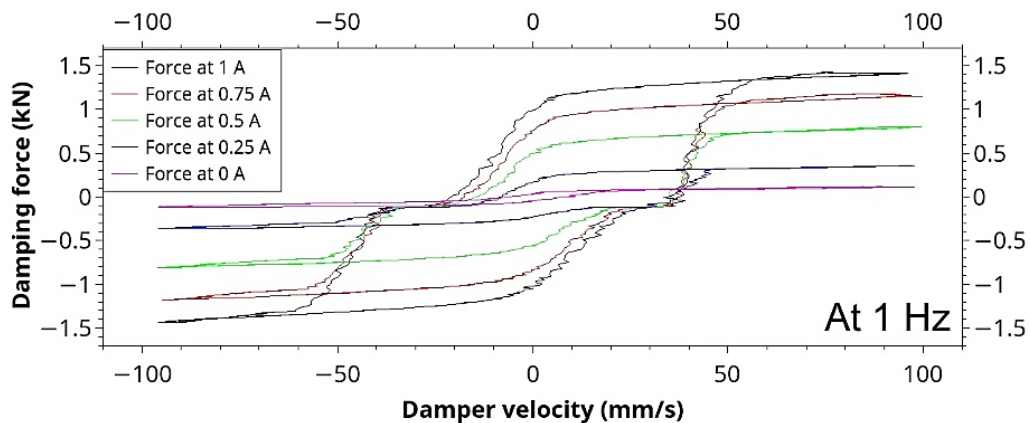
(a)
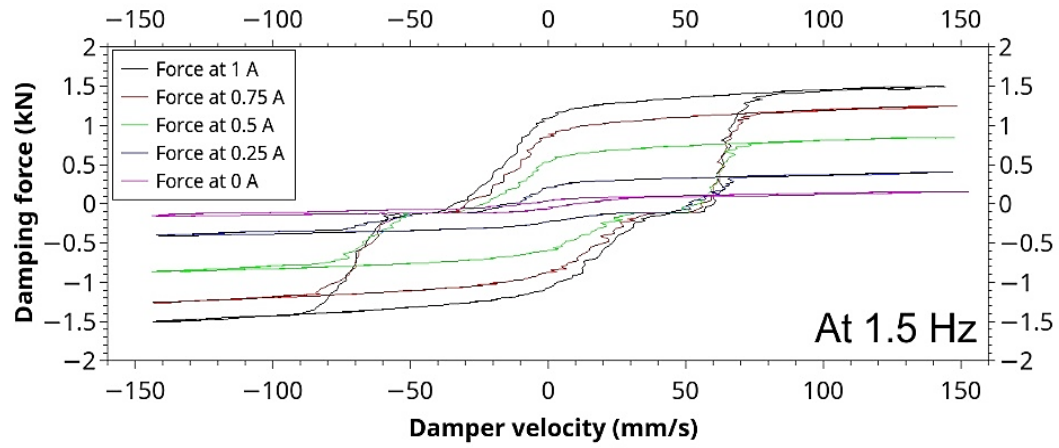
(b)
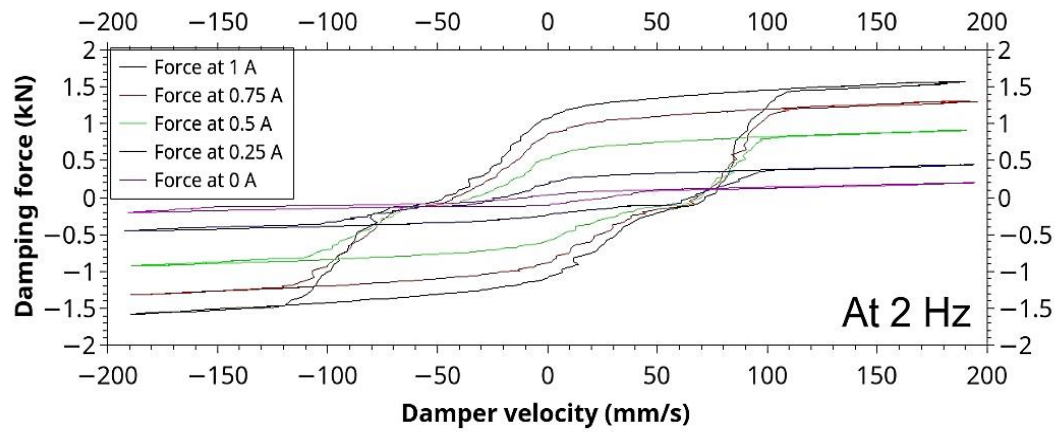
(c)
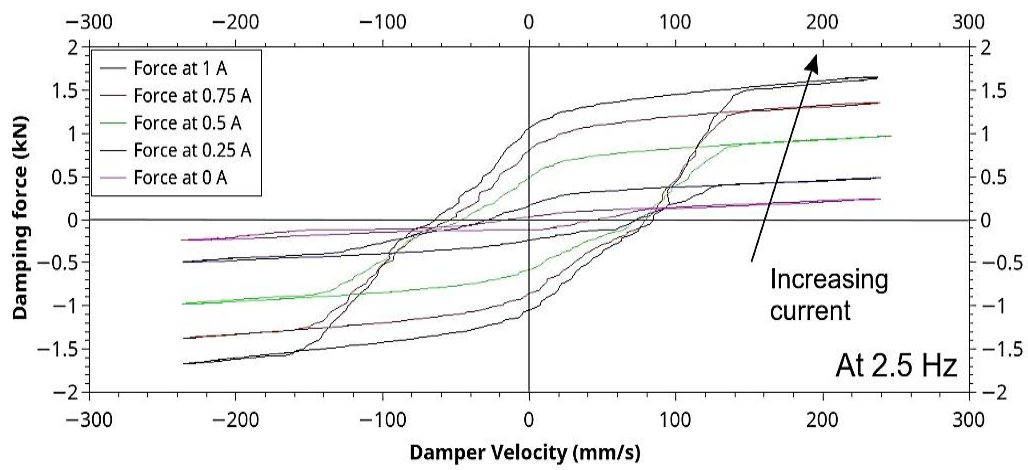
(d)
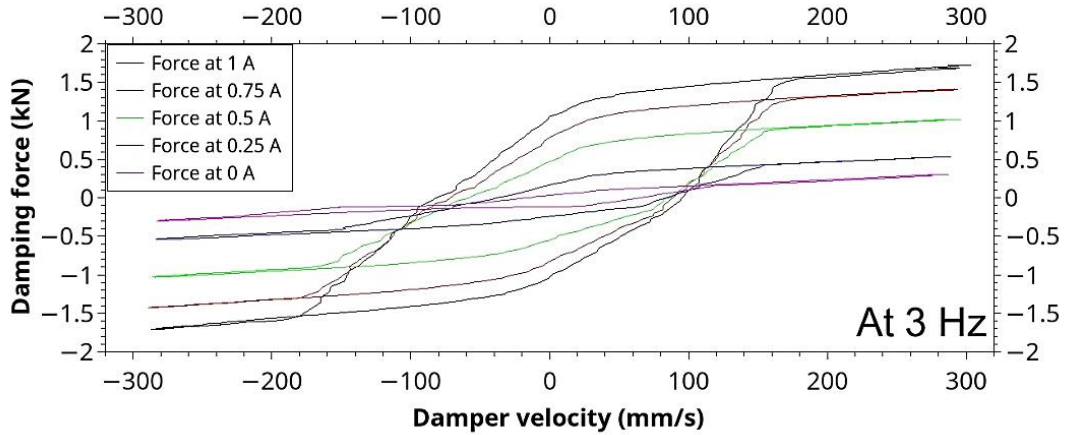
(e)

Figure 6.3 Force vs velocity of MR damper for different values of currents supplied (a) 1 Hz (b) 1.5 Hz (c) 2 Hz (d) 2.5 Hz (e) 3 Hz

As per convention, damping force during compression is taken as negative force and that during extension is taken positive. Similarly, compressive displacement from mean position is taken as negative displacement and that during extension is taken positive. The graph for each frequency shows the hysterical behaviour of MR damper at varying levels of current. It can be observed in Figure 6.3 that for any given frequency of excitation, the damping force increases with increase in the current supplied for a given velocity. Also, the area contained by the hysteresis loops increase with increase in current supplied. Since the area under force-velocity graph represents power, it can be inferred that the rate of energy dissipation by the MR damper increases as the current given is increased.

6.2.4 Polynomial model for force-velocity graph of commercial MR damper

A mathematical model was developed for the hysteresis behaviour of the MR damper. The experimental data for 2.5 Hz excitation frequency, as shown in Figure 6.3 (d) was used for this. A fifth-degree polynomial equation is used to fit the experimental data of force vs velocity behaviour of the MR damper using

$$F_d = q_0 + q_1\dot{x} + q_2\dot{x}^2 + q_3\dot{x}^3 + q_4\dot{x}^4 + q_5\dot{x}^5 \qquad (6.1)$$

Where F_d is the damping force and $\dot{x}$ is the damper velocity. The value of the coefficients q_i for different currents is given in Table 6.2.

Table 6.2 Values of polynomial coefficients for force vs velocity curve of commercial MR damper

Current (A)	q_0	q_1	q_2	q_3	q_4	q_5
0	-2.43284E-02	1.54319E-03	2.0805E-06	-2.3491E-08	-3.2283E-11	2.6262E-13
0.25	-4.74096E-02	3.42742E-03	2.3382E-06	-3.5844E-08	-2.9457E-11	1.9981E-13
0.5	-4.2707E-02	6.85805E-03	1.698E-06	-5.6038E-08	-1.8407E-11	1.011E-13
0.75	-3.67396E-02	8.94015E-03	1.7411E-06	-3.5804E-08	-2.157E-11	-4.1804E-13
1	-1.0213E-02	9.77831E-03	3.7514E-07	5.3304E-09	-6.0116E-12	-1.0383E-12

In order to show the accuracy of the fit, plot of damping force vs damper velocity for 2.5 Hz excitation and at 0.75 A current is shown in Figure 6.4. It is a fit for the average of the upper and lower curve, where upper curve is for extension stroke of damper and lower curve is for compression stroke.
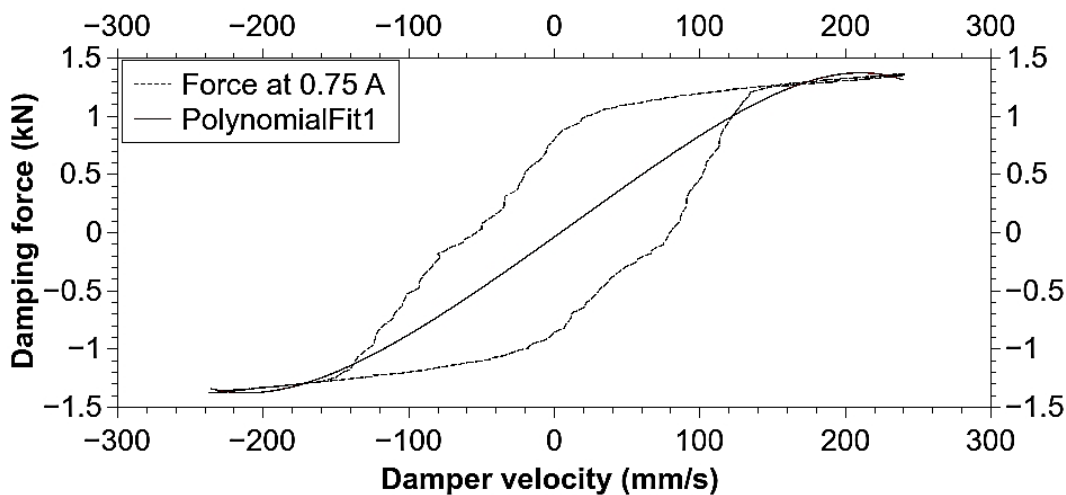
Figure 6.4 Polynomial model for force vs velocity of commercial MR damper

6.3 POLYNOMIAL MODEL FOR TWIN-TUBE MR DAMPER

The experimental results presented in section 4.7 were used to develop a polynomial model for twin-tube MR damper force vs velocity characteristics. Specifically, the data presented in Figure 4.13 was used. A fifth-degree polynomial equation, as shown in equation 6.1, is used to fit the experimental data of force vs velocity behaviour of the twin-tube MR damper. The value of the coefficients for minimum current (0 A) and maximum current (1.5 A) is given in Table 6.3.

Table 6.3 Values of polynomial coefficients for force vs velocity curve of twin-tube MR damper

Current (A)	q_0	q_1	q_2	q_3	q_4	q_5
0	0.0053847	0.0019793	-8.67925E-07	-7.087E-09	1.3827E-12	1.8411E-14
1.5	0.0040501	0.0043334	-6.09168E-07	-2.33E-08	1.0908E-12	5.7251E-14

In order to show the accuracy of the fit, plot of damping force vs damper velocity for 0 A and at 1.5 A current is shown in Figure 6.5. It can be observed that the polynomial fit closely matches the experimental data. Hence, using the coefficients of the polynomial model given in Table 6.3, the damper force can be evaluated at any velocity in the range.
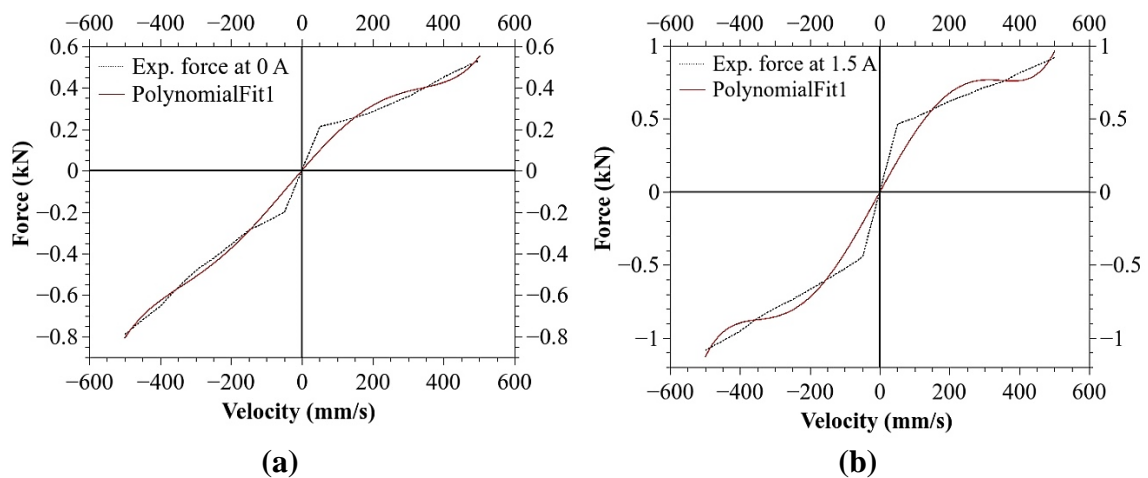
Figure 6.5 Polynomial model for force vs velocity for twin-tube MR damper **(a)** Minimum current 0 A **(b)** Maximum current 1.5 A

6.4 QUARTER CAR SIMULATION

The diagrams of quarter car model for both semi-active and passive control are shown in Figure 6.6. Here, M is the sprung mass, m is the unsprung mass, suspension spring stiffness is K_s, suspension damping coefficient is C_s, K_t is the tyre stiffness and C_t is the tyre damping coefficient. The heave of the sprung mass and unsprung mass are taken as x(t) and y(t) and road input is taken as z(t).

(a)

(b)
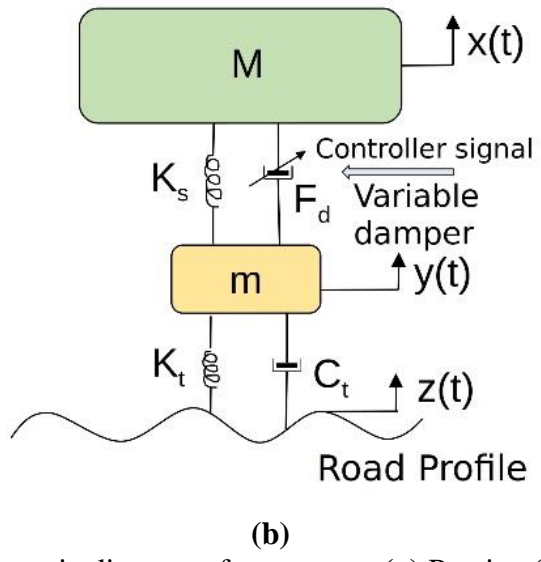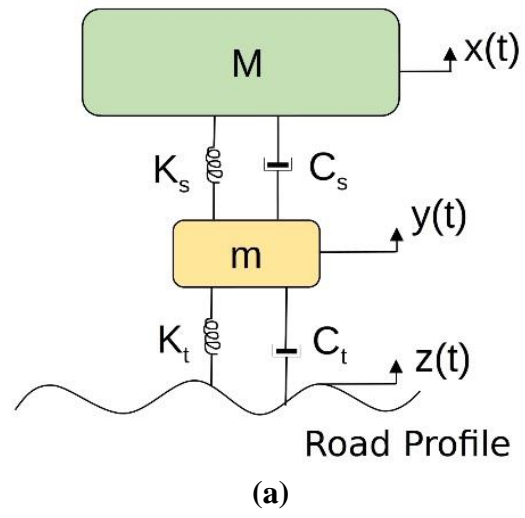
Figure 6.6 Schematic diagram of quarter car (a) Passive (b) Semi-active

6.4.1 Parameters of quarter car model

Table 6.4 shows the parameters of the quarter car model that were taken as fixed and those which are variables. Since the contribution of damping from tyre is very small, it has been neglected for the present analysis.

Table 6.4 Parameters of quarter car model

Fixed parameters	Variable parameters
Tyre stiffness K_t	Damper current I
Sprung mass M	Input frequency f
Unsprung mass m	Input amplitude Z
Suspension spring stiffness K_s	

The various parameter values used in the simulation are given in Table 6.5. Tyre damping coefficient C_t is taken as zero as its value is negligibly small. The suspension

134

damping coefficient C_s for SUV was calculated using energy dissipated method as explained in section 3.3.2. The force vs displacement plot for SUV damper based on experimental testing, as shown in Figure 7.3 of Chapter 7 is used for this calculation, particularly the loop for 250 mm/s velocity. The stiffness of the coil spring K_s used in SUV was also experimentally measured. In the simulation, commercial MR damper based semi-active suspension is compared with passive suspension of car and twin-tube MR damper based semi-active suspension is compared with passive suspension of an SUV.

Table 6.5 Parameter values for quarter car model for car as in Metered and Bonello (2010) and SUV

Parameter	Value for car	Value for SUV
Sprung mass M	240 kg	300 kg
Unsprung mass m	36 kg	36 kg
Suspension spring stiffness K_s	16 kN/m	41 kN/m
Suspension damping coefficient C_s	980 Ns/m	3,168 Ns/m
Tyre stiffness K_t	160 kN/m	200 kN/m

6.4.2 Equations of motion for the quarter car model

The quarter car model is a dynamic system with two degree of freedom. Hence its motion can be described with the help of two second order differential equations. From the free body diagram of the sprung mass, unsprung mass and using Newtons laws of motion, equations 6.2 and 6.3 can be written for the passive suspension system.

$$M\ddot{x} + K_s(x - y) + C_s(\dot{x} - \dot{y}) = 0 \tag{6.2}$$

$$m\ddot{y} + K_s(y - x) + C_s(\dot{y} - \dot{x}) + K_t(y - z) + C_t(\dot{y} - \dot{z}) = 0 \tag{6.3}$$

Similarly, for the semi-active suspension shown in Figure 6.6 (b), equations 6.4 and 6.5 can be written.

$$M\ddot{x} + K_s(x - y) + F_d = 0 \tag{6.4}$$

$$m\ddot{y} + K_s(y - x) - F_d + K_t(y - z) + C_t(\dot{y} - \dot{z}) = 0 \tag{6.5}$$

Here, F_d is given by equation 6.1.

6.5 INPUT EXCITATIONS AND SKYHOOK CONTROL

When the vehicle moves on a rough road surface, the wheels roll over bumps, potholes and other unevenness on road surface. This translates into an input displacement to the wheel which is represented by $z(t)$ in the quarter car model in Figure 6.6. Two types of displacements are considered for $z(t)$, sine wave and random road excitation.

6.5.1 Sine wave excitation

A sinusoidal displacement of amplitude 0.015 m and of frequency 2.5 Hz is the input to the wheel of the quarter car model. Equation 6.6 represents the displacement function *z(t)*.

$$z(t) = 0.015 \, \sin(2\pi * 2.5 * t) \tag{6.6}$$

This input displacement is used in the quarter car model of car, where the commercial MR damper is used for building the semi-active suspension.

6.5.2 Random road excitation

Random road profile can be used to simulate the random excitations coming to the vehicle suspension when it travels over uneven road surface. When the motion of the vehicle is uniform, the road unevenness can be represented by a random road profile given by

$$\dot{Z}_r(t) = -2\pi u n_0 Z_r(t) + \sqrt{G_q(\Omega_0)u} \, w(t) \tag{6.7}$$

Where $Z_r(t)$ is the road roughness amplitude, $G_q(\Omega_0)$ is the coefficient of road roughness at wave number $\Omega_0 = 0.1$ rad/min, u is the vehicle speed, n_0 is the spatial frequency and $w(t)$ is white noise signal. Figure 6.7 shows the time domain plot for random road excitation input for a vehicle speed of 15 m/s (54 km/hr). Two types of road surface, average road with $G_q(\Omega_0)$ value of 256 (10^{-6} m²/(cycle/min)) and bad road with $G_q(\Omega_0)$ value of 1024 (10^{-6} m²/(cycle/min)) at $n_0 = 0.1$ cycle/min are used for simulation.
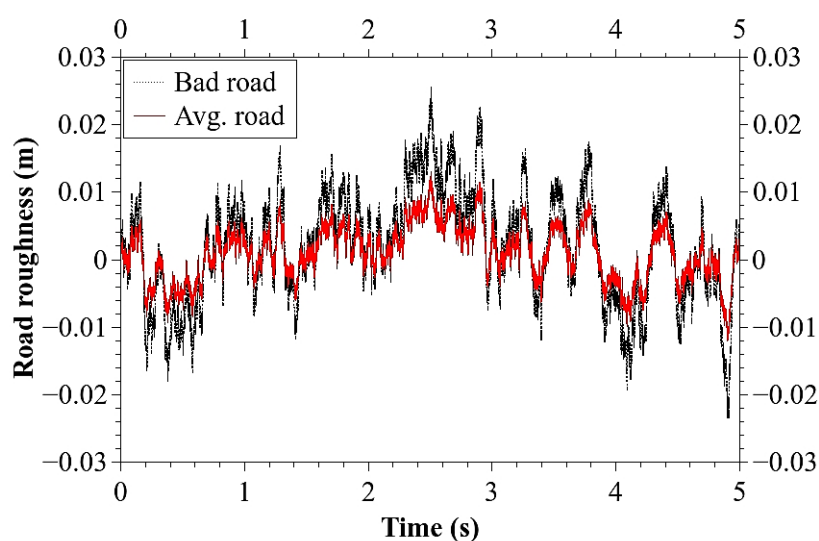
Figure 6.7 Random road profile in time domain for vehicle speed of 15 m/s (54 km/hr)

The Power Spectral Density (PSD) of the random road profile for average and bad road for constant vehicle speed of 15 m/s (54 km/hr) is shown in Figure 6.8.
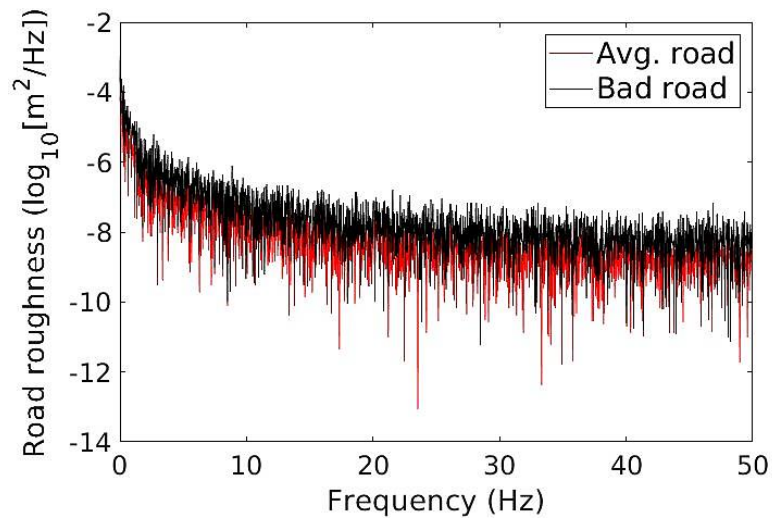
Figure 6.8 PSD of random road profile for vehicle speed of 15 m/s (54 km/hr)

6.5.3 Skyhook control of semi-active suspension

For implementing semi-active suspension, an On-Off Sky-hook control algorithm is used, given by

$$F_d = F_{dmax} \; if \; \dot{x}(\dot{x} - \dot{y}) > 0$$
$$= F_{dmin} \; if \; \dot{x}(\dot{x} - \dot{y}) \leq 0 \qquad (6.8)$$

Here, F_{dmax} is the maximum damping force obtained at maximum current given and F_{dmim} is the minimum damping force obtained at zero current given to the MR damper. This is implemented with the help of a conditional switch block and MATLAB function blocks. The function blocks take the damper piston velocity as input and computes the damping force F_d using equation 6.1. When the coefficients used in the polynomial are those corresponding to maximum current, the damping force calculated will be F_{dmax} and when the coefficients correspond to minimum current (0 A), the damping force calculated will be F_{dmin}.

6.6 SIMULATION RESULTS AND DISCUSSION

MATLAB Simulink software was used for simulating the quarter car model of the vehicle suspension. The values of the variables used are as shown in Table 6.5.

6.6.1 Semi-active suspension with commercial MR damper

For the semi-active suspension with commercial MR damper, skyhook control and sinusoidal excitation was used. The performance is compared with passive suspension of a car. The heave of the sprung mass and sprung mass acceleration are plotted against time in Figure 6.9 (a) and (b) respectively. It can be observed that when compared to passive suspension, heave is more for the semi-active suspension but the peaks arrive much farther apart. However, the sprung mass acceleration is lower for the semi-active suspension when compared to passive suspension.

(a)

(b)
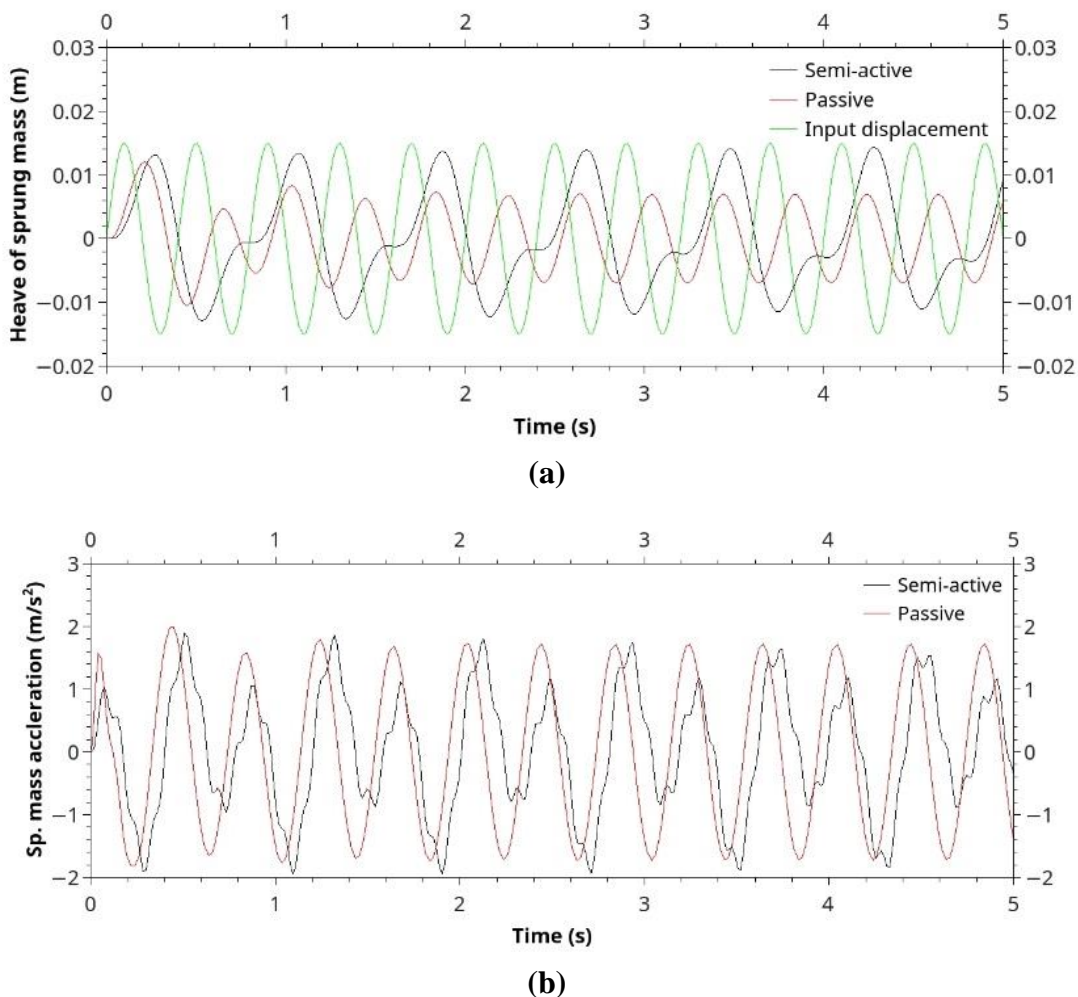
Figure 6.9 Time domain plots for Sine wave excitation **(a)** Heave of sprung mass **(b)** Sprung mass acceleration

In Figure 6.9, though the displacement of the semi-active suspension is higher, the sprung mass acceleration of semi-active suspension is lower when compared to passive suspension. The sprung mass acceleration is more significant than displacement with regards to the ride comfort of the vehicle. Hence semi-active suspension will provide better

ride comfort when compared to passive suspension system, which is the objective of the present study. The waviness of the semi-active suspension seen in Figure 6.9 (b) is due to chattering phenomenon which happens when either the damper piston velocity $(\dot{x} - \dot{y})$ or the sprung mass velocity $\dot{x}$ as mentioned in equation 6.8, is very close to zero. This can be solved by using suitable control logic to prevent the chattering.

The normalized amplitudes for heave and acceleration of the sprung mass are plotted against frequency for sine wave excitation in Figure 6.10 (a) and (b) respectively. These were obtained by performing Fast Fourier Transformation (FFT) on the time domain data.
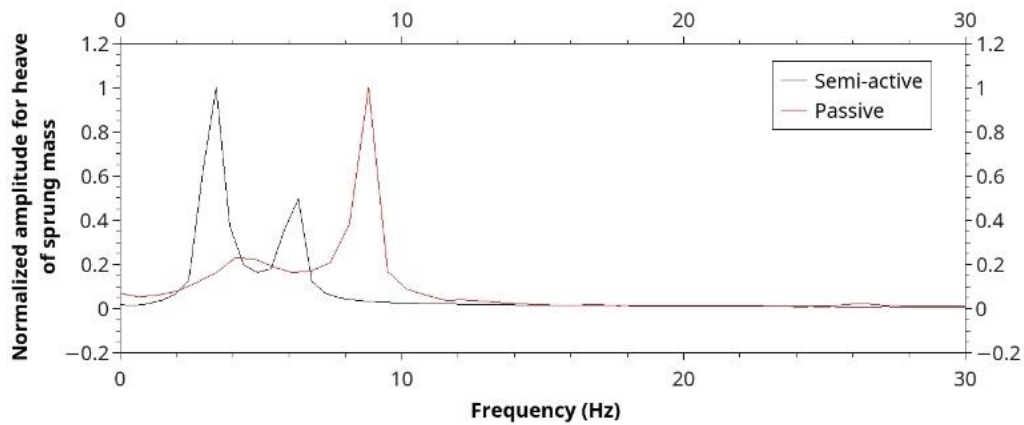
(a)
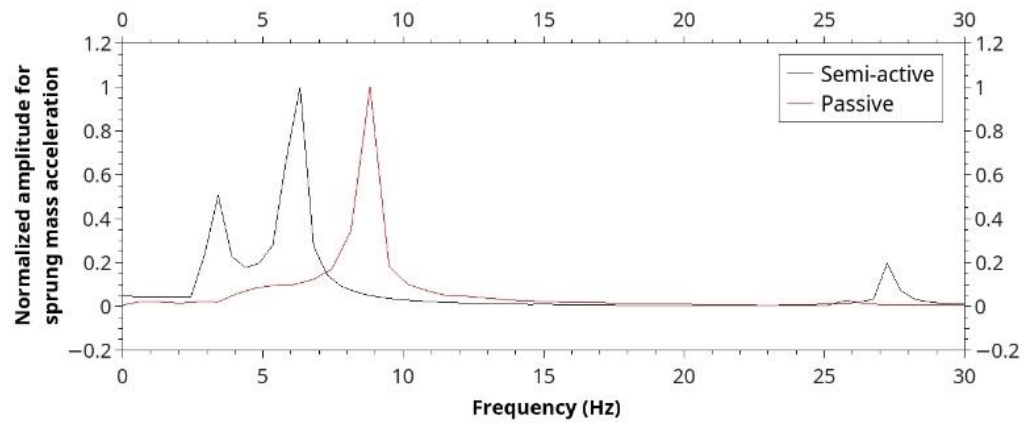
(b)

Figure 6.10 Frequency domain plots for Sine wave excitation **(a)** Heave of sprung mass **(b)** Sprung mass acceleration

Plots for both passive and semi-active type are shown and it can be seen that for both heave and acceleration, the peaks arrive at a lower frequency for the semi-active type when compared to passive type. There are multiple peaks for the semi-active type but there is a single peak for passive type.

6.6.2 Semi-active suspension with twin-tube MR damper

For the semi-active suspension with twin-tube MR damper, skyhook control and random road excitation was used. The performance is compared with passive suspension of an SUV. The vertical acceleration response of the sprung mass for a constant vehicle speed of 15 m/s (54 km/hr) for two kinds of road surfaces, average road and bad road are shown in Figure 6.11 and Figure 6.12 respectively.

(a)   **(b)**
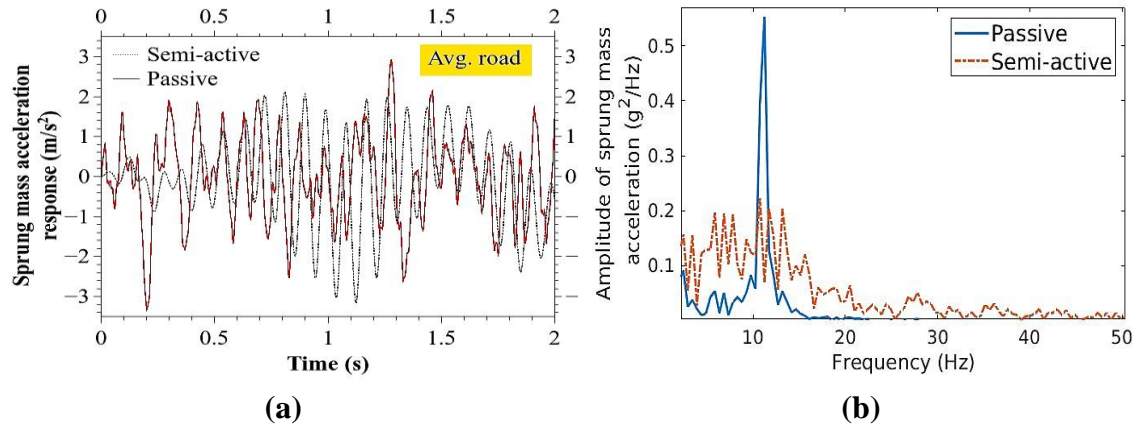
Figure 6.11 Sprung mass acceleration response for average road **(a)** Time domain **(b)** Frequency domain

Both time domain and frequency domain data are shown. It can be observed in time domain plots that the peak acceleration values for semi-active suspension with twin-tube MR damper are lower when compared to passive suspension for both average road and bad road. From the frequency domain plots, it can be seen that semi-active suspension has much lower acceleration and without any sudden peaks, when compared to passive suspension. From this, it can be inferred that semi-active suspension will provide better ride comfort when compared to passive suspension.

(a)   **(b)**
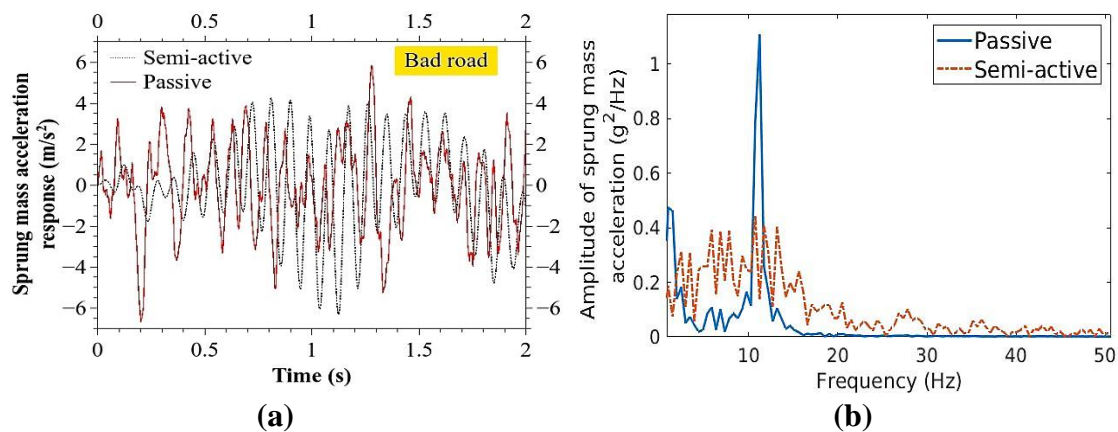
Figure 6.12 Sprung mass acceleration response for bad road **(a)** Time domain **(b)** Frequency domain

140

In order to study the performance of the suspension at different vehicle speeds, the root mean square (RMS) acceleration of the sprung mass is plotted against vehicle speed for average road and bad road as shown in Figure 6.13 (a) and (b) respectively.
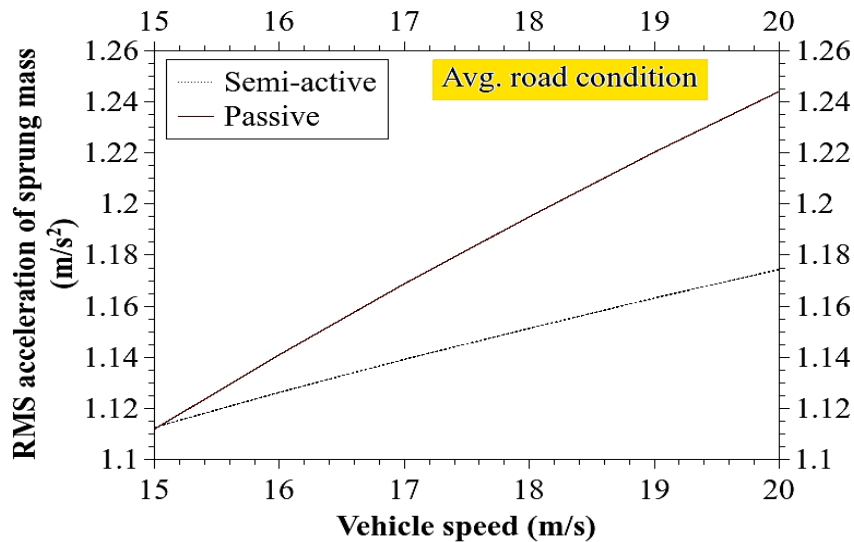
(a)
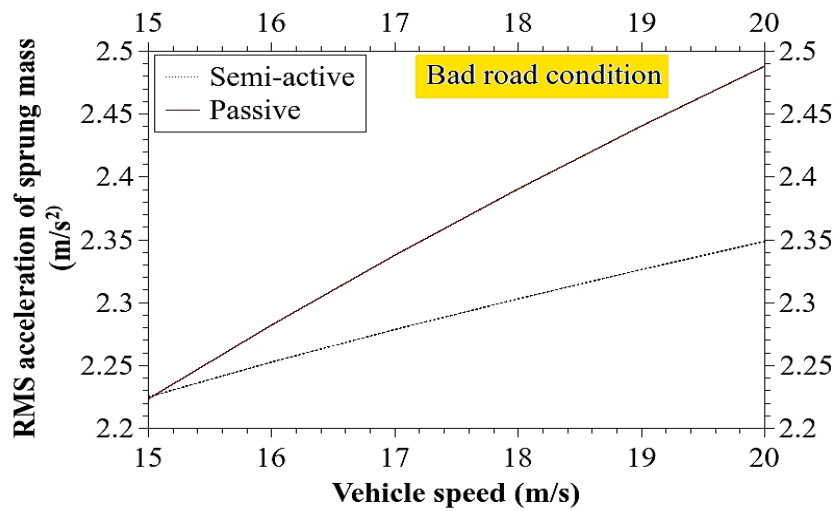
(b)

Figure 6.13 RMS acceleration of sprung mass vs vehicle speed **(a)** Average road **(b)** Bad road

It can be seen that semi-active suspension with twin-tube MR damper results in a lower RMS acceleration of sprung mass when compared to passive suspension of SUV, for both average and bad road condition. In addition to that, the advantage of semi-active suspension increases as the vehicle speed increases, with higher reduction in RMS acceleration when compared to passive suspension as the vehicle speed increases. Thus,

semi-active suspension with twin-tube MR damper provides better ride comfort than passive suspension.

6.7 SUMMARY

The dampers used in a passive suspension have fixed damping coefficient and hence they are a compromise between good ride comfort and better road holding. MR dampers provide variable damping which can be modulated by controlling the current supplied to the electromagnetic coil of the MR damper. Based on experimental characterization, polynomial models were proposed to mathematically model the hysteresis behaviour of commercial and twin-tube MR damper. MATLAB Simulink was used to study the performance of the semi-active suspension which uses the MR damper by mathematically modeling a quarter car setup. Sine wave excitation and random road excitation were used to simulate different types of excitation input to the suspension when the vehicle travels over uneven road surface. Two different types of random road profiles, average road and bad road, were considered. The variation of RMS acceleration of sprung mass with vehicle speed was also studied. The results of the simulation which consider the acceleration of the sprung mass show that semi-active suspension with skyhook control gives better ride comfort when compared to passive suspension. The twin-tube MR damper which was designed, fabricated and evaluated in the previous chapters has been used in a single degree of freedom (SDOF) quarter car suspension experimental setup in the next chapter to demonstrate the semi-active control of the suspension.

CHAPTER 7

PERFORMANCE EVALUATION OF A SINGLE SENSOR CONTROL SCHEME USING A TWIN-TUBE MR DAMPER BASED SEMI-ACTIVE SUSPENSION

7.1 INTRODUCTION

In this chapter, a single degree of freedom (SDOF) quarter car suspension is built for experimental evaluation of twin-tube MR damper based semi-active suspension. The semi-active control presented here makes use of only one sensor for obtaining input from the system. The performance is compared with other semi-active control method which uses more than one sensor to obtain system input.

7.2 METHODOLOGY

The methodology followed is as shown in Figure 7.1. A commercially available damper of passive type, used in a SUV is tested in damper testing machine to obtain graphs of force vs displacement and peak force vs velocity. With these results as basis, a valve mode MR damper of twin-tube construction was designed and fabricated. This MR damper is also tested in damper testing machine to obtain plots of peak force vs amplitude of velocity and force vs displacement. A single degree of freedom (SDOF) quarter car suspension is built using the suspension test rig. This quarter car suspension setup includes a sprung mass supported by a spring and damper and it is given vertical displacement input with the help of an actuator. Passive suspension is built using the passive damper and suspension of semi-active type is built using the MR damper. Displacement input in the form of fixed amplitude sinusoidal wave and rounded ramp wave are given at different frequencies. Different semi-active control methods are used such as Skyhook control and Rakheja-Sankar (RS) control along with constant current control. The response of the sprung mass and the ground force in each case is compared to determine the best type of suspension.
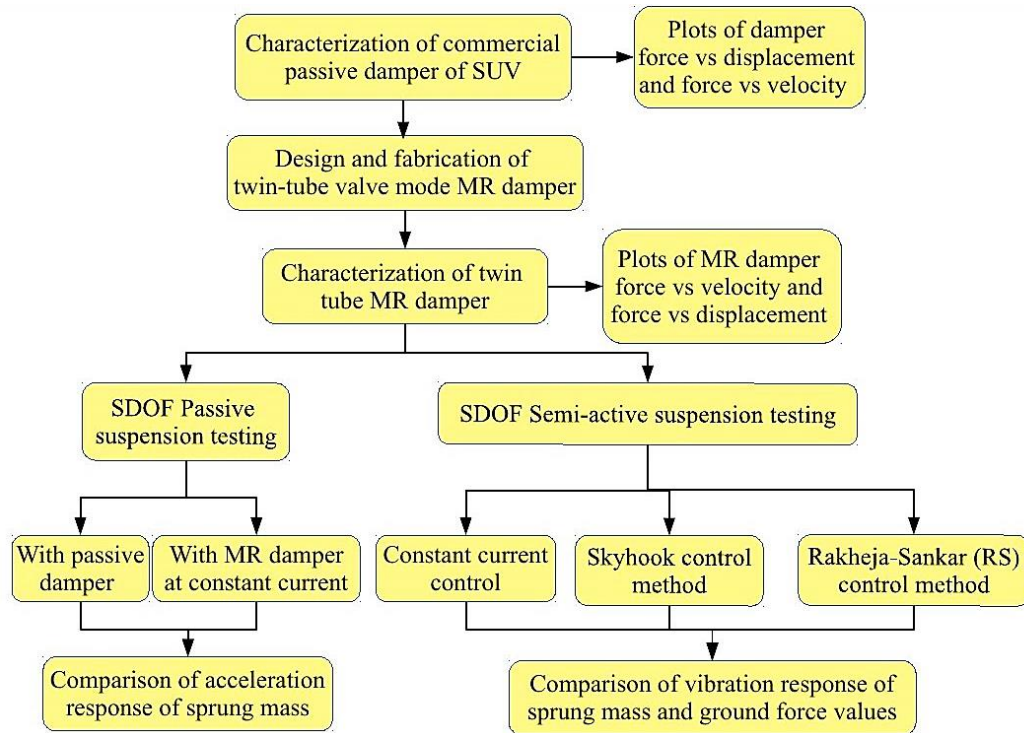
Figure 7.1 Flowchart of methodology followed

7.3 DAMPER CHARACTERIZATION

7.3.1 Characterization of commercial passive damper of SUV

The damper of Gabriel make, of front suspension in an SUV (Bolero by Mahindra) is characterized experimentally in the damper testing machine. The damper has 135 mm stroke and a fully compressed length of 345 mm as measured from eye to eye as shown in Figure 7.2.
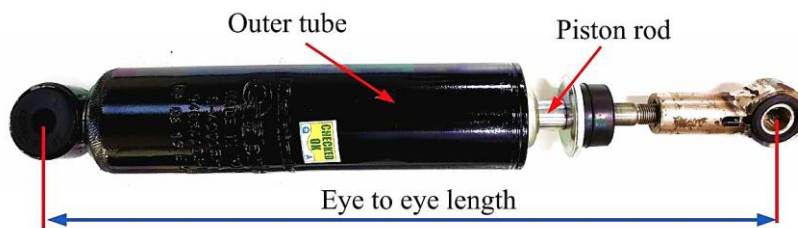
Figure 7.2 Passive damper of front suspension of SUV (Make: Gabriel)

The damper was given harmonic oscillations at a fixed amplitude of 15 mm and increasing frequency to experimentally measure the damping developed at different velocities. The variation of damper force with displacement as well as time is measured at frequencies of oscillation corresponding to a peak velocity of 50 to 300 mm/s in steps of 50 mm/s as shown in Table 7.1.

144

Table 7.1 Different frequencies of sinusoidal input oscillation at a fixed amplitude of 15 mm and corresponding peak velocities

Sinusoidal input frequency f (Hz)	Velocity amplitude (mm/s)
0.53	50
1.06	100
1.59	150
2.12	200
2.65	250
3.18	300

The damper is held between the two jaws of the damper testing machine which is shown in Figure 7.8. The lower jaw is fixed and the upper jaw is part of a hydraulic actuator. The actuator is servo controlled with the help of a MOOG electronic controller. When the damper is thus made to oscillate, the damping force generated is measured with the help of a force transducer placed below the fixed jaw and the damper displacement is measured by a position sensor. A 1 kHz sampling rate is used. Damping force is plotted against displacement for different peak velocities of piston as shown in Figure 7.3. Damping force in compression is given negative sign by convention and during rebound is given positive sign. It can be observed that as the peak piston velocity increases due to increased frequency of oscillation, the force-displacement loop becomes larger with higher peak compression and rebound force. Also, there is an asymmetry of the damping forces observed in compression and rebound. Damping force during rebound is observed to be more than twice the corresponding damping force during compression. This is intended and a design requirement, as the damper is not expected to provide high force during compression when most of the vibration energy is being absorbed by the spring. During rebound, when the spring releases the absorbed energy, the damper dissipates this energy by providing a high damping force during rebound. A slip is observed near zero force where displacement is happening without increase in force. This is due to play in the experimental setup, particularly between the eye of damper and the clamps in the damper testing machine which hold the damper during testing. When the actuator which is providing input oscillation to damper, changes the direction of motion during the course of sinusoidal excitation, a small play in the experimental setup is developed which can be seen at the extreme positions of displacement in Figure 7.3
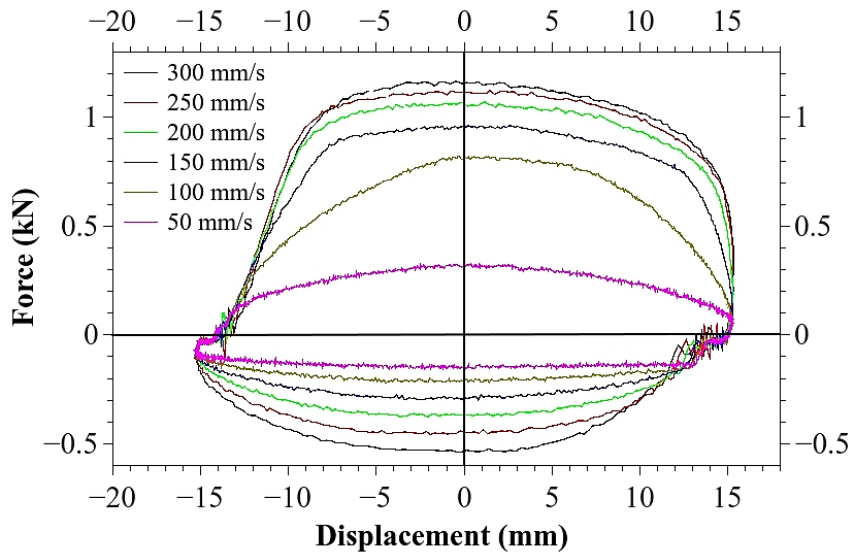
Figure 7.3 Damping force vs displacement for various peak velocities of piston

Plotting peak force during compression and rebound against the corresponding peak piston velocity shows that force increases with increase in peak piston velocity, both in compression and in rebound, as shown in Figure 7.4. In this figure, each data point corresponds to one of the frequencies of input excitation as given in Table 7.1
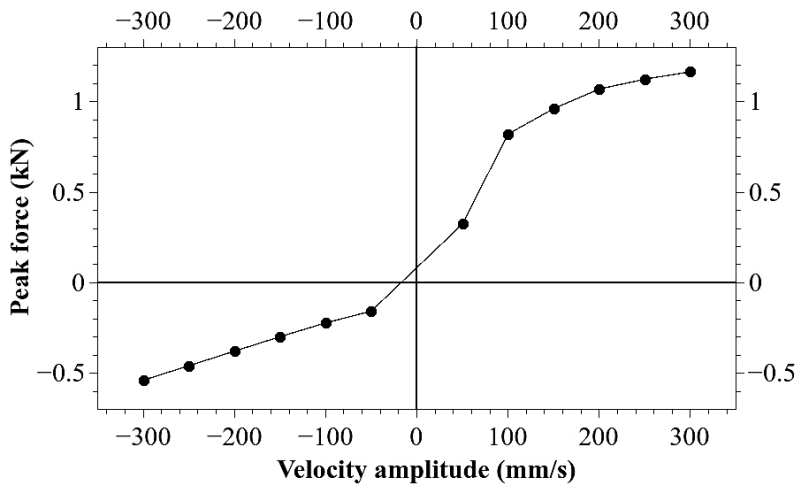
Figure 7.4 Peak damping force vs peak velocity

7.3.2 Characterization of twin-tube MR damper

A twin-tube MR damper working in flow mode, which was previously designed and manufactured, is used here. In this design, the piston of the damper incorporates an electromagnet and its construction is as shown in Figure 7.5. The copper coil is wound on the piston core and covered by an aluminium inner sleeve. An outer sleeve made of low

146

carbon steel along with top and bottom plate complete the piston assembly. MR fluid flows between the inner and outer sleeve. The construction is made in a way so that the magnetic flux is forced to cut through and magnetise the MR fluid present in annular gap.
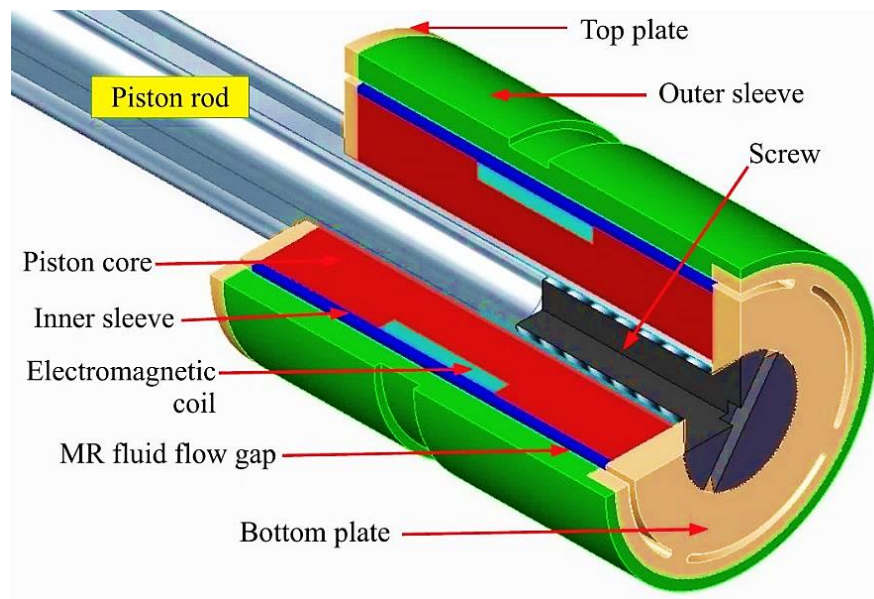
Figure 7.5 MR damper piston sectional view

This piston assembly is fastened on to the piston rod with the help of a countersunk screw fixed at the bottom plate. As shown in Figure 7.6, there is a hole in the piston core, which is concentric to another hole on the hollow piston rod through which the wires needed to supply electric power to the coil is routed.

Figure 7.6 Piston assembly with piston rod

The piston and rod assembly are inserted into the inner tube of the damper, which in turn is placed in the outer tube. It is located and held in place with the help of piston rod guide, an O ring seal and a fastener cap. A commercial MR fluid, Lord MRF 132DG was used in the MR damper. The fluid has carbonyl iron particles suspended in silicone oil, which acts as the carrier fluid. The MR damper after full assembly has a stroke of 170 mm and a fully compressed length of 397 mm measured from end to end as shown in Figure 7.7.
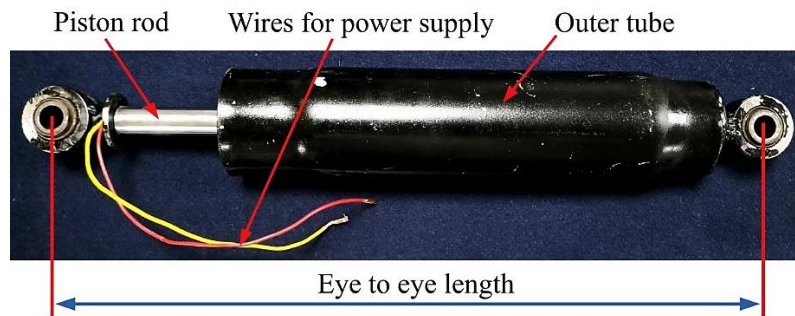
Figure 7.7 Twin-tube MR damper

Damper testing machine is used to test MR damper as explained in the previous section. Harmonic displacement input of fixed amplitude of 15 mm is given. Frequency of excitation is increased so as to vary the peak velocity starting from 50 mm/s to 300 mm/s in steps of 50 mm/s.
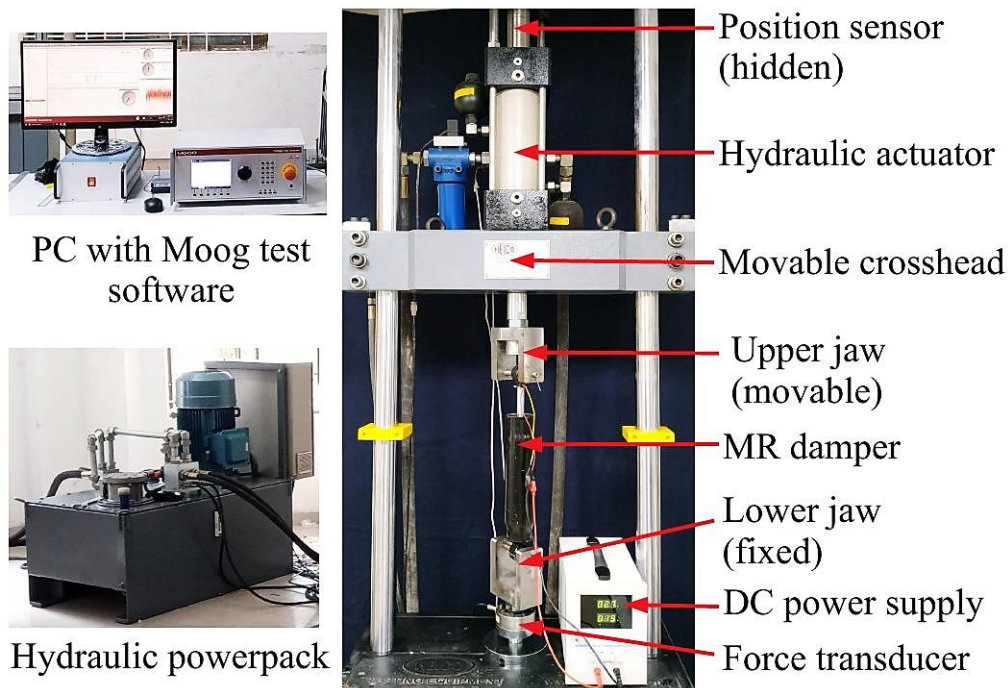
Figure 7.8 MR damper testing machine setup

148

Electric power is supplied to the MR damper with the help of a DC power supply unit as shown in Figure 7.8. The experiment is repeated for various fixed levels of current. Current is increased from 0 A to 0.6 A in steps of 0.15 A.

The plot of peak damper force during compression and rebound stroke against the velocity amplitude of harmonic oscillation is as shown in Figure 7.9. Here, each data point corresponds to one of the frequencies of input excitation as given in Table 7.1. It can be seen that the force values are increasing with increase in current. This is true both during compression and rebound. The corresponding peak force values for passive damper are also shown in the same plot to verify that force developed by MR damper are in a comparable range to that of the passive damper used in SUV front suspension.
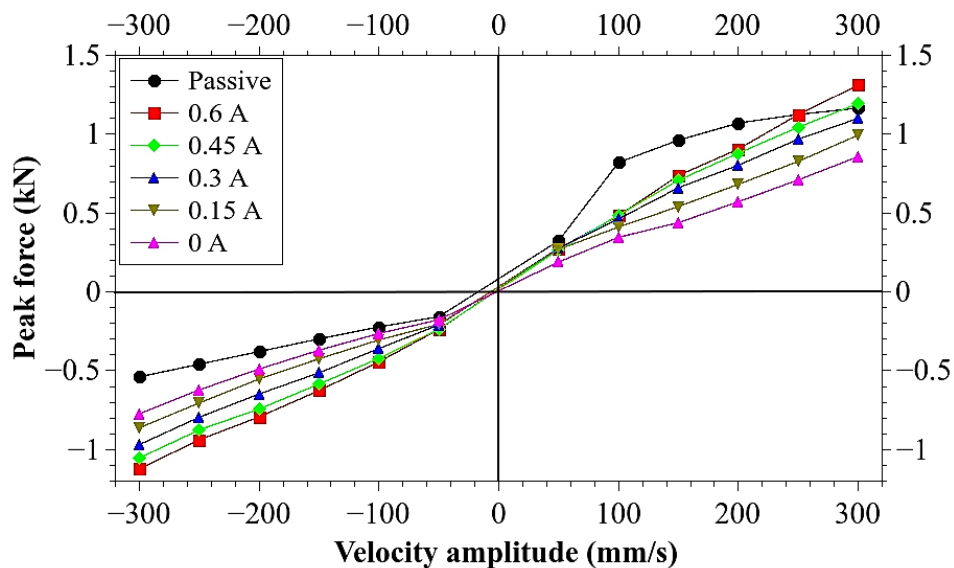
Figure 7.9 Peak force vs velocity amplitude at different current supplied

Variation of damping force with the damper displacement provides an estimate of the energy dispelled by the damper in single cycle of operation. A harmonic excitation of 10 mm fixed amplitude is given and frequency is varied from 2 Hz to 5 Hz in steps of 1 Hz. For each frequency of excitation, the current is varied from 0 A to 0.6 A in steps of 0.15 A. Such a plot for 5 Hz excitation is shown in Figure 7.10. It can be observed that as the current increases, the size of the force vs displacement loop increases. This shows that the MR damper is capable of dissipating higher energy at higher levels of current.
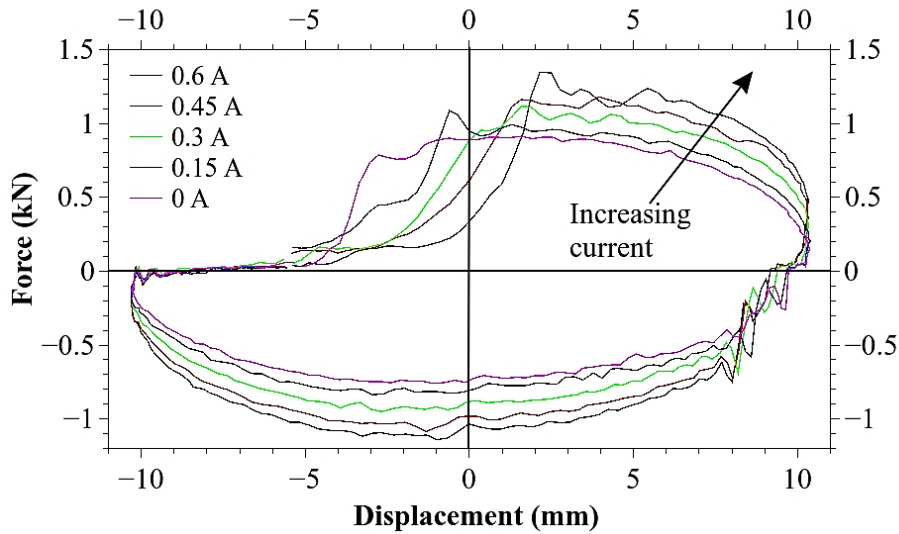
Figure 7.10 Damping force vs displacement at 5 Hz

7.4 SDOF SUSPENSION TESTING

7.4.1 Passive Suspension Test Setup

A single degree of freedom (SDOF) passive suspension consisting of a suspended mass supported by a passive damper and coil spring in parallel arrangement is shown schematically in Figure 7.11.
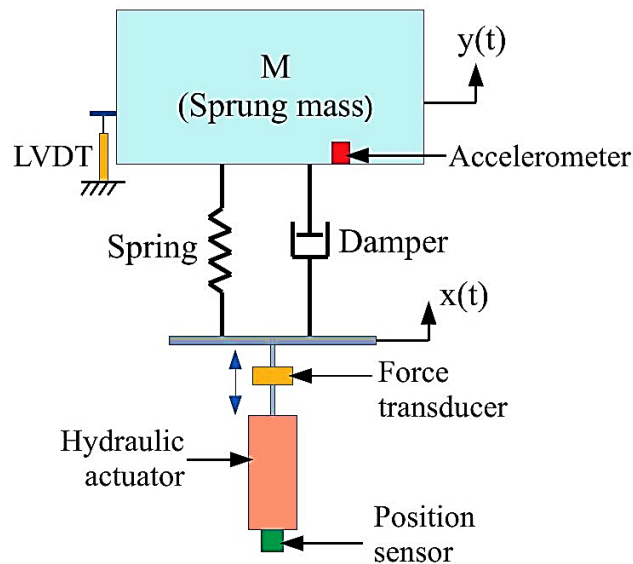
Figure 7.11 Schematic diagram of a SDOF passive suspension

Input displacement is given by means of a hydraulic actuator mounted at the bottom. It is connected to the bottom of the spring and damper through a force transducer. A

position sensor in the actuator measures the input displacement. The absolute vertical displacement of the sprung mass is measured by a Linear Variable Differential Transformer (LVDT). A uniaxial accelerometer mounted on the sprung mass measures its vertical acceleration. The hydraulically powered suspension testing machine is fabricated by HEICO Ltd and it can test automotive suspensions of different types and sizes as shown in Figure 7.12.
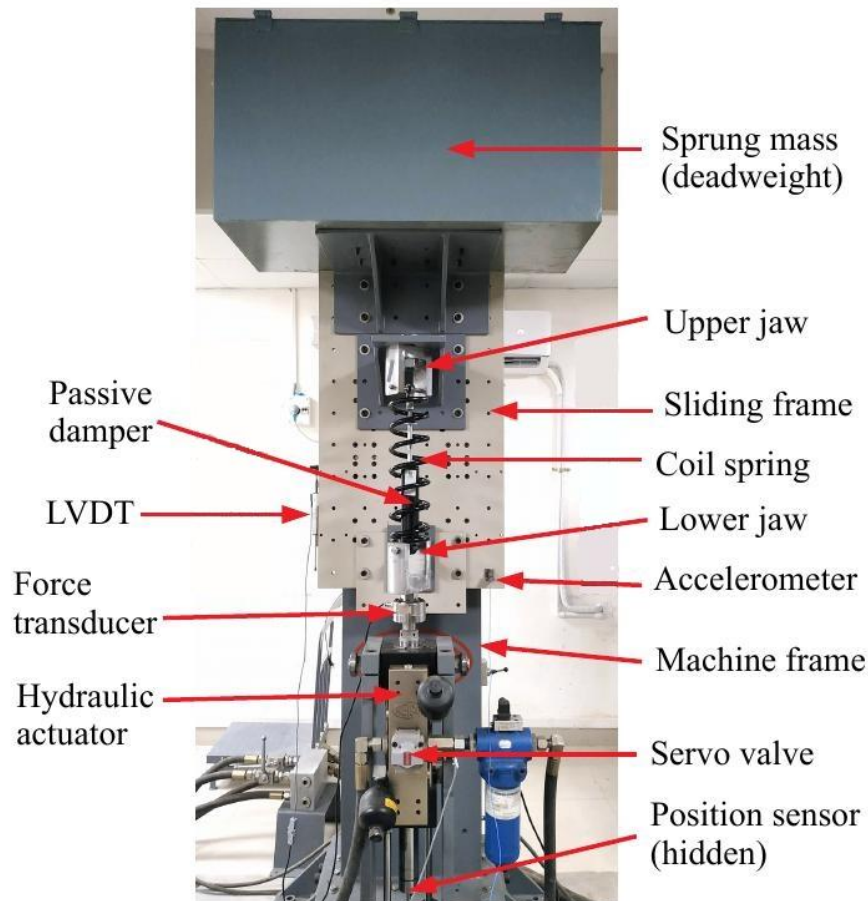
Figure 7.12 SDOF passive suspension test setup

A deadweight with a total weight of 300 kg, fastened to a vertical plate, is sprung mass in this case. This vertical plate is free to slide in the vertical direction on low friction guideways provided in the machine frame. The Gabriel make passive damper of SUV characterized previously, along with a coil spring taken from the same SUV are fixed between the upper and lower jaws of the test setup. The coil spring has a mean diameter of 101.5 mm and a wire diameter of 14 mm. One end of the spring is plain while the other end is squared with the total number of active coils being 6.5. The experimentally measured stiffness of the coil spring is 40.8 N/mm. The upper jaw is rigidly fixed to the sliding vertical plate and the lower jaw is fastened to rod end of hydraulic actuator. The hydraulic

actuator is servo controlled with the help of MOOG electronic controller. This actuator is equipped with a position sensor for displacement measurement. There is also a force transducer mounted between the actuator and the lower jaw which measures the force applied by actuator to suspension base. Both these sensors record the data with a sampling rate of 1000 Hz. There is a displacement sensor in the form of a LVDT mounted on the machine frame which measures the vertical displacement of the sprung mass. A uniaxial accelerometer mounted on the vertical sliding plate measures the vertical acceleration response of the sprung mass.

The suspension is given two types of input excitation, rounded ramp wave and harmonic oscillation with the help of the hydraulic actuator. Two levels of displacement amplitude, lower one at 5 mm and higher one at 10 mm along with four different frequencies from 2 Hz to 5 Hz with increments of 1 Hz are given as shown in Figure 7.13.
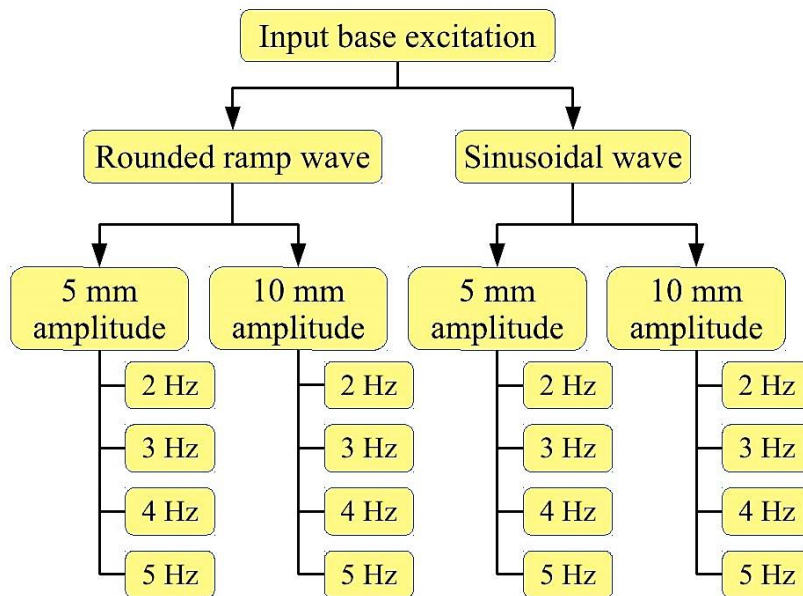
Figure 7.13 Input base excitation waveforms

7.4.2 Semi-active Suspension Test Setup

The same setup that was used for testing SDOF passive suspension is used to test the semi-active suspension, but with a few modifications as shown in Figure 7.14. The passive damper is replaced with the twin tube MR damper while retaining the same coil spring. The upper and lower jaws were modified with better support and safety for the spring in the form of tubular housings. This will prevent accidental damage to the MR damper under heavy loads and high amplitudes of vibration. The MR damper is connected to a DC power supply unit. A double ended and double acting hydraulic actuator of ± 20

152

kN capacity is used to provide the input displacement from the bottom to the suspension setup. A hydraulic power pack with maximum operating pressure of 210 bar is used to power the actuator. The capacity of power pack is 40 HP. It is also provided with a fan cooled radiator to bring down the temperature of the hydraulic fluid, as it heats up due to continuous operation at high loads. A PC running Moog Integrated Test Suite application along with a controller from Moog provides the control signal to the servo valve of the actuator. Another PC running NI LabVIEW software captures the accelerometer data. For the case with 0.3 A supplied to MR damper, a constant current DC power supply was used. This case with constant current will be used as reference to compare performance of the semi-active control methods.
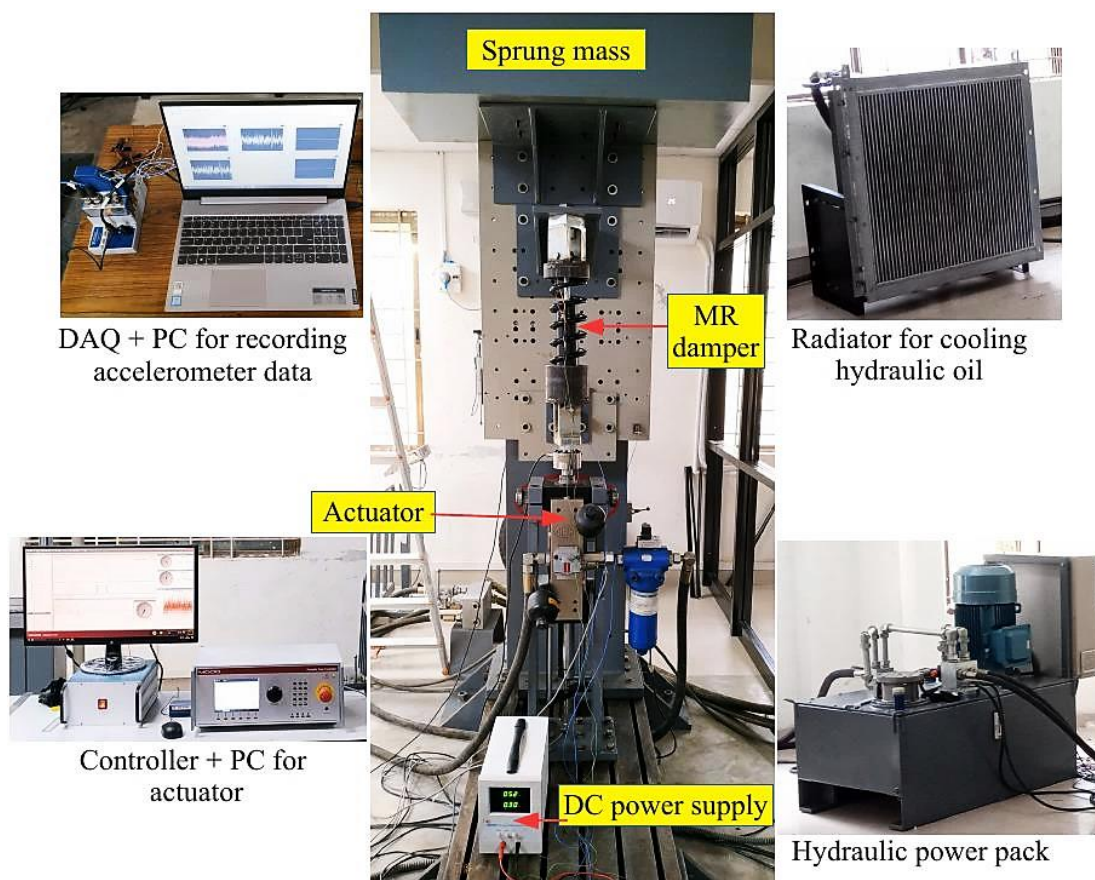
Figure 7.14 Semi-active SDOF suspension test setup

7.4.2.1 Skyhook control method

Skyhook control method is a well-accepted control method for semi-active suspension and the experimental setup is shown schematically in Figure 7.15. It prioritises passenger comfort by reducing displacement and acceleration of sprung mass. An imaginary damper of damping coefficient C_{sky} is connected between sprung mass and sky.

This damper reduces the absolute motion of the sprung mass in vertical direction by dissipating kinetic energy of sprung mass rapidly. The skyhook control method is implemented with the help of two uniaxial accelerometers a0 and a1 measuring the vertical acceleration of the unsprung mass and sprung mass respectively.
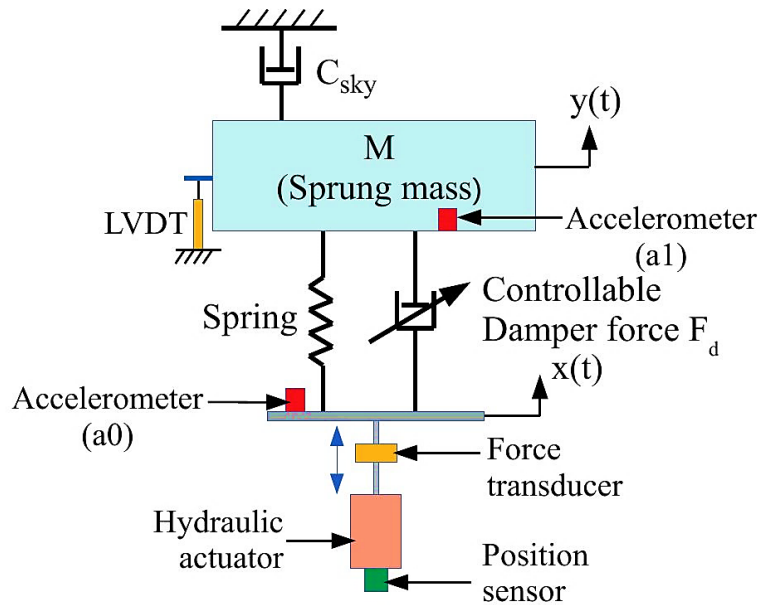
Figure 7.15 Schematic diagram of Skyhook control

Skyhook control method with on-off control is implemented according to the algorithm given by equation 7.1. Here, F_{dmax} is the maximum damping force achieved by supplying the maximum current to MR damper. F_{dmin} is minimum damping force achieved by cutting off the supply of current to the MR damper.

$$F_d = \begin{cases} F_{dmax} & \dot{y}(\dot{y} - \dot{x}) \geq 0 \\ F_{dmin} & \dot{y}(\dot{y} - \dot{x}) < 0 \end{cases} \tag{7.1}$$

The experimental setup for Skyhook control method is shown in Figure 7.16. Real time data from accelerometers a0 and a1 is captured with the help of DAQ NI 9234, which is a four input, 24-bit IEPE module and it is processed by NI LabVIEW software in the PC. The acceleration data is integrated to obtain the velocity of the unsprung and sprung mass needed in equation 7.1. Based on the outcome of the Skyhook control algorithm, the current supplied to the MR damper is controlled through a LabVIEW program with the help of NI 9403, which is a digital input output module. Both NI 9234 and NI 9403 communicate with the PC with the help of NI-CDAQ 9174 which is a four input CDAQ with power adaptor. The digital control signal output from NI 9403 is given to a battery powered current

controller, which then supplies the MR damper with either zero current or a maximum current of 0.6 A based on the digital input signal.
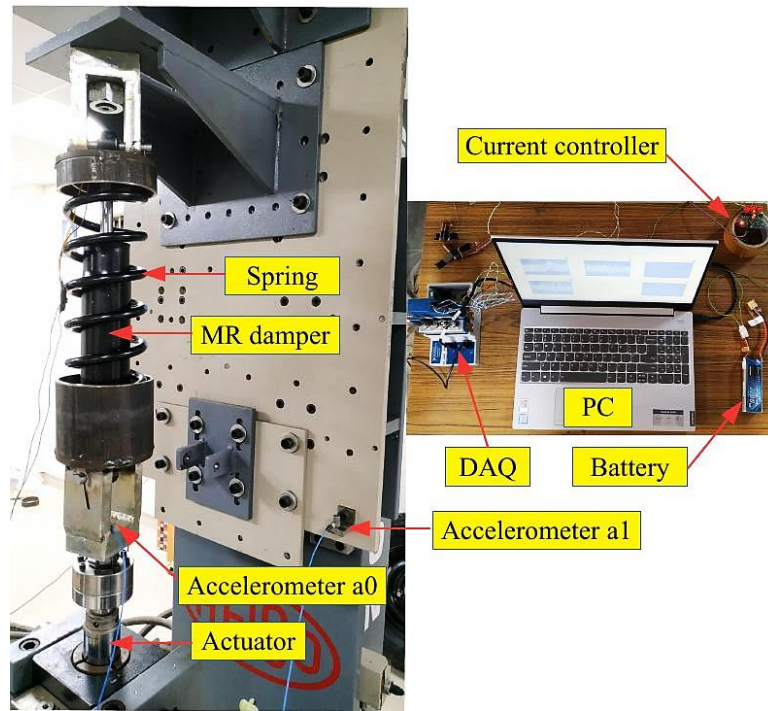
Figure 7.16 Skyhook control method suspension test setup

7.4.2.2 Rakheja-Sankar (RS) control method

In this control method, the relative velocity and relative displacement between unsprung mass and sprung mass is used as an input to calculate the current given to the MR damper. The control algorithm is given by equation 7.2. The basic idea is to have minimum damping force when spring and damping forces are in same direction and maximum damping force when they are in the opposite direction.

$$F_d = \begin{cases} F_{dmax} & (y - x)(\dot{y} - \dot{x}) \leq 0 \\ F_{dmin} & (y - x)(\dot{y} - \dot{x}) > 0 \end{cases} \tag{7.2}$$

The schematic of RS control method experimental setup is shown in Figure 7.17. A second LVDT mounted between the sprung mass and actuator measures the displacement between sprung mass and actuator. The data from the LVDT is filtered and differentiated with respect to time to obtain relative velocity between sprung mass and input displacement from actuator.
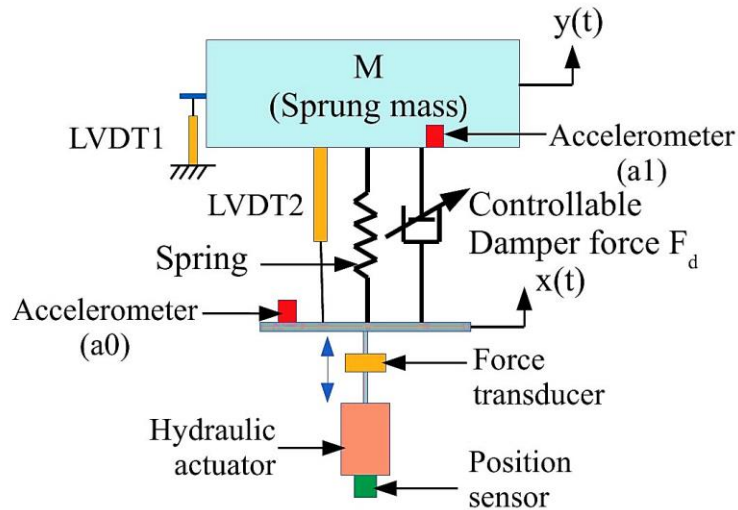
Figure 7.17 Schematic diagram of RS control method

The experimental setup for RS control method is shown in Figure 7.18. Sensor data from LVDT2 is captured with the help of DAQ NI 9234. This is the relative displacement $(y - x)$. This data is filtered and differentiated to obtain the relative velocity $(\dot{y} - \dot{x})$. Based on the outcome of the calculations of equation 7.2, the current given to MR damper is controlled through NI 9403, which is a digital input output module.
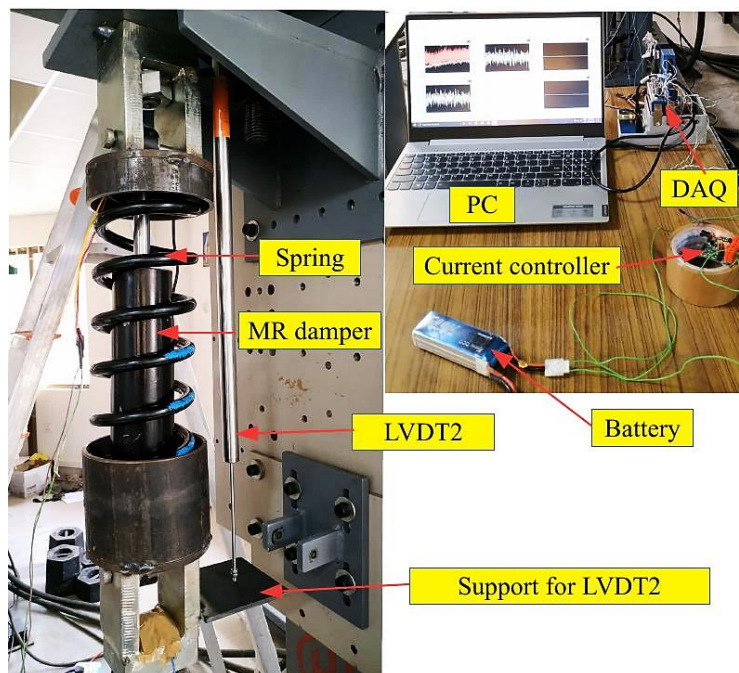
Figure 7.18 RS control method suspension test setup

Whereas the Skyhook control method uses input from two accelerometers, which are then integrated separately to evaluate the current to be given to the MR damper, in RS control method, data from a single displacement sensor mounted between sprung and

unsprung masses gives $(y - x)$ which upon differentiation gives $(\dot{y} - \dot{x})$. Though in the experimental work presented, a LVDT was used for higher accuracy, in practical implementation for a vehicle, a rotary encoder with a crank arm can be used. The encoder can be fixed to the chassis which is the sprung mass and the spring-loaded crank can be made to rest on any of the unsprung components of the vehicle suspension. This can measure the displacement between the chassis and the wheel axle (y-x). Hence RS control method requires fewer sensors and lower computational capacity. Therefore, it is simpler and less expensive when compared to Skyhook control.

7.5 RESULTS

7.5.1 Equivalence of passive suspension system and semi-active suspension with constant current

The comparison of passive suspension system and semi-active suspension with constant current is shown in Figure 7.19. Vertical acceleration response of the sprung mass is shown plotted against time for sinusoidal base displacement input. A low amplitude case of 5 mm and high amplitude case of 10 mm is used and low frequency of 2 Hz and high frequency of 5 Hz is used. Response for all combinations of these amplitudes and frequencies is shown in Figure 7.19. Between passive suspension and semi-active suspension, the spring used is identical but the commercial passive damper was replaced with MR damper. A constant current of 0.3 A which is mid-way between zero current and maximum current of 0.6 A is supplied to the MR damper. It can be observed from Figure 7.19 that the semi-active suspension under constant current behaves nearly the same as the passive suspension. Peak acceleration response of sprung mass is almost the same in the two cases for all combinations of amplitudes and frequencies tested.
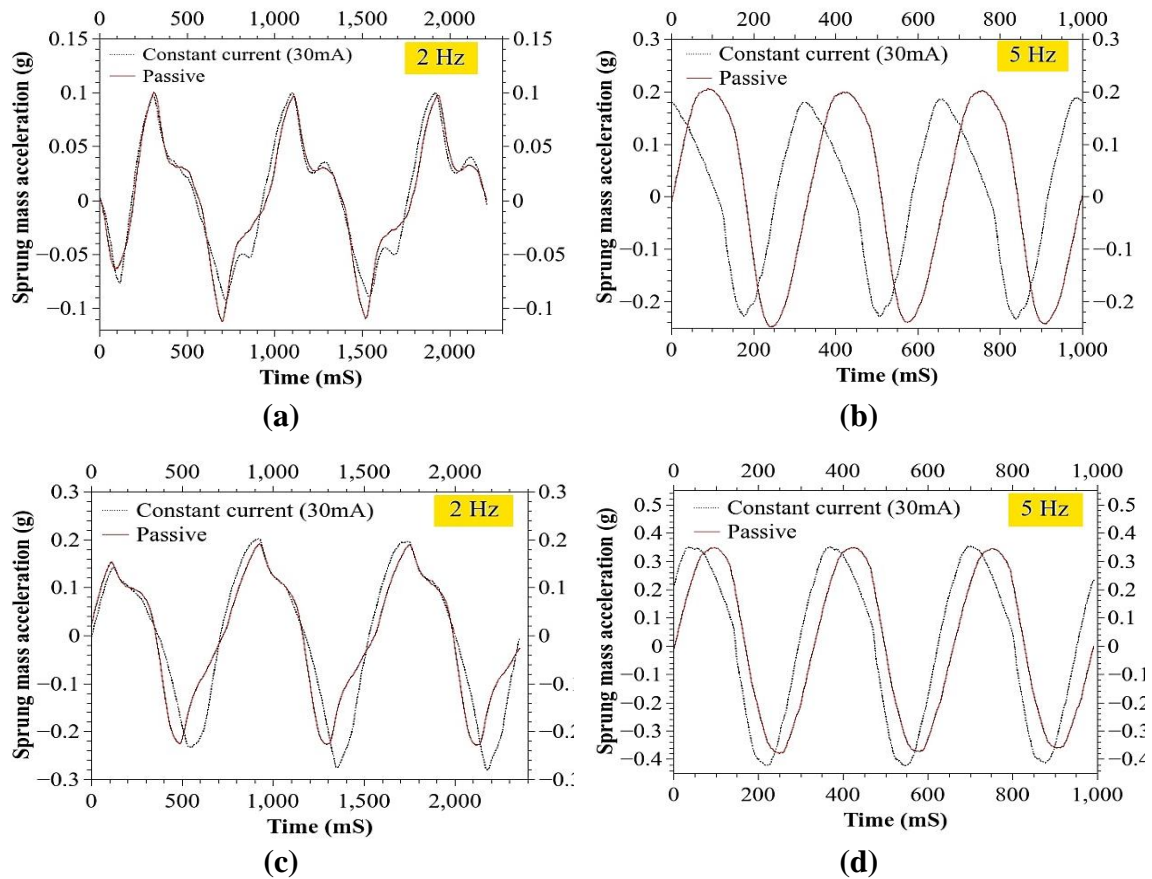
Figure 7.19 Sprung mass acceleration comparison of passive and semi-active suspension for sine wave input **(a)** 5 mm amplitude of 2 Hz frequency **(b)** 5 mm amplitude of 5 Hz frequency **(c)** 10 mm amplitude of 2 Hz frequency **(d)** 10 mm amplitude of 5 Hz frequency

This establishes the equivalence of passive suspension of SUV and newly designed semi-active suspension with constant current control. This result will be used in further comparisons of MR damper based semi-active suspension.

7.5.2 Response to rounded ramp input

Sprung mass acceleration response for rounded ramp displacement input of 5 mm amplitude and 10 mm amplitude plotted against time is shown in Figure 7.20 and Figure 7.21 respectively. Response under constant current of 0.3 A is compared to the response under Skyhook control method and Rakheja-Sankar (RS) control method. Each plot shows the response for 2 Hz, 3Hz, 4 Hz and 5 Hz excitation, run for 5 cycles each.
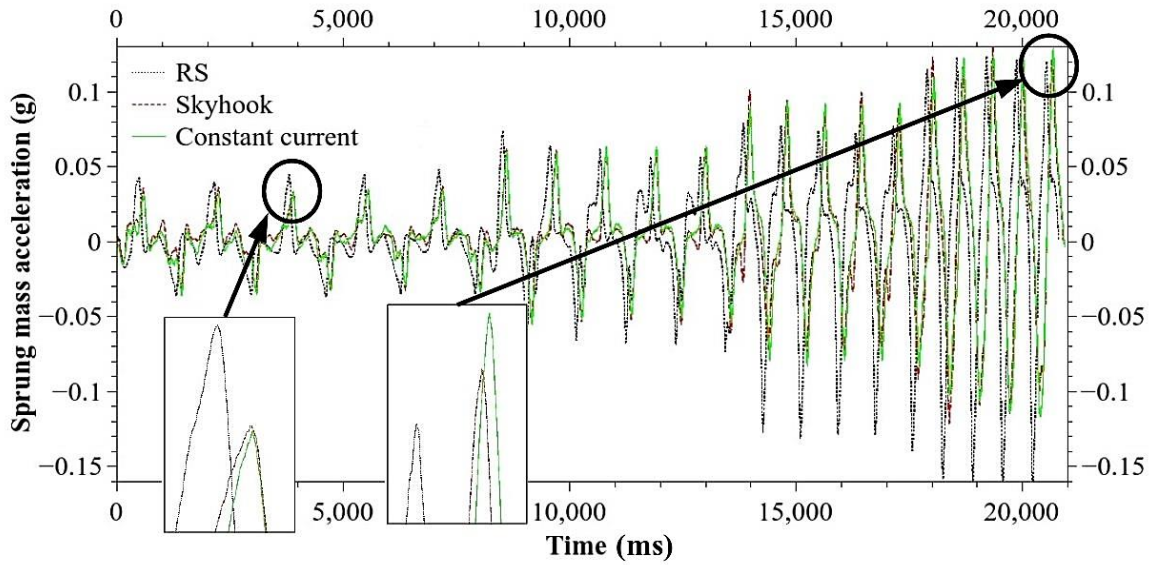
Figure 7.20 Sprung mass acceleration response for rounded ramp input of 5 mm
amplitude
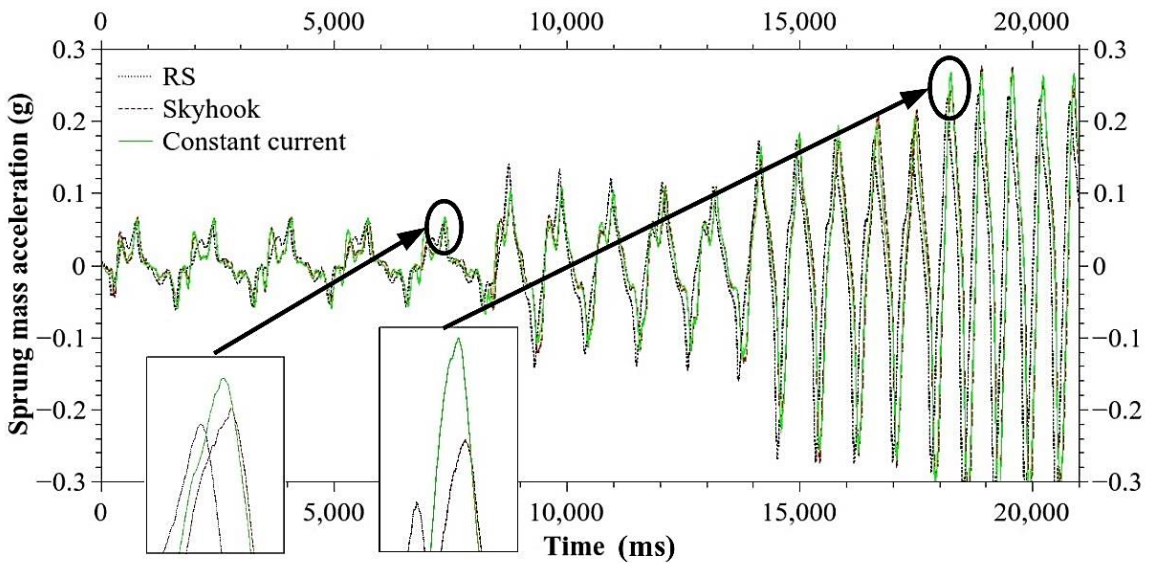
Figure 7.21 Sprung mass acceleration response for rounded ramp input of 10 mm
amplitude

7.5.3 Response to sine wave input

Similarly, the sprung mass acceleration response for sine wave displacement input
of 5 mm amplitude and 10 mm amplitude plotted against time is shown in Figure 7.22 and
Figure 7.23 respectively. Response under constant current of 0.3 A is compared to the
response under Skyhook control method and Rakheja-Sankar (RS) control method.
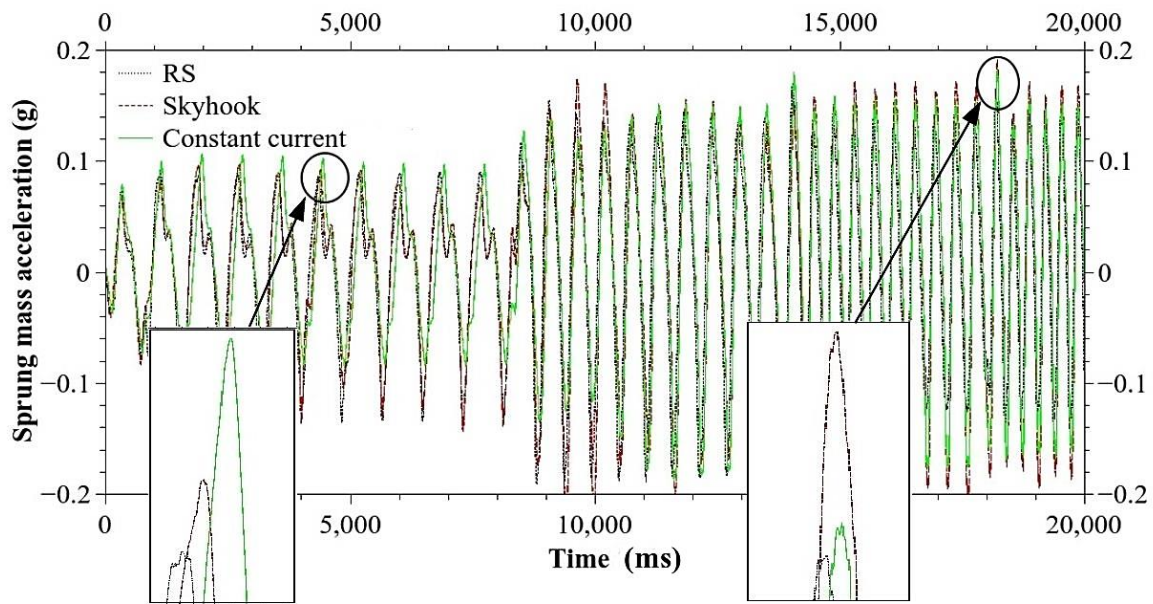
Figure 7.22 Sprung mass acceleration for sine wave input of 5 mm amplitude
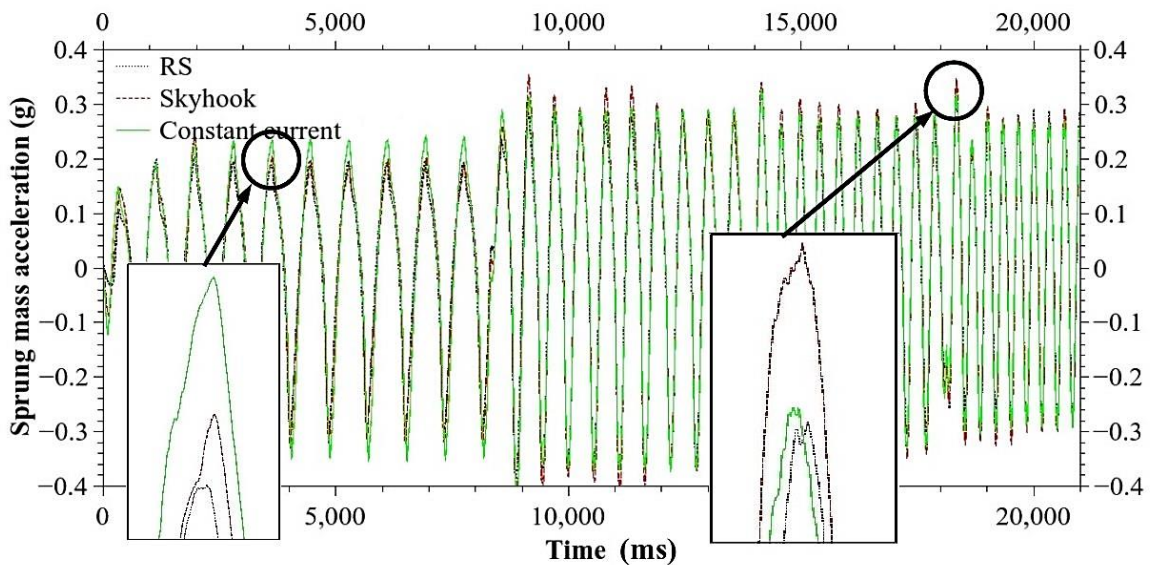
Figure 7.23 Sprung mass acceleration for sine wave input of 10 mm amplitude

7.5.4 Comparison of peak value of sprung mass acceleration

In order to compare different semi-active controls used, peak sprung mass acceleration response is plotted as a bar graph for different types of input displacement, rounded ramp input of 5 mm and 10 mm amplitude and sine wave input of 5 mm and 10 mm amplitude as shown in Figure 7.24. Four frequencies were tested, out of which the lowest of 2 Hz and highest of 5 Hz is shown.
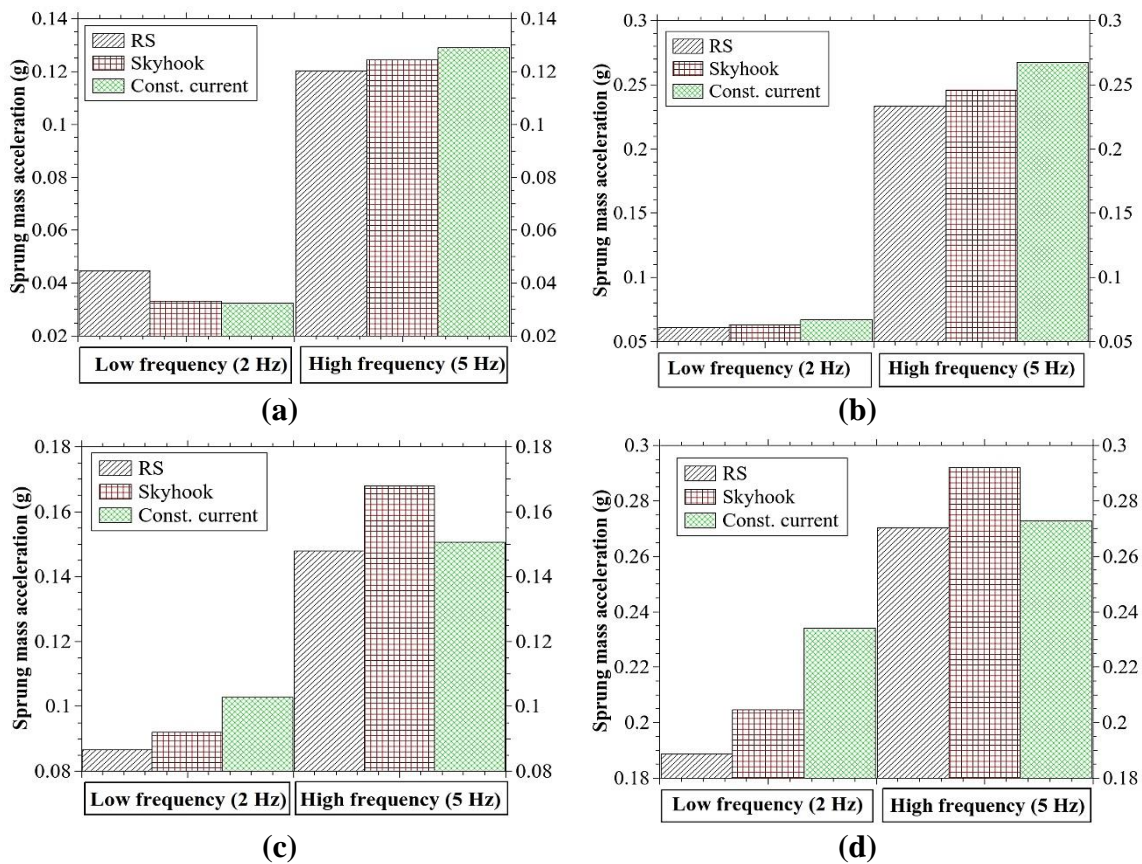
Figure 7.24 Peak sprung mass acceleration values for different semi-active control methods **(a)** Rounded ramp input of 5 mm amplitude **(b)** Rounded ramp input of 10 mm amplitude **(c)** Sine wave input of 5 mm amplitude **(d)** Sine wave input of 10 mm amplitude

A lower value of peak acceleration response of sprung mass corresponds to better ride comfort of vehicle passengers. Hence, a lower peak value of sprung mass acceleration is desirable. It can be observed that for rounded ramp input of higher frequency, RS control method gives the lowest peak acceleration value followed by Skyhook control method and then constant current control. So, RS control method provides the best ride comfort followed by Skyhook control method and constant current control. The same result is true for rounded ramp input of lower frequency at 10 mm amplitude. For rounded ramp input of lower frequency at 5 mm amplitude, it appears that Skyhook control method and constant current control provide better ride comfort than RS control method. For sine input of lower frequency, for both 5 mm and 10 mm amplitude, RS control method gives the lowest peak acceleration value followed by Skyhook control and then constant current control. So, RS control provides the best ride comfort followed by Skyhook control and constant current control. For higher frequency input, both RS control and constant current control provide

lower peak acceleration values than Skyhook control method. Hence, it can be concluded that except for rounded ramp input of low frequency and low amplitude, RS control method provides the best ride comfort in all conditions.

7.5.5 Ground force response

Ground force is the force developed at the contact between the road surface and the tyre of the vehicle. In terms of the quarter car test setup, it is the force between the actuator and the unsprung mass of the suspension. It is important because excessive ground force is detrimental to the road surface and causes damage to the road. This ground force is also transmitted to the unsprung mass and it may damage the tyres and suspension elements of the vehicle. Hence, ground force must be kept under control and a lower value is desirable. The variation of ground force with time for different control methods for sine wave input of 5 mm and 10 mm amplitude is shown in Figure 7.25 and Figure 7.26 respectively.
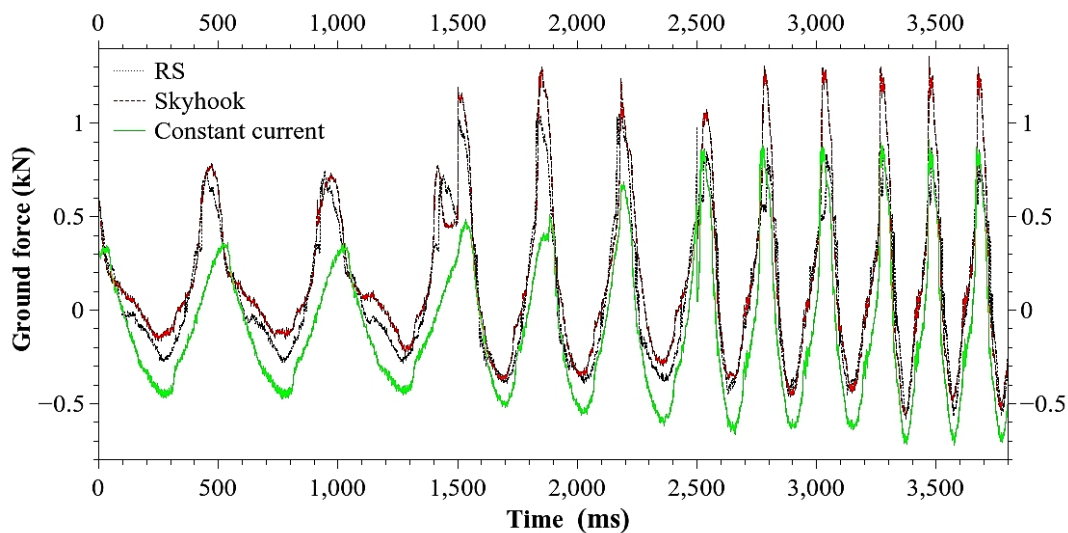
Figure 7.25 Ground force response for sine wave input of 5 mm amplitude
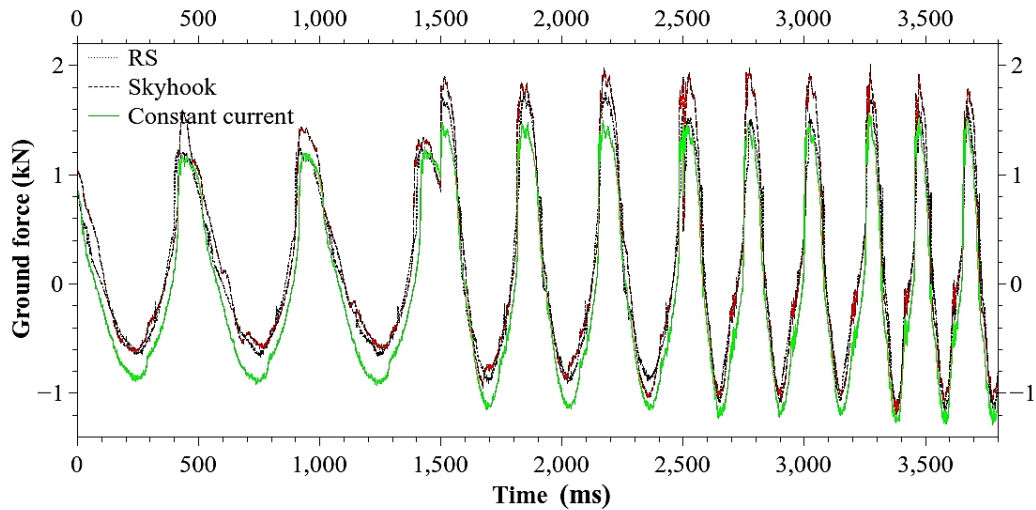
Figure 7.26 Ground force response for sine wave input of 10 mm amplitude

For comparison of different control methods, the peak ground force response values are plotted as bar graphs for sine wave input of 5 mm and 10 mm amplitude, as shown in Figure 7.27.

(a)   **(b)**
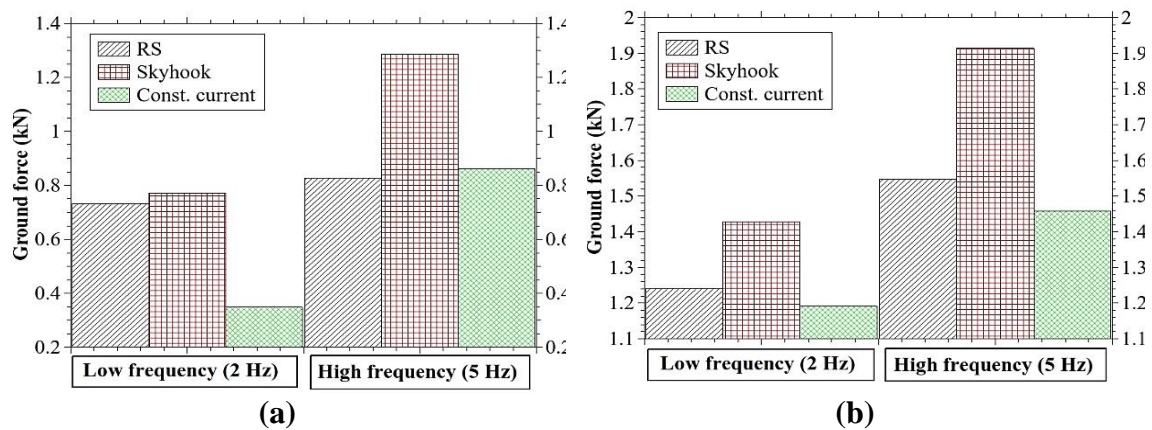
Figure 7.27 Comparison of peak values of ground force **(a)** Sine wave input of 5 mm amplitude **(b)** Sine wave input of 10 mm amplitude

It can be observed from the ground force bar graph that Skyhook control method generates the highest ground force for all conditions of frequencies and amplitudes. Except for low frequency and low amplitude case, RS control method provides much lower ground force when compared to Skyhook control method and it is similar to that provided by constant current control. Hence RS control method provides low peak ground force values and it is the preferred control method.

7.6 SUMMARY

A twin-tube valve mode MR damper was created for use in the suspension of a SUV automobile. Experimental characterization of the MR damper on damper testing machine confirmed MR behaviour of the damper with following conclusions.

- The damping force developed by MR damper increases with increase in current. Energy dissipated by the damper can be varied by controlling the current.

- The magnitude of force developed at various excitation frequencies and peak damper velocities is comparable to that of a passive damper used in the SUV automotive suspension.

- The MR damper can be deployed as semi-active element in vehicle suspension.

A single degree of freedom (SDOF) quarter car suspension test rig was built on a suspension testing machine to test the performance of semi-active suspension and compare it with passive suspension. Various types of excitations in the form of input displacement were used with constant current control, Skyhook control and Rakheja-Sankar (RS) control method as different cases. The conclusions are.

- The passive suspension system of the SUV and the newly designed MR damper semi-active suspension with constant current control have nearly identical sprung mass acceleration response.

- For sinusoidal displacement input in the low frequency range (2-3 Hz), RS control method provides the least value of peak vertical acceleration of sprung mass, followed by Skyhook control and constant current control. In the high frequency range (4-5Hz), RS control provides much lower vertical acceleration than Skyhook control and similar to constant current control.

- For rounded ramp displacement input, except for the low frequency low amplitude case, RS control method provides the least value of peak vertical acceleration of sprung mass, followed by Skyhook control and constant current control.

- Thus, for a semi-active suspension using twin-tube MR damper, RS control method provides better ride comfort to passengers due to lower peak vertical acceleration when compared to constant current control or Skyhook control method.

- For sinusoidal displacement input, RS control method generated much lower peak ground force values when compared to Skyhook control, especially in the high frequency region. For example, for 5 Hz excitation of 5 mm amplitude, RS control method led to 36 % reduction of peak ground force when compared to Skyhook

control. Thus, for preventing damage to road surface as well as to vehicle suspension elements, RS control method is a much better choice.

The next chapter presents the significant conclusions of the present work.

CHAPTER 8

CONCLUSIONS AND FUTURE WORK

8.1 CONCLUSIONS

In this research work, a twin-tube valve mode MR damper was designed and developed for application in a semi-active automotive suspension. With reference to the objectives mentioned in section 2.9, an automotive passive damper was experimentally tested to determine the levels of damping force required at different velocities. MR fluid was successfully synthesized and characterised in a rheometer. Mathematical models were developed based on the experimental data as well as MR fluid rheology and damper geometrical data. Effectiveness of MR damper based semi-active suspension was demonstrated with the help of a SDOF quarter car test rig using skyhook and RS control method. The significant contributions from this dissertation research are as follows:

8.1.1 Automotive passive damper

The passive damper used in a SUV automobile was tested in the damping force testing machine. Sinusoidal excitations of fixed amplitude and varying frequencies were used for evaluation. Damper force and corresponding displacement were measured along with time data. The force vs displacement plots show that the size of the loops increase with increase in frequency of excitation. As the area of the loops represent the amount of dissipated energy in one cycle, one can conclude that the passive damper dissipates higher amount of energy at higher frequencies of excitation keeping amplitude of vibration as constant. From the maximum force vs velocity amplitude plot, it was found that for the same velocity values, the damping force in bounce is more than twice that in compression. Plots of damper force vs damper velocity demonstrated the hysteresis behaviour of the damper. Results for several frequencies were plotted and to demonstrate the method, mathematical models were built for two of the frequencies, the medium and the highest one (1.99 Hz and 3.98 Hz). The simulated curves follow the experimental plots closely and for all practical purposes, the mathematical models can be used to estimate the damper force at any given damper velocity or any combination of sinusoidal excitation frequency and amplitude. These results can be utilized in designing a new suspension system for the vehicle under study as these data are not provided by the damper manufacturers.

8.1.2 Commercial MR damper

A commercially available MR damper was evaluated in a damping force testing machine at various excitation frequencies and current supplied. Plots of force vs displacement show that damping force was increasing with velocity as well as current supplied. Calculation of area of the force vs displacement loops lead to evaluation of energy dissipated values and which in turn gave values of equivalent damping of the MR damper. The increase in equivalent damping with current supplied and plots showing high dynamic range of MR damper at frequencies between 0.5 Hz and 3 Hz, made the MR damper suitable for application in commercial vehicle driver's seat suspension. Mathematical model of the MR damper behaviour was developed using Bouc-Wen hysteresis operator and genetic algorithm (GA) provided in Optimization toolbox of MATLAB. A good match between the simulated and experimental plots confirms the veracity of the method used. It was successfully shown that by controlling the current supplied to the MR damper, the suspension can be made to work as an underdamped, critically damped or overdamped system. The current supplied also controls the amount of energy dissipated by the MR damper in one cycle of input oscillation. These can be used to design a semi-active control strategy for the seat suspension using MR damper to provide a comfortable and fatigue free ride.

8.1.3 Twin-tube valve mode MR damper

A twin tube MR damper was designed based on the damping values of a passive damper used in a passenger van. The damper piston was modified to accommodate an electromagnetic coil in order to generate a magnetic field in the fluid flow gap for the activation of MR fluid. The MR damper operates in valve mode. The magnetic flux density at the fluid flow gap was evaluated analytically by using laws of the magnetic circuit and the value obtained closely matches with that obtained using the FEMM software. Experiments were carried out by using commercially available MR fluid by Lord Corporation. Different levels of current were supplied to the MR damper and input oscillations at operating frequencies and amplitudes were given. The force generated by the damper and displacement of the damper piston were measured. The plots of force vs displacement reveal that the damping force increases with increase in the current supplied and hence demonstrates the field dependent yield stress nature of the MR fluid. Plots of

force vs velocity further confirm the MR behaviour which show that for a particular damper piston velocity, as the current supplied increases, the damping force increases.

Mathematical models were developed to simulate the MR damper behaviour at various values of current supplied and input oscillation frequency. The Bouc-Wen equation was used to simulate the force vs displacement, force vs velocity and force vs time plots. The eight parameter values needed for this simulation were arrived at using GA provided in the optimization toolbox of the MATLAB software. This was done for selected values of current supplied at a particular input oscillation frequency to demonstrate the method used. The plots showing comparison between experimental and simulated values for 1.59 Hz input oscillation frequency for three values of current 0 A, 0.5 A and 1 A, confirm close agreement and validates the values of parameters used in the mathematical model. The maximum input current used for the MR damper operation was 1.5 A and this can be comfortably supplied by the vehicle's alternator or battery without any modifications needed. The power requirement of the MR damper is less than 18 W, which is very low. A PID controller was used to track the desired damping force in the time domain. A pulse waveform was used as input. The actual force of the MR damper tracks the desired force closely with very little lag and no overshoot. Hence the MR damper can be used to implement a semi-active suspension system in the passenger van with PID controller. Thus, this twin tube valve-mode MR damper can be used as a replacement for the passive damper in the passenger van.

8.1.4 Synthesis of MR fluid

MR fluid was prepared with CIP and silicone oil as the principal components. This fluid was characterized in a rheometer and its behaviour under varying magnetic field strengths was studied. The shear stress developed at any given shear strain was experimentally observed to increase with the applied magnetic field. The shear thinning behaviour of shear stress vs shear rate plot for MR fluid is non-linear in nature. This was successfully modelled using the HB model and the parameters of the model were expressed as polynomial functions of strength of magnetic field so that shear stress of MR fluid can be found at any given strength of the magnetic field. A twin tube valve mode MR damper containing this MR fluid was experimentally characterized in the damper testing machine under varying values of current given. Damper force vs displacement, peak velocity and instantaneous velocity plots were generated. The strength of the magnetic field at the fluid flow gap in the piston of the MR damper at different levels of current were evaluated using

an axisymmetric 2D model of piston in FEMM software. It was found that the damper force increases with current given at all frequencies of excitations tested. The value of analytically calculated force increases with current. Some important conclusions are:

- Dimensionless numbers along with HB model for MR fluid behaviour can be used to predict the damping force of MR damper at any given piston velocity and current.
- Dynamic range of MR damper was evaluated and it was found that it decreases with an increase in excitation frequency.
- The experimental and analytical damper force were compared to conclude that the methods used are valid.

Hence, a twin tube MR damper operating in valve mode can be designed for application in an automobile using an in-house prepared MR fluid. The damping force is the sum of controllable and uncontrollable force. The controllable force can be varied by controlling the current supplied to the MR damper and thus it can be used to implement a semi-active suspension system. The MR damper piston which acts as a MR valve can be analyzed using non-dimensional equations involving pressure number G, yield stress number S and flow index m. The pressure loss across the damper piston due to a field-controlled yield stress of MR fluid was calculated at different velocities using flow rate and geometrical design parameters along with dimensionless numbers.

8.1.5 Dynamic analysis of quarter car vehicle model

The dampers used in a passive suspension have fixed damping coefficient and hence they are a compromise between good ride comfort and better road holding. MR dampers provide variable damping which can be modulated by controlling the current supplied to the electromagnetic coil of the MR damper. Based on the experimental characterization of a commercial MR damper, a polynomial model was proposed to mathematically model the hysteresis of the MR damper. Plots of damping force vs damper piston velocity at different currents supplied show that the damping force increases with increase in current. MATLAB Simulink was used to study the behaviour of the semi-active type suspension which uses the MR damper by modeling a quarter car setup. Sine wave excitation and step input were used to simulate different types of excitation input to the suspension when the vehicle travels over uneven road surface. The results of the simulation which consider the heave of the sprung mass and acceleration of the sprung mass show that semi-active type suspension system gives better ride comfort when compared to a passive suspension.

170

8.1.6 Single sensor control scheme

A twin-tube valve mode MR damper was created for the suspension of a SUV automobile. Experimental characterization of the MR damper on damper testing machine confirmed MR behaviour of the damper with following conclusions.

- The damping force developed by MR damper increases with increase in current. Energy dissipated by the damper can be varied by controlling the current.

- The magnitude of force developed at various excitation frequencies and peak damper velocities is comparable to that of a passive damper used in the SUV automotive suspension.

- The MR damper can be deployed as semi-active element in vehicle suspension.

A single degree of freedom (SDOF) quarter car suspension test rig was built on a suspension testing machine to test the performance of semi-active suspension and compare it with passive suspension. Various types of excitations in the form of input displacement were used with constant current control, Skyhook control and Rakheja-Sankar (RS) control as different cases. The conclusions are:

- The passive suspension system of the SUV and the newly designed MR damper semi-active suspension with constant current control have nearly identical sprung mass acceleration response.

- For sinusoidal displacement input in the low frequency range (2-3 Hz), RS control method provides the least value of peak vertical acceleration of sprung mass, followed by Skyhook control and constant current control. In the high frequency range (4-5Hz), RS control provides much lower vertical acceleration than Skyhook control and similar to constant current control.

- For rounded ramp displacement input, except for the low frequency low amplitude case, RS control method provides the least value of peak vertical acceleration of sprung mass, followed by Skyhook control and constant current control.

- Thus, for a semi-active suspension using twin-tube MR damper, RS control method provides better ride comfort to passengers due to lower peak vertical acceleration when compared to constant current control or Skyhook control method.

- For sinusoidal displacement input, RS control method generated much lower peak ground force values when compared to Skyhook control, especially in the high frequency region. For example, for 5 Hz excitation of 5 mm amplitude, RS control

method led to 36 % reduction of peak ground force when compared to Skyhook control. Thus, for preventing damage to road surface as well as to vehicle suspension elements, RS control method is a much better choice.

8.2 SCOPE OF FUTURE WORK

In the present work, based on the results of experimental evaluation of an automotive passive damper and a commercial MR damper, a twin-tube valve mode MR damper was designed and developed for application in automotive semi-active suspension. MR fluid was also synthesized, characterised and mathematical model was developed for its behaviour. A SDOF quarter car test rig was used to evaluate the semi-active suspension performance using skyhook and RS control methods. This study can be further extended as given below:

- A two degree of freedom quarter car test rig can be developed so that the effect of tyre damping and stiffness can be studied.
- Effect of temperature variation on the performance of twin-tube MR damper can be studied.
- Damper design can be further improved to reduce cost, increase dynamic range of damper force and to reduce the response time.
- Response of the semi-active suspension to random road vibration under non-linear control methods can be studied.

REFERENCES

Acharya, S., Saini, T.R., and Kumar, H. (2019). "Determination of optimal magnetorheological fluid particle loading and size for shear mode monotube damper". *J. Braz. Soc. Mech. Sci. Eng.*, 41(10), 392.

Ahmadian, M. (2017). "Magneto-rheological suspensions for improving ground vehicle's ride comfort, stability, and handling". *Veh. Syst. Dyn.*, 55(10), 1618-1642.

Allien, J. V., Kumar, H., and Desai, V. (2020). "Semi-active vibration control of SiC-reinforced Al6082 metal matrix composite sandwich beam with magnetorheological fluid core". *Proc. Inst. Mech. Eng. Pt. L J. Mater. Des. Appl.*, 234(3), 408-424.

Arachchige, D. D., Tharangi, S., Ireshika, O. N., and Karimi, H. R. (2013). "New results on mathematical modelling and simulation of semi active suspension systems with magneto-rheological damper". *J. Pure Appl. Math.: Adv. Appl.*, 10(2), 191-226.

Arjon Turnip., Seonghun Park., and Keum-Shik Hong (2010). "Sensitivity Control of a MR-Damper SemiActive Suspension". *Int. J. Precision Engineering and Manufacturing*. 11(2), 209-218.

Aruna, M. N., Rahman, M. R., Joladarashi, S., and Kumar, H. (2019). "Influence of additives on the synthesis of carbonyl iron suspension on rheological and sedimentation properties of magnetorheological (MR) fluids". *Mater. Res. Express*, 6(8), 086105.

Ashtiani, M., Hashemabadi, S. H., and Ghaffari, A. (2015). "A review on the magnetorheological fluid preparation and stabilization". *J. Magn. Magn. Mater.*, 374, 716-730.

Ata, W. G., and Salem, A. M. (2017). "Semi-active control of tracked vehicle suspension incorporating magnetorheological dampers". *Veh. Syst. Dyn.*, 55(5), 626-647.

Baltzis, K. B. (2008). "The FEMM Package: A Simple, Fast, and Accurate Open Source Electromagnetic Tool in Science and Engineering". *J. Eng. Sci. Technol. Rev.*, 1(1).

Bossis, G., Lacis, S. and Meunier, A. (2002). "Magnetorheological fluids". *J. Magnetic and Magnetic Materials*. 224-228.

Butz, T. and O. Von Stryk. (2002). "Modelling and simulation of electro-and magnetorheological fluid dampers". *ZAMM* 82.1.

Chen, Y. (2009). "Skyhook surface sliding mode control on semi-active vehicle suspension systems for ride comfort enhancement". *Engineering*, *1*(1), 23-32.

Cheng, M., Chen, Z. B., and Xing, J. W. (2018). "Design, analysis, and experimental evaluation of a magnetorheological damper with meandering magnetic circuit". *IEEE Trans. Magn.*, 54(5), 1-10.

Chi, Z., He, Y., and Naterer, G. F. (2008). "Design optimization of vehicle suspensions with a quarter-vehicle model". *Trans. Can. Soc. Mech. Eng.*, 32(2), 297-312.

Choi, S. B., Li, W., Yu, M., Du, H., Fu, J., and Do, P. X. (2016). "State of the art of control schemes for smart systems featuring magneto-rheological materials". *Smart Mater. Struct.*, 25(4), 043001.

Cortes R, J. A., Villarreal-Gonzalez, L. S., and Martinez M, M. (2005). "Characterization, modeling and simulation of magnetorheological damper behavior under triangular excitation". *Adv. Technol. Mater. Mater. Process. J.*, 7(2), 135.

Dixon, J. C. (2007). "The shock absorber handbook". *John Wiley & Sons.* pp.16.

Dutta, S., Narahari, S., and Chakraborty, G. (2013). "Semi-active vibration isolation of a quarter car model under random road excitations using magnetorheological damper". In *1st International and 16th National conference on Machines and Mechanisms* (pp. 999-1005).

Faruque Ali and Ananth Ramaswamy (2009). "Testing and modeling of MR damper and its application to SDOF Systems using integral backstepping technique". *J.Dynamic Systems, Measurement, and Control,* 131.

García-Baños, I., Ikhouane, F., and Aguirre-Carvajal, N. (2017). "An asymmetric-friction based model for magnetorheological dampers". *IFAC-PapersOnLine*, 50(1), 14076-14081.

Georgiou, G., Verros, G., and Natsiavas, S. (2007). "Multi-objective optimization of quarter-car models with a passive or semi-active suspension system". *Veh. Syst. Dyn.*, 45(1), 77-92.

Gołdasz, J. (2013). "Electro-mechanical analysis of a magnetorheological damper with electrical steel laminations". *Przegląd Elektrotechniczny*, *89*(2a), 8-12.

Gołdasz, J., and Sapiński, B. (2015). "Insight into magnetorheological shock absorbers". *Switzerland: Springer International Publishing*, pp.17-21, pp.52-73.

Gołdasz, J., and Sapiński, B. (2017). "Magnetostatic analysis of a pinch mode magnetorheological valve". *Acta Mech. Autom.*, 11(3), 229-232.

Gołdasz, J., Sapinski, B., and Jastrzębski, Ł. (2018). "Assessment of the magnetic hysteretic behaviour of MR dampers through sensorless measurements". *Shock Vib.*, 2018, 3740208-21.

Gong, X. L., Zhang, X. Z. and Zhang, P. Q. (2005). "Fabrication and characterization of isotropic magnetorheological elastomers". *Polymer Testing*, 24(5), 669-676.

Guan, X. C., Guo, P. F., and Ou, J. P. (2011). "Modeling and Analyzing of Hysteresis Behavior of Magneto Rheological Dampers". *Procedia Engineering*, *14*, 2756-2764.

Guglielmino, E., Sireteanu, T., Stammers, C. W., Gheorghe, G., and Giuclea, M. (2008). "Dampers and vehicle modelling". *Semi-active Suspension Control: Improved Vehicle Ride and Road Friendliness*, 17-42.

Gurubasavaraju, T. M., Hemantha, K., and Arun, M. (2018). "A study of influence of material properties on magnetic flux density induced in magneto rheological damper through finite element analysis". *MATEC Web Conf.*, 144, 02004.

Gurubasavaraju, T. M., Kumar, H., and Arun, M. (2017). "Evaluation of optimal parameters of MR fluids for damper application using particle swarm and response surface optimization". *J. Braz. Soc. Mech. Sci. Eng.*, 39(9), 3683-3694.

Gurubasavaraju, T. M., Kumar, H., and Mahalingam, A. (2018). "An approach for characterizing twin-tube shear-mode magnetorheological damper through coupled FE and CFD analysis". *J. Braz. Soc. Mech. Sci. Eng.*, 40(3), 139.

Hato, M. J., Choi, H. J., Sim, H. H., Park, B. O., and Ray, S. S. (2011). "Magnetic carbonyl iron suspension with organoclay additive and its magnetorheological properties". *Colloids and Surfaces A: Physicochemical and Engineering Aspects*, *377*(1), 103-109.

Havelka, F., and Musil, M. (2012). "Optimal semi-active preview control of a quarter car model with magnetorheological damper with respect to tire lift off". *Eng. Mech.*, 175.

Hemanth, K., Ganesha, A., Kumar, H., and Gangadharan, K. V. (2014). "Analysis of MR damper based on finite element approach". *Appl. Mech. Mater.,* 592, 2006-2010.

Hemanth, K., Kumar, H., and Gangadharan, K. V. (2016). "Vertical dynamic analysis of a quarter car suspension system with MR damper". *J. Braz. Soc. Mech. Sci. Eng.*, *39*(1), 41-51.

Hemanth, K., Kumar, H., and Gangadharan, K. V. (2018). "Dynamic analysis of half car model with MR damper as semi-active suspension element". *Int. J. Acoust. Vib.*, 23, 138-46.

Hrovat, D., and Margolis, D. L. (1981). "An experimental comparison between semi–active and passive suspensions for air–cushion vehicles". *Int. J. Veh. Des.*, 2(3), 308-321.

Hu, G., Liu, Q., Ding, R., and Li, G. (2017). "Vibration control of semi-active suspension system with magnetorheological damper based on hyperbolic tangent model". *Adv. Mech. Eng.*, 9(5), 1687814017694581.

Imaduddin, F., Mazlan, S. A., and Zamzuri, H. (2013). "A design and modelling review of rotary magnetorheological damper". *Materials and Design*, *51*, 575-591.

Jaehwan, K. and Kyoung-Mi, P. (2004). "Material characterization of MR fluid at high frequencies". *J. Sound Vibr.*, 121-133.

Jamali, M. S., Ismail, K. A., Taha, Z., and Aiman, M. F. (2017). "Development of Matlab Simulink model for dynamics analysis of passive suspension system for lightweight vehicle". *J. Phys. Conf. Ser.*, 908, 012066.

Jastrzębski, Ł., and Sapiński, B. (2017). "Experimental investigation of an automotive magnetorheological shock absorber". *Acta Mech. Autom.*, 11(4), 253-259.

Jiang, W., Zhang, Y., Xuan, S., Guo, C., and Gong, X. (2011). "Dimorphic magnetorheological fluid with improved rheological properties". *J. Magnetism and Magnetic Materials*, *323*(24), 3246-3250.

Jun, J. B., Uhm, S. Y., Ryu, J. H. and Suh, K. D. (2005). "Synthesis and characterization of monodisperse magnetic composite particles for magnetorheological fluid materials. Colloids and Surfaces A". *Physicochemical and Engineering aspects*, 260(1), 157-164.

Kamble, V. G., and Kolekar, S. (2014). "Analysis of rheological properties of MR fluid based on variation in concentration of iron particles". *American J. Nanotechnology*, 5(2), 12.

Kasemi, B., Muthalif, A. G., Rashid, M. M., and Fathima, S. (2012). "Fuzzy-PID controller for semi-active vibration control using magnetorheological fluid damper". *Procedia Engineering*, 41, 1221-1227.

Kciuk., S. K. and Turczyn, R. (2009). "Magnetorheological characterization of carbonyl iron based suspension". *J. Achievements in Materials and Manufacturing Eng.,* V33.

Keshav, M., Bhagyarajan, A., and Chandramohan, S. (2019). "Regression models for magnetic flux density using DoE techniques and geometric optimization of MR valve". *Smart Mater. Struct.*, 28(7), 075008.

Kim, W. H., Park, J. H., Kaluvan, S., Lee, Y. S., and Choi, S. B. (2017). "A novel type of tunable magnetorheological dampers operated by permanent magnets". *Sens. Actuators A: Phys.*, 255, 104-117.

Kim, Y., Choi, S., Lee, J., Yoo, W. and Sohn, J. (2011). "Damper modeling for dynamic simulation of a large bus with MR damper". *Int. J. Automotive Tech.,* 12(4), 521-527.

Krishna, H., Kumar, H., and Gangadharan, K. (2017). "Optimization of magneto-rheological damper for maximizing magnetic flux density in the fluid flow gap through FEA and GA approaches". *J. Inst. Eng. (India) Ser. C*, 98(4), 533-539.

Krishnan Unni, R., and Tamilarasan, N. (2018). "Design and analysis of a magneto-rheological damper for an all terrain vehicle". *MS&E*, 310(1), 012128.

Kubik, M., and Goldasz, J. (2019). "Multiphysics Model of an MR Damper including Magnetic Hysteresis". *Shock Vib.*, 2019.

Kubík, M., Macháček, O., Strecker, Z., Roupec, J., and Mazůrek, I. (2017). "Design and testing of magnetorheological valve with fast force response time and great dynamic force range". *Smart Mater. Struct.*, 26(4), 047002.

Kumbhar, B. K., and Patil, S. R. (2014). "A study on properties and selection criteria for magneto-rheological (MR) fluid components". *Int. J. ChemTech Research*, 6, 3303-3306.

Kwok, N. M., Ha, Q. P., Nguyen, M. T., Li, J., and Samali, B. (2007). "Bouc–Wen model parameter identification for a MR fluid damper using computationally efficient GA". *ISA transactions*, *46*(2), 167-179.

Liu, Y., Waters, T. P., and Brennan, M. J. (2005). "A comparison of semi-active damping control strategies for vibration isolation of harmonic disturbances". *J. Sound Vib.*, 280(1-2), 21-39.

Manjeet, K., and Sujatha, C. M. (2018). "Modeling and optimization of non-linear Herschel-Bulkley fluid model based magnetorheological valve geometry". *IEEE/ASME Inter. Conf. Adv. Intell. Mechatron.*, 413-420.

Metered, H. A., and Bonello, P. (2010). "Modelling and control of magnetorheological dampers for vehicle suspension systems" (Doctoral dissertation, University of Manchester).

Montgomery, D. (1997) "Design and Analysis of Experiments" (4th edn), *John Wiley and Sons, New York,* pp. 622-629.

Morales, A. L., Nieto, A. J., Chicharro, J. M., and Pintado, P. (2018). "A semi-active vehicle suspension based on pneumatic springs and magnetorheological dampers". *J. Vib. Control*, 24(4), 808-821.

Nam, Y. J., and Park, M. K. (2009). "Electromagnetic design of a magnetorheological damper". *J. Intell. Mater. Syst. Struct.*, 20(2), 181-191.

Nguyen, Q. H., Choi, S. B., and Wereley, N. M. (2008). "Optimal design of magnetorheological valves via a finite element method considering control energy and a time constant". *Smart Mater. Struct.*, 17(2), 025024.

Nie, S., Zhuang, Y., Liu, W., and Chen, F. (2017). "A semi-active suspension control algorithm for vehicle comprehensive vertical dynamics performance". *Veh. Syst. Dyn.*, 55(8), 1099-1122.

Omar, M., El-Kassaby, M. M., and Abdelghaffar, W. (2017). "A universal suspension test rig for electrohydraulic active and passive automotive suspension system". *Alexandria Eng. J.*, 56(4), 359-370.

Palomares, E., Morales, A. L., Nieto, A. J., Chicharro, J. M., and Pintado, P. (2019). "Modelling magnetorheological dampers in preyield and postyield regions". *Shock Vib.*, 2019, 5636053, 23.

Pang, H., Liu, F., and Xu, Z. (2018). "Variable universe fuzzy control for vehicle semi-active suspension system with MR damper combining fuzzy neural network and particle swarm optimization". *Neurocomputing*, 306, 130-140.

Park, B. J., Fang, F. F., and Choi, H. J. (2010). "Magnetorheology: materials and application". *Soft Matter*, *6*(21), 5246-5253.

Park, B. J., Song, K. H., and Choi, H. J. (2009). "Magnetic carbonyl iron nanoparticle based magnetorheological suspension and its characteristics". *Materials Letters*, *63*(15), 1350-1352.

Park, J. H., Kim, W. H., Shin, C. S., and Choi, S. B. (2016). "A comparative work on vibration control of a quarter car suspension system with two different magneto-rheological dampers". *Smart Mater. Struct.*, 26(1), 015009.

Parlak, Z., Engin, T., and Şahin, İ. (2013). "Optimal magnetorheological damper configuration using the Taguchi experimental design method". *J. Mech. Des.*, 135(8).

Parlak, Z., Engin, T., Ari, V., Sahin, I., and Calli, I. (2010). "Geometrical optimisation of vehicle shock dampers with magnetorheological fluid". *Int. J. Veh. Des.*, 54(4), 371-392.

Pavel Kuzhir., George Bossis., Victor Bashtovi and Olga Volkova (2003). "Flow of magnetorheological fluid through porous media". *European J. Mechanics B/F Fluids*, 22, 331-343.

Peng, G. R., Li, W., Tian, T. F., Ding, J., and Nakano, M. (2014). "Experimental and modeling study of viscoelastic behaviors of magneto-rheological shear thickening fluids". *Korea-Australia Rheology Journal*, *26*(2), 149-158.

Peng, Y., Yang, J., and Li, J. (2018). "Parameter identification of modified Bouc–Wen model and analysis of size effect of magnetorheological dampers". *J. Intell. Mater. Syst. Struct.*, 29(7), 1464-1480.

Phule, P. P. (2001). "Magnetorheological (MR) fluids: principles and applications". *Smart Materials Bulletin*, *2001*(2), 7-10.

Poynor, J. C. (2001). "Innovative designs for magneto-rheological dampers" (Doctoral dissertation, Virginia Tech).

Prabakar, R. S., Sujatha, C., and Narayanan, S. (2009). "Optimal semi-active preview control response of a half car vehicle model with magnetorheological damper". *J. Sound Vib.*, 326(3-5), 400-420.

Prabakar, R. S., Sujatha, C., and Narayanan, S. (2013). "Response of a quarter car model with optimal magnetorheological damper parameters". *J. Sound Vibr.*, *332*(9), 2191-2206.

Qin, Y., Zhao, F., Wang, Z., Gu, L., and Dong, M. (2017). "Comprehensive analysis for influence of controllable damper time delay on semi-active suspension control strategies". *J. Vib. Acoust.*, 139(3).

Rabinow, J. (1948). "The magnetic fluid clutch". *Electr. Eng.*, 67(12), 1167-1167.

Rahman, M., Ong, Z. C., Julai, S., Ferdaus, M. M., and Ahamed, R. (2017). "A review of advances in magnetorheological dampers: their design optimization and applications". *J. Zhejiang Univ. Sci. A*, 18(12), 991-1010.

Rakheja, S., and Sankar, S. (1985). "Vibration and shock isolation performance of a semi-active "on-off" damper". *Trans. ASME: J. Vib. Acoust. Stress Reliab. Des.*, 398-403.

Rao, L. G., and Narayanan, S. (2008). "Preview control of random response of a half-car vehicle model traversing rough road". *J. Sound Vib.*, 310(1-2), 352-365.

Rao, S.S., and Yap, F.F. (2011) "Mechanical vibrations" (Vol. 4). *Upper Saddle River: Prentice hall*, pp. 179.

Salem, M. M. M., and Aly, A. A. (2009). "Fuzzy control of a quarter-car suspension system". *World Acad. Sci. Eng. Technol.*, 53(5), 258-263.

Sapiński, B., and Filuś, J. (2003). "Analysis of parametric models of MR linear damper". *J. Theoretical and Applied Mechanics*, *41*(2), 215-240.

Seong, M. S., Choi, S. B., and Sung, K. G. (2011). "Control Strategies for Vehicle Suspension System Featuring Magnetorheological (MR) Damper". *Vibration Analysis and Control-New Trends and Developments*. InTech.

Shen, Y., Golnaraghi, M. F., and Heppler, G. R. (2006). "Semi-active vibration control schemes for suspension systems using magnetorheological dampers". *J. Vibr. Control*, *12*(1), 3-24.

Shiao, Y. J., Nguyen, Q. A., and Lai, C. C. (2013). "Application of Magneto Rheological Damper on Semi-Active Suspension System". *Applied Mechanics and Materials* (Vol. 284, pp. 1754-1758). Trans Tech Publications.

Shivaram, A. C., and Gangadharan, K. V. (2007). "Statistical modelling of a magneto-rheological fluid damper using the design of experiments approach". *Smart Mater. Struct.,* 16(4), 1310.

Simon, T. M., Reitich, F., Jolly, M. R., Ito, K., and Banks, H. T. (2001). "The effective magnetic properties of magnetorheological fluids". *Mathematical and Computer Modelling,* 33(1), 273284.

Song, X. (2009). "Cost-effective skyhook control for semi-active vehicle suspension applications". *Open Mechanical Engineering Journal*, *3*, 17-25.

Song, X., Ahmadian, M., and Southward, S. C. (2005). "Modeling magnetorheological dampers with application of nonparametric approach". *J. Intell. Mater. Syst. Struct.*, *16*(5), 421-432.

Spaggiari, A., Castagnetti, D., Golinelli, N., Dragoni, E., and Scirè Mammano, G. (2019). "Smart materials: Properties, design and mechatronic applications". *Proc. Inst. Mech. Eng. Pt. L J. Mater. Des. Appl.*, 233(4), 734-762.

Spencer, B. F., Dyke, S. J., Sain, M. K., and Carlson, J. (1997). "Phenomenological model for magnetorheological dampers". *J.Eng. Mechanics*, 123(3), 230-238.

Sultoni, A. I., Sutantra, I. N., and Pramono, A. S. (2014). "Modeling, prototyping and testing of regenerative electromagnetic shock absorber". *Appl. Mech. Mater.*, 493, 395-400.

Sunil Jha and Jain, V. K. (2009). "Rheological characterization of magnetorheological polishing fluid for MRAFF". *Int. J. Adv. Manufac. Tech.*, 42: 656-668.

Thakkar, R.M., Shah, K., and Mohammed, Y.M. (2013). "Modeling and simulation of magnetorheological fluid damper for predicting the saturation limit to applied field current". *Global Research Analysis*, 2(3).

Tharehalli Mata, G., Kumar, H., and Mahalingam, A. (2018). "Performance analysis of a semi-active suspension system using coupled CFD-FEA based non-parametric modeling of low-capacity shear mode monotube MR damper". *Proc. Inst. Mech. Eng. Pt. D J. Automob. Eng.*, 233(5), 1214-1231.

Tu, F., Yang, Q., He, C., and Wang, L. (2012). "Experimental study and design on automobile suspension made of magneto-rheological damper". *Energy Procedia*, *16*, 417-425.

Türkay, S., and Akçay, H. (2005). "A study of random vibration characteristics of the quarter-car model". *J. Sound Vib.*, 282(1-2), 111-124.

Upadhyay, R. V., Laherisheth, Z., and Shah, K. (2013). "Rheological properties of soft magnetic flake shaped iron particle based magnetorheological fluid in dynamic mode". *Smart Mater. Struct.*, *23*(1), 015002.

Verros, G., Natsiavas, S., and Papadimitriou, C. (2005). "Design optimization of quarter-car models with passive and semi-active suspensions under random road excitation". *J. Vib. Control*, 11(5), 581-606.

Wang, D. H., and Liao, W. H. (2011). "Magnetorheological fluid dampers: a review of parametric modelling". *Smart Mater. Struct.*, *20*(2), 023001.

Wereley, N. (Ed.). (2013). "Magnetorheology: advances and applications". *Cambridge: Royal Society of Chemistry*, pp.158.

Wong, P. L., Bullough, W. A., Feng, C., and Lingard, S. (2001). "Tribological performance of a magneto-rheological suspension". *Wear*, 247(1), 33-40.

Yang, G., Spencer, B. F., Carlson, J. D., and Sain, M. K. (2002). "Large-scale MR fluid dampers: modelling and dynamic performance considerations". *Eng. Structures,* 24(3), 309-323.

Yao, G.Z., Yap, F.F., Chen, G., Li, W.H. and Yeo, S.H. (2002). "MR damper and its Application for semi-active control of vehicle suspension system". *Mechatronics,* 12, 963-973.

Yerrawar, R. N., and Arakerimath, R. R. (2017). "Development of methodology for semi active suspension system using MR damper". *Mater. Today: Proc.*, 4(8), 9294-9303.

Yıldız, A. S., Sivrioğlu, S., Zergeroğlu, E., and Çetin, Ş. (2015). "Nonlinear adaptive control of semi-active MR damper suspension with uncertainties in model parameters". *Nonlinear Dyn.*, 79(4), 2753-2766.

Zapateiro, M., Pozo, F., Karimi, H. R., and Luo, N. (2012). "Semiactive control methodologies for suspension control with magnetorheological dampers". *IEEE/ASME Transactions on Mechatronics*, *17*(2), 370-380.

Zhang, H. H., Liao, C. R., Chen, W. M., and Huang, S. L. (2006). "A magnetic design method of MR fluid dampers and FEM analysis on magnetic saturation". *J. Intell. Mater. Syst. Struct.*, *17*(8-9), 813-818.

APPENDIX-A

Specification of instruments used

Lord MR damper RD-8040-1 and RD-8041-1

Lord MR damper

Parameter	Specification	
	RD-8040-1	**RD-8041-1**
Stroke in mm (inches)	55 (2.17)	74 (2.91)
Extended Length in mm (inches)	208 (8.2)	248 (9.76)
Body Diameter in mm (inches)	42.1 (1.66) max	42.1 (1.66) max
Shaft Diameter in mm (inches)	10 (0.39)	10 (0.39)
Tensile Strength in N (lbf)	8896 (2000) max	8896 (2000) max
Damper Forces in N (lbf) Peak to Peak at 5 cm/sec @ 1 A	>2447 (>550)	>2447 (>550)
Damper Forces in N (lbf) Peak to Peak at 20 cm/sec @ 0 A	<667 (<150)	<667 (<150)
Operating Temperature °C (°F)	71 (160) max	71 (160) max

Lord Wonder box

Lord Wonder box

Parameter	Specification
Overall Dimensions (LxWxH), mm (in)	63.5 x 27.9 x 88.9 (2.5 x 1.1 x 3.5)
Input Receptacle	1 mm, Female
Pulse Width Modulation (PWM) Frequency, kHz	30
Output Current, Amp	2 max

Lord MRF 132 DG

Lord MR fluid MRF 132 DG

Parameter	Specification
Appearance	Dark Gray Liquid
Viscosity, Calculated as slope 800-1200 sec-1, Pa-s @ 40°C (104°F)	0.112 ± 0.02
Density, g/cm3 (lb/gal)	2.95-3.15 (24.6-26.3)
Solids Content by Weight, %	80.98
Flash Point, °C (°F)	>150 (>302)
Operating Temperature, °C (°F)	-40 to +130 (-40 to +266)

Damper testing machine at Rambal Ltd., Chennai

Damper testing machine at Rambal Ltd.

Parameter	Specification
Capacity of hydraulic actuator	1 ton (1000 kg) or 9.81 kN
Maximum stroke of actuator	250 mm
Maximum velocity of actuator	1 m/s
Force transducer capacity (Interface make)	1200 kg or 11.77 kN
Sampling rate	10,000 samples per second
Resolution of position sensor	0.0001 mm

HEICO Damper testing machine at NITK

HEICO damper testing machine at NITK

1. Hydraulic power pack

Hydraulic power pack

Parameter	Specification
Flow of the pump	64 LPM
Max. Operating Pressure	210 bars
Oil tank capacity	200 litres

Power rating of motor	40 HP
Length of hoses	5 m. (each)
Electric power supply	440V, 3 phase (AC supply)

2. Hydraulic actuator
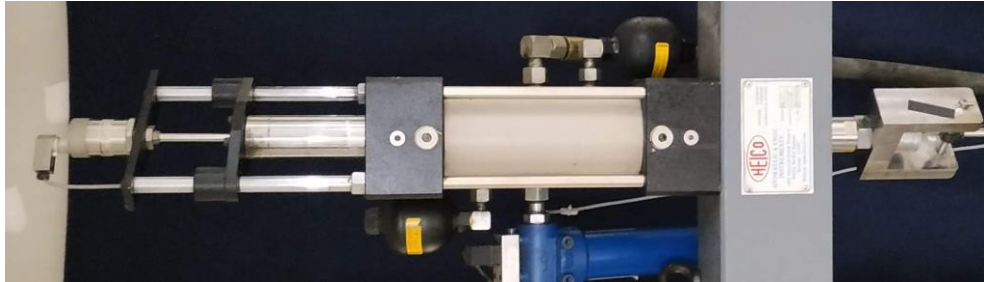
Hydraulic actuator

Parameter	Specification
Type	Double acting double ended
Capacity	+/- 20 kN
Stroke	150 mm (+/- 75 mm)
Max. working pressure	210 bars
Max. sustained velocity	0.8 m/s
Peak velocity	1.2 m/s
Servo valve	63 LPM
Pressure line filter	180 LPM with 3 microns filtration
Accumulator (2 No.)	0.36 litre capacity

A servo valve with pressure line filter and accumulators (1.5 litres) in pressure and return valve is fitted on the manifold block. It controls the movement of the ram as per given command signal from control electronics. The servo valve is a throttle valve for 4-way applications and rated for a pressure drop of 1,000 PSI (70 kg/cm^2). The output stage is a closed centre four way sliding spool. The servo valve is of MOOG make with a flow rate of 63 LPM.

3. Force transducer

Force transducer

Parameter	Specification
Capacity	+/- 30 kN
Resolution	0.001 kN
Full scale output	2 mV/V
Excitation Voltage	10 Volts DC
Non-linearity	< +/- 0.15 % FSO
Safe overload	150 %
Operating temperature	0 to +60 deg. C
Accuracy	0.5% of indicated value as per ISO7500-1

4. Position sensor/ Displacement transducer

Position sensor/ Displacement transducer

Parameter	Specification
Range	200 mm
Make	Gefran/Balluff

Full scale output	10 volts
Repeatability	<0.01 mm
Pressure withstand	Up to 600 bars
Excitation voltage	24 volts DC
Sampling rate	2 kHz
Operating temperature	-30 to +75 deg. C

5. Signal conditioning and controlling unit

Computer with signal conditioning and controlling unit

- Signal conditioning unit consists of conditioning modules for different transducers (position transducer, load cell etc.) that receives output signal from these sensors and processes the signal as per the requirement and transfers it to the computer where it is accepted by the data acquisition system.
- The controlling unit controls the movement of the ram with respect to the signal input on feedback basis either from force transducer or displacement transducer.
- It consists of a dedicated Servo-controller card that gives the desired processed signal through an automatic PID controller to the servo valve to operate in load mode or displacement mode.
- It also sends the signal to the computer and accepts the command from the software to operate in the desired manner.

Specifications of controller

- Auto PID operation with auto zeroing, auto tuning and auto-adjustment feature servo operation.

- Digital signal processing (DSP) based closed loop servo controller with closed loop update rate of 10 kHz.
- Number of control channels - 4 (Load/Displacement/External channel strain 1 and strain2).
- Demand wave generation - Sine, Triangular, Square and ramp signal.
- High-speed 32-bit data acquisition with 6 kHz sampling rate on all primary channels.
- Auto calibration and digital auto zero capability.

6. Computer with control software for controlling and data acquisition

The system consists of a dedicated computer of latest available configuration with built in data acquisition card and latest OS installed. Computer configuration consists of Intel i5 processor with 4GB RAM and 500 GB HDD, 6 USB ports and 24" LCD monitor.

Control software in the system is the Windows based user-friendly software. The loading can be given in the form of sine, triangular, square and ramp signal. Multi-velocity performance and plotting with desired parameters make this software user friendly.

HEICO Suspension test rig

Suspension test rig with PC and controller

Suspension test rig

1. Base frame

Parameter	Specification
Length of the frame	1500 mm
Width of the frame	1000 mm
Working height of the frame	500 mm
T slots size	M16
Vertical loading capacity	30 kN
Number of T slots	4

2. Vertical frame

Parameter	Specification
Base of the frame	600 mm
Length of the frame	400 mm
Height of the frame	3000 mm

Main carriage adjustment	1500 mm
Front plate of the carriage	Matrix of 100x100xM12
Travel of slide carriage (linear bearing)	100 mm

3. Frame for mounting shock absorbers or dampers

Parameter	Specification
Capacity	20 kN
Horizontal clearance	400 mm
Vertical clearance (adjustable)	200-1000 mm

4. LVDT on suspension test rig
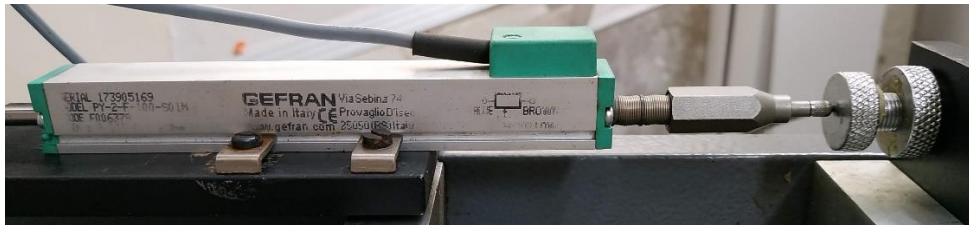
LVDT on suspension test rig

It measures motion of vertical frame. It is Gefran make and has a stroke of 100 mm (+/- 50 mm). It has stainless steel ball tip with M2.5 thread. It has double support of control rod with return spring and has infinite resolution. It can measure displacement speeds up to 10 m/s and has a working temperature range of -30^0C to 100^0C.

5. Uniaxial accelerometer (PCB make)

Uniaxial accelerometers (2 Nos.)

Parameter	Specification
Sensitivity	± 100 mV/g
Range	± 50 g
Frequency	0.5 to 10kHz
Resonance frequency	Greater than or equal to 50 kHz
Temperature Range	-54 to 93 °C
Cable Length	5m

6. Long stroke LVDT
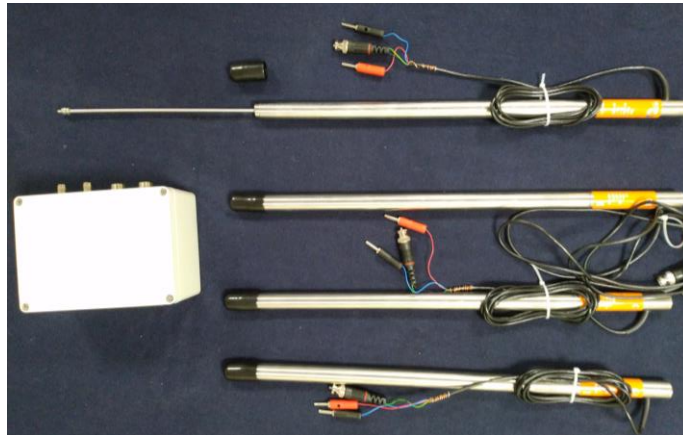
Long stroke LVDT (4 Nos.)

Parameter	Specification
Stroke range	0 mm to 200 mm
Sensitivity	49.04mV/mm
Shocks	50g
Vibrations	10g RMS (20Hz to 2000Hz)
Linearity	±0.16 % of Full scale
Operating temperature	-40°C to +85°C

7. DAQ and semi-active controller (NI CDAQ 9174, NI 9234, NI 9403)

NI CDAQ 9174

Parameter	Specification
Input FIFO size	127 samples per slot
Timing accuracy	50 ppm of sample rate
Timing resolution	12.5 ns
Resolution (Timers and counters)	32 bits
No. of slots for modules	4 slots

NI 9234 C series

Parameter	Specification
IEPE channels	4 channel sound and vibration input
Resolution	24-bit resolution
Operational Range	±5 V, 0 to 20mA Input range
Connectivity type	BNC connectivity only

Sampling rate	51.2 kS/s

NI 9403 with DSUB 32 Ch, TTL Digital Input/Output Module

Parameter	Specification
Module type	5V, TTL digital I/O
No. of input output channels	32 - Channel
Speed of operation	7µ S
Isolation	60 VDC, CAT I
Operational Temperature	-40 °C to 70 °C
Operating Acceleration	5 g vibration, 50 g shock

Particle size analyser CILAS 1064

Particle size analyser CILAS 1064

Parameter	Specification
Particle size range	0.04 to 500 µm
Number of lasers	2
Laser source	Fibre and collimated laser diodes
Wavelength	635 and 830 nm
Power	3/7 mW
Beam diameter	2 and 20 mm
Repeatability	± 0.5 %
Reproducibility	< 2 %

FESEM Zeiss Sigma make

FESEM Zeiss Sigma make

Parameter	Specification
Electron Source	Schottky Thermal Field Emitter
Resolution at 30 kV (STEM)	1.0 nm
Resolution at 15 kV	1.0 nm
Resolution at 1 kV	1.6 nm

Resolution at 30 kV (VP Mode)	2.0 nm
Maximum Scan Speed	50 ns/pixel
Accelerating Voltage	0.02 – 30 kV
Magnification	$10\times – 1,000,000\times$
Probe Current	3 pA - 20 nA (100 nA optional)
Image Framestore	$32 \text{ k} \times 24 \text{ k}$ pixels

Anton Paar Rheometer MCR 702

Anton Paar Rheometer MCR 702

Parameter	Specification
Minimum torque, rotation	1 nNm
Maximum torque, rotation	230 mNm
Minimum torque, oscillation	0.5 nNm
Maximum angular frequency	628 rad/s
Normal force range	0.005 to 50 N
Maximum temperature range	-160 to +1000 °C
Pressure range	up to 1000 bar
Rheometer Software RheoCompass™ Professional	Running under Microsoft Windows 7/8/8.1/10 (64bit versions only) - Recommended hardware: Intel i5, 2.67 GHz or higher, 8 GB RAM or more, SSD with 240 GB or more

Magnetorheological Device Cell	Magnetic Flux density up to 1 Tesla Temperature range -10 to 170°C
Hood with Peltier Heating/Cooling	Temperature range: -40 to 200 °C
Compressor	230/50 V/Hz, 55 l/min, OILFREE Motor Power: 0.55 kW Output (5 bar): 55 l/min max. Pressure: 8 bar Tank Volume: 10 l Weight: 59 kg Dimensions: 510x530x515 mm
Peltier Temperature Control Device	Temperature range: -5 to 200 °C
Power Supply Magneto Cell	230V HCP 14-12500,12.5,1 mA
Tesla meter	1 Tesla

MATLAB software details

Parameter	Specification
Name of the software	MATLAB/SIMULINK
Version	R2018b, R2019a, R2019b, R2020b
Licensed to	NITK
Company	MathWorks

FEMM software details

Parameter	Specification
Name of the software	Finite Element Method Magnetics
Version	4.2 (Current version)
Licensed to	Open-Source software

LabVIEW software

| Parameter	Specification
Name of the software	LabVIEW
Version	2014, 2017
Licensed to	NITK
Company	National Instruments

DC Power supply (Scientific make)

DC Power supply (Scientific PSD 3005)

- Built in over-heat and over-voltage protection.

- Constant current and constant voltage operation.

- Digital display for voltage and current.

- Adjustable current limiter.

- Protection against over-load and short circuit.

- Compact and light weight.

| Parameter	Specification
Make	Scientific
Model	PSD 3005
DC output	0 to 30V / 5A
Settling resolution	V: 10 mV, I : 5 mA
Load Regulation	<= +/-(0.05% + 10 mV)
Input Supply	230 AC +/- 10% / 50-60 Hz
Internal resistance	<=10 milliOhms

APPENDIX-B

Simulink model of quarter car model for passive suspension with sine wave input
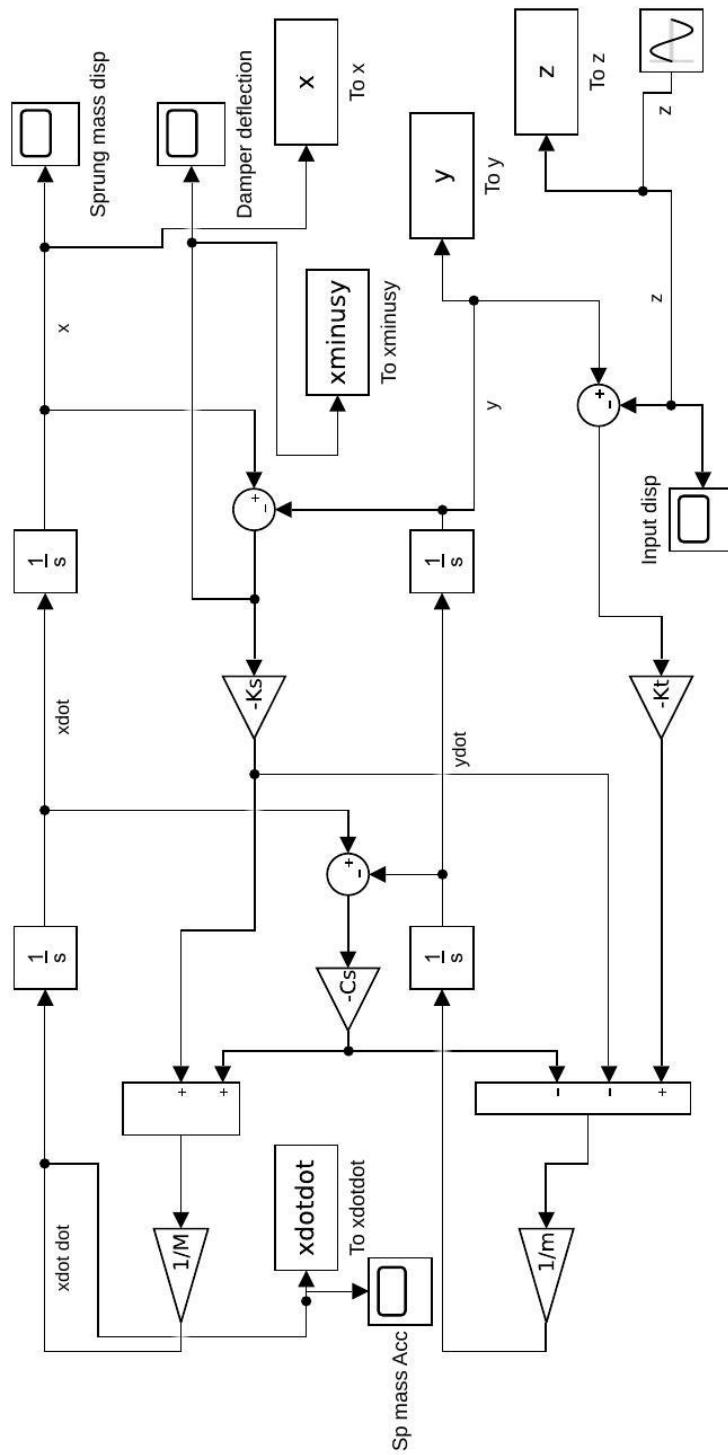
Simulink model of quarter car model for semi-active suspension with sine wave input,
made according to equations 6.4 and 6.5
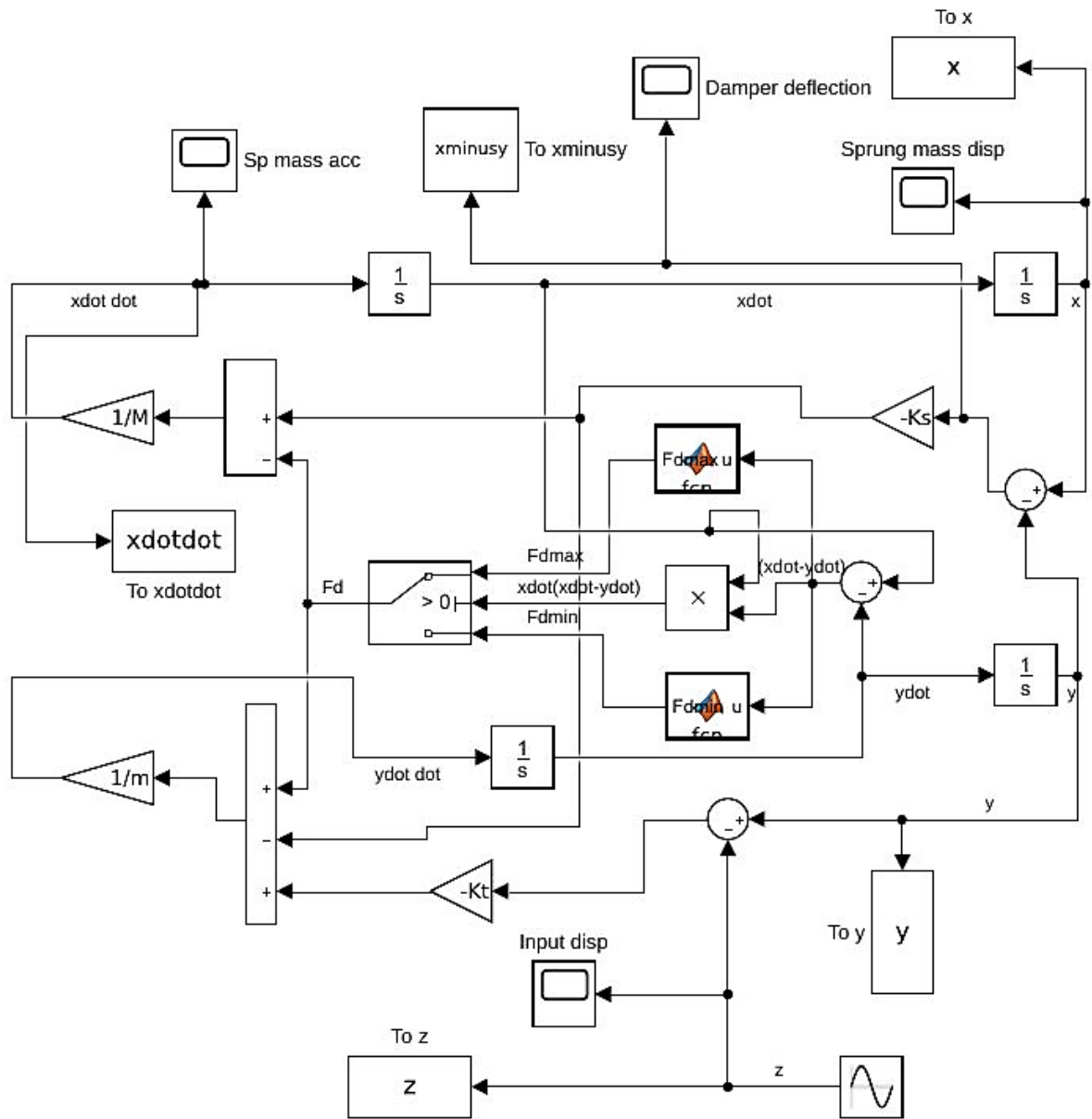
Simulink model for generating random road profile
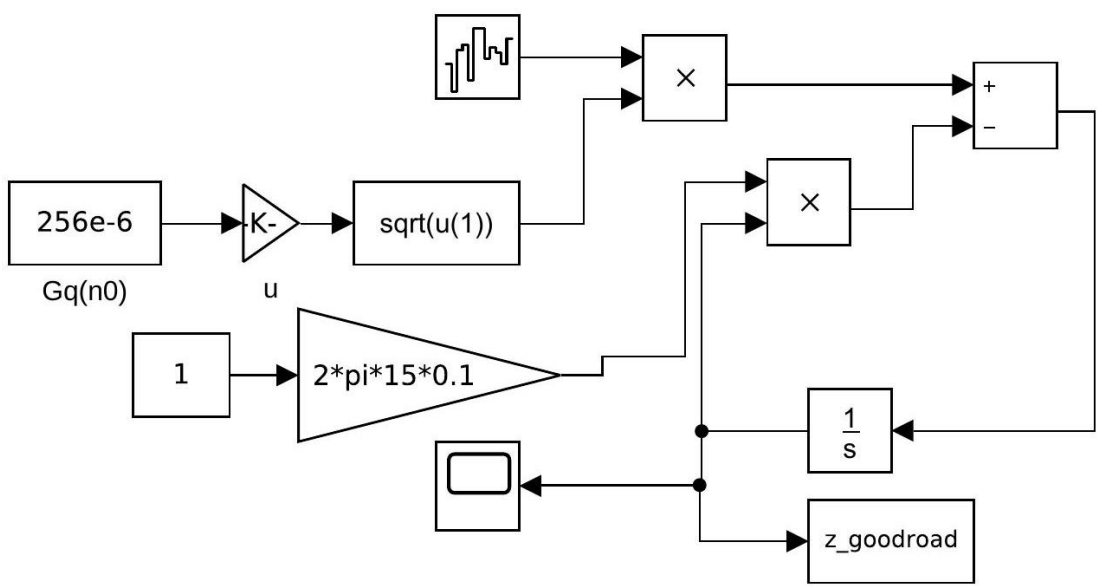
LIST OF PUBLICATIONS

INTERNATIONAL JOURNALS

1. **Rangaraj Madhavrao Desai**, Mohibb E. Hussain Jamadar, Hemantha Kumar, Sharnappa Joladarashi and Rajasekaran S.C. (2019). "Design and Experimental Characterization of a Twin Tube MR Damper for a Passenger Van". *Journal of the Brazilian Society of Mechanical Sciences and Engineering*. 41: 332. **(SCIE and SCOPUS indexed, Impact factor 2.22 for 2020)** https://doi.org/10.1007/s40430-019-1833-5

2. **Rangaraj Madhavrao Desai**, Subash Acharya, Mohibb-e-Hussain Jamadar, Hemantha Kumar, Sharnappa Joladarashi and SC Raja Sekaran. (2020). "Synthesis of magnetorheological fluid and its application in a twin-tube valve mode automotive damper". *Proc IMechE Part L: Journal of Materials: Design and Applications*. 234: 7. **(SCIE and SCOPUS indexed, Impact factor 2.31 for two years)** https://doi.org/10.1177/ 1464420720925497

3. **Rangaraj Madhavrao Desai**, Mohibb-e-Hussain Jamadar, Hemantha Kumar and Sharnappa Joladarashi. (2021). "Performance evaluation of a single sensor control scheme using a twin-tube MR damper based semi-active suspension". *Journal of Vibration Engineering and Technologies*. 1:18. **(SCIE and SCOPUS indexed, Impact factor 1.89 for 2020)** https://doi.org/10.1007/s42417-021-00290-1

INTERNATIONAL CONFERENCES

1. **Rangaraj Madhavrao Desai**, Mohibb E. Hussain Jamadar, Hemantha Kumar, Sharnappa Joladarashi, S.C. Rajasekaran and G. Amarnath. "Evaluation of a Commercial MR Damper for Application in Semi-active Suspension". *International Conference on Advances in Mechanical Engineering and Nanotechnology* (ICAMEN 2019), Manipal University Jaipur, INDIA, March 8-9, 2019. **(Received the Best Paper award).** Published in SN Applied Sciences – A Springer Nature Journal. (2019) 1:993. https://doi.org/10.1007/s42452-019-1026-y

2. **Rangaraj Madhavrao Desai**, Mohibb E. Hussain Jamadar, Hemantha Kumar and Sharnappa Joladarashi. "Experimental Investigation and Mathematical Modeling of

Automotive Passive Damper for SUV Suspension System". *Second International Conference on Design, Materials & Manufacture* (ICDEM 2019), National Institute of Technology Karnataka, Surathkal, INDIA, December 6-8, 2019. Published in AIP Conference Proceedings 2247, 020015 (2020). https://doi.org/10.1063/5.0003954

3. **Rangaraj Madhavrao Desai**, Mohibb E. Hussain Jamadar, Hemantha Kumar and Sharnappa Joladarashi. "Dynamic Analysis of Quarter Car Vehicle Model with Semi-active Suspension for Better Ride Comfort". *7th International Congress on Computational Mechanics and Simulation* (ICCMS 2019), IIT Mandi, Himachal Pradesh, INDIA, December 11-13, 2019.

BIODATA

Name   : RANGARAJ MADHAVRAO DESAI

Date of Birth   : 07-03-1985

Mobile No.   : +91 9482575659

Email   : rangarajmdesai@gmail.com

ADDRESS:

S/O M. D. Desai, Ranga Nilaya, Near railway station, Koppal, Karnataka-583231.

QUALIFICATION:

Degree	Board/Institute	Year	Percentage/ CGPA
Ph. D. (course work)	NITK, Surathkal	2016	8.46/10
M. Eng (Mechanical Systems)	Concordia University Montreal, Canada	2010-12	3.99/4.3
B.E. (Mechanical Engg.)	NITK, Surathkal	2002-06	78.4%

EXPERIENCE:

Sl. no	Name of the company/institute	Designation	From	To
1.	Tata Motors Ltd. PCBU, Pimpri, Pune	Assistant Manager	July 2006	April 2007
2.	TVS Motor Company Ltd. Hosur, Tamil Nadu	Senior Executive	June 2008	July 2009
3.	Reva University, Yelahanka, Bengaluru	Assistant Professor	June 2014	July 2016

Journal Publications   : 5

Conference Publications   : 3